ASSESSMENT OF SURFACE WATER POTENTIAL AND DEMAND OF UPPER GENALE RIVER BASIN UNDER THE IMPACT OF CLIMATE AND LAND USE LAND COVER CHANGE, ETHIOPIA.

PhD DISSERTATION

MEHARI SHIGUTE WOLDEYOHANNES

August 2024

Addis Ababa

Assessment of Surface Water Potential and Demand of Upper Genale River Basin under the Impact of Climate and Land Use Land Cover Change, Ethiopia.

By

Mehari Shigute Woldeyohannes

A Dissertation Submitted

to

Ethiopian Institute of Water Resources

Presented in Fulfillment of the Requirements for the Degree of Doctor of Philosophy

in

Water Resources Engineering and Management

Major Advisor: Dr. Tena Alamirew

Addis Ababa University (AAU), EIWR

Co-Advisor: Dr. Adane Abebe

Arba Minch University

Addis Ababa University

Addis Ababa, Ethiopia

August 2024

Addis Ababa University

School of Graduate Studies

This is to certify that the dissertation presented by Mehari Shigute entitled "**Assessment of Surface Water Potential and Demand of Upper Genale River Basin under the Impact of Climate and Land Use Land Cover Change, Ethiopia"** and submitted in fulfillment of the requirements for the degree of Doctor of Philosophy (Water Resources Engineering and Management) complies with the regulations of the University and meets the accepted standards with respect to originality and quality.

Approved by Board of Examiners:

Dr. Tena Alamirew		22/10/2024
Main Advisor	Signature	Date
Dr. Adane Abebe		25/10/2024
Co - Advisor	Signature	Date
Dr. Fasikaw Atanaw	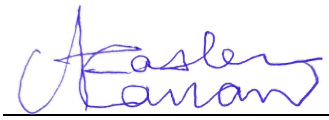	22/10/2024
External Examiner	Signature	Date
Dr. Sirak Tekleab	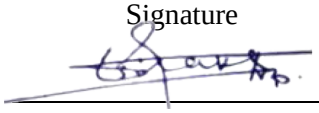	22/10/2024
Internal Examiner		Date
Dr. Ermias Teferi		23/10/2024
Internal Examiner	Signature	Date
Dr. Gebremedhin Tesfaye		26/10/2024
Chair Person	Signature	Date
Dr. Tilahun Derib		
EIWR Education Coordinator	Signature	Date
Dr. Zeleke Agide		
EIWR Director	Signature	date

ACKNOWLEDGMENTS

Above all, I thank Almighty God for his assistance throughout my life. Next, I'd like to express my heartfelt gratitude to my dissertation advisors, Dr. Tena Alamirew and Dr. Adana Abebe, for their consistent guidance and invaluable comments and suggestions on the dissertation work. I would also like to express my heartfelt gratitude to Dr. Christopher Ndehedehe and Dr. Habtamu Tilahun Kassahun, who assisted me with manuscript review and financial support during the journal publication process, and without whom I would not be at this stage of the dissertation work. I am also deeply indebted to Dr. Gebremedhin Tesfaye for his guidance and encouragement, which helped me navigate the challenges of the PhD program.

I am very grateful to EIWR, Addis Ababa University, Dilla University, and the Australian Rivers Institute, Griffith University, Brisbane, for funding my Ph.D. study. I would also like to thank the Ethiopian National Meteorological Service Agency (including Hawassa and Bale Robe Meteorological Branch Offices), the Ethiopian Central Statistical Agency, the Ministry of Water, Irrigation, and Energy for providing meteorological, demographic, and streamflow data, and Sidama and Oromia Regional State Bureau of Water and Irrigation Development and Agriculture for providing me with the relevant data and information required for my study. My gratitude goes to the staff at EIWR and Dilla University's Department of Natural Resource Management, who have always been able to provide administrative support.

I am grateful to my entire family, especially my mom, brothers and sisters (Zewdu, Ejigayehu, Zegeye, Yeshi, Wubayehu, Tamiru, Mistre, Eng. Sintayehu) for always being there for me. Their constant encouragement, unwavering support, and heartfelt prayers have given me the strength and courage to keep going. I adore each and every one of them. Special thanks to my beloved mother, W/ro Abebech Tura, and my sister, Wubayehu Shigute, for all of your support and prayers. Their love and support have been invaluable to me, and I am truly blessed to have them in my life.

Most importantly, I would like to express my deepest gratitude to my supportive wife, Timelis Gashu. Throughout my PhD studies, she has been my rock, my confidante, and my partner in every way. Her love, care, and support have been invaluable. I could not have reached this point without her by my side. Her patience during my long absences from home and her unwavering care for our

children have been truly incredible. My dear, without your love and unwavering patience, this achievement would not have been possible. This success belongs to both of us.

Special thanks also go to my lovely boys, Natan, Dagim, and Yafet. They are a constant source of strength, happiness, and inspiration for me. I love you all unconditionally.

DEDICATION

I dedicated this work for my beloved Mom, W/ro Abebech Tura, My wife Timelise Gashu, my three sons (Nati, Dagi, & Yafu), and for all my brothers and sisters.

LISTS OF ABBREVIATIONS AND ACRONYMS

AGRL	Agricultural land
ANN	Artificial Neural Network
AR5	Fifth Assessment Report
ARS	Agricultural Research Services
BARR	Bare Land
BCM	Billion Cubic Meter
BRT	Buishand test
CIWD	Commercial and Institutional Water Demand
CMIP5	Coupled Model Intercomparison Project five
CN	Curve Number
CREAMS	Chemicals, Runoff, and Erosion from Agricultural Management Systems
CSA	Central Statistical Agency
CV	Coefficient of variation
DEM	Digital Elevation Model
DJF	December, January, February
DOY	Day of the Year
EGIA	Ethiopian Geospatial Information Agency
ENACT	Enhancing National Climate Services
ENSO	El-Nino Southern Oscillation
EOS	End of the Season
EPCC	Ethiopian Panel on Climate Change
EPIC	Erosion Productivity Impact Calculator
ERF	Effective Rainfall
ESGF	Earth System Grid Federation
EUMET-SAT	European Organisation for the Exploitation of Meteorological Satellites
FAO	Food and Agricultural Organizations
FRST	Forest Land
GCM	General Circulation Model
GD	Genale Dawa
GHG	Greenhouse Gas
GIS	Geographic Information System
GLEAMS	Groundwater Loading Effects of Agricultural Management Systems
GPS	Global Positioning System
GRAS	Grassland
HBV	Hydrologiska Byrns Vattenbalansavdelning
HEC-HMS	Hydrologic Modeling System
HRB	Shrubland
HRU	Hydrologic Response Units
IPCC	Intergovernmental Panel on Climate Change

ITCZ	Inter-Tropical Convergence Zone
IWR	Irrigation Water Requirement
IWRM	Integrated Water Resources Management
JJA	Jun, July, August
LGP	Length of Growing Period
LH-OAT	Latin Hypercube One-factor-At-a-Time
LULC	Land Use Land Cover
MAM	March, Aril, May
MICE	Multivariate Imputation by Chained Equations
MK	Mann–Kendall test
MoWE	Ministry of Water and Energy
NMA	National Meteorological Agency
NSE	Nash – Sutcliff's simulation Efficiency
OLI	Operational Land Imagery
PBIAS	Percent Bias
PCI	Precipitation Concentration Index
RCM	Regional Climate Models
SD	Standard deviation
SDSM	Statistical Downscaling Model
SEI	Stockholm Environment Institute
SNHT	Standard Normal Homogeneity Test
SNNP	Southern Nations, Nationalities, and Peoples'
SON	September, October, November
SRA	Standard Rainfall Anomaly
SRTM	Shuttle Radar Topography Mission
SUFI -2	Sequential Uncertainty Fitting -2
SWAT	Soil and Water Assessment Tool
SWRRB	Simulator for Water Resources in Rural Basin
TM	Thematic Mapper
URBN	Urban/Settlement area
USGS	United State Geological Survey
VNRT	Von Neumann ratio test
WATR	Water body
WEAP	Water Evaluation and Planning

TABLE OF CONTENTS

LIST OF TABLES

LIST OF FIGURES

LIST OF APPENDICES

Appendices: Tables

Appendices: Figures

Appendices: Published Articles

LIST OF MANUSCRIPTS

The dissertation consists of the following manuscripts in the chapters:

3. Analysis of rainfall and temperature variability for agricultural water management in the upper Genale river basin, Ethiopia. Scientific African, 20, e01635 (2023). https://doi.org/10.1016/j.sciaf.2023.e01635

4. Understanding Hydrological Processes under Land Use Land Cover Change in the Upper Genale River Basin, Ethiopia. Water, 14(23), 3881 (2022). https://doi.org/10.3390/w14233881

5. Assessing the Impacts of Climate Change on Hydrological Processes in the Upper Genale River Basin, Ethiopia. Environ Earth Sci 83, 297 (2024). https://doi.org/10.1007/s12665-024-11586-2

6. Evaluating Streamflow Potential and Demand of the Upper Genale River Basin Under Current and Future Development Plan, Ethiopia (Under preparation to a journal).

ABSTRACT

Understanding how climate and land-use changes affect water availability and demand in a watershed is crucial for planning and managing water resources effectively. This study addresses this need by examining the Upper Genale River Basin in Ethiopia. It investigates long-term trends in rainfall and temperature to inform agricultural water management. It also analyzes the impact of land use land cover (LULC) change on water flow and future climate change on water resources. Finally, the study assesses the potential for developing water resource systems and future water demand scenarios, providing valuable insights for adaptation and mitigation strategies in the basin. To achieve these objectives, long-term climate data from the Ethiopian National Meteorological Service Agency (NMA) were collected, and 30 m-resolution Landsat imageries were used to assess the impact on watershed hydrology and analyze the dynamics of LULC change. Future climate scenarios for the 2021-2050 and 2051-2080 time periods were developed using four different GCM-RCM combinations from the CORDEX-Africa projections under the RCP 4.5 and RCP 8.5 scenarios. Additionally, to investigate water resource demand and allocation under current and future scenarios, socioeconomic data (population, livestock, irrigation) was collected from federal and regional sources. The Coefficient of Variation (CV), Standard Rainfall Anomaly (SRA), and Precipitation Concentration Index (PCI) were used to evaluate the observed climate characteristics of rainfall and temperature. In addition, the Mann-Kendall test and Sen's slope estimator were used to assess the trend and magnitude of changes in rainfall and temperature. The Soil and Water Assessment Tool (SWAT) model was calibrated and validated in SWAT-CUP using the sequential uncertainty fitting (SUFI-2) algorithm using monthly measured flow data. The model performed well, with a coefficient of determination (R^2) > 0.74, Nash-Sutcliffe efficiency (NSE) > 0.72, and percent bias (PBIAS) ranging from -5% to 5% for the calibration and validation periods. The annual, winter, spring, summer, and autumn rainfall variability in the basin was high, with coefficients of variation (CVs) of 20%, 89%, 30%, 45%, and 32%, respectively. The standardized rainfall anomalies indicated that the basin had a drier season than a wet season. The mean length growing season ranges in 43 to 79 days in *Belg* and 38 to 170 days in *Kiremt* seasons. Most rainfall stations showed no significant increasing trend in annual, summer, and autumn rainfall, but there was a decreasing but statistically insignificant trend in spring rainfall at all stations except Bensadaye, Bore, Telamokentise, and Yirba Muda. The analysis result also shows to minimize yield reduction and crop failure during spring and autumn supplementary irrigation is essential. For instance, maize and sorghum varieties require supplementary irrigation of up to 202 mm and 252 mm,

respectively. Over the past 30 years, annual and seasonal maximum and minimum temperatures in the basin have been increasing trend in most stations, and the landscape has changed significantly. Satellite images analyses show that settlements, cultivated land, and bare land have all increased in area from 0.16% to 0.28%, 24.4% to 47.1%, and 0.16% to 0.62%, respectively, while forests, shrublands, and grasslands have decreased from 29.6% to 13.5%, 23.9% to 19.5% and 21.8% to 18.9%, respectively, in the area. These changes in LULC have affected the water cycle in the basin, leading to increased runoff and total water yield, and decreased lateral and groundwater flow. Under the two RCPs, annual and seasonal precipitation is expected to decrease while temperatures rise during the 2030s (2021-2050) and 2060s (2051-2080). The simulation result indicated a significant change in hydrological aspects. Under MPI-ESM-LR, EC-EARTH, and MIROC5 climate models, the study area's total water yield, surface runoff, ground waterflow, and lateral flow all decrease annually. However, all climate models (MPI-ESM-LR, EC-EARTH, CNRM-CM5, and MIROC5) show an increase in evapotranspiration of up to 8.1% due to an increase in temperatures. The decrease in rainfall and increase in temperatures will reduce annual water yield, surface runoff, ground waterflow, and lateral flow by up to 39.8%, 39%, 50%, and 40%, respectively, for the entire study basin. The observed and predicted annual and seasonal rainfall variability, as well as rising temperatures and LULC modification over the study area, have a significant impact on hydrological processes, resulting in droughts, flooding, and extreme water loss due to evaporation. These changes have consequences for agricultural and livestock production, domestic water supply, and municipal services. In addition, the WEAP model was used to evaluate water demand and allocation under different scenarios, the results predict a dramatic rise in water demand across the upper Genale River basin by 2050, driven by population growth, irrigation expansion, and the climate change. Water scarcity is expected to worsen, especially for irrigation, due to combined pressures from increasing consumption, potential climate change impacts, and limited water resources. As a result, natural resource managers, policymakers, and stakeholders in the study area will be better able to design and implement effective and sustainable land use planning and water resource management in order to deal with the ongoing impacts of climate, LULC change, and variability. It is also critical to develop strategic adaptation measures and a long-term approach to climate risk management.

Keywords: Upper Genale river basin, Rainfall and Temperature Trend, LULC change, Climate change, Regional climate models, Hydrological processes, SWAT model

CHAPTER ONE:

1. GENERAL INTRODUCTION

1.1. Background

Water is a natural resource that all social, economic, and ecosystem functions rely on. It is the most important element for life on Earth, and it is also critical to agriculture in many parts of the world, as well as a means to achieve sustainability in production systems (Shiva Shankar et al., 2021). However, its scarcity is the most limiting factor for socioeconomic growth and development (Dolan et al., 2021).

The availability of freshwater is the vital driving of socio-economic progress in Sub-Saharan Africa. It fuels a wide range of activities, from irrigation and sanitation to industry and recreation. These activities create jobs, generate income, and ultimately strengthen the region's economy. Furthermore, freshwater plays a critical role in tackling hunger, poverty, and health, making it a cornerstone of national and global development programs (Kankam-Yeboah et al., 2013).

However, freshwater supplies are inconsistent and unpredictable in terms of location, timing, and quantity. Ethiopia's hydrology is an excellent example for explaining the spatial and temporal variability of rainfall (Berihun et al., 2023; Ketema & Dwarakish, 2021a). Despite the fact that the resources vary in space and time, Ethiopia's twelve river basins provide a significant amount of water resources. The total annual runoff from these basins is estimated to be about 122 billion cubic meters (Awulachew et al., 2007; Ayalew, 2018; Woldegebriel et al., 2022). In addition, estimates of the groundwater resource of the country ranges from 12 BCM to 30 BCM (EPCC, 2015). And the country has more than 12 wetlands, 4 crates lakes, 9 saline lakes, and 11 fresh lakes. The major lakes have an estimated storage capacity of 70 BCM to 87 BCM of water (Ayalew, 2018; Berhanu et al., 2014; Getaneh et al., 2022). As a country, Ethiopia boasts a wealth of rivers and lakes, forming a diverse aquatic ecosystem. These ecosystems hold significant scientific value and contribute greatly to the nation's economy (Berhanu et al., 2014; Ermias, 2019)

Despite having abundant water and land resources, Ethiopia struggles to fully utilize these rich water resources (Berhanu et al., 2014; Ketema & Dwarakish, 2021a). Limited technical expertise, financial resources, social and environmental concerns, and legal frameworks restrict

development. As a result, the country has been labeled as technical and economical water scarce country (Berhanu et al., 2014; Ketema & Dwarakish, 2021a).

Among the environmental factors, climate and LULC change are significant problems that can heavily impact watershed hydrology (Dibaba et al., 2020b; Teklay et al., 2020). Climate change, in particular, exerts various impacts on humanity. Among these, droughts and floods stand out as primary consequences, significantly impacting people's means of living. In Ethiopia, rising temperatures and alterations in rainfall patterns have led to detrimental outcomes, such as diminishing soil moisture, decreased availability of freshwater, and recurrent occurrences of droughts and floods (Ketema & Dwarakish, 2021a).

Moreover, the adverse effects of drought and unpredictable rainfall patterns have severely impeded agricultural progress and access to clean water for rural communities in Sub-Saharan African nations, particularly Ethiopia. This is exacerbated by the country's heavy reliance on subsistence farming, which is highly susceptible to LULC and climate change and variability (Berihun et al., 2019; Jilo et al., 2019; Serdeczny et al., 2017; Temam et al., 2019). As a result, changes in LULC and climate variability have a direct impact on food production and other economic activities. Additionally, both climate and LULC changes are significant factors that can influence flow regimes and water resource availability (Wang et al., 2013).

Various studies in various parts of Ethiopia have shown that Ethiopia's water resources are highly sensitive to climate and land use land cover change (Chimdessa et al., 2019; Dibaba et al., 2020b; Gedefaw et al., 2023; Kuma et al., 2023; Mengistu et al., 2023; Mitiku et al., 2023; Teklay et al., 2020; Tesfaw et al., 2023; Woldesenbet et al., 2018). For instance, a study by Kuma et al. (2023) in southern Ethiopia showed that Land use land cover changes resulted in an increase in actual evapotranspiration, potential evapotranspiration, surface runoff, and water leaving the root zone by 201.71 mm/year, 593.85 mm/year, 514.86 mm/year, and 962.02 mm/year, respectively. Another study in the Awash River basin by Mitiku et al. (2023) found that climate change results in changes of up to 100.5% and 77.5% in the wet season and annual river flow, respectively.

Land use and climate change are intricately linked, and their effects significantly impact the hydrologic characteristics. These changes may intensify the water cycle, potentially leading to

water scarcity and uneven distribution. This has serious consequences in water resource development sectors such as for water supply for cities and rural areas, irrigation, and hydropower (Megersa et al., 2019). Quantifying these impacts is vital for addressing future water challenges in domestic, agricultural, industrial, and hydropower sectors. Ultimately, such knowledge is crucial for planning, managing, and protecting our water resources and environment.

The Genale Dawa, one of Ethiopia's largest river basins, currently underutilized its surface water. Water currently supplies major towns and some irrigation projects, with minimal competition between users (MoWE, 2007b). However, future scenarios predict a rise in water demand due to population growth, land-use changes, and potential development projects like irrigation and hydropower (MoWE, 2007b). This will shift the situation, water will become a scarce resource, and competition will likely arise. Dry periods could exacerbate this situation, with upstream users potentially impacting downstream supplies.

Therefore, understanding and predicting how water systems, climate change, and land use interact is crucial scientific research and a major challenge. Climate and land-use changes, along with their impacts on water resources, have been a major focus area in recent years (Chakilu & Moges, 2017). Integrating various climate, land use and hydrologic models can lead to the development of better water resource management plans, climate change adaptation strategies, and water resource development projects. A systematic, high-resolution assessment of water availability across the basin is crucial for strategic decision-making. To successfully manage water and restore the environment, a comprehensive understanding of the basin's hydrological processes is essential. This necessitates the use of geospatial analysis tools and mathematical models to study these processes and responses.

Furthermore, understanding the hydrological characteristics is essential for managing the interaction between human and natural systems in the Ethiopia river basin. It's also a cornerstone of the country's economic and social development. Therefore, understanding the impacts of climate change, land-use alterations, current and future water potential and demand on the basin's water resources is critical for designing effective adaptation, mitigation, and management strategies.

1.2. Statement of Problems

For sustainable water management, a basin's total water resources and their seasonal variations must be thoroughly understood. Accurate assessment of this potential is fundamental for designing long-term, sustainable water management systems. Without a clear grasp of available water, planning and development projects risk failure, ultimately hindering the ability to meet diverse water needs within the basin (Loucks & van Beek, 2017).

A major challenge for integrated water resource management in most Ethiopian river basins are the lack of accurate and up-to-date information on surface water availability, water needs for different purposes, future water demand projections, unfair water allocation, and how supply and demand interact within river basins (Dinsa & Nurhusein, 2023). To address these limitations, Ethiopia's water resource policy aims to improve data collection and promote efficient, equitable, and sustainable water use for social and economic development (MoWE, 2007b). This policy encourages utilizing the potential of the country's river basins and developing stronger water management strategies. One example of this approach is the development of a master plan for integrated water resource development in the Genale-Dawa basin (MoWE, 2007b).

The Genale Dawa, Ethiopia's third largest river basin (by area), after Wabi Shebelle and Abbay, has the potential to satisfy the water demands of existing and proposed projects. This includes agriculture, hydropower, industry, and water supply. However, very little of this potential has been developed (MoWE, 2007b). The lack of in-depth studies on LULC, climate change impacts, surface water potential, and water demand assessment using updated information and suitable methods is a major reason for this underdevelopment. Additionally, there's a gap in implementing clear, a more effective, and dynamic approach to managing the basin's watershed.

Hence, understanding how climate change affects water resources is crucial for scientists and policymakers to develop effective water management plans and mitigate negative impacts (Touseef et al., 2021). This includes assessing how the river basin responds to climate shifts, land-use changes, and water demands. Sustainable water allocation and conflict prevention rely on understanding these dynamics (Zhang et al., 2007). Therefore, ongoing research on catchment processes, climate, and land-use changes is essential. Scientific studies that explore the interactions between climate change, land-use changes, and their effects on water availability and demand are

necessary for effective water management in the face of future uncertainties. Complex hydrological models are valuable tools for such exploration (Dibaba et al., 2020b; Knutti, 2008). Ultimately, water resource management and hydrological modeling are inherently linked to understanding the spatial processes of the water cycle.

Therefore, a comprehensive understanding of the Genale River basin's water resource characteristics is essential. This can be achieved by assessing the full potential of both water and land resources, alongside predicting future water demand scenarios. Determining water resource availability within the basin is critical for developing long-term solutions to water quality and quantity issues. Before implementing management strategies, a thorough analysis of the current and future water resource situation is necessary to avoid environmental harm and resolve potential user conflicts (Xu & Singh, 2004).

The report on the Genale Dawa master plan (MoWE, 2007b) indicated that the basin's water resources are under threat due to increasing population, new infrastructure, large-scale hydropower development (such as Genale Dawa III Hydroelectric Power Plant (GD3)), and global warming. To address these threats, it's crucial to investigate how changes in LULC, climate change, and various water demand scenarios will affect the basin's water potential. Therefore, assessing the basin's surface water resources and predicting water demands under different development plans are fundamental steps for achieving sustainable water management.

In this study, the surface water resource potential and water demand of the river basin under the impact of climate and LUCC change was investigated by analyzing outputs from GCM models using the SWAT and WEAP models. This work aims to improve our understanding of how water flows in the basin and how vulnerable the water system is to land use and climate changes in the upper Genale River basin with a view to provide information for developing strategies to adapt to and lessen the negative effects of these changes in the entire river basin.

Unlike other studies on the basin (Abebe et al., 2024; Alemayehu & Kabite Wedajo, 2023; Eshete et al., 2024; Mengistu et al., 2022; Negewo & Sarma, 2021), this research examines several aspects crucial for integrated water resource management. For example, the study by Alemayehu and Kabite Wedajo (2023) explores the variations in climate and vegetation, along with their spatial and temporal relationships, to support effective drought monitoring, flood risk assessment, and

agricultural planning. Eshete et al. (2024) analyzed the hydrological effects of LULC changes in the Welmel watershed from 1990 to 2020, and projected the impact of these changes on hydrological conditions in 2050. Similarly, Negewo and Sarma (2021) used the Soil Water Assessment Tool (SWAT) model to evaluate the water yield and water balance components in the Genale Watershed under future climate change scenarios, to better understand the status of water resources.

In contrast, this study tackles crucial aspects such as estimating surface water potential, analyzing the impacts of LULC changes and climate change on water resources, and forecasting future water demands across various sectors, including large-scale projects. Furthermore, it investigates the potential impacts of these large-scale projects on future water supply and demand, and explores the relationship between these factors to inform the development of a more integrated water management system for the basin.

1.3. Objectives

The main objective of this dissertation was to investigate the hydrologic responses and surface water availability due to land use land cover dynamics and climate change in the Genale Dawa river basin, Ethiopia.

The specific objectives were to:

- Investigate the historical rainfall and temperature characteristics in the basin.
- Evaluate the impact of land use land cover change on special and temporal variation of streamflow in the basin.
- Evaluate the impact of climate change on spacial and temporal variation of streamflow availability in the basin.
- Evaluate the streamflow availability and demand due to the current and future development plan in the basin.

1.4. Research Questions

The research questions that the study strived to answer include:

- How does the rainfall and temperature of the basin be characterized?
- What are the dominant hydrological processes in the basin?
- How climate and land use land cover change affect the hydrological processes and water availability in the basin?
- How well can the surface water potential of the Genale River basin satisfy future water resource development and demand changes under various climate and socio-economic scenarios?

1.5. Significance of the Study

Numerous researchers emphasize the necessity of evaluating surface water to effectively plan and sustainably manage water resources globally. Challenges persist in water resource utilization due to alterations in the hydro-geo-morphological attributes of basins. The Ministry of Water and Electricity in Ethiopia, a governmental body tasked with overseeing the nation's water and energy development, aims to contribute significantly to Ethiopia's socio-economic advancement by sustainably developing and managing its water and energy resources. It is evident that changes in hydro-geo-morphology significantly impact the surface water potential of the Genale River basin.

This research addresses a critical aspect of sustainable water management by analyzing the upper Genale River basin's water resources. It employs relevant techniques and models to estimate surface water potential and predict major water demands under the influence of climate change and LULC changes. These findings contribute to the development of a dynamic and integrated water resource management plan for the basin.

In addition, analyzing water potential and demand under LULC and climate change scenarios in the upper Genale River basin offers valuable information at the catchment scale. These insights can then be used to develop appropriate adaptation and mitigation strategies or sustainable water management. Furthermore, the study's findings can assist local governments in implementing watershed management plans, and promote regional socio-economic development through effective land-use planning and climate change adaptation. Additionally, the study's findings can

aid in planning future water resource development projects. Ultimately, the research aims to reduce ecological hazards linked to climate change and improve understanding of the basin's water resource vulnerability. These findings also provide a strong foundation for further research in the Genale River basin.

1.6. Scope and Limitations of the Study

This research offers a comprehensive analysis of how climate change, land-use alterations, and water resources interact within Ethiopia's Upper Genale River Basin. It delves into historical rainfall and temperature trends to understand their impact on agricultural water management practices. Furthermore, the study investigates how changes in LULC affect water flow patterns within the basin. A crucial aspect of the research is assessing the potential impacts of future climate change on water availability. This includes exploring the feasibility of developing water resource systems to meet future demands and analyzing future water demand scenarios to inform decision-making. By investigating these various elements, the research aims to provide valuable insights on the vulnerability of the hydrological process and water resource systems to land-use land cover dynamics and climate change. Ultimately, the goal is to develop adaptation and mitigation strategies for sustainable water resource management in the Upper Genale River Basin.

While the research offers valuable insights, it acknowledges certain limitations. The projections of future climate scenarios and the downscaling models used introduce a degree of uncertainty that can potentially affect the analysis results. Additionally, data collected from meteorological and streamflow stations may have inherent drawbacks due to missing data points, outliers, and potential observation errors. Furthermore, climate models used to drive hydrological simulations often have inherent uncertainties in their projections, which can propagate through the modeling process and lead to uncertain predictions of future hydrological responses. The study also acknowledges potential limitations in the accuracy of socioeconomic data collected from regional sources. Political instability, the presence of informal armed groups, security issues, and the inaccessibility of some areas due to transportation challenges have further limited the ability to conduct frequent visits. Lastly, budgetary or financial constraints may have restricted the scope of the research and data collection processes.

1.7. Overall Research Framework

The water resource potentials and demand in relation to climate and land use change in the Genale River basin were analyzed using the SWAT and WEAP models. Historical climatic characteristics, land use and land cover change dynamics, and future climate models were used to assess the impacts on the water potential and demand of the study basin. Future daily climate data for four GCM-RCM combinations were obtained from CORDEX-Africa projections under two Representative Concentration Pathways (RCP 4.5 and RCP 8.5). Accordingly, the study's scope is divided into four major themes. The investigation examines long-term changes in annual and seasonal rainfall and temperature for agricultural water management, the impact of land use and land cover change on hydrological variables, the future impact of climate change on hydrology and water resources, and the surface water potential and demand of the upper Genale River basin using hydrological models. The general framework for the research is shown on Figure 1-1.

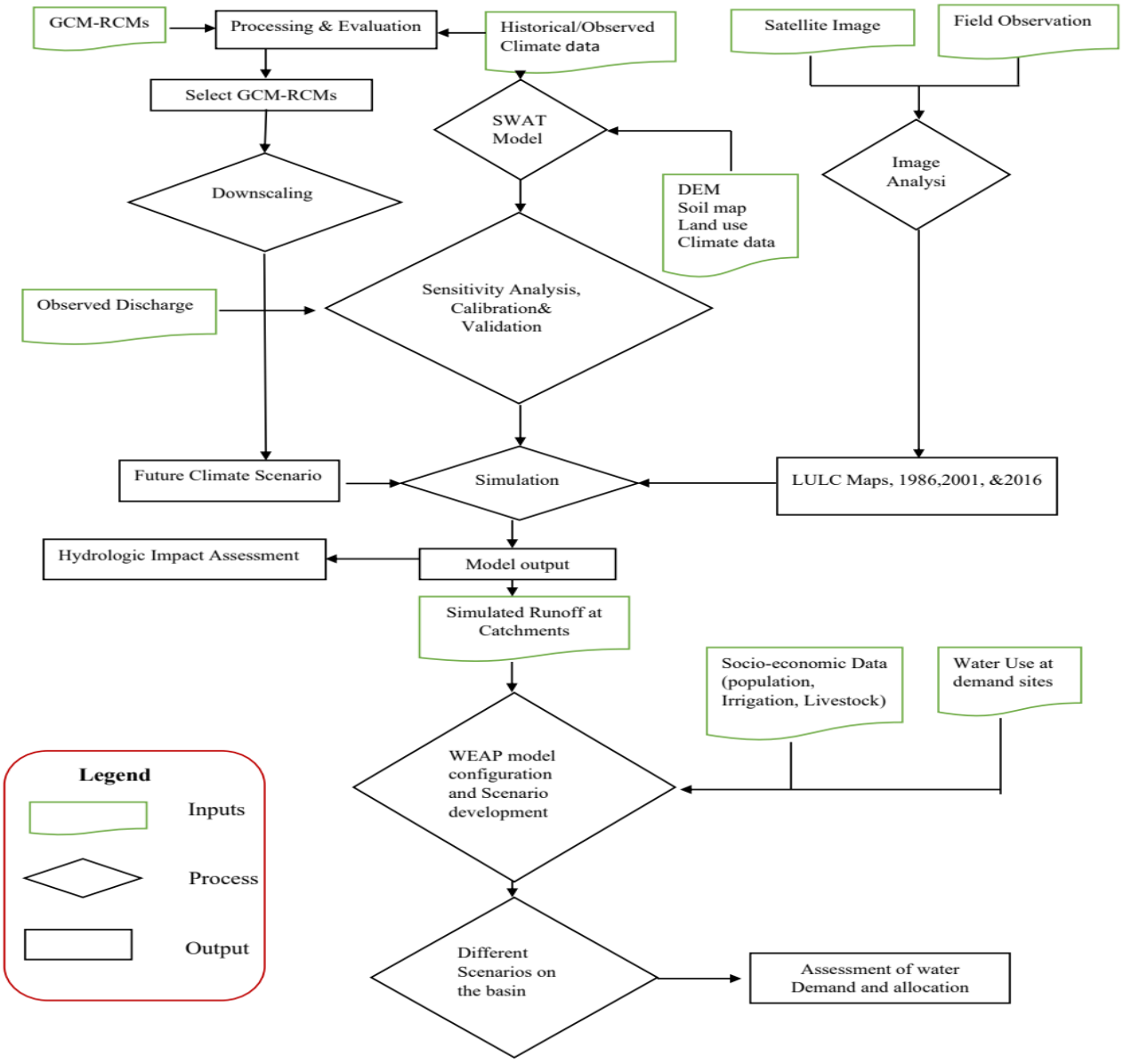

Figure 1-1. General methodological flowchart for the research

1.8. Dissertation Organization

This thesis is organized in eight chapters. Each chapter is set in such a way that it is addressing one topic and can standalone. The first chapter introduces the subject matter of the research and provides the problem statement and objective of the dissertation. Chapter two contains a review of pertinent literature. Chapter three deals with analysis of rainfall and temperature variability for agricultural water management of the study basin. In chapter four, land use land cover change

detection and analyses along with its impact on hydrological processes are discussed. Chapter five explain the impact of climate change on hydrological characteristics. While demand and allocation of water resource analysis is covered in Chapter six, Chapter seven provides the summary of the dissertation work.

CHAPTER TWO:

2. LITERATURE REVIEW

2.1. Overview and Assessment of Water Availability

Life on Earth depends entirely on water – it's essential for humans, animals, and plants (Babel et al., 2005; Pedro-Monzonís et al., 2015). Beyond survival, water underpins everything from health and sanitation to food production, energy generation, and recreation. However, urbanization, growing population, and increased industrial activity threaten this vital resource, leading to competition and potential conflict (Babel et al., 2005; Insan & Kuntiyawichai, 2022). Environmental degradation like deforestation and climate change, coupled with inadequate water management in some regions, further exacerbates the challenges, leaving people and industries vulnerable to water scarcity (Papa et al., 2023).

Ethiopia's geographical location, combined with its favorable climate, leads to a greater volume of rainfall within the country. This rainfall serves as the primary replenishment for its water resources, which are essential for agriculture, hydropower generation, and socioeconomic development. The average annual precipitation varies across the country, ranging from 141 mm in the arid eastern and northeastern regions to as much as 2,275 mm in the southwest highlands; this potential makes the country Africa's water tower.

Ethiopia's water resources can be divided into two main categories: blue water, which includes surface and groundwater, and green water, which is the moisture in the soil that plants use. Blue water encompasses the total flow of water in streams, including surface runoff, subsurface flow, and shallow groundwater flow, as well as deep aquifer recharge and water storage in lakes, ponds, and wetlands (Serur, 2020). Ethiopia is home to numerous river systems, lakes and reservoirs. In general, the country has 12 river basins: eight are river basins, three are dry basins with no outflow in the drainage system, and one is a lake basin (Berhanu et al., 2014). Estimates suggest an annual surface runoff of approximately 122 BCM and a groundwater resource ranging from 12 BCM to 30 BCM derived from these basins (Awulachew et al., 2007, 2010; Ayalew, 2018; Berhanu et al., 2014; EPCC, 2015). Green water refers to the portion of rainfall that infiltrates and stored in the soil and utilized by plants(Teferi et al., 2020). It is a key resource for rain-fed agriculture, which

accounts for the vast majority of Ethiopia's agricultural activities. Given that more than 80% of Ethiopia’s population depends on agriculture for their livelihoods, green water plays a crucial role in food security and rural development (Teferi et al., 2020).

The Genale Dawa river basin, one of Ethiopia's largest alongside the Wabi Shebelle and Abbay river basins, is a transboundary water system. It stretches over 172,889 square kilometers and drains into the Indian Ocean through Somalia's deserts. Its primary drainage network consists of the Genale, Dawa, and Weyb rivers, along with their sub-basins. Annually, the entire basin yields approximately 6.6 billion cubic meters of runoff. Of this total, the Genale sub-basin contributes around 70%, amounting to 4.6 billion cubic meters or an average annual runoff of 80 millimeters (MoWE, 2007b).

Despite Ethiopia's abundant water resources, a significant portion of the country struggles with inconsistent access and uneven water distribution across space and time (Awulachew et al., 2010). This limits development for water supply, irrigation, hydropower, and other uses. Consequently, populations remain vulnerable to water scarcity and climate variability, unable to fully benefit from the land and water resources.

Developing the water sector is hindered by natural factors, technical limitations, institutional weaknesses, and financial constraints (Ayalew, 2018). Ethiopia's diverse climate, geography, and water resources require a comprehensive knowledge base. Unfortunately, organized information on the country's water resources is scarce or unavailable. Existing data is scattered, and detailed studies at the necessary scale and depth are lacking (Berhanu et al., 2014).

Recently, numerous studies have been conducted to determine the water resource potential and generate detailed information that is important for water resource development (Alemayehu et al., 2010; Awulachew et al., 2007; Berhanu et al., 2014; Dananto et al., 2022; Kemal & Adeba, 2021; Negasa Jaleta et al., 2019). To accurately assess a basin's water potential, these studies first determine the total amount of water available within the system. This requires a comprehensive understanding of the basin's hydrologic system, and a clear picture of water flow entering and exiting the basin.

Several factors influence the amount of water available in a river basin for various users. These include the total water flow, water quality, legal frameworks, economic considerations, and

regulations governing water use. The key concept is that water demand and supply are inherently connected - a basin's capacity limits the total amount of water that can be withdrawn sustainably. While complete fulfillment of all user demands might not be possible, management strategies can minimize water losses and achieve a more balanced relationship between supply and demand. Unfortunately, poor management is common in developing countries' river basins, leading to economic and social losses for water users in those regions (Weragala, 2010). This emphasizes the critical importance of understanding how water resources fluctuate in response to environmental changes, allowing for more scientific management, utilization, and assessment of these vital resources (Qin et al., 2020).

Understanding how much water a catchment holds is vital. This allows us to estimate the usable amount, ultimately driving economic growth through efficient water management for essential purposes like drinking water, irrigation, and hydropower generation (Kemal & Adeba, 2021). Understanding how water flows within the catchment is equally important for economic development. For this reason, having tools to measure the water entering the catchment is crucial. These measurements help us determine how much water is stored and how much is lost.

Hydrologic models are recognized as the most effective tools for predicting water availability and how water will be distributed under different demands and operating conditions (Guug et al., 2020). Many hydrologic models have been developed and used worldwide to assess water resources, potential water availability, water demand, and how water availability changes over time in response to environmental shifts. For example, the SWAT and WEAP models are popular choices for water resource assessments in various regions of Ethiopia (Adgolign et al., 2016; Hussen et al., 2018).

2.2. Water Demand

Water is vital for survival; therefore, all sectors must have sufficient water for use. It would be inappropriate to give each sector the same amount of water because they have different water needs. When estimating demands for these sectors, it is important to take into account the fact that some uses are impacted by variations in the monthly or seasonal water demand. Water demand is referred to as the amount of water required by users to meet their needs. It is frequently considered

synonymous with water consumption, despite the fact that the two terms do not have the same conceptual meaning.

The rising population and urbanization, coupled with industrialization and increased irrigation, are placing a growing strain on resources. To effectively manage these demands and ensure sustainable development, it is essential to develop the necessary knowledge and skills to address river basin demands without compromising socio-economic progress (Genjebo et al., 2023).

The report on the Genale Dawa River Basin's integrated water resources master plan highlights the basin's importance in supporting various ecosystems and livelihoods. The distribution of water resources among different activities and stakeholders is determined by their specific water needs. These needs vary depending on the watershed and time period being considered. Factors such as water productivity, affordability, and type of use (consumptive or non-consumptive) also influence water demand (MoWE, 2007b).

The annual water demand per unit of area (m3/ha) or person/capita, as well as the monthly variations, are used to calculate the water demand per site (Shumet & Mengistu, 2016). Water demands in a basin are classified into five categories: domestic, irrigation, livestock, and industrial water demand, as well as environmental and instream flow requirements (Cai & Rosegrant, 2002).

2.2.1. Water demand for domestic and livestock use

Water is a vital resource for humans and livestock, crucial for health maintenance, agricultural support, and overall well-being. The growing population, intensified agriculture, and climate change have highlighted the need to study water demand in the domestic and livestock sectors as a key aspect of water resource management (de Fraiture & Wichelns, 2010).

2.2.1.1. Domestic water demand

Domestic water demand refers to the amount of water required for daily household activities, such as drinking, cooking, bathing, washing, and sanitation. Numerous factors influence the level of domestic water demand, including population size, socioeconomic status, cultural practices, climate, and household technology.

Domestic water demand typically ranges from 20 to 100 liters per capita per day (LPCD), depending on regional factors (Howard et al., 2020). In developed nations may have higher consumption rates, often exceeding 100 LPCD due to lifestyle factors and infrastructure availability. Conversely, developing countries, per capita water consumption is often lower due to limited access to piped water and sanitation services. In Ethiopia, the national GTP-2 plan outlined the country's water needs. This plan set new water supply standards, allocating 25 LPCD for rural areas and 40-100 liters for urban areas (NPC, 2016).

Water demand for the current population is estimated by multiplying the current population by the per capita water consumption rate, which is typically expressed in liters per capita per day (lpcd) (Vijayan et al., 2022). For future demand, future population is forecasted using demographic models, and the projected per capita consumption rate is used to estimate future water needs. The total water demand is calculated by multiplying the population by the per capita water demand, following the formula (Kifle Arsiso et al., 2017; Vijayan et al., 2022):

$$P_n = P_i(1 + G_r)^n \quad (1)$$

Where P_n is population after n years, P_i initial population, G_r is Growth rate in percentage, and n is years.

This calculation is essential for planning water supply infrastructure and ensuring sufficient water resources to meet the needs of a growing population.

2.2.1.2. Livestock water demand

Water demand for livestock varies by type of livestock species, climatic conditions, and management practices. Cattle, for example, typically consume between 25 and 60 liters of water per day, sheep and goats consume between 5 and 15 liters per day, poultry consume 0.2 and 0.4 liters per bird per day (Adeba et al., 2015; Sileshi et al., 2003; Vijayan et al., 2022). Water is also required for cleaning barns, washing equipment, and feed processing, contributing to overall livestock water use. The total water consumption by livestock in the basin is estimated by multiplying the average daily water requirement per animal by the total livestock population.

2.2.2. Irrigation water demand

Agriculture is an important sector in Ethiopia, supporting food security and the economy. It plays a significant role in the country's economy (Shigute et al., 2023). Irrigated agriculture is especially important because it is typically two to three times as productive as rain-fed farming. Irrigation benefits the national economy in several ways. On a smaller scale, it increases crop yield per hectare, resulting in higher income, more consumption, and better food security. Furthermore, irrigation enables small farmers to diversify their crops and transition from low-value subsistence farming to higher-value, market-oriented production, lowering the risk of crop failure caused by droughts (Hagosa et al., 2009).

To effectively manage water resources, the amount of water used for irrigation must be precisely measured. Many farmers apply too much water because they believe their fields are dry or require additional water. This can cause waterlogged soil and nutrient loss. On the other hand, using too little water can damage crops and reduce yields. Thus, calculating the appropriate amount of water for crops is critical. CropWat software estimates crop water requirements using a scientific method known as the FAO Penman-Monteith equation. This method uses weather information to determine how much water crops require, allowing farmers to use water more efficiently.

To calculate the reference evapotranspiration (ETo) shown in equation 2, FAO Panman-Monteith method (Allen et al., 1998) is used.

$$ETo = \frac{0.408\Delta(R_n - G) + \gamma * \frac{900}{T + 273} * U_2(e_a - e_d)}{[\Delta + \gamma(1 + 0.34U_2)]} \quad (2)$$

Where ETo = reference crop evapotranspiration (mm/day), Rn = net radiation at crop surface (MJ/m^2.day), G = soil heat flux (MJ/m^2.day), T = average temperature (°C), U2 = wind speed measured at 2m height (m/s), $e_a - e_d$ = vapor pressure deficit (kpa), Δ = Slope vapor pressure curve (KPa/°C), γ = Psychometric constant (KPa/°C), 900 = conversion factor.

Calculation of crop water requirements (ETc) using CROPWAT model over the growing season determined from ETo using equation 3:

$$ETc = Kc * ETo \quad (3)$$

Where ETc = Crop water requirement, Kc = Crop coefficient, ETo = reference evapotranspiration.

Irrigation water demand depends on factors like crop type, acreage, growing cycles, evapotranspiration, and effective precipitation. It varies annually with rainfall—decreasing during wet years and increasing in dry years. Methods to estimate this demand include empirical formulas, flow measurements, or field assessments, though field measurements are complex and costly. Typically, empirical formulas are used, requiring data on crop evapotranspiration, soil type, rainfall, and irrigation efficiency to provide accurate estimates of water needs (Allen et al., 1998).

2.2.3. Commercial and institutional water demand

Commercial and institutional (C&I) water demand, which includes industries, public facilities, and businesses plays an important role in urban water management. In Ethiopia, where rapid urbanization and economic growth are occurring, understanding and forecasting C&I water demand is critical for long-term water resource planning. Metal, textile industries, chemicals, pharmaceuticals, paper, and liquor, all rely heavily on water during the manufacturing process. However, gathering data on industrial water consumption is difficult because many industries use private water sources that are not registered with municipalities. In Ethiopia, the city's water supply and sewerage agency estimates that industrial water use accounts for approximately 5 -10% of total daily domestic water demand (Adeba et al., 2015).

2.2.4. Hydropower demand

To assess hydropower water demand, the Water Year Index Method (WYIM) and Spill Demand Method (SDM) are frequently employed. The WYIM focuses on energy demand and is used to simulate historical reservoir releases to hydropower plants, relying on past data to approximate operational rules. In contrast, the SDM is based on water demand rather than energy demand and aims to model operators' efforts to minimize spills, which typically represent lost revenue. Energy demand is explicitly modeled (WYIM) for powerhouses that receive water directly from large reservoirs, while the SDM is applied to all reservoirs (Engdaw, 2016).

The SDM requires that any excess inflow, beyond current demands, be directed toward hydropower generation. This ensures that hydropower plants make the most use of water that

cannot be stored and would otherwise be released as spill (Rheinheimer, 2011). Hydropower will only be generated for flows up to the maximum turbine flow. “Tail water Elevation defines the working water head on the turbine. The power generated in a given month depends on the head available, which is computed as the drop from the reservoir elevation to the tail water elevation. The Plant Factor specifies the percentage of each month that the plant is running. The plant Generating Efficiency defines the generator's overall operation effectiveness in converting the energy of the falling water into electricity” (Sieber & Purkey, 2015).

In WEAP, hydropower facilities are modeled using a reservoir element, incorporating data such as storage capacity, conservation levels, and inactive storage volume to define the usable water for power generation. Monthly evaporation losses are accounted for, while the maximum turbine flow and plant factor dictate the water withdrawal rate for energy production. Additionally, information on tailwater elevation and full supply levels helps set operational rules for the reservoir, guiding water releases and power generation. By simulating inflows and outflows based on these parameters, WEAP estimates the water demand required to meet the facility’s targeted average annual energy output (Sieber & Purkey, 2015).

2.2.5. Environmental flow water demand

Environmental flow requirements refer to the minimum streamflow necessary to sustain the riverine ecosystem and support downstream socio-economic activities. As a result, determining these flows is inherently a multidisciplinary task (Pastor et al., 2014). In many countries around the world, the environment is now being recognized as a legitimate water user. As a result, it has become necessary to estimate the water requirements needed to sustain environmental needs (Bianucci et al., 2024).

Decisions regarding the allocation of water for environmental purposes are ultimately made by society and are somewhat subjective. Reserve flow, which is intended to meet both basic human needs and ecological demands, can be estimated through thorough analyses of river discharge patterns and the corresponding biological or ecological responses (Richter et al. 2003; Acreman and Dunbar 2004).

The amount of water allocated to the environment will inevitably fall short of what the ecosystem ideally needs, which is the natural, undisturbed flow of a river. As a result, society must balance the potential costs and benefits to both the environment and other water users when deciding how much water to allocate to the environment. In making these decisions, society accepts some degree of alteration to the natural environment. This accepted level of modification can vary from one river to another and is often categorized by "ecological management classes."

An environmental instream flow can serve various purposes. Although the concept appears straightforward, accurately determining environmental flow (EF) values can be challenging. This difficulty mainly stems from a limited understanding and lack of quantitative data on how river flows interact with different aspects of river ecology. Depending on the priority of its demand, a flow requirement may be met before, after, or simultaneously with other uses of the river (Sieber & Purkey, 2015).

There is a range of methods available for assessing Instream flow requirements:

- ✓ Simple hydrological indices;
- ✓ Hydrological simulations;
- ✓ Consensus and discussion based approaches;
- ✓ Historical data analysis;
- ✓ Biological response simulation techniques often referred to as habitat simulation methods

Hydrological index methods represent the most straightforward approach to assessing environmental flows, requiring minimal data and primarily using historical hydrological records to guide flow recommendations. These records typically consist of long-term, historical daily or monthly discharge data.

In flow duration curve analysis, historical flow records—whether naturalized or representing present-day conditions—are evaluated over specific periods to generate curves that depict the relationship between discharge levels and the percentage of time each is met or surpassed. For this river basin, assuming a relatively low reserve flow threshold at 95% exceedance to account for environmental considerations, the concept of low-flow analysis is applied. To sustain the ecological functions and preserve the natural channel habitat tied to the river's historical flow

patterns, a reserve flow must be maintained, potentially classifying it as an independent sectoral demand (Verma et al., 2017).

The limitation of the Q95% approach lies in its ineffectiveness for rivers with natural catchment conditions, where flow variations are generally minimal. This causes the Q95% value to be high, often nearing Q80% or the average discharge level. To address this issue, the Tennant Method (Shaeri Karimi et al., 2012) can be utilized. In this method, the maintenance flow is calculated as a percentage of the river's average discharge, with a minimum threshold set at 10%. To account for seasonal variations, this 10% value is adjusted for each month throughout the year (Hatmoko et al., 2020).

2.3. Land Use and Land Cover Changes in Ethiopia

LULC changes refer to the modification and/or transformation of various land uses based on how humans utilize the land (Guida-Johnson & Zuleta, 2013). These changes are a significant aspect of global environmental change and have a profound impact on ecosystem processes and services (Shiferaw et al., 2019). In Ethiopia, LULC change has become a major concern in recent years. The country's rapidly growing population places increasing pressure on land resources, further accelerating the pace of LULC change (Minta et al., 2018; Sisay et al., 2021).

Many developing nations, including Ethiopia, experience a fast-growing population. This pressure on land leads to changes in how land is used (LULC changes). One way this happens is deforestation to create more farmland. Studies show that Ethiopia faces significant LULC changes, mainly involving the conversion of natural areas to farms and settlements (Aredo et al., 2021; Negese, 2021; Kindu et al., 2013). These changes happen quickly and vary depending on location. In fact, many studies have been conducted in recent years to track these LULC changes across different parts of Ethiopia (Alemu et al., 2015; Ayele et al., 2019; Dibaba et al., 2020a; Hailemariam et al., 2016; Hailu et al., 2020; Hassen & Assen, 2018; Kibret et al., 2016; Kindu et al., 2013; Mathewos et al., 2019; Minta et al., 2018; Woldeyohannes et al., 2018; Yesuph & Dagnew, 2019).

The studies revealed significant variation in the extent, direction, and pattern of land use and cover change across different locations. Minta et al. (2018) showed that over the study time, the central Ethiopian highlands have seen a significant decline in forests, pastureland, and woodlands due to the expansion of cultivated land, settlements, and plantations. A study in Finchaa Catchment, Northwestern Ethiopia by Dibaba et al. (2020) reported in the last 30 years, commercial agriculture, cultivated land, water bodies, and settlement areas have increased. On the other hand, forests, rangelands, pastures, and wetlands have all shrunk. Study by Mathewos et al. (2019) in southern Ethiopia indicated that the area of built-up and cultivated land significantly increased by 53.2% and 67.4%, respectively, while grass and shrub land and forest areas decreased by 18.4 % and 66.4%, respectively, between 1972 and 2017. All of these researches underscored that LULC change has an impact on water resources, biodiversity, forestlands and local livelihoods, among others. These changes are largely driven by the need for more farmland and by a growing population (Hailemariam et al, 2016; Berihun et al., 2019; Fasika et al., 2019; Bufebo & Elias, 2021).

While analyzing LULC changes has been a global research priority for decades (Lambin et al., 2003; Temesgen et al., 2021), studies in Ethiopia started much later (Minta et al., 2018) and focused mainly on the Northern highlands. This neglect extends to the Southern highlands (Babiso et al., 2016), particularly the upper Genale watershed, where LULC change detection remains understudied. This lack of data hinders the development of effective land management plans for the region, which are crucial for the success of ongoing and future development projects in the Genale Dawa basins.

Hence, understanding LULC is critical for various reasons. Information on land cover types and their optimal uses is essential for selecting land for development, planning its use sustainably, and managing resources effectively (Tewabe & Fentahun, 2020). Additionally, studying LULC changes provides crucial insights for land use planners, decision-makers, and communities. This knowledge help them to create efficient and appropriate policies and strategies for land management, generate data for comprehensive land use plans, and ultimately realize the causes of environmental changes within a basin. In short, LULC analysis empowers decision-makers to

ensure sustainable development and navigate the complexities of a changing environment (Berihun et al., 2019).

2.4. Climate Change

Earth's climate made up of five key parts: the land surface, the hydrosphere, the biosphere, the cryosphere, and the atmosphere. The atmosphere is the most rapidly changing and unstable component of the system (IPCC., 2014). Climate can be described as the weather conditions for a particular place, such as precipitation, air temperature, wind, humidity, cloud cover, sunshine, and atmospheric pressure, determined over a duration of at least 30 years. (Ibe & Amikuzuno, 2019; Tripathi et al., 2016). Any changes in these phenomena over several years are known as climate change (Tripathi et al., 2016). Climate change can happen naturally, like from volcanic eruptions or changes in the sun's activity. But human actions, like altering land use or adding greenhouse gases to the air, are now the main culprits (IPCC., 2014). Throughout history, Earth's climate has constantly changed due to both natural and human influences. However, human activity is the leading driver of climate change today (IPCC., 2014).

Water availability on Earth is primarily controlled by three main climate factors: temperature, precipitation, and how much water evaporates. Evaporation itself depends on temperature, sunlight reaching the ground, wind speed, and air humidity. When climate change alters surface temperatures, it sets off a chain reaction. These changes can disrupt the natural water cycle, impacting how much water is available for households, farms, and industries. Research overwhelmingly suggests that climate change will significantly alter global water patterns and availability (Kiparsky et al., 2014). To mitigate these negative effects, policymakers and researchers need to understand the link between climate and water resources, and implement effective water management strategies. This understanding is supported by numerous studies demonstrating the connection between changes in streamflow, precipitation, and temperature (Touseef et al., 2020, 2021).

2.5. Climate Change in Ethiopia

Ethiopia faces a significant development obstacle due to climate change. Rising temperatures, altered rainfall patterns (both amount and distribution), and more frequent droughts and floods are

all signs of a changing climate. These impacts are expected to be widespread, affecting all social groups, economic sectors, and ecological regions. Agriculture, heavily reliant on predictable rainfall, is particularly vulnerable (Bewket et al., 2015).

The past study has demonstrated that the country's water resources are extremely vulnerable to changes in climate and variability (Bewket et al., 2015; Ketema & Dwarakish, 2021a; Taye et al., 2018). Research indicates that because of their geographical locations, climatic characteristics, and economic circumstances, developing countries like Ethiopia will be more susceptible to climate change. The National Meteorological Service Agency of Ethiopia reports that since 1950, the country's average annual maximum temperature has seen a rise of approximately 0.1 °C every ten years. Similarly, the average annual minimum temperature has also been on an upward trend, increasing by around 0.25 °C per decade during the same timeframe (NMA, 2007). Since the beginning of the 20th century, Ethiopia has experienced a rise in its average temperature by approximately 1 degree Celsius. It is anticipated that this trend of warming will persist, with a projected increase in the average temperature by an additional 2-3 degrees Celsius by the end of the 21st century (World Bank, 2017). Precipitation patterns in Ethiopia are also being influenced by climate change. Droughts are becoming more intense and frequent, and heavy rains are becoming more common. These alterations in precipitation patterns are anticipated to continue, resulting in more extreme weather events (Bewket et al., 2015). The NMA. (2007) reports showed that Ethiopia's annual rainfall has exhibited significant variability in recent years, despite the overall average remaining relatively constant. Climate change's most significant impact is on water availability. A warmer climate will speed up the hydrological cycle, varying the amount and timing of both rainfall and runoff (Ketema & Dwarakish, 2021a).

In Ethiopia, many studies on the effects of climate change on water resources have been conducted. For example (Bekele et al., 2021; Daba & You, 2020; Emiru et al., 2022; Fentaw et al., 2018; Mengistu et al., 2020; Merga et al., 2022; Takele, Gebrie, et al., 2022; Taye et al., 2018; Worqlul et al., 2018), these studies revealed that rainfall across the country is highly variable seasonally and annually. Because of this variability, the country experiences frequent droughts and famines. Furthermore, the findings disclosed that alterations in temperatures and precipitation would have a significant impact on streamflow and surface runoff, potentially reducing total water availability in the subbasin. Hence, understanding the local impact of climate change on watersheds, as well

as quantifying its hydrological effects, is essential for addressing potential water resource management challenges (Shawul et al., 2016).

2.6. Prediction of Climate Change

Scientists use complex computer programs called climate models to understand how Earth's climate system works. These models consider how the atmosphere, land, oceans, and ice interact with each other (IPCC., 2014). The IPCC is the principal international organization that develops these models to assess climate change (IPCC., 2014). Many scholars use different versions of these models, incorporating factors like population growth, economic activity, environmental changes, and industrialization, all of which influence greenhouse gas (GHG) levels. Regional climate models (RCMs) and GCMs are the most widely used types of climate models (Adugna et al., 2021).

GCMs simulate the Earth's climate using mathematical equations that represent the complex interactions and feedbacks between atmospheric, oceanic, and biological processes. For researchers, these models serve as the primary tools for generating reliable climate data at global, hemispheric, and continental scales, aiding in understanding current climate conditions and predicting future scenarios under rising greenhouse gas levels (Trzaska & Schnarr, 2014). RCMs, on the other hand, allowing researchers to focus on specific regions and understand how these global trends will manifest at a more local level (Chokkavarapu & Mandla, 2019).

General Circulation Models, or GCMs, are complex computer programs that factor in the physics of land, atmosphere, ice, and oceans (Hartmann, 2016; Reichle, 2023). GCMs are the most comprehensive tools for simulating the global climate system's response that are currently available. For impact assessment studies IPCC (2014) identified wide ranges of GCM models. Among these, (CNRM-CM5) National Center of Meteorological Research, France, (EC-EARTH) EC-EARTH consortium, Netherlands/Ireland, (MIROC5) Atmosphere and Ocean Research Institute University of Tokyo, National Institute for Environmental Studies, and Japan Agency for Marine-Earth Science and Technology, Japan, (MPI-ESM-LR) Max Planck Institute for Meteorology, Germany, (GFDL-ESM2M) NOAA Geophysical Fluid Dynamics Laboratory,

USA, and (CanESM2) Canadian Center for Climate Modeling and Analysis, are the commonly used ones.

Current Global Climate Models (GCMs) rely on a coarse grid system (ranging from 1.25° to 3.75° latitude/longitude) to represent Earth's climate, which creates limitations for impact assessments (Parkinson et al., 2006). This coarse resolution hinders the models' ability to capture crucial details like El Niño events and local weather phenomena driven by smaller-scale processes like clouds, leading to uncertainties in their predictions (Mendez et al., 2020; Worku et al., 2020).

To address these limitations, scientists use two main downscaling techniques: dynamical and statistical. Dynamical downscaling involves nesting high-resolution models within GCMs. Statistical downscaling establishes relationships between large-scale atmospheric patterns and regional climate. Both techniques aim to bridge the gap between global climate predictions and what's happening on a more regional level (Fowler et al., 2007).

2.6.1. Dynamic downscaling

Dynamic downscaling, first established by Dickinson et al. (1989), uses regional climate models (RCMs) to translate broad-scale climate patterns from general circulation models (GCMs) into more detailed local climate projections. By integrating finer grids (down to 10-20 km or less) within the coarser GCM framework, this method provides high-resolution data that accurately reflects spatial correlations and relationships between climate variables. Although initially limited by high computational demands, advancements in computing have made dynamic downscaling increasingly viable for long-term and multi-scenario climate studies.

The core idea behind dynamic downscaling is that while GCMs are effective at simulating global climate responses to large-scale influences like greenhouse gas emissions, RCMs are specifically designed to refine these projections by incorporating regional characteristics such as topography, land cover, and coastlines. This approach enhances the spatial and temporal accuracy of climate models, making it particularly useful for analyzing localized phenomena and their impacts on the environment (Giorgi et al., 2001).

Despite these benefits, RCMs can be highly sensitive to initial conditions, which may cause

deviations from the broader GCM results. In addition, systematic errors may arise due to the limited representation of some climate processes, which can be partially corrected through bias adjustment techniques (Keller et al., 2022). Furthermore, dynamic downscaling often involves a one-way data flow, meaning RCMs rely on GCM inputs without feeding refined data back into the larger-scale models. This limitation, along with the potential for reduced accuracy when over-downscaling, necessitates close collaboration between global and regional climate modelers to optimize results (Giorgi et al., 2001).

2.6.2. Statistical down scaling model (SDSM)

Statistical downscaling works by establishing empirical relationships between large-scale atmospheric patterns and local climate conditions based on historical data. Once this relationship is validated, it can be applied to future large-scale atmospheric projections from General Circulation Models (GCMs) to predict local climate characteristics (Keller et al., 2022). The Statistical Downscaling Model (SDSM) serves as a tool to bridge the gap between global climate simulations and localized climate needs, translating coarse GCM outputs into detailed, location-specific data. This approach allows researchers to generate precise daily climate information, which is essential for studying localized climate change impacts (Gebrechorkos et al., 2019).

Statistical downscaling is also computationally less demanding than dynamical methods like Regional Climate Models (RCMs), which rely on complex simulations of physical processes. As a result, statistical methods are often a practical alternative for institutions with limited computational resources or expertise. Unlike RCMs, which typically provide downscaled data over spatial scales of 20–50 kilometers, statistical techniques can deliver climate information at the station level, offering finer spatial resolution. SDSM is one of several statistical techniques used in climate change research, alongside methods like weather typing, stochastic weather generators, and regression analysis (Fowler et al., 2007; Gebrechorkos et al., 2019; Sunyer et al., 2012).

Table 2-1 below (adapted from Trzaska & Schnarr, 2014) outlines the main advantages and disadvantages of dynamic and statistical downscaling methods, emphasizing the compromises researchers must take into account when choosing a downscaling technique for particular studies.

Table 2-1. Advantages and disadvantages of dynamic and statistical downscaling

	Statistical downscaling	Dynamic downscaling
Requires	➢ Medium/low volume of inputs data ➢ Sufficient amount of good quality observational data ➢ Reliable GCM simulations ➢ Low/medium computational resources	➢ High volume of input data ➢ Reliable GCM simulations ➢ High computational resources and expertise
Advantages	➢ Computationally inexpensive and efficient, which allows for many different emissions scenarios and GCM pairings ➢ Methods range from simple to elaborate and are flexible enough to tailor for specific purposes ➢ The same method can be applied across regions or the entire globe, which facilitates comparisons across different case studies ➢ Relies on the observed climate as a basis for driving future projections ➢ Can provide point-scale climatic variables for GCM-scale output ➢ Tools are freely available and easy to implement and interpret; some methods can capture extreme events	➢ Based on consistent, physical mechanism ➢ Resolves atmospheric and surface processes occurring at sub-GCM grid scale ➢ Not constrained by historical record so that novel scenarios can be simulated ➢ Experiments involving an ensemble of RCMs are becoming available for uncertainty analysis
Disadvantages	➢ High quality observed data may be unavailable for many areas or variables ➢ Assumes that relationships between large and local-scale processes will remain the same in the future (stationarity assumptions) ➢ The simplest methods may only provide projections at a monthly resolution	➢ Computationally intensive ➢ Due to computational demands, RCMs are typically driven by only one or two GMC/emission scenario simulations ➢ Limited number of RCMs available and no model results for many parts of the globe ➢ May require further downscaling and bias correction of RCM outputs ➢ Results depend on RCM assumptions; different RCMs will give different results ➢ Affected by bias of driving GCM

Source (Trzaska & Schnarr, 2014)

2.6.3. Biases Correction

Both global and regional climate models (GCM and RCM) often have systematic errors or biases, such as predicting too many rainy days or underestimating extreme rainfall (Teutschbein & Seibert, 2012). These errors can affect the accuracy of forecasts regarding onset, length of growing season, and cessation timing, seasonal rainfall, or temperature, which may be consistently too high or low. The causes include factors like limited spatial resolution, simplified physics, and incomplete understanding of climate systems. Using uncorrected climate model outputs can lead to unrealistic results in climate impact assessments. To address these biases, various correction methods have been developed (Mendez et al., 2020).

Some of the methods for bias correction include linear scaling (LS), delta-method (DT), power transformation of precipitation (PTR), Local intensity scaling (LOCI) of precipitation, distribution mapping (DM) for precipitation and temperature.

2.6.3.1. Linear scaling (LS)

Linear scaling is a simple and widely-used technique for bias correction, where a correction factor is applied to modeled data by accounting for the difference or ratio between the modeled and observed historical data (Abera & Gebeyehu, 2023; Azman et al., 2022; Galata et al., 2021; Mahmood et al., 2018; Mahmood & Jia, 2017; Takele et al., 2022). The goal of the linear scaling (LS) method is to ensure that the long-term monthly average of the corrected data aligns precisely with that of the observed data. To adjust the RCM simulation for temperature and rainfall, the linear scaling method applies additive factors for temperature and multiplicative factors for rainfall, as represented by the following formula. By design, the corrected simulations from GCM-RCM will perfectly match the observed monthly mean values. The LS method uses monthly correction values derived from the differences between the observed control data and the uncorrected model data (Mendez et al., 2020).

Precipitation is corrected using a multiplicative factor based on the ratio between long-term monthly mean observed and simulated values (Teutschbein & Seibert, 2012).

$$P^*_{contr}(d) = P_{contr}(d) * \left(\frac{l_m(P_{obs}(d))}{l_m(P_{contr}(d))}\right) \quad (4)$$

$$P^*_{scen}(d) = P_{scen}(d) * \left(\frac{l_m(P_{obs}(d))}{l_m(P_{contr}(d))}\right) \quad (5)$$

Temperature is adjusted using an additive term using equations 6 and 7

$$T^*_{contr}(d) = T_{contr}(d) + l_m\big(T_{obs}(d)\big) - l_m(T_{contr}(d)) \quad (6)$$

$$T^*_{scen}(d) = T_{scen}(d) + (l_m\big(T_{obs}(d)\big) - l_m(T_{contr}(d)) \quad (7)$$

Where:

- ✓ $P^*_{contr}(d)$, $P^*_{scen}(d)$ represent the bias-corrected precipitation for the control period (contr) and scenario period (scen), respectively, on a specific day d.
- ✓ $P_{contr}(d)$, $P_{scen}(d)$ represent the raw, uncorrected precipitation from the Regional Climate Model (RCM) for the control and scenario periods, respectively, on a specific day d.
- ✓ $l_m(P_{obs}(d))$ is the long-term monthly mean of observed precipitation on day d in month m.
- ✓ $l_m(P_{contr}(d))$ is the long-term monthly mean of the RCM-simulated precipitation during the control period.
- ✓ $l_m\big(T_{obs}(d)\big)\ abd\ l_m(T_{contr}(d))$ refer to the long-term monthly mean of observed and RCM-simulated temperature, respectively.

2.6.3.2. Delta or change factor (DT)

The delta or change factor method modifies climate scenarios by applying the projected changes (anomalies) from GCM-RCM simulations to observational datasets, rather than directly using the simulations of future conditions. This approach follows a specific formula and involves adjusting future climate data based on the differences (or ratios) between historical observed and modeled data (Teutschbein & Seibert, 2012).

For precipitation:

$$P^*_{scen}(d) = P_{obs}(d) * \left(\frac{l_m(P_{scen}(d))}{l_m(P_{contr}(d))}\right) \quad (8)$$

$$T^*_{scen}(d) = T_{obs}(d) + (l_m\big(T_{scen}(d)\big) - l_m(T_{contr}(d)) \quad (9)$$

Where:

- ✓ $P^{*}_{scen}(d)$ This is the bias-corrected precipitation for the scenario period on a specific day d.
- ✓ $P_{obs}(d)$ This represents the observed precipitation on a specific day d,
- ✓ $l_m(P_{scen}(d))\ and\ l_m(P_{contr}(d))$ represent the long-term monthly means of the RCM-simulated precipitation for the scenario period and control period, respectively.
- ✓ $T^{*}_{scen}(d)$ is the bias-corrected temperature for the scenario period on day d.
- ✓ $T_{obs}(d)$ is the observed temperature on day d.
- ✓ $.l_m\big(T_{scen}(d)\big)\ and\ l_m(T_{contr}(d))$ refer the long-term monthly means of the RCM-simulated temperature for the scenario period and control period, respectively.

2.6.3.3. Power transformation (PT)

Power Transformation (PT) is a method used to adjust precipitation data by applying a mathematical transformation. The PT technique employs exponential equations to modify the standard deviation of rainfall series. In this approach, each daily rainfall value Praw is converted into a corrected value Pcor using the following formula.

$$P_{cor} = P^{b}_{raw} \tag{10}$$

Where: P_{cor} is corrected precipitation, P_{raw} is raw/uncorrected precipitation and b is a parameter identified by matching the coefficient of variation (CV) of the corrected daily RCM precipitation with the CV of observed daily precipitation (Pobs) for each month.

2.6.3.4. Local intensity scaling of precipitation (LOCI)

Local Intensity Scaling (LOCI) for precipitation modifies the intensity and frequency of wet days in Regional Climate Model (RCM) simulations, which tend to overestimate the occurrence of light rainfall (Schmidli et al. 2006). Initially, a rainfall threshold (Ptresh,m) is set based on the daily RCM rainfall data, ensuring the frequency of days exceeding this threshold matches the observed wet day frequency. Then, the scaling factor is determined using Equation 11.

$$S_f = \frac{\mu(P_{obs,m,d}|P_{obs,m,d} > 0)}{\mu(P_{hst,m,d}|P_{hst,m,d} > P_{thres,m})} \tag{11}$$

$$P_{hst,m,d}^{cor} = \begin{cases} P_{hst,m,d} \times S_f P_{hst,m,d} > P_{thres,m} \\ 0 \; if \;\; P_{hst,m,d} < P_{thres,m} \end{cases} \quad (12)$$

2.6.3.5. Distribution mapping (DM)

The Distribution Mapping (DM) method adjusts rainfall and temperature parameters, including the mean, standard deviation, and quintiles. This correction is done by using the distribution of the raw data alongside the adjusted data functions. DM operates on the assumption that the probability distributions of both observed and raw weather variables are identical, which introduces some uncertainty (Teutschbein & Seibert, 2012). For precipitation data, the Gamma distribution, as proposed by Thom (1958), is commonly considered appropriate, characterized by a shape parameter (k) and a scale parameter (θ) (Eq. (13)). In the case of temperature time series, the Gaussian distribution, as suggested by Cramér (1999), with location parameter (μ) and scale parameter (δ) (Eq. (12)), is typically regarded as the best fit.

$$F_{gamma}(P) = \frac{1}{\Gamma(k)} \int_0^p x^{k-1} e^{-x/\theta} dx \quad (13)$$

For temperature time series, the Gaussian distribution:

$$f(T) = \frac{1}{\delta\sqrt{2\pi}} exp\left(-\frac{(T-\mu)^2}{2\delta^2}\right) \quad (14)$$

Where: p is precipitation value, $\Gamma(k)$ is gamma function, T is temperature value, μ is mean temperature of the time series.

2.7. Climate Change Scenarios

2.7.1. Representative concentration pathways (RCPs).

The IPCC's Fifth Assessment Report (AR5) in 2014 introduced four new climate futures, known as RCPs (Representative Concentration Pathways). These RCPs act like roadmaps, outlining different possibilities for how Earth's climate might change depending on the amount of greenhouse gases released in the coming years.

The four RCPs are RCP2.6, RCP4.5, RCP6, and RCP8.5. Each represents a distinct pathway for future emissions, leading to a specific level of heat trapped by the atmosphere (radiative forcing) by the year 2100. The higher the number, the more intense the greenhouse gas concentration and the greater the potential for climate change. For example, RCP8.5 represents a scenario with the most significant greenhouse gas emissions and the most substantial potential warming. The RCPs are named after their 2100 radiative forcing values of 2.6, 4.5, 6.0, and 8.5 watts per square meter (W/m2) (IPCC., 2014).

Global annual GHG emissions (in CO2-equivalents) will peak from 2010 to 2020, followed by a significant decline, as assumed in RCP2.6. RCP 4.5 emissions peak around 2040 and then decline. Around 2080, RCP6.0 emissions peak and then decline, resulting in a continuous rise in emissions throughout the twenty-first century (IPCC., 2014; van Vuuren et al., 2011). The mid- and late-twentieth-century averages and projections are 2046-2065 and 2081-2100, respectively, based on the RCPs for the twenty-first century. van Vuuren et al. (2011) found that the higher the value, the higher the emissions.

2.8. Impacts of Climatic and Land Use and Land Cover Change on Hydrology

Water is an essential part of every element in the Earth's climate system, from the land surface to the atmosphere and even the living things. This close connection means that changes in climate directly impact how water circulates around the globe (hydrological cycle). Global warming, a major concern for the coming century (IPCC., 2014), is a key driver of these changes (Kundzewicz, 2008; Papa et al., 2023).

Shifts in climate, particularly precipitation and temperature, can significantly affect how water behaves on land. For example, these changes can influence surface runoff, evapotranspiration (ET), and streamflow (Kundzewicz, 2008). Rising temperatures and altered radiation balance are tightly linked to these hydrological processes.

Scientists have observed consistent connections between increasing temperatures and changes in various aspects of the hydrological cycle. This includes modifications in the intensity, patterns,

and extremes of rainfall, along with rising evapotranspiration rates, more frequent melting of snow and ice, and alterations in runoff and soil moisture (Sun et al., 2023).

The IPCC warns that Africa is likely to experience more significant warming than the rest of the world by the year 2100 (IPCC, 2014). This warming is expected to have a dramatic impact on water resources across the continent. Water scarcity is already a major challenge in Africa, and climate change is poised to worsen the situation by reducing the availability and quality of freshwater (IPCC., 2014).

According to Papa et al. (2023), this issue has become a top priority for policymakers and scientists concerned with the combined effects of climate change, land use changes, and biodiversity loss. The IPCC (2014) further emphasizes that climate change creates new risks and exacerbates existing ones for both society and the environment. Water scarcity, compounded by natural resource degradation due to climate change, is becoming a major driver of food insecurity, particularly in developing nations across Sub-Saharan Africa (Urama & Ozor, 2010).

In Sub-Saharan Africa, water, fertile land for crops, and grazing land are essential for subsistence agriculture, the backbone of many economies. This makes the region highly sensitive to changes in land use and climate. Droughts in the Horn of Africa, for example, have resulted in severe food insecurity, impacting over 44% of the population according to UNEP (2011). This region is particularly vulnerable because it can experience both floods and droughts within a short timeframe.

Several factors contribute to this vulnerability. Poor water management systems, limited resources, and low-tech practices make it harder for communities to adapt to climate changes (Urama & Ozor, 2010). In Ethiopia, for instance, population growth, unsustainable agricultural practices, and a long history of settlements in the highlands put immense pressure on the land (Alemu, 2015; Dubale, 2002).This pressure has led to widespread deforestation, land degradation, and increased land cultivation over the past century (Berihun et al., 2019; Bishaw, 2001). In a similar way in southern Ethiopia, growing population has been a significant driver of agricultural land expansion in recent years (Mathewos et al., 2019; Woldeyohannes et al., 2018).

Climate change and land use alterations significantly impact water resources in Ethiopia. These changes modify streamflow, surface runoff, and groundwater recharge (Dibaba et al., 2020b). Combined with erratic rainfall patterns, this leads to water scarcity and food shortages, ultimately contributing to poverty and environmental degradation (Hamza & Iyela, 2012).

A major driver of these changes is population growth. As populations increase, people cultivate more land, often abandoning traditional fallow periods that allow the soil to recover According to (Hurni et al.,2005). This intensifies land use and leads to severe soil degradation and increased sediment loss, particularly in the highlands (Bishaw, 2001). Soil erosion not only reduces agricultural productivity but also creates downstream problems by accumulating sediment in reservoirs, shortening their lifespan. Furthermore, the lack of a national water management policy hinders effective water resource development (MoWR, 2001).

Recently, there's been a growing interest regarding how land use and land cover changes unfold over time and space in Ethiopia, particularly how they affect water flow (hydrological characteristics) and soil erosion (Negese, 2021). The degradation of land and water resources is a major concern, especially for rural communities that depend on these resources for their livelihoods. This growing awareness emphasizes the urgent need for proper watershed management strategies (Alemayehu et al., 2009).

Effective water management requires balancing positive and negative impacts on water resources. Understanding the environmental challenges caused by land-use changes is crucial for managing watersheds effectively. Research combined on hydrological modeling along with LULC and climate change, which are major drivers of water scarcity and degradation, plays a vital role in achieving sustainable water management practices (Mango et al., 2011; Mitiku et al., 2023).

2.9. Overview of the Hydrological Model

A model serves as a refined depiction of a real-world system, comprising a defined set of logical operations embedded within a computer program (Wheater, 2008). Specifically, a watershed model is an amalgamation of algorithms utilizing climatic data and watershed attributes to replicate natural land-based processes like hydrology and pollutant movement over a specified duration.

The purpose for which the model is developed determines its framework and design. Due to its capability to simulate in-stream phenomena, a watershed model serves as a valuable tool for establishing a measurable connection between external influences and in-stream reactions (Wolde, 2017).

Watershed hydrologic models are designed to help us understand and predict the water cycle in a watershed, and to assess how it may be affected by changes in the watershed itself or in the climate. They can also be used to generate simulated hydrologic data for specific purposes, such as designing water facilities or forecasting floods. They also provide useful data for researching the potential effects of changes in climate and/or land use (C. Xu, 2002).

Now a day, because of the sophistication of technological advances in computers, hydrological models now differ greatly in their computing abilities and the requirements of input data to the model (Devries & Hromadka, 1993). Hydrological models are essential tools for understanding and predicting the water cycle in a catchment, and for assessing how it may be affected by changes in land use, land cover, and climate. However, it is important to choose the right model for the job, taking into account the complexity of the scenarios that need to be simulated (Lund et al., 2010).

Currently, many hydrologic models are used to assess the effects of land use and climate change on water resources (Johnston & Smakhtin, 2014; Singh, 2018). Among these models, rainfall-runoff models have been particularly valuable for water resource management in catchments. These models play a significant part in the most effective management and planning of the water resources in catchments (Leitzke & Adamatti, 2021).

However, using rainfall-runoff models effectively can be challenging. A major hurdle is the limited availability of data, particularly regarding the spatial distribution of rainfall across the catchment area. Since precipitation is the primary input for any hydrologic model, this lack of data can be problematic. Additionally, reliable streamflow data is crucial for calibrating and validating the model's parameters. Without this data, it's difficult to ensure the model's accuracy (Chiew et al., 2018).

Watershed modeling approaches are classified into three types based on the algorithms they employ: physically-based, conceptual, or empirical. Empirical models are the most basic type of

model, and they use mathematical functions to approximate or fit available data (Daniel et al., 2011). Models can be classified as stochastic or deterministic, depending on the techniques used in the modeling process. In stochastic models, the inputs are denoted by statistical distributions resulting in a variety of outputs, while in deterministic models, outcomes are found by means of known associations between events and states (Abdulkareem et al., 2018). Models can be divided into lumped, semi-distributed, and distributed categories based on their spatial distribution. While the watershed's spatial variability of hydrologic processes and boundary conditions is taken into account by semi-distributed and distributed models, the lumped modeling approach treats the entire watershed as a single unit for computations and averages its parameters and variables (Pechlivanidis et al., 2011). Watershed models can also be divided into two types: continuous models and event-based. The former produces continuous output, whereas the latter produces output only during specific time periods (Devia et al., 2015).

Understanding how water systems will respond to climate change caused by CO2 emissions is crucial. This knowledge is essential for developing effective strategies to adapt to and mitigate these changes, ensuring sustainable water management for agriculture in the long term (Wodaje et al., 2021). A lot of research has been carried out to examine long-term hydrologic variability influenced by climate change (Awotwi et al., 2021; Bekele et al., 2019; Birkinshaw et al., 2017; Eisner et al., 2017; Lotfirad et al., 202; Näschen et al., 2019; Takele et al., 2022; Worku et al., 2021; Zhang et al., 2018). Hydrologic models, coupled with climate scenarios derived from GCMs, are used to predict the effects of climate change on water resources (Merga et al., 2022).

Effectively managing and planning water resources requires a deep understanding of how watersheds respond to changes in climate and land use (Mitiku et al., 2023). This involves analyzing the movement of water within a watershed. Key factors influencing water flow include rainfall, runoff, and infiltration, all of which are impacted by the watershed's topography, natural climate patterns, and climate change. To adapt water resource planning to these changing conditions, we use watershed runoff models that can simulate water flow under various climate change scenarios (Wolde, 2017).

However, due to a lack of high spatiotemporal observational data in a watershed, studies frequently depend on hydrologic models to predict and understand basin hydrologic characteristic (Sridhar &

Nayak, 2010). Over time, a number of operational, conceptual or lumped, watershed models have been created. The soil water assessment tool (SWAT), the Hydrologiska Byrns Vattenbalansavdelning (HBV), the hydrologic modeling system (HEC-HMS) model, the artificial neural network (ANN), the European Hydrological System Model (MIKE-SHE), the water resource allocation and simulation model (WAS), the MODSIM, and the Cooperative Water Allocation Mode are just a few of the models used today to model water resources among physically-based, empirical, and conceptual (Aredo et al., 2021; Berhe et al., 2013; Birhanu et al., 2019; Bizuneh et al., 2021; Dibaba et al., 2020b; Gedefaw et al., 2019; Goshime et al., 2021; Takele et al., 2022; Tassew et al., 2019; Teklay et al., 2020; Tufa & Sime, 2020; Wang et al., 2008; Yan et al., 2017; Yan et al., 2018; Zelelew & Melesse, 2018).

2.9.1. Soil and Water Assessment Tool (SWAT)

The SWAT model, created by the USDA's Agricultural Research Services, is a user-friendly tool specifically designed for watersheds [areas that drain into a body of water]. Unlike some models, SWAT doesn't require a lot of hard-to-find data to get started, making it accessible for many users (Neitsch et al., 2011). It excels at simulating how water runoff and nutrients flow over long periods, particularly in rural areas dominated by agriculture (Arnold et al., 1998; Arnold & Fohrer, 2005).

This powerful model operates on a daily basis and combines physical principles with data distributed throughout the watershed (Arnold et al., 2012). The tool functions primarily as a strategic planning resource. It can estimate the impact of changes in land use and agricultural practices on water flow in watersheds with varying characteristics over extended periods (soil types, land use, management). It also has a variety of other applications such as sediment and nutrient flow simulation (Arnold et al., 1998; Taylor et al., 2016).

SWAT has the advantage of being able to be combined with GIS in ArcSWAT and ArcGIS (Shukla & Gedam, 2018). It incorporates features from several ARS models and is a direct descendant of the SWRRB (Simulator for Water Resources in Rural Basins) model (Arnold & Williams, 1987). The CREAMS model (Knisel, 1980), the GLEAMS model (Leonard et al., 1987), and the EPIC model (Izaurralde et al., 2006), which initially known as the Erosion Productivity Impact Calculator (Williams, 1990), all made significant contributions to the development of SWAT.

SWAT's effectiveness in simulating hydrological processes around the world is well-documented in scientific research (Marahatta et al., 2021; Nasiri et al., 2020; Takele et al., 2022; Touseef et al., 2021; Zhang et al.,2007). Additionally, the SWAT literature database at http://swatmodel.tamu.edu offers easy access to current research on the model.

Researchers have found the SWAT model to be a valuable tool for a variety of applications in watersheds. These include accurately simulating streamflow in watersheds of various sizes (Khoi & Thom, 2015; Nasiri et al., 2020; Roba et al., 2021; Tufa & Sime, 2020), assessing how land-use changes affect a watershed's annual water balance and seasonal flow patterns (Awotwi et al., 2019; Kuma et al., 2023; Tesfaw et al., 2023), and even predicting potential impacts of climate change on water resources (Chaemiso et al., 2016; Insan & Kuntiyawichai, 2022; Kankam-Yeboah et al., 2013; Näschen et al., 2019). This global research confirms SWAT's effectiveness in simulating catchment flows and highlights the vulnerability of catchments to climate change and land-use alterations.

The SWAT model has proven successful in simulating hydrological processes across various Ethiopian watersheds. Studies have applied SWAT in the Awash (Bekele et al., 2019; Daba & You, 2020; Mitiku et al., 2023), Blue Nile Basin (Chakilu & Moges, 2017; Kemal & Adeba, 2021; Mengistu et al., 2020; Woldesenbet et al., 2018), Baro Akobo river basin (Mengistu et al., 2023; Zantet oybitet et al., 2023), Wabi Shebelle basin (Fita & Abate, 2022; Roba et al., 2021), Omo Gibi basin (Chaemiso et al., 2016; Orkodjo et al., 2022), Genale Dawa river basin (Messele & Moti, 2019; Negewo & Sarma, 2021; Shigute et al., 2022). These studies successfully modeled hydrological processes, sediment yield, and water balance, demonstrating the model's effectiveness in Ethiopia.

SWAT simulates a watershed's hydrology in two stages: the land phase and the routing phase. The former controls the amount of water, nutrients, sediment, and pesticides that enter each subbasin's main channel and simulates surface runoff, infiltration, canopy storage, evapotranspiration, lateral flow, and return flow, whereas the latter is the movement of water, chemicals, and sediments to the outlet via the watershed channel network (Neitsch et al., 2011).

The SWAT model's hydrological components are governed by the water balance components as shown in equation 15, (Neitsch et al., 2011).

$$SW_t = SW_o + \sum \left(R_{day} - Q_{surf} - E_a - W_{seep} - Q_{gw}\right) \quad (15)$$

where SW_t is the soil water content (mm), SW_0 is the initial soil water content on day i (mm), t is time (days), R_{day} is the amount of precipitation on day I (mm), Q_{surf} is the amount of surface runoff on day i (mm), E_a is the amount of evapotranspiration onday i (mm), W_{seep} is the amount of water entering the vadose zone from the soil profile on day i (mm), and Q_{gw} is the amount of return flow on day i (mm).

The water balance of each HRU has four storage volumes: snow, soil profile (0–2 m), shallow aquifer (2–20 m), and deep aquifer (>20 m). The surface runoff is estimated using the SCS curve numbers or the Green and Ampt infiltration formula (Neitsch et al., 2011). The SCS curve number equation is stated by Equation 16 (Arnold & Fohrer, 2005).

$$Rsurf = \frac{(Pday - 0.2S)^2}{(Pday + 0.8S)} \quad (16)$$

Where, R_{surf} is depth of daily accumulated runoff (mm), S is a retention parameter, and Pday is the daily rainfall depth (mm). The above equation indicates that surface runoff in a watershed occurs when the value of the depth of rainfall in a day (Pday) is greater than 0.2S.

In terms of curve number (CN), the parameters S is computed by equation 17. The parameter S is affected by slope, types of soil, and land use management practices.

$$\frac{S}{25.4} = \left(\frac{1000}{CN} - 10\right) \quad (17)$$

According to Arnold et al. (2012), CN is significant parameter which determines the surface runoff of the catchment during the model calibration.

Channel flood routing is estimated using the Muskingum method (Zhang et al., 2007). Potential evaporation is estimated using Hargreaves, Priestly-Taylor or Penman-Monteith formulas and percolation is modelled with a layer storage routing method combined with a crack flow model (Arnold et al., 1998).

2.9.2. Water Evaluation and Planning (WEAP) model

WEAP is a computer-based, a practical semi-theoretical, semi-distributed, and deterministic tool that assists water resource planners in making decisions about how to manage a basin's water resources. It considers both the supply of water (for example, from rivers and lakes) and the demand for water (for agriculture, industry, and drinking). WEAP also takes into account water quality and ecosystem needs. This comprehensive approach is critical because it allows for more sustainable water management (Touseef et al., 2021). The model simulates water operations using water accounting principles. Users can define the time step, which is usually a month. The model can be used to assess the impacts of various water policies, such as conservation programs, changes in water demand, or new infrastructure projects (SEI, 2015; Yates et al., 2005). The WEAP model is developed by the Stockholm Environment Institute (SEI) in Boston and the model offers a comprehensive way to analyze how water systems behave when affected by development projects (SEI, 2015).

This model incorporates two interacting components (Yates et al., 2005). One component simulates natural water processes like evaporation, runoff, and infiltration, allowing researchers to assess water availability within a watershed. The other component simulates human activities that affect these natural systems, such as water use for consumption or other purposes. This allows us to evaluate the impact of human water use on the overall water resources.

Numerous nations face difficulties in managing and developing their water resources. Policymakers are currently concerned about the allocation of scarce water resources, quantity of water, watershed protection of water, as well as suitable policies for efficient water utilization and management. The WEAP model employs an integrated technique to simulate both natural and engineering aspects like groundwater discharge, reservoirs, and water supply and demand. WEAP can provide water planners with a more comprehensive picture of the many factors that must be considered when managing water resources for current and future uses (Tena et al., 2019).

The model essentially performs a mass balance of flow sequentially down a river system, making allowance for abstractions and inflows (using equation 18).

$$Q_s = Q_i - Q_0 - Q_l \quad (18)$$

where Q_s, Q_i, Q_o, and Q_{sl} stand for the actual water supply at each demand point, the node's overall water intake, output, and loss, respectively.

The system is usually set up to simulate a recent baseline year, for which the water availability and demands can be accurately predicted. The impact of various development and management options is then evaluated by simulating alternative scenarios (i.e., potential futures based on what-if statements). As a result, WEAP is viewed as an integrated water management tool for assessing water use and allocation with a stronger emphasis on balancing supply and demand quickly and transparently.

Several studies have reported effective applications of the WEAP model in managing water resources in different regions. For instance, in the Tributary Basin of Tonle Sap Lake, Cambodia, the WEAP model has been applied to integrated demand and supply modeling under the impacts of climate change as well as management options (Touch et al., 2020). In Ziway Meki Sub Basin, Ethiopia, the WEAP model was used to estimate water demand by taking into account the current state of development and anticipated future development of water resources through scenario analysis (Shumet & Mengistu, 2016). In Ethiopia, the WEAP model was used to simulate subbasin hydrology in the Central Rift Valley basin (Goshime et al., 2021).

In general, the WEAP model is a helpful tool for managing and planning water resources. It offers a comprehensive, adaptable, and simple framework for analyzing environmental and water policy. The model has been successfully used to simulate water demand, subbasin hydrology, and manage water resources in various regions.

CHAPTER THREE:

3. ANALYSIS OF RAINFALL AND TEMPERATURE VARIABILITY FOR AGRICULTURAL WATER MANAGEMENT IN THE UPPER GENALE RIVER BASIN, ETHIOPIA

Abstract

A better understanding of climate-induced changes and support for adaptation strategies requires understanding the spatiotemporal dynamics of climatic variables. This study aims to assess long-term changes in annual and seasonal rainfall and temperature for agricultural water management in the upper Genale river basin, Ethiopia. To achieve this objective, long-term climate data from 13 stations between 1975 and 2018, as well as maximum and minimum temperatures for six stations were collected from the Ethiopian National Meteorological Service Agency (NMA). The characteristics of rainfall (onset, cessation, length of growing season, and crop water requirement) were assessed using the Coefficient of Variation (CV), Standard Rainfall Anomaly (SRA), and Precipitation Concentration Index (PCI). Additionally, the Mann–Kendall test and Sen's slope estimator were used to assess the trend and magnitude of changes in rainfall and temperature. The annual, winter, spring, summer and autumn CVs were 20%, 89%, 30%, 45%, and 32%, respectively. The standardized anomalies of annual and seasonal rainfall for the climate stations indicated that the basin had a drier season than a wet season. The mean length of the growing season in Belg and Kiremt ranged from 43 to 79 days and 38 to 170 days, respectively. On an annual, summer, and autumn season basis, most rainfall stations showed a non-significant trend. In contrast, in the spring season, rainfall showed a decreasing but statistically insignificant trend in all stations except Bensadaye, Bore, Telamokentise, and Yirba Muda stations. According to the analysis of the crop water requirements in the studied basin, supplemental irrigation is essential to reducing yield reduction and crop failure during spring and autumn. In these seasons, maize and sorghum varieties required supplementary irrigation up to 202 mm and 252 mm, respectively. Annual and seasonal maximum and minimum temperatures showed an increasing trend at all the stations except Hagre Selam station. Generally, there was a spatially and temporally variable trend in rainfall while the temperature trend was increasing irrespective of the temporal and spatial factors. Thus, this study contributes to a better understanding of climate change in the basin and these findings can be used in planning for adaptation measures against a changing climate.

Keywords: Upper Genale river basin, Rainfall and Temperature Trend, Rainfall variability, Mann-Kendall trend test.

3.1. Introduction

Climate change is dominating discussion on international agenda because of its impacts on global environmental change. Even though climate change is a global issue, smallholder subsistence farmers who rely on rainfed agriculture, cultivate marginal areas, and have limited adaptive capacity are severely affected (Harvey et al., 2018; Tripathi & Mishra, 2016). Similarly, due to high vulnerability and inadequate adaptive capacity of socio-economic systems, Africa is one of the most at risk continent to climate change impacts (IPCC., 2014). More specifically, studies (Chapman et al., 2020; Stuch et al., 2020) showed that sub-Saharan Africa is severely affected by climate change and variability. This is due to their livelihood dependence on climate sensitive rain-fed agricultural activities and livestock production (Ibe & Amikuzuno, 2019). Among climate variables, precipitation and temperature are the two principal variables in the field of climatology and hydrology that enables our understanding of climate change and key hydrological metrics, including the frequency, magnitude and variability in extreme events, at different spatial and temporal scales (Beyene, 2016).

The projected temperature trend for Africa is expected to rise more faster than in other land areas (IPCC, 2014). As a result, by the end of the 21st century, Africa could be several degrees warmer than the global average, with temperatures rising 3–4 °C. Similarly, a rapid temperature increase has also been reported in Ethiopia. A study conducted by Suryabhagavan (2017) has revealed that the minimum and the mean surface temperature has shown increasing trend over Ethiopia. Other region-specific case studies(e.g., Belay et al., 2021) like in Southern Ethiopia, confirmed significant increasing trends for mean maximum and minimum temperature. As with temperature, rainfall is also rapidly changing in its characteristics. These characteristics include, spatiotemporal irregularities in precipitation patterns and variability in its onset, increased frequency and intensity of large storms etc. are the common ones (Ibe & Amikuzuno, 2019).

A review by Gezie (2019) and Zewdie (2014) showed that climate change in the form of increased rainfall variability, change in rainfall amount and distribution, higher temperature, and change in climatic variability and extreme events reduces food production especially to susceptible smallholder subsistence farmers in Sub Saharan African countries where there are no well-established technological and institutional capacity to cope with climate change (Zewdie, 2014).

Report on NMA (2007) and Gezie (2019) showed that, developing countries in general and least developed countries like Ethiopia, in particular, are more vulnerable to the adverse impacts of climate variability and change. This vulnerability mainly arises from its high levels of poverty, low level of adaptive capacity, and a higher dependence on climate sensitive natural resources base for livelihood (Alemayehu & Bewket, 2016; Alemu & Mengistu, 2019; EPCC, 2015; NMA, 2007).

Agriculture is a major contributor to Ethiopia's economy. About 43% of Gross Domestic Product (GDP) and, 96% of rural employment earnings come from this sector, and it accounts for 90% of export earnings as well (Biru et al., 2020). Although agriculture contribute significantly to Ethiopia's overall economy, the sector is challenged by climatic, institutional, and edaphic factors, of which climate related impact such as climate extremes and variability in seasonal rainfall amount and distributions are the major ones (Suryabhagavan, 2017). For instance, in Lake Tana basin, rainfall is one of the most significant climatic variables that impact on natural environment and agricultural production (Weldegerima et al., 2018). In a country like Ethiopia, whose economy is largely dependent on rain-fed agriculture, precipitation patterns and temperature analysis have paramount importance for adaptation to future climate change and to cope with impacts on agricultural production and ecosystem services (Asfaw et al., 2018; Miheretu, 2020; Wagesho et al., 2013). Evaluating long-term trend and variability of rainfall and temperature in Ethiopia is crucial to understand how the climate has changed there over recent decades (Mengistu et al., 2014). To achieve this, a rigorous statistical analysis examining the spatial and temporal dynamics of these climate variables is essential. This comprehensive approach allows for a thorough assessment of climate-related changes, ultimately leading to the recommendation of appropriate adaptation measures (Asfaw et al., 2018).

The non-parametric MK test and Sen's slope estimator have been used in Ethiopia to study climatic variability and trend analysis at different spatial and temporal scales (Ademe et al., 2020; Asfaw et al., 2018; Suryabhagavan, 2017; Wagesho et al., 2013). Recently, a study conducted by Suryabhagavan (2017) found that rainfall in Ethiopia showed high variability over the study period. Due to change in altitude, there was also a significant variation in annual rainfall and temperature was observed. Wagesho et al. (2013) had also conducted a study on the spatial and temporal variability of annual and seasonal rainfall over Ethiopia. The trend analysis revealed that annual rainfall was increasing in the eastern parts. In contrast, *Kiremt* and annual rainfall decreased

in the country's north, northwest, and west. A study on North central Ethiopia by Asfaw et al.(2018) showed a statistically significant declining trend of annual and *Kiremt* rainfall. For the case of temperature, an increasing trend was observed. Another study in the Great Rift valley basin by Ademe et al. (2020) showed non-significant trends in annual precipitation at most of the stations.

Even though various trend and climatic variability analysis studies have been conducted at different parts of Ethiopia, detailed scientific studies on spatiotemporal rainfall and temperature variability for agricultural water management and trend detection have not been conducted over the study area. In addition, most trend analysis studies conducted in Ethiopia to date have not been conclusive, which requires additional investigation (Asfaw et al., 2018). Moreover, previous studies examining rainfall and temperature impacts on agricultural activities have focused on their annual amounts and distributions. However, seasonal reliability is more important for agricultural activities than annual reliability. Therefore, this study was mainly designed to explore annual and seasonal rainfall and temperature variability for agricultural water management and trend over the study basin of the upper Genale river basin. The basin encompasses varying topographic and climatic regimes. The main river, the Genale, is a multi-purpose river that has been used for a variety of water-related projects, and additionally, the federal government of Ethiopia has designed huge development plans to develop the water resources of the river basin (MoWE, 2007c). Hence, knowledge of climate variability, trend and characteristics of the growing season in a river basin is essential to plan possible climate change adaptation and mitigation measures. In addition, the output of this study may be utilized to design and implement effective water resources development and management in the area. Therefore, this study was conducted with the objectives to analyze the spatial and temporal characteristics of rainfall and temperature for agricultural water management, and to analyze the variability and trend in the upper Genale river basin, Ethiopia.

3.2. Materials and Methods

3.2.1. Description of the study area

The Genale Dawa river basin lies in the southern part of Ethiopia, covering parts of Southern Nations, Nationalities, and Peoples', Somali, and Oromia regional states. Geographically located between 3°30' and 7°20' North latitude and 37°05' and 43°20' East longitude. The basin covers an

area of about 172,713 km^2 (Awulachew et al., 2007; MoWE, 2007c). Specifically, the upper Genale Sub-River basin (study area) is located between 6° 52’ and 5°20’ North latitude and 38°30' and 39°45' East longitude and lies in the upper central area of the basin. It has a basin area of about 10,582.19 km^2 (Figure 3-1). Due to the north-south oscillation of the Inter-Tropical Convergence Zone (ITCZ) and effects of topography, the basin experiences bimodal type I (three season type) and bimodal type II (double wet and dry seasons) annual rainfall cycle in northern (highland) and southeastern (lowland) parts, respectively. The northern and highland area characterized by the three wet seasons types, March–May (locally known as *Belg*), June–September (locally known as *Kiremt*) and September–November (locally known as *Meher*) (MoWE, 2007c). The southern and the southeastern parts of the study area experienced by double wet season, the first runs from March to May and the second from September to November (Degefu et al., 2021; MoWE, 2007). The mean total annual rainfall ranges from 1617.7 mm to 591 mm. The mean annual minimum and maximum temperatures range between 18.9 to 27.7^{o}C and 6.9 to 16.2 ^{o}C, respectively (Shigute et al., 2022). The altitude of the study basin varies from 901 m to 3751 m. The topography comprises a great diversity with uneven, rugged mountain, low lands and flood plains, deep river valleys and gorges. Traditionally, the study area has four climatic zones, such as Wurch with an altitude >3000 m, Dega with an altitude range of 2500 m – 3000 m, Woina Dega with an altitude of 1500 m – 2500 m, and Kola with an altitude of less than 1500 m. According to Koppen's classification system, the study area has warm temperate climate (in the north and Sidamo mountains), tropical climate (in the lower central area), and hot arid climate (in the lower and southern parts) (MoWE, 2007c).

Pastoralism and mixed farming (crop cultivation and livestock rearing) are the dominant livelihood systems in the lowland and highland parts of the area, respectively. Maize, wheat, sorghum and barley are widely grown crop in the Basin (MoWE, 2007g). Coffee in the southcentral highlands particularly in Sidamo is an important cash crop grown in the region (Degefu et al., 2021a).

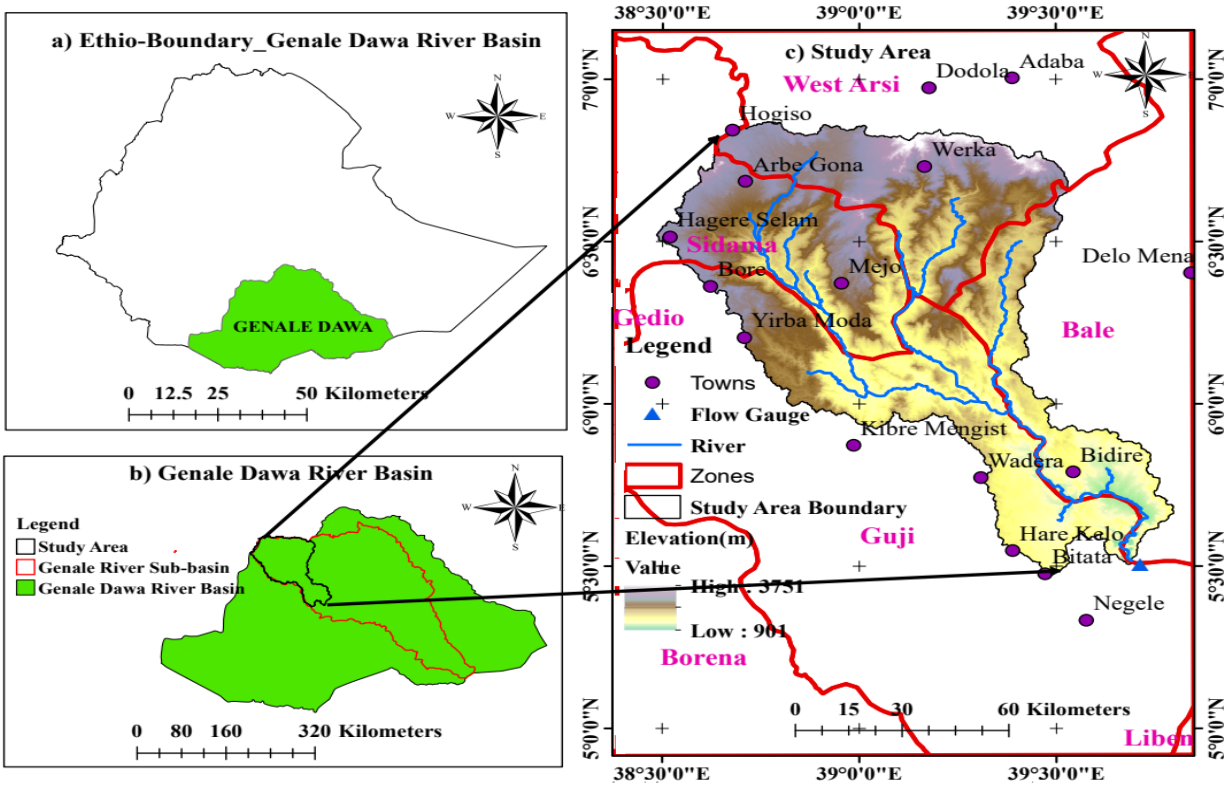

Figure 3-1. Location of the study area

3.2.2. Research design and data source

The upper Genale river basin was purposefully chosen as the study watershed due to the diversity of climate conditions, varying topographic nature, and diversity of farming systems. Despite the fact that the natural resources in the study area have the potential to ensure the community's livelihood, they have been underutilized for agricultural development and other purposes (MoWE, 2007c).This is due to a lack of comprehensive scientific research on climate and other related fields, as well as agricultural development.

For this study, a long-term climatic data was used to analyze and quantify rainfall and temperature variability and trends. Daily rainfall data for thirteen stations and maximum and minimum temperature data for six stations within and around the study area were collected from the Ethiopian National Meteorological Service Agency (NMA) (Table 3-1). Data from three locations (Arbegona, Bidere and Harokelo) were extracted from the Enhancing National Climate Services (ENACTS) dataset. Details of the ENACT dataset are presented at (Dinku et al., 2014, 2016). The

missing values were generated and filled by multiple imputations using Fully Conditional Specification (FCS) implemented by the MICE (Multivariate Imputation by Chained Equations) algorithm as described in van Buuren & Groothuis-Oudshoorn (2011). Then, to summarize the daily data into annual, monthly, and seasonal totals and to analyse the variability and trend, XlSTAT, R-INSTAT and R software were used. The XlSTAT 2018 software was used to test the homogeneity of rainfall data. This software was also used to summarize the daily temperature (minimum and maximum) and rainfall data in to annual, monthly and seasonal totals. The INSTAT was used to calculate the start and end dates of the growing season as well as the length of the growing season. To analyze the trend, SRA, and PCI, R software were used.

Table 3-1. List of meteorological stations in the study river basin and their data points

Stations	Latitude	Longitude	Altitude	Rainfall	Temperature
	(N°)	(E°)	(m)	Period	Periods
Arbegona	6°40'48"	38°43'30"	2600	1983-2016	1983-2016
Bensadaye	6°31'35"	38°49'35"	1914	1998-2018	1998-2018
Bore	6°20'30"	38°38'29"	2712	1982-2018	
Bidere	5°46'19"	39°36'46"	1400	1983-2016	1983-2016
Dolo Mena	6°26'1"	39°41'21"	1330	1987-2017	
Hager Selam	6°30'47"	38°31'18"	2809	1975-2018	1984-2017
Harokelo	5°33'19"	39°23'17"	1600	1983-2016	1983-2016
Kibre Mengist	5°53'46"	38°58'1"	1680	1975-2018	
Kofele	7°2'52"	39°35'43"	2620	1987-2017	
Neghele	5°26'1"	39°35'43"	1544	1982-2017	1982-2017
Telamokentise	6°50'1"	38°30'38"	1911	1990-2018	
Woreka	6°30'6"	39°12'45"	2450	1987-2018	
Yirba Muda	6°13'17"	39°35'43"	2560	1987-2018	

3.2.3. Data quality

To control the quality of the dataset, outlier detection and homogeneity tests were conducted. The Tunky fency method as described by Ngongondo et al. (2011). Potential outliers in the weather data were identified using Inter Quartile Range (IQR), which uses median and the lower and upper quartile (25th and 75^{th} percentile) to create fences to identify extreme values in the tails of distribution. Lower fence is Quartile1–1.5×(IQR) and upper fence Quartile3+1.5×(IQR) were used to identify outliers in the data.

To evaluate the homogeneity of the annual precipitation data series, four statistical absolute homogeneity tests, such as the standard normal homogeneity test (SNHT) (Alexandersson, 1986), the Buishand range test (Buishand, 1982), the Pettitt test (Pettitt, 1979), and the Von Neumann ratio test (von Neumann, 1941), were applied. Kang & Yusof (2012) have described and elaborated these tests.

For all these four tests, the computed P values for observed data were compared with the critical values at 95% level of confidence. If the computed P values exceeds the critical values, the data series is considered as homogenous (the data are independent with similar distribution). If the critical value exceeds the test statistic, the data series considered as inhomogeneous (the data have a break in the mean). Under the alternative hypothesis, the VNR test cannot detect the year break because it assumes that the series is not randomly distributed (Chang et al., 2017).

Table 3-2 shows the summary results of the homogeneity tests for the stations. According to the Wijngaard et al. (2003) classification, the test result revealed that all rainfall stations were homogeneous and classified as "useful" series. However, a break was detected for the Buishand test at Woreka station. In addition, the VNR test identified inhomogeneity at Neghele, Telamokentise and Yirba Muda stations.

Table 3-2. Homogeneity test results using different methods at 95% significance level.

Station	**P-Value**				
	Pettitt	**SNHT test**	**Buishand**	**von Neumann**	**Result**
Arbegona	0.291	0.17	0.286	0.606	Usefull
Bensadaye	0.505	0.113	0.260	0.084	Usefull
Bidere	0.751	0.808	0.783	0.097	Usefull
Bore	0.402	0.412	0.339	0.116	Usefull
Dolo Mena	0163	0.273	0.206	0.759	Usefull
Hager Selam	0.382	0.306	0.315	0.151	Usefull
Harokelo	0.683	0.604	0.870	0.206	Usefull
Kibre Mengist	0.407	0.613	0.299	0.777	Usefull
Kofele	0.075	0.235	0.079	0.053	Usefull
Neghele	0.447	0.099	0.199	**0.001***	Usefull
Telamokentise	0.577	0.119	0.329	**0.021***	Usefull
Woreka	0.152	0.058	**0.036***	0.064	Usefull
Yirba Muda	0.102	0.050	0.074	**0.031***	Usefull

* Shows inhomogeneity at $\alpha = 0.05$

Figure 3-2 shows the rainfall time series of selected stations for SNH, BR, and Pettitt tests. The plots in Figure 3-2 showed that the change point occurred only in 2004 for BRT at Woreka station. Therefore, the overall homogeneity test results showed that the record appears to be sufficiently homogenous and can be used for further analysis.

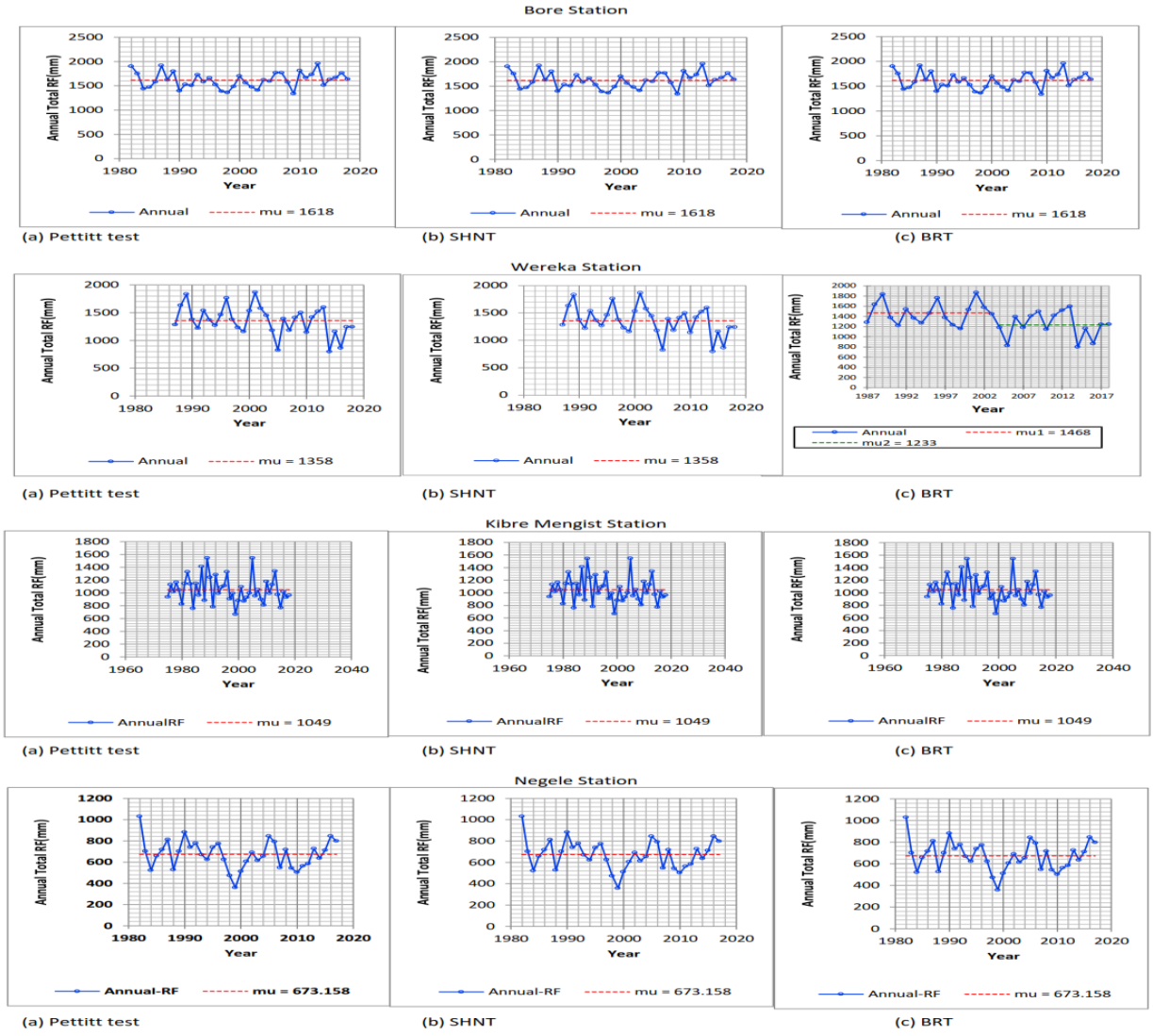

Figure 3-2. Result for Bore, Woreka, Kibre Mengist and Neghele stations using different homogeneity test methods (mu represent the mean annual rainfall)

3.2.4. Methodology

3.2.4.1. Variability analysis

Analysis of rainfall variability were computed using coefficient of variation (CV) (see the details NMSA, 1996; Asfaw et al., 2018), precipitation Concentration Index (PCI) (see De Luis et al. 2011), and standardized anomalies of rainfall (SRA) (see Bewket & Conway, 2007; Hadgu et al., 2013; Viste et al., 2013), CV was computed to measures the overall variability of the rainfall and temperature in the study area. PCI is an indicator of whether there is a low concentration of monthly rainfall distribution or not in the annual rainfall data series. SAR it is used to determine the frequency and severity of droughts, as well as the wet and dry years of the rainfall record.

3.2.4.2. Trends

The non- parametric MK test and Sen's slope estimator were employed to detect and compute the magnitude of trends in the observed time series data of precipitation and temperature. The advantages of using the non- parametric Mk test is that, its low sensitive to outliers due to inhomogeneous time series data and the data need not required to be normally distributed (Gummadi et al., 2018). In the MK test, the positive or negative test statistic, S, indicates an increasing or a decreasing trend and is computed by equation 1 (Kendall, 1975; Mann, 1945):

$$S = \sum_{i=1}^{n-1} \sum_{j=i+1}^{n} Sgn(X_j - X_i) \quad \text{..... (1)}$$

Where *S* is the Mann-Kendal's test statistics; X_i and X_j are the consecutive data values of the time series in the years i and j (j>i), respectively and *N* is the length of the time series. The sign function is given as equation 2:

$$Sgn = (X_j - X_i) = \begin{cases} +1 \; if(X_j - X_i) > 0 \\ 0 \; if(X_j - X_i) = 0 \\ -1 \; if(X_j - X_i) < 0 \end{cases} \quad \text{..... (2)}$$

According to Mann (1945) and Kendall (1975), when the number of observed data is more than 10 ($n \geq 10$), the statistic 'S' is approximately behaves as normally distributed with the mean and E(S) becomes 0. In this case, the variance statistic (Var (S)), is calculated as:

$$Var\ (S) = \frac{1}{18}\left[N(N-1)(2N+5) - \sum_{p=1}^{q} tp(tp-1)(2tp+5)\right] \quad \ldots\ldots (3)$$

Where, q = the number of tied groups in the data set; tp = the number of data points in the i^{th} tied group; N = the number of data points

In cases where the sample size n > 10, the standardized MK test statistic (Z_{MK}), is calculated using equation 4 (Kendall, 1975; Mann, 1945).

$$Z_{MK} = \begin{cases} \frac{S-1}{\sqrt{Var(S)}}\ if\ S > 0 \\ 0\ if\ S = 0 \\ \frac{S+1}{\sqrt{Var(S)}}\ if\ S < 0 \end{cases} \quad \ldots\ldots (4)$$

Where Var(S) and Z_{MK} is variance and standardized MK test statistic, respectively. Z_{MK} value was used to evaluate the presence of a statistically significant trend. In this trend test, the null hypothesis (Ho = μ = μo) states that the dataset under evaluation is no monotonic trend; the alternate hypothesis (Ha ≠ μ) states that there exists a monotonic (increasing or decreasing) trend over time. In a two-sided test for trend, the null hypothesis should be accepted if $|Z_{MK}| < Z_{1-\alpha/2}$ at a given level of significance, where $Z_{1-\alpha/2}$ is the critical value of Z_{MK} from the standard normal Table.

Estimating the Magnitude of the Trend

The magnitude of the trend can be estimated with Sen's slope method, developed by Theil (1950) and Sen (1968). To obtain the slope estimate Q, the slopes of a pairs of all data value calculated as follows:

$$Q_i = \frac{Y_j - Y_i}{X_j - X_i} \qquad i = 1, 2, \ldots . N, j > i. \quad \ldots\ldots (5)$$

where, xi is the time of the ith observation, and yi is the value of the ith observation of the rainfall variable. The Sen's estimator of slope is the median of these N values of Qi. The N values of Qi are ranked from the smallest to the largest, and then the Sen's slope estimator computed as:

$$Q_{med} = \begin{cases} Q * \left[\frac{(N+1)}{2}\right], if\ N\ is\ odd \\ \frac{Q*\left[\frac{N}{2}\right] + Q*\left[\frac{(N+2)}{2}\right]}{2}, if\ N\ is\ even \end{cases} \quad \text{......} (6)$$

In Equation (6), the sign of Qmed reflect the trend direction. A positive or a negative value indicates an increasing (upward) or decreasing (downward) trend in the data series over time, respectively.

3.2.4.3. Onset, cessation and length of rainy season

Stern et al. (2006) definition was used to determine the onset, cessation date, and length of growing period (LGP). Accordingly, the onset of the rain season in Days of the Year (DOY) was defined as the first wet-spell of at least three days totaling with 20 mm or more rainfall, provided no dry spell of 10 days or more within the following 30 days. To determine the cessation date of rain season in DOY, the method used by Tesfaye & Walker (2004), was employed. Accordingly, the end of the rainy season is marked by the date when soil water drops to a certain threshold. This threshold is set at an average of 5 mm of ET per day and 10 mm per meter of the maximum soil water holding capacity of the area. This threshold is chosen because it reflects the point at which the soil no longer provides sufficient water for plant growth (Tesfaye & Walker, 2004). By using this definition, the built-in R-Instat statistical software was used for the analysis and on the way LGP was determined by taking the difference between the end date and the onset.

3.2.4.4. Determination of seasonal deficit in crop water requirement

In the study watershed to compute the seasonal crop water requirements from planting to maturity for major crops (maize and sorghum) CROPWAT 8 model were used.

$ET_C = K_C * ET_O$...(7)

Where ET_C, ET_O, and K_C represent crop water requirement, reference evapotranspiration, and crop coefficient, respectively. Maize and sorghum Kc values for each growth stages were derived from

FAO guidelines (No56). Based on the long-term climate data, reference evapotranspiration was calculated using FAO Penman-Monteith.

To calculate the supplemental irrigation water requirement effective rainfall and crop water requirements were used using the following formulas:

$$IWR = ET_C - ERF \quad \text{.....(8)}$$

Where IWR and ERF represent supplemental irrigation water and effective rainfall. Effective rainfall is a portion of rainfall effectively utilized by the crop after loss from percolation and runoff has been considered and computed using dependable formula developed by FAO.

3.3. Results and Discussion

3.3.1. Rainfall characteristics

3.3.1.1. Rainfall Distribution

The study area consists of various agro-ecology with varying patterns of precipitation. It is characterised by bimodal rainfall seasons. The first wet season runs from March to May (spring) and the second from September to November (Autumn), with a highest in April and October (Appendix Figure 1). This aligns with the studies undertaken by Alhamshry et al. (2019) in Ethiopia and Degefu et al., (2021a) and (2021b) in Southeastern Ethiopia. Therefore, analysing rainfall characteristics for different seasons (winter, spring, summer, autumn and annual) is crucial to rainfed agriculture in Ethiopia.

The mean total annual rainfall distribution across the climate stations in the study basin varies from 1617.7 mm in Bore to 591.27 mm in Harokelo (Table 3.3). On seasonal bases, during MAM, the mean rainfall varies from 529.97 mm (at bore) to 336.53mm (at Harokelo), during JJA, the mean rainfall varied from 24.2 mm at Neghele to 506.19 mm at Bore. During SON season the mean rainfall distribution varies from 478.81 mm at Bore to 205.85 mm at Harokelo. On the other hand, during DJF, the rainfall across station varied from 140.63 mm at Hagere Selam to 28.76 mm at Bidere stations. The seasonal weighted average rainfall for annual, winter, spring, summer, and autumn over the stations is 1118.45 mm, 82.21 mm, 432.65 mm, 274.57 mm and 329.74.5 mm, respectively, which indicated that, winter (DJF), spring (MAM), summer (JJA) and autumn (SON) contributes about 7.35%, 38.68%, 24.54% and 29.48% of the annual total rainfall. This implies, spring rain is the major rainfall period for the near-equatorial regions of extreme southern and southeastern Ethiopia that are associated with the long rainy season of equatorial East Africa (Ademe et al., 2020; Berhanu et al., 2014; Dandesa et al., 2017; Degefu et al., 2021a; Gummadi et al., 2018).

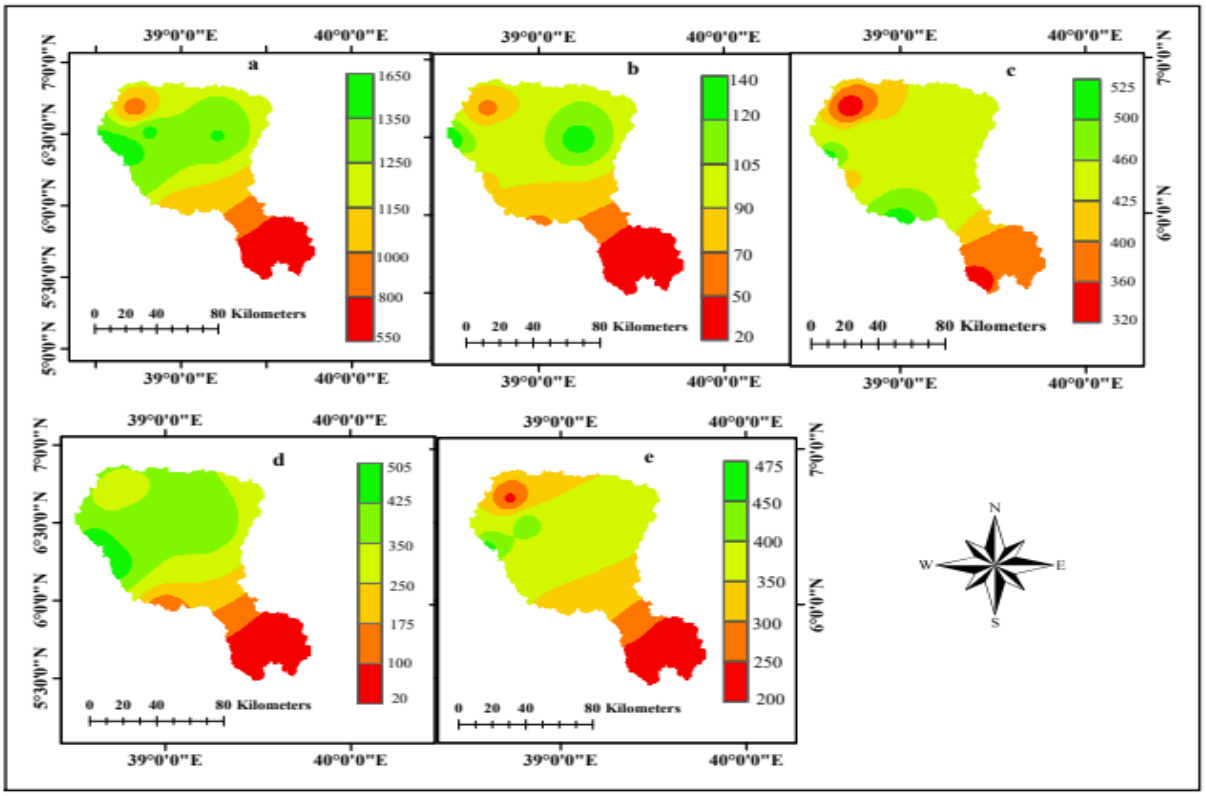

Figure 3-3. Spatial distribution mean rainfall a) Annual, b) Winter (DJF), c) Spring (MAM), d) Summer (JJA) and e) Autumn (SON).

The spatial mean annual and seasonal rainfall distribution of the study basin is presented in Figure 3-3 (a–e). In the annual and seasonal periods, the maximum rainfall values were observed in the highland and northern parts of the study area, while the minimum was observed in the lowland and southeastern parts (Figure 3-3 a-e). Much of the northern parts of the study areas received more than 1200 mm of rainfall annually, on the contrary the southern parts received less than 800 mm rainfall annually. During the spring season (MAM), most parts of the norther parts received more than 425 mm of rainfall, whereas the southeastern parts received less rainfall (Figure 3-3c). Different authors reported that the high-altitude regions, where the climate is typically arid to semi-arid, received more rainfall than the low-altitude areas (Anose et al., 2021; Degefu et al., 2021a; Gummadi et al., 2018).

The annual and seasonal mean, CV, and SD of rainfall (Table 3.3) indicated that the weighted average of annual, winter, spring, summer, and autumn rainfall showed CV of 20%, 89%, 30%, 45%, and 32% with the standard deviation of 216.95, 65.22, 127.79, 82.86, and 104, respectively.

Pair comparison of rainfall at temporal scales indicated seasonal variability is higher than the annual variability. Rainfall variability is very high during dry seasons and lowers during wet seasons. On seasonal time scales, inter-annual rainfall variability is higher in winter (DJF) and summer (JJA) than the case for spring (main rainy season: MAM) and autumn (SON) rainfalls. This is consistent with previous studies by Alemayehu & Bewket (2017), Degefu et al. (2021) and Viste et al.(2013). They concluded that higher rainfall variability was experienced during the small rainy season than the main rainy season and annual rainfall. Hare (2003) stated that, a rainfall amount with a CV of less than 0.20 is less variable, CV between 0.20 and 0.30 is moderately variable, and CV greater than 0.30 is highly variable. The study site experienced moderate and high rainfall variability. Stations Bidere, Harokelo, Kibre Mengist, Neghele, Dolo Mena, Telamokentise, and Yirba Muda shows high coefficient of variation (CV>30%) in all seasons. In the annual basis, the stations Bidere, Dolo Mena, Harokelo, Neghele, Telamokentise, and Yirba Muda showed moderate variation (CV between 20–30%). However, the other stations showed less variable rainfall (< 20%). During the spring season, the CV value greater than 30% in Arbegona, Bidere, Dolo Mena, Harokelo and Yirba Muda, which indicate considerably high rainfall variability. In general, most of the rainfall stations showed less and moderate variation in annual and high variation in seasonal rainfall patterns. This finding is consistent with past studies (Alemu & Bawoke, 2019 ; Anose et al., 2021; Asfaw et al., 2018; Bekele et al., 2017; Belay et al., 2021; Gummadi et al., 2018; Harka et al., 2021). According to Alhamshry et al.,(2019) and Seleshi & Zanke, (2004), the reasons for annual and seasonal inter-annual variability of rainfall over Ethiopia were due to the impacts of topography, the equatorial eastern Pacific sea level pressure, the forward and retreat pace of the African sector of the intertropical convergence zone (ITCZ) migration, and hydro-climate system interaction in the region.

The spatial distribution of annual and seasonal CV is presented in Figure 3-4 (a–e). During annual seasons, the variability of CV value is less than 20% in large portion of highland and northern parts of the study area, while the southern parts exhibited moderate rainfall variability (Figure 3-4a). On the other hand, the winter season, the CV value is greater than 40% in all basin areas (Figure 3-4b), which indicates very high rainfall variability. During the spring season, all the southern parts and a small portion of northern parts exhibited highly variable rainfall (CV between 30% and 40%). On the contrary a large portion of the northern part showed moderate rainfall variability (Figure 3-4c). As shown in Figure 3-4d, during the summer season, the southern part

showed very high variability (CV >40%), whereas the northern parts exhibited, moderately variable and highly variable rainfall. On the other hand, during the autumn season most part of the study basin showed high variation of rainfall (Figure 3-4e). Gummadi et al. (2018) stated that rainfall in Ethiopia shows excessive spatial variability due variations in topography. In general, in annual and seasonal time scales, the CV values have relatively high variability in southern and lowland areas of study basin, which received a relatively minimal amount of rainfall distribution. Recent studies in different parts of Ethiopia reported similar results (Alemu & Bawoke, 2019; Gummadi et al., 2018; Harka et al., 2021). They found out that the areas with high rainfall amounts showed low coefficient of variations whereas areas with low rainfall showed high coefficient of variations. In general, the results on mean annual and seasonal rainfall amounts, CV, inter-annual rainfall variability, and spatial pattern of annual rainfall cycle confirmed very high spatio-temporal rainfall variability in the study area.

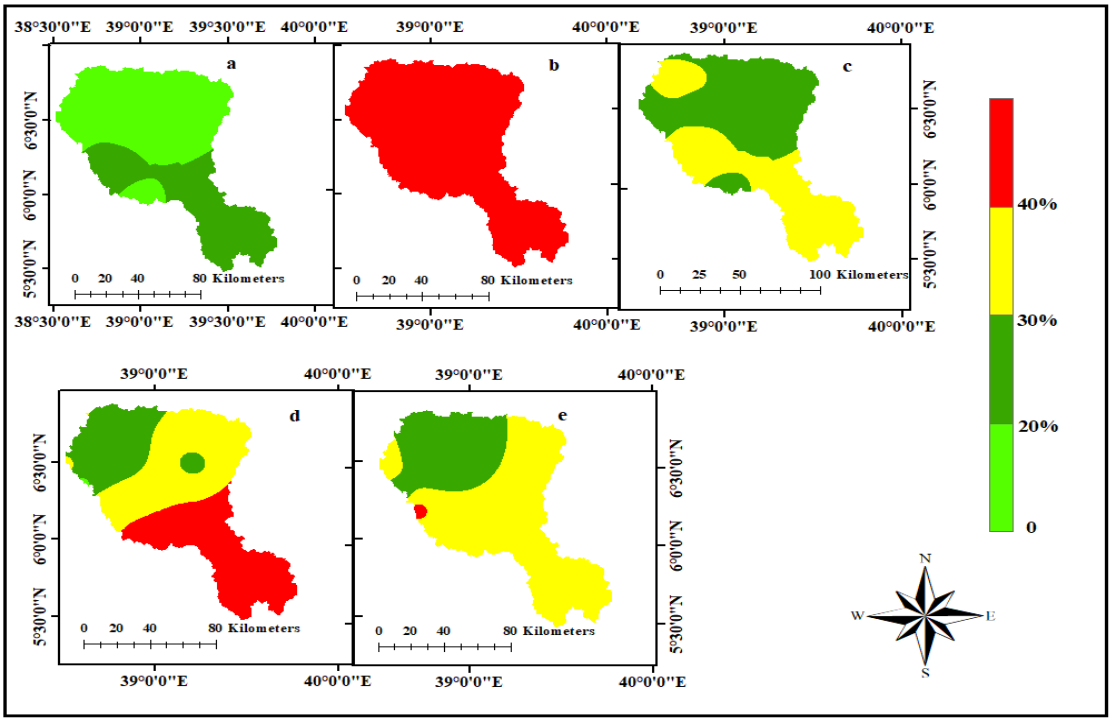

Figure 3-4. Spatial distribution (CV%) a) Annual, b) Winter (DJF), c) Spring (MAM), d) Summer (JJA), e) Autumn (SON) rainfall

3.3.1.2. Rainfall – Elevation relationships

The relation of mean annual and seasonal rainfall and CV with elevation was analysed and presented in Figure 3-5. The scatter plot between rainfall characteristics and elevation helps to observe and estimate their relationships. During the annual, DJF, and JJA seasons, the correlation between mean rainfall and elevation was found to be moderate in the study area (R2>0.5). During the MAM and SON seasons, the relation between mean rainfall and elevation was very weak. This could be because the amount and distribution of rainfall in low-lying areas is greater during these seasons. The relationship between CV and elevation showed that, on annual and seasonal time scales, the CV values in the study basin have relatively high variability in lowland areas and less variability in highland areas. The change in rainfall amount and distribution and variability was in line with the change in altitude in the study area. This result is consistent with related studies conducted in the country (Anose et al., 2021; Gummadi et al., 2018).

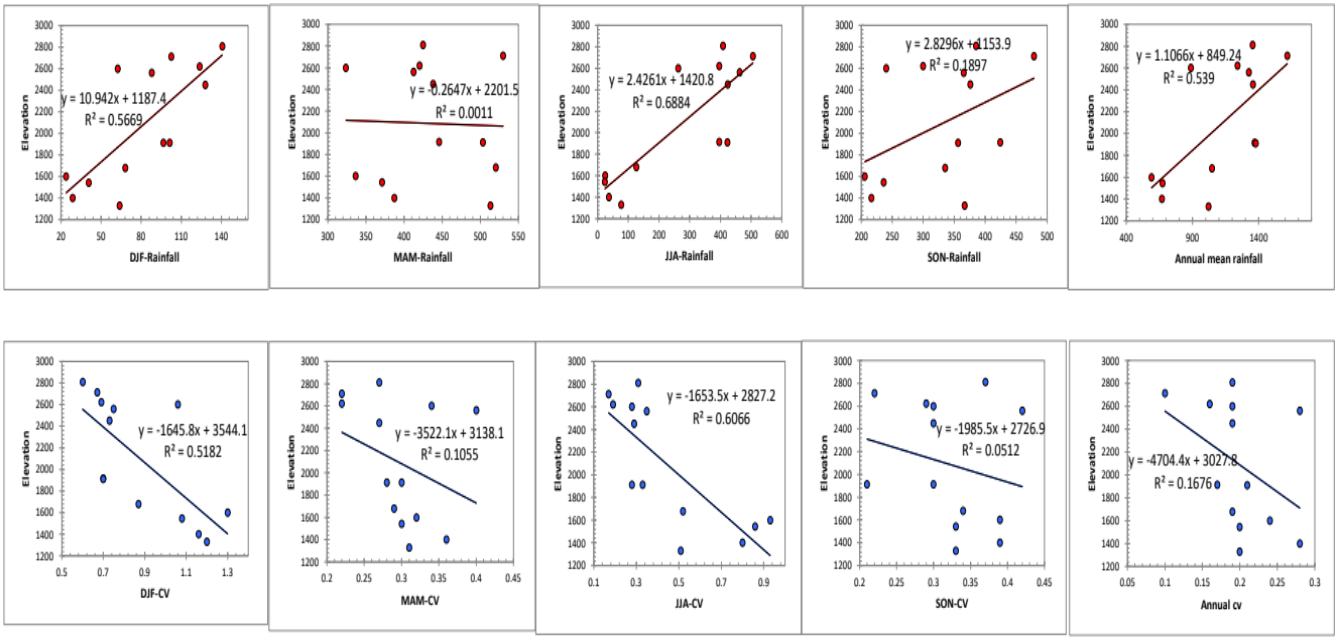

Figure 3-5. Scatter plot of rainfall characteristic and elevation, the above panel shows the relationship between seasonal rainfall and elevation and the lower panel shows the relationship between seasonal rainfall CV and elevation

4.3.1.3. Precipitation concentration index

The yearly Precipitation Concentration Index (PCI) was calculated on an annual basis. According to Oliver, (1980), the calculated PCI value indicate uniform monthly distribution of rainfall (PCI < 10), moderate concentration (PCI is between 11 to 15), high concentration (PCI is between 16 to 20), and very high concentration (PCI > 21). The yearly distribution of PCI showed that, the highest and the smallest value of 22.2 and 11.5 was recorded at Harokelo and Kofele station, respectively. PCI values indicated moderate monthly rainfall distribution in all stations, except for Bidere, Dolo Mena, Harokelo, kibremengist, and Neghele stations. PCI values at Dolo Mena (18.4%) and Kibre Mengist (16.8%) stations indicated irregular monthly rainfall distribution while Bidre (21.4%), Harokelo (22.2%) and Neghele (21.6%) showed strong irregularity of monthly rainfall distribution. This indicates the existence of spatial variations in monthly precipitation distribution in the study basin.

Previous researches in Ethiopia reported a moderate to high interannual rainfall distribution in various regions. Study by Ayalew et al. (2012) in the Amhara Region; Kassie et al. (2014) in Central Rift Valley of Ethiopia and Abegaz & Mekoya (2020) in central Ethiopia reported moderate to high interannual rainfall concentration. On the other hand, Hadgu et al. (2013) from their study undertaken in the northern Ethiopia indicated high to very high concentration of rainfall. Another study (Eshetu et al., 2016) in South western part of Ethiopia and Northwest Ethiopia (Geremew et al., 2020), indicated annual PCI with values greater than 16. This is similar to PCI values of this study found at Bidere, Delo Mena, Harokelo, Kibre Mengist and Neghele stations (Table 3-3).

Table 3-3. Annual and seasonal rainfall mean average, standard deviation (SD), coefficient of variation (CV) and Precipitation concentration index (PCI) in the study area

	DJF			MAM			JJA			SON			Annual			
Stations	**Mean**	**SD**	**CV**	**Mean**	**SD**	**CV**	**Mean**	**SD**	**CV**	**Mean**	**SD**	**CV**	**Mean**	**SD**	**CV**	**PCI%**
Arbegona	62.45	66.99	106%	323.82	110.34	34%	262.74	73.58	28%	240.03	72.71	30%	888.38	170.98	19%	12.58
BensaDaye	101.26	71.16	70%	446.02	125.21	28%	396.10	111.15	28%	424.24	89.82	21%	1369.61	236.31	17%	11.76
Bidere	28.76	33.80	116%	387.27	140.23	36%	37.53	30.49	80%	216.18	85.71	39%	669.62	186.75	28%	21.39
Bore	102.60	68.45	67%	529.97	117.44	22%	506.19	83.79	17%	478.81	103.77	22%	1617.74	159.58	10%	12.22
Dolo Mena	63.94	77.20	120%	513.30	159.10	31%	77.50	39.20	51%	367.10	120.20	33%	1021.10	207.50	20%	18.38
Hagere Selam	140.63	84.11	60%	424.95	114.58	27%	408.73	127.28	31%	385.30	142.56	37%	1355.21	263.79	19%	12.01
Harokelo	23.94	31.70	130%	336.53	108.96	32%	24.82	23.41	93%	205.85	81.70	39%	591.27	142.92	24%	22.22
KibreMengist	68.24	59.29	87%	520.24	151.99	29%	125.91	65.74	52%	335.31	115.28	34%	1048.78	201.08	19%	16.75
Kofele	123.68	84.95	69%	420.16	92.29	22%	396.65	73.96	19%	299.81	87.45	29%	1240.55	199.84	16%	11.50
Neghele	40.77	43.97	108%	371.31	112.28	30%	24.20	20.91	86%	236.10	77.68	33%	673.16	133.73	20%	21.56
Telamokentise	96.60	67.88	70%	503.49	148.58	30%	422.75	140.87	33%	356.40	107.30	30%	1379.05	287.56	21%	12.06
Woreka	127.94	92.87	73%	438.31	116.96	27%	423.89	124.52	29%	375.90	114.38	30%	1357.68	258.46	19%	12.14
Yirba Muda	87.87	65.48	75%	412.40	163.27	40%	462.44	162.26	35%	365.60	153.56	42%	1327.64	371.85	28%	12.74
Mean	82.21	65.22	89%	432.65	127.79	30%	274.57	82.86	45%	329.74	104.01	32%	1118.45	216.95	20%	15.18

DJF (December-February), MAM(March-May) JJA(June-Augest) and SON (September-November)

3.3.1.4. Standardize rainfall anomaly

The proportion of positive and negative SRA of annual and seasonal rainfall for the climate stations presented in (Table 3-4). The result of the SRA of annual rainfall revealed, the negative anomalies ranged from 41% (Arbegona) to 67% (Bensadaye) of the total number of observations. On a seasonal basis, 70% (Harokelo), 66% (Telamokentise), 71% (Bensadaye), and 66% (Woreka) of the study period of the years showed negative rainfall anomalies during DJF, MAM, JJA, and SON, respectively. The stations weighted mean rainfall anomalies of annual, DJF, MAM, JJA, and SON seasons exhibited negative anomalies of 51.8% ,63%, 54.5%, 56.6%, and 53.2% of the years during the study years, respectively. The result shows that the rainfall stations in the basin had a drier season than a wet season. The finding in line with the study by Alemayehu & Bewket (2017) in the central highlands of Ethiopia. They found that the portion of negative rainfall anomalies ranged from 37% to 71%.

Table 3-4. Percentage of positive and negative standardized anomaly index for annual and seasonal rainfall of the selected stations in the study basin.

	Positive Anomaly					**Negative Anomaly**				
Stations	**DJF**	**MAM**	**JJA**	**SON**	**Annual**	**DJF**	**MAM**	**JJA**	**SON**	**Annual**
Arbegona	32	41	47	56	59	68	59	53	44	41
Bensadaye	38	38	29	48	33	62	62	71	52	67
Bidere	38	44	41	44	50	62	56	59	56	50
Bore	46	51	46	38	51	54	49	54	62	49
Dolo Mena	32	55	55	52	52	68	45	45	48	48
Hagere Selam	39	43	36	48	45	61	57	64	52	55
Harokelo	30	47	41	47	44	70	53	59	53	56
Kibre Mengist	36	43	43	41	43	64	57	57	59	57
Kofele	35	55	42	48	45	65	45	58	52	55
Neghele	36	47	36	50	50	64	53	64	50	50
Telamokentise	41	34	45	52	52	59	66	55	48	48
Woreka	38	53	50	34	56	63	47	50	66	44
Yirba Muda	41	41	53	50	47	59	59	47	50	53
Mean	37.1	45.5	43.4	46.8	48.2	63	54.5	56.6	53.2	51.8

DJF (December-February), MAM(March-May) JJA(June-Augest) and SON (September-November)

The time-series analysis of the rainfall dataset (Appendix Figure 3) showed that the study area was characterised by periodic fluctuation of the dry and wet years. Even though it is not in consecutive years, the most extremely dry incidents happened in 1993 at (Dolo Mena), 1999 at (Neghele and Telamokentise), 1984 at (Bidere and Harokelo) and 2005 and 2014 at (Woreka). In addition, significantly large areas in the study region experienced differing magnitude of anomaly during all the other years. Severely dry years (anomaly b/n -1.5 to -1.99) were experienced in 1981(Hagere Selam),1988 (Yirba Muda), 1999 (Bensadaye, Kibre Mengist, Harokelo and Dolo Mena), 1998(Bore and Neghele), 1994 and 2012(Kofele), 1990, 1991 (Arbegona, Talamkantisso), 2014 and 2016 at Dolo Mena, and Woreka stations, 2015 at Bidre, Telamokentise, Kibre Mengist, Harokelo and Woreka, respectively.

The result from Appendix Figure 3 also showed, the most extremely wet conditions were found at Hagre Selam (1977= 2.03), Harokelo (1996=2.25), Neghele (1982=2.68), Telamokentise (2006=2.06), Kibre Mengist (1989 and 2005=2.47), Bore (2013=2.13). The result agrees with the recent study by Teshome & Zhang (2019), they showed that the change in rainfall over Ethiopia causing periodic fluctuation of droughts and floods from the 1980s onwards. Since 1990 extreme drought and flood were recorded during 1990-92, 1996, 1997, 2002, 2005-06, 2009, 2015 and 2016 (Teshome & Zhang, 2019). Most of the drought years were mostly related with El Nino events, while extreme wet years were associated with La Nina events. For instance, the recent El Nino-induced drought in 2015 was one of Ethiopia's driest years on record, and the *Belg* (Spring) and *Kiremt* (Summer) seasons were severely impacted. As a result, crops failed in the field, livestock died and millions of people have remained food insecure (Belay et al., 2021).

Previous studies also revealed historical occurrences of drought in Ethiopia in 11 years from 1952 to 2002 and occasional floods in 1993, 1996, 1998 and 2006 (Gissila et al., 2004; Haile, 1988; Mera, 2018). Segele & Lamb (2005) also indicated that during the last 35 years, Ethiopia has been ravaged by severe drought, owing to variations in the start and end of its major rain season. A recent study by Suryabhagavan (2017) during 1983 to 2012 showed that several drought events were detected across Ethiopia. Major droughts that occurred during the last three decades across Ethiopia were related to ENSO events, which negatively affected the livelihoods of millions of people over 60% of the country (Belay et al., 2021).

The annual rainfall anomaly analysis showed in Appendix Figure 3, indicated variations in the amount of rainfall received at different years and parts of the basin. It demonstrated that rainfall in the study basin happened above and below normal average which resulted flood and drought events. Climate change and extreme weather events are threatening the livelihoods of many people around the world. Over the last fifty years, extreme weather events in Ethiopia have shown a spatial and temporal distribution. Droughts affect certain regions of the country more frequently than others; the eastern and south-eastern regions, as well as the rift valley, are the most affected (Mera, 2018). Recently, it was observed that the reoccurrence of extreme weather events shortens and devastating impacts occurred in three successive years (Haile, 1988; Mera, 2018). It is believed that high temperature and low rainfall have played a significant role in shortening the recurrence frequency of the climate extremes in Ethiopia. If climate variability and extreme weather events continue in the future, the vulnerability of smallholder and subsistence farmers may be exacerbated, resulting in additional economic loss (Miheretu, 2020).

3.3.2. Annual and seasonal rainfall trend

The Mann–Kendall (MK) test and Sen's slope estimator were applied to investigate the trend in the hydrological time series data of the study area. The results of the MK test for trend analysis of annual and seasonal rainfall at 95% confidence level are presented in Table 3-5. The MK trend test showed both positive and negative trends for rainfall time series, which indicated the existence of local variations. The result of the MK test for annual rainfall data revealed an insignificant trend in most of the stations, but it showed an increasing tendency with rates varying from 2.18 to 10.86 mm per year for the study period (Table 3-5). This output agrees with the findings of Abegaz & Mekoya (2020); Ademe et al. (2020) and, Wagesho & Yohannes (2016), which all reported statistically non-significant increasing tendency in annual rainfall across different parts of Ethiopia. However, 16.96 mm per year of statistically significant increasing trend was observed at Yirba Muda station. Another grid-based (Alemayehu & Bewket., 2017) in the central highlands of Ethiopia revealed statistically non-significant increasing annual rainfall trends. On the contrary, several stations including Arbegona, Harokelo, Kibre Mengist, Kofele, Neghele and Woreka showed decreasing trend in annual rainfall. The detected trends were significant at 5% significant level only at Kofele station.

Table 3-5. The trend of annual and seasonal rainfall at study stations.

Station	DJF		MAM		JJA		SON		Annual_RF	
	p-value	Sen's slope	p-value	Sen's slope	p-value	Sen's slope	p-value	Sen's slope	p-value	Sen's slope
Arbegona	0.477	-0.33	0.218	-2.40	0.836	0.61	0.859	-0.15	0.302	-2.9
Bensadaye	0.526	-1.11	0.139	6.93	0.450	2.33	**0.012***	7.41	0.110	10.86
Bidere	0.835	0.00	0.744	-0.86	1	0.00	0.573	0.74	1.000	0.36
Bore	0.804	0.26	1.000	-0.02	0.314	-1.42	0.139	2.07	0.410	2.18
Dolo Mena	0.440	-0.62	0.590	-1.95	0.130	1.14	**0.016***	5.87	0.250	4.65
Hager Selam	**0.045***	-1.88	0.122	2.23	0.927	-0.13	0.051	3.29	0.192	5.46
Harokelo	0.80	0.00	0.286	-2.42	0.988	0.00	0.988	0.00	0.142	-4.29
Kibre Mengist	0.401	0.48	0.229	-2.06	0.769	0.21	0.800	-0.44	0.307	-2.58
Kofele	0.126	-2.03	0.708	-0.74	0.083	-2.35	0.973	-0.18	**0.027***	-7.60
Neghele	0.859	-0.33	0.169	-2.84	0.446	0.21	0.406	1.17	0.605	-1.17
Telamokentise	0.616	-0.89	0.402	2.35	**0.005***	9.71	0.616	1.44	0.150	10.35
Woreka	0.835	-0.15	0.266	-2.43	0.141	-3.70	0.160	-2.61	0.083	-8.42
Yirba Muda	0.910	0.22	0.376	3.18	**0.008***	8.31	0.083	6.08	**0.042***	16.96

DJF (December-February), MAM(March-May) JJA (June-August and SON (September-November). * Show significance at $\alpha = 0.05$

On a seasonal basis, spring (MAM) season rainfall showed statistically insignificant decreasing trend in all stations except Bensadaye, Hager Selam, Telamokentise and Yirba Muda stations. This agrees with the result of the study by Abegaz & Mekoya (2020), Belay et al. (2021), and Getachew (2018). They showed that the spring rainfall had non-significant decreasing trend at South Gondar, Centeral Ethiopia and Southern Ethiopia, respectively. The MAM season rainfall is used to grow crops and agro-pastoral activities in the highland and lowland of southern, southeastern and eastern Ethiopia (Bekele-Biratu et al., 2018). A delay or reduction of MAM rain means absence of water and pasture, which can lead to drought and have a negative impact on Ethiopian agricultural and pastoral activities. On the other hand, summer (JJA) and autumn (SON) seasons revealed an increasing trend in most stations, but stations at Bensadaye, Delo Mena, Telamokentise, and Yirba Muda showed a statistically significant increasing trend of 7.41, 5.87, 9.71, and 8.3 mm per year, respectively (Table 3-5). Furthermore, Wagesho & Yohannes (2016) and Gummadi et al. (2018) also reported that kiremt seasonal rainfall shows an increasing trend in southern and the south-eastern parts of Ethiopia, respectively, although some stations show a decreasing trend. Generally, the direction and magnitude of the seasonal rainfall trend was not uniform throughout different stations.

In general, the study area showed significant spatiotemporal variability in amount and distribution of annual and seasonal rainfall. As indicated in the result, MAM season contributed significant amount of rainfall. The rainfall from this season is very important for the performance of agriculture and livestock production, furthermore, it has impact on crop production during the JJA and SON season by affecting soil moisture availability and planting date. The declining trend in rainfall during the MAM season have / and will have a significant impact on agriculture in this largely bimodal rainfall areas.

3.3.3. Variability and trend in temperature at annual and seasonal time scales

To examine the trends and variability of mean annual and seasonal minimum and maximum temperature, meteorological stations such as Arbegona, Bensadaye, Bidere, Hagere Selam, Harokelo and Neghele were used (Table 3-6). Based on the year-to-year variation of annual and seasonal maximum and minimum temperatures analysis, the mean annual maximum temperature varied between 18.88 and 27.73 °C. The annual CV and SD for mean maximum temperature ranged from 1.69 to 5.78% and 0.47 to 1.09 °C, respectively. The annual mean minimum temperature for the study area ranged from 6.91 to 16.19 °C. The highest mean maximum temperature and the lowest mean minimum temperature was recorded at Bidere station (27.73 °C) and Hagere Selam Station (6.9 °C), respectively.

At the seasonal level, the weighted average of maximum mean temperature for winter (DJF), spring (MAM), summer (JJA) and autumn (SON) varied between 22.4 to 26.2 °C, with SD and CV from 0.7 to 1.01 °C and 3.2 to 4.7%, respectively. The highest maximum temperature observed during the DJF period. This result agrees with the findings of Dandesa et al. (2017) where highest maximum temperature was disclosed during DJF in Borena Zone. As it can be depicted in Table 3-6, the weighted average mean seasonal minimum temperature ranged from 11.6 to 13.2 °C with SD and CV from 1.1 to 1.6 °C and 10.5 to 15.2%, respectively. Throughout the seasons, Hagere Selame and Bidere station experienced lowest and highest temperature, respectively.

Table 3-6. Annual and seasonal maximum and minimum temperature trend and slope change, standard deviation (SD) and coefficient of variation (CV) in the study area.

Seasons	Parameters	Maximum Temperature (°C)						Mean	Minimum Temperature (°C)						Mean
		Arbegona	B/daye	Bidere	H/ Selam	Harokelo	Negele		Arbegona	B/daye	Bidere	H/ Selam	Harokelo	Negele	
Annual	P-value	**<0.0001****	1	0.374	**<0.0001****	**0.00013****	**<0.0001****		**<0.0001****	0.1235	**<0.0001****	**0.0015****	**<0.0001****	**<0.0001****	
	Sen's slope	0.051	0.36	0.009	0.081	0.043	0.049		0.058	0.059	0.087	-0.077	0.067	0.06	
	Mean	21.22	25.47	27.73	18.88	26.22	26.59	24.35	9.26	12.32	16.19	6.91	14.58	15.50	12.46
	SD	0.71	0.76	0.47	1.09	0.64	0.64	0.72	1.00	1.05	1.00	1.76	0.81	1.25	1.14
	CV	3.34	2.98	1.69	5.78	2.45	2.42	3.11	10.78	8.51	6.16	25.51	5.55	8.04	10.76
DJF	P-value	**0.008****	0.61	0.163	**0.0002****	**0.0003****	**0.01****		**0.0006****	0.11	**0.0003****	**0.0214****	**0.0128****	**<0.0001****	
	Sen's slope	0.04	-0.026	0.012	0.076	0.046	0.035		0.07	0.12	0.09	-0.054	0.047	0.072	
	Mean	22.46	26.81	29.62	20.55	28.83	28.92	26.20	7.96	11.61	14.51	6.46	13.52	15.44	11.58
	SD	0.83	1.10	0.70	1.78	0.80	0.84	1.01	1.33	2.29	1.30	1.75	1.01	1.76	1.57
	CV	3.70	4.11	2.35	8.66	2.79	2.90	4.08	16.69	19.70	8.93	27.17	7.46	11.41	15.23
MAM	P-value	**<0.0001****	0.83	0.08	**<0.0001****	**0.0002****	**0.003****		**0.0019****	0.32	**0.0002****	**0.0009****	**0.0001****	**<0.0001****	
	Sen's slope	0.069	0.003	0.02	0.056	0.058	0.04		0.049	0.033	0.068	-0.11	0.06	0.08	
	Mean	21.82	26.43	28.02	19.53	26.58	27.11	24.92	10.14	12.64	17.11	7.40	15.48	16.31	13.18
	SD	0.90	0.88	0.69	0.96	0.91	0.89	0.87	1.23	1.10	1.04	2.20	0.86	1.30	1.29
	CV	4.10	3.31	2.47	4.92	3.42	3.28	3.58	12.10	8.72	6.09	29.80	5.55	8.00	11.71
JJA	P-value	**<0.0001****	0.174	0.91	**<0.0001****	**0.0076****	**<0.0001****		**0.0003****	0.98	**0.0002****	**0.0009****	**0.0001****	**<0.0001****	
	Sen's slope	0.064	0.04	0.004	0.11	0.046	0.074		0.057	0.00	0.063	-0.069	0.066	0.07	
	Mean	19.90	24.15	25.68	17.20	23.47	24.14	22.42	9.96	12.54	16.96	6.84	14.76	14.83	12.65
	SD	0.99	0.91	0.75	1.43	0.87	1.13	1.01	1.14	1.01	0.86	1.77	0.86	1.04	1.11
	CV	4.97	3.78	2.93	8.32	3.69	4.70	4.73	11.41	8.03	5.07	25.85	5.80	6.99	10.52
SON	P-value	**<0.0001****	0.93	0.373	**<0.0001****	0.22	**<0.0001****		**<0.0001****	0.29	**0.0006****	**0.0096****	**<0.0001****	**<0.0001****	
	Sen's slope	0.04	0.003	-0.014	0.06	0.018	0.041		0.067	0.047	0.08	-0.06	0.071	0.063	
	Mean	20.72	24.50	27.62	18.25	26.04	26.17	23.88	9.00	12.50	16.23	6.96	14.58	15.41	12.45
	SD	0.63	0.73	0.70	1.05	0.73	0.61	0.74	1.04	1.12	1.09	1.82	0.87	1.20	1.19
	CV	3.03	2.96	2.53	5.74	2.79	2.32	3.23	11.52	8.97	6.73	26.16	5.98	7.79	11.19

** and * show significance at $\alpha = 0.01$ and 0.05, respectively; DJF (December-February), MAM(March-May) JJA (June-Augest and SON (September-November)

The result from the Mk analysis on mean annual maximum and minimum temperature had shown statistically significant increasing trend at 0.05 and 0.01 levels of significance for all the stations in the study area except at Bensadaye and Bidre station, which were found insignificant (Table 3-6). Similarly, several studies in different parts of Ethiopia reported significant increasing trend in maximum and minimum temperature (Addisu et al., 2015; Alemayehu & Bewket, 2017; Asfaw et al., 2018; Belay et al., 2021; Gedefaw et al., 2018). The rising temperatures are attributable to a rise in minimum temperatures, which could be due to an increase in anthropogenic emissions throughout time (Suryabhagavan, 2017). However, only at Hagere Selam station the annual minimum temperature shows a significantly decreasing trend of 0.08 °C per year. This agrees with study by the Yirga et al. (2017) and Kassie et al. (2014), as they reported a decreasing trend for annual minimum temperature by -0.2 °C and - 0.12 °C at Indibir and Butajira station, respectively.

The Mk trend analysis for mean maximum and minimum temperatures also presented on a seasonal basis in Table 3-6. The seasonal trend for winter, spring, summer, and autumn over the stations showed an increasing trend for all stations except Hagre Selam, showed statistically significant decreasing trends for all seasons of minimum temperature at 0.01 and 0.05 significance levels. While Bensadaye and Bidre stations showed statistically insignificant decreasing trend of mean maximum temperature for DJF and SON seasons, respectively. Arbegona, Hagere Selam and Neghele showed statistically significant increasing trend for maximum temperature while for the minimum temperature, Arbegona, Bidere, Harokelo and Negle showed significant increasing trends at 0.05 and 0.01 confidence level. This finding also agrees with several reports with regards to annual and seasonal maximum and minimum temperature in different parts of Ethiopia, which revealed an increasing trend (Addisu et al., 2015; Beyene, 2016; Dandesa et al., 2017; Gedefaw et al., 2018; Mekonen & Berlie, 2020; Mengistu et al., 2014) at Lake Tana sub-basin, Mekelle city, Borena area, Awash river basin, Northeastern Highlands of Ethiopia and Upper Blue Nile River Basin, respectively.

Moreover, the changes in slope of annual and seasonal temperature in the study period also summarized in Table 3-6. Accordingly, the annual minimum temperature slope of change was greater than the annual maximum temperature in all station except Hagereselam and Bensadaye stations. The highest slope of change was found at Bidre (0.087 °C per annual). In general, the rate of increasing of the minimum temperature is more pronounced than the maximum temperature.

The result is in line with the findings of Asfaw et al. (2018), Belay et al. (2021) and Mekonen & Berlie, 2020). They showed that the increasing trends in the minimum temperature were higher than those in the maximum temperature in many parts of Ethiopia. During the MAM period, all stations except Arbegona and Hagere Selam, experienced higher rate of changes on minimum temperature than maximum temperature. During the JJA period, Bidre and Harokelo showed higher slope change on minimum temperature. On the other hand, Arbegona, Bidre, Harokelo and Neghele experienced higher rate of change on minimum temperature than the maximum temperature in the DJF and SON seasons.

3.3.4. Onset, cessation and length of rain season

Table 3-7 and 3-8 summarize and present the mean SD and CV of onset, cessation, and length of rain season of the *Belg* and *Kiremet* growing seasons. The result showed that the mean onset date of the *Belg* growing season ranged from Julian day number 69 (March 9th) to 96 (April 6th), while the corresponding value for the *Kiremt* growing season is 160 (June 8th) to 275 (October 1st). The result also revealed that, on average, the *Belg* season starts on March 24th of the year (DOY, 84) in the study area. The output aligns with previous studies by Legese et al. (2018) and (2019). They reported that the *Belg* season starts or onset period over the Bale highlands on average was March 28th Day of the year (DOY, 88) and March 25th Day of the year (DOY, 85), respectively. The earliest onset for *Belg* was recorded on March 9 at Telamokentise, which is in the northern part, while the most late was recorded on April 6 at Harokelo meteorological site, which is located in the southern part of the study area. The CV for the start of the *Belg* and *Kiremt* growing seasons ranged from 16% to 29% and 6.4% to 20%, respectively. The result revealed a higher CV observed in the *Belg* season than in the *Kiremt* season. This agrees with Bekele et al. (2017) and Legese et al. (2018), who also reported a higher inter-annual variability of start of season (SOS) observed in the *Belg* season than in the *Kiremt* season.

The end of the season(EOS) is governed by stored soil water and its availability to the crop after the rainfall stops (Ademe et al., 2020). The mean potential cessation date of the *Belg* and *Kiremt* growing seasons in the study area ranged from Julian day numbers 139 to 149 (i.e., 18 May to 29 May) and 297 to 330 (i.e., 24 October to 25 November) respectively (Table 3-7 and 3-8). The SD

for the cessation of the season of the *Belg* and *Kiremt* growing seasons ranged from 4 to 9 and 11 to 19 days, respectively, with a CV of 2.2% to 6.3% for *Belg* and 3.5 to 6.1% for *kiremt*. The SD of cessation dates and CV are less than the onset dates in all stations of the basin. This agrees with the study conducted by Bekele et al. (2017) in the Awash River Basin. Higher SD and CV of the start of the season indicate that rainfall patterns may be difficult to understand, and thus practicing crop planting and related agricultural activities should be undertaken with caution. According to Segele & Lamb (2005), the average onset and cessation dates vary depending on the geographical location of the stations.

Table 3-7. The mean, standard deviation and coefficient of variance of onset, cessation, and length of the growing period of *Belg* season.

	FMAM			FMAM					
Stations	**SOS**	**StDV**	**CV(%)**	**EOS**	**StDV**	**CV(%)**	**LGP**	**StDV**	**CV(%)**
Arbegona	93	18	19	143	8	5.8	50	21	43
Bensa	78	23	29	146	6	4.2	67	25	37
Bidere	94	15	16	140	9	6.2	47	18	38
Bore	80	22	27	149	3	2.2	69	22	33
Delo Mena	83	18	22	144	8	5.4	61	20	33
Hagre Selam	77	22	29	148	4	2.6	71	23	33
Harokelo	96	16	17	139	9	6.3	43	19	44
Kibre Mengist	86	17	20	145	7	4.5	59	19	32
Kofele	71	19	26	147	5	3.3	76	19	25
Neghele	90	17	19	140	8	5.9	50	17	35
Telamokentise	69	20	29	148	5	3.2	79	21	28
Woreka	84	24	29	148	6	3.9	64	26	41
YirbaMuda	89	19	21	149	4	2.4	59	20	34

SOS= start of season; EOS=end of season; LGP= length of growing period

The mean LGP of the *Belg* and *Kiremt* growing seasons ranged from 43 to 79 days and 38 to 170 days, respectively (Table 3-7 and 3-8). The SD and CV of LGP for the *Belg* growing season ranged from 17 to 26 days and 28% to 44%, respectively. The SD and CV of LGP for the *Kiremt* growing season ranged from 21 to 44 days and 13% to 62%, respectively. The results revealed that in the *Belg* season, higher inter-annual variability of LGP was observed than in the *Kiremt* season. This is due to high CV at the onset and cessation date for the *Belg* season. The delayed start of the rain season and/or early withdrawal of the rain season resulted in a shorter length of growing period, and this indicates significant uncertainty and risk associated with the *Belg* season agricultural

activities. Different researches have shown that the LGP varied considerably between different geographical locations. Hadgu et al. (2013) reported length of rain season stretched from 66 to 85 days in northern Ethiopia, while Bekele et al. (2017) in Awash River Basin reported that the mean potential LGP of the *Kiremt* and *Belg* growing season ranged from 35 to 127 days and 0 to 82 days respectively. Abegaz & Mekoya (2020) also reported length of the rainy season varied from 55 to 138 days over central Ethiopia.

Table 3-8. The mean, standard deviation and coefficient of variance of onset, cessation, and length of the growing period of *Kiremt* season.

Stations	JJAS SOS	StDV	CV(%)	JJAS EOS	StDV	CV(%)	LGP	StDV	CV (%)
Arbegona	203	34	17	297	18	6.1	94	34	36
Bensa	168	17	10	320	12	3.6	153	23	15
Bidere	274	23	8.4	312	14	4.4	38	24	62
Bore	160	10	6.5	330	19	5.8	170	22	13
Delo Mena	255	32	13	319	11	3.5	64	33	52
Hagre Selam	173	24	14	316	16	5.1	143	31	21
Harokelo	274	22	8.0	313	15	4.7	39	21	53
Kibre Mengist	226	45	20	318	12	3.8	92	44	47
Kofele	169	18	11	308	16	5.3	139	23	16
Neghele	275	22	8.0	317	12	3.7	42	24	58
Telamokentise	170	22	13	307	19	6.1	137	28	21
Woreka	168	19	12	316	13	4.2	147	24	17
YirbaMuda	163	11	6.4	314	18	5.7	150	22	15

SOS= start of season; EOS=end of season; LGP= length of growing period; JJAS= June, July, August, September

3.3.4.1. Trends of onset, cessation and length of rain season

The Mann-Kendall trend test on the onset date of *Belg* rainfall showed a statistically insignificant trend. All the stations showed an increasing tendency except Hagere Selam, which shows a decreasing tendency (see Table 3-9). The cessation date of *Belg* rainfall showed an increasing trend in all stations except Arbegona, Bidre, Delo Mena, Harokelo, and Neghele. However, stations Kibre Mengist and Yirba Muda showed a statistically significant trend at a 95% confidence level.

Table 3-9. Trends of *Belg* and *Kiremt* onset, cessation days and length of growing period of study area

Statiom	Belg						Kiremt					
	Onset		Cessation		LGS		Onset		Cessation		LGS	
	p-value	Sen's slope	p-value	Sen's slope	p-value	Sen's slope	p-value	Sen's slope	p-value	Sen's slope	p-value	Sen's slope
Arbegona	0.44	0.38	0.49	-0.11	0.23	-0.75	0.49	-0.36	**0.01***	0.92	**0.04***	1.39
Bensaday	0.24	1.00	0.40	0.13	0.20	-1.11	0.76	-0.07	**0.02***	0.55	0.26	0.65
Bidre	0.22	0.25	0.25	-0.20	0.15	-0.50	0.57	0.07	0.50	0.21	0.92	0.00
Bore	0.72	0.12	0.54	0.00	0.70	-0.12	**0.03***	-0.14	0.51	0.18	0.18	0.47
DeloMena	0.92	0.00	0.27	-0.15	0.32	-0.48	0.84	-0.08	**0.003***	0.82	0.06	0.91
Hagre Selam	0.54	-0.13	0.06	0.05	0.41	0.21	0.16	-0.14	0.07	0.34	0.06	0.46
Harokelo	0.75	0.11	0.50	-0.13	0.48	-0.29	0.38	0.13	0.73	-0.09	0.41	-0.33
KibreMengist	0.73	0.05	**0.04***	0.11	1.00	0.00	0.22	0.59	0.37	0.14	0.28	-0.50
Kofele	0.21	0.43	0.40	0.05	0.27	-0.43	1.00	0.00	0.46	-0.25	0.84	0.15
Neghele	0.65	0.09	0.36	-0.15	0.49	-0.19	0.15	0.22	0.29	0.21	0.95	0.00
Telamokentise	0.33	0.54	0.61	0.00	0.41	-0.45	0.20	-0.25	0.13	0.67	0.07	1.09
Woreka	0.91	0.06	0.79	0.00	0.67	-0.25	0.33	0.38	0.96	0.00	0.10	-0.90
YirbaMuda	0.47	0.29	**0.02***	0.10	0.55	-0.16	**0.03***	-0.38	0.70	0.11	0.12	0.62

* Show significance at $\alpha = 0.05$

In the *Kiremt* season, stations Arbegona, Bensadaye, Bore, Delo Mena, Hagre Selam, Telamokentise, and Yirba Muda showed a decreasing trend (Table 3-9). Only the Bore and Yirba Muda stations showed statistically significant trends, while the remaining stations did not show any trends at the 0.05 level of significance. On the other hand, the cessation date of *Kiremt* showed an increasing trend in all stations except Kofele and Harokelo stations.

The length of the growing period (LGP) for Belg season indicated a non significant declining trend in all stations except Hagere Selam, which shows statistically insignificant increasing trend. This agrees with the result of the study by Bekele et al. (2017) who showed that decreasing trend in all stations except Koka in the Awash Basin. Hence, during this season more cautions should be taken on planning agricultural activities and to cope with the uncertainty and risk associated with the *Belg* season agricultural practice different climate change adaptation and mitigation measures need to be practiced (e.g adopting rainwater water harvesting schemes, improving water use efficiency, selecting drought-tolerant varieties or early maturing crops, and using soil moisture conservation practices are needed). If these are not put into practices, crop production sustainability and food security in the study basin will be jeopardized. However, the LGP for the *Kiremt* season indicated an increasing trend in all stations except for Kibremengist, Harokelo and Woreka stations. Arbegona station shows statistically significant increasing trend at a 95% confidence level.

3.3.5. Supplementary irrigation water requirement for the selected crops

The analysis of crop water requirements in the study basin revealed that supplementary irrigation is crucial to prevent crop failure and yield reduction during the two cropping seasons. To offset the impact of water stress on crop yield during the MAM season, Hagre Selam and Neghele areas required the least (34.8 mm and 15.6 mm) and the highest (202.4 mm and 181.2 mm) amounts of supplementary irrigation water for maize and sorghum crops, respectively. During the same season, Delo mena and Kibre Mengist required supplementary irrigation of 158.6 mm and 146.6 mm for maize, and 162.1 mm and 146.8 mm for sorghum, respectively. During SON season, sorghum required a 206 mm, 166.6 mm, 217.7 mm, and 252.2 mm depth of supplementary irrigation water for Delo Mena, HagereSelam, Kibre Mengist, and Negehl stations, respectively (Table 3-10). This implies that the MAM season required less supplementary irrigation than the SON season. Crops are extremely sensitive to water stress during the flowering and yield formation stages (Bekele et al., 2017). As a result, the lack of supplemental irrigation water at these stages would result in lower maize and sorghum yields.

Table 3-10. Seasonal crop water requirement, effective rainfall, and supplementary irrigation for maize and sorghum in selected location of the study watershed.

Seasons	Crops	Units	Location			
			Delo Mena	Hagre Selam	Kibre Mengist	Neghele
MAM	Maize	Crop water Requirement (mm)	357	329.3	361.6	342.8
		Effective rainfall (mm)	322.4	383	328.8	166
		Irrigation Requirement (mm)	158.6	34.8	146.6	202.4
	Sorghum	Crop water Requirement (mm)	277.8	259.3	282.7	270.2
		Effective rainfall (mm)	278.7	378.3	291.1	144.9
		Irrigation Requirement (mm)	162.1	15.6	146.8	181.2
SON	Sorghum	Crop water Requirement (mm)	327.3	282.4	310.2	324
		Effective rainfall (mm)	210.6	211	184.9	121
		Irrigation Requirement (mm)	206	166.6	217.7	252.2

The intermittent nature of the moist periods, combined with variable rainfall, and high temperatures, has made the available moisture in the soil insufficient to maintain crop productivity

for the majority of the year (MoWE, 2007g). Hence, the area's administration should work to develop small and medium-scale irrigation and water harvesting technology to mitigate the incoming effects of climate change and variability. During rainfall shortages and extended dry spells, irrigation is expected to play a significant role in enhancing and sustaining crop production systems.

3.3.6. Potential impacts of rainfall and temperature variability on crop production

The observed spatiotemporal variability in rainfall and temperature could have far-reaching consequences for smallholder farmers' agricultural practices and crop production. Having adequate and timely rainfall during the cropping seasons (*Belg* and *Kiremt* seasons) is critical for farming practices. However, the short growing season caused by the variability and inconsistency of rainfall during cropping seasons, as well as the inadequacy of soil moisture to support crop production for the majority of the year, discourages agricultural practices and reduces crop production across the region (MoWE, 2007g). The variability in the onset, cessation, and length of the growing period affects planting and harvesting. This has caused uncertainty in the cropping calendar, which has an impact on agricultural production (Mekonen & Berlie, 2020). During the study period, the rising trend of annual and seasonal minimum and maximum temperatures could have had a significant impact on smallholder farmers' crop production processes. Rising temperatures will amplify the impact of droughts, reducing soil moisture availability and cropland productivity.

In general, climate variability could have a significant impact on agricultural production because it is highly sensitive to changes in rainfall and temperature. Variability in temperature and rainfall would substantially reduce agricultural production and, in some cases, result in crop failure (Lemi & Hailu, 2019). Based on the abovementioned discussions, it is possible to conclude that crop yield is reduced by rainfall and temperature variability, which in turn has an impact on the agricultural sector, which is a significant contributor to national income. When climate change and variability is at its worst level, it causes total crop failure, resulting in hunger and the deaths of people and animals. These are common circumstances in Ethiopia’s especially in the study basin.

3.4. Summary and Conclusion

The analysis result of rainfall characteristics of the Upper Genale river basin showed various agroecology with varying precipitation patterns. It is characterized by bimodal seasons. The first wet season runs from March to May (spring) and the second from September to November (autumn), with a highest on April and October. The mean total annual rainfall distribution across the climate stations in the study basin varies from 1617.7 mm to 591.27 mm. The seasonal weighted average rainfall for annual, winter, spring, summer, and autumn over the stations is 1118.45 mm, 82.21 mm, 432.65 mm, 274.57 mm and 329.74.5 mm, respectively. This implies is that, spring rain is the major rainfall period for the study area and contributes about 31–58% to the annual rainfall.

The spatial distribution of seasonal and annual rainfall was heterogeneous in the study area. During the annual and spring seasons, large portion of the northern parts showed less rainfall variability (CV<20) and the southern and the low land areas exhibited moderately and highly variable rainfall. During the summer and autumn seasons, the northern and highland areas showed moderate and high variability while the lowland and the southern parts exhibited high and extremely high rainfall variability, respectively. The SRA and the PCI values of the time-series analysis of the rainfall dataset showed that the study area was characterised by a periodic fluctuation of the dry and wet years and substantial irregularity of monthly rainfall distribution. The Mk trend test result showed both positive and negative trends for rainfall time series, which indicated the existence of local variations. During the spring (MAM) season rainfall showed a statistically non-significant decreasing trend in most stations. The Mk trend analysis test result also revealed that the mean annual and seasonal maximum and minimum temperature had shown statistically significant increasing trend at 0.05 and 0.01 levels. Furthermore, the MK trend analysis showed that the onset of the main rainy season was insignificantly increased whereas the cessation date and LGS were decreased over most of the stations during the study period. This indicated the occurrence of late-onset and early cessation in the study area.

The occurrences of extremely dry conditions and irregularities in rainfall distribution, along with the observed decrease in MAM rainfall and the late onset and early cessation of the cropping seasons over the study area, made crop planting and growth unpredictable. The increasing trend of

temperature and the decreasing trend of rainfall were the major threat to the agricultural sector. This could have a negative impact on the agricultural system by shortening the growing season and making available moisture in the soil insufficient to sustain crop productivity across the region. To avoid the growing season moisture deficit, a reduction in yield, and crop failure in the study basin, application of supplementary irrigation is crucial in both seasons. This is particularly important in the middle and southern parts. Moreover, most of the supplementary irrigation is needed at the end of both growing seasons. Hence, to enhance and stabilize crop production in the study area, developing rainwater harvesting technology and small and medium-scale irrigation have to be considered as the primary options. Besides that, developing and implementing appropriate adaptation and mitigation strategies in the study area as well as in other similar environmental areas is essential to minimize the impacts of climate change and variability on agricultural activities.

In general, the variability in annual and seasonal rainfall totals, as well as rising temperatures over the study area, create droughts, flooding, and outbreaks of human and livestock diseases, as well as extreme water loss due to evaporation. This affects agriculture and livestock production, domestic water supply, and municipal services. Therefore, to cope with the ongoing impacts of climate change and variability in the study area, developing strategic adaptation measures and a sustainable climate risk management approach is important. In line with this, to enhance the capacity to withstand climate change and variability, it is essential to adopt strategies and policies that improve the crop production systems in the study basin. An increase in agricultural research and extension services, as well as implementing improved agricultural practices for reducing crop production losses caused by climate change and variability, would be one approach. In addition, the present study has provided valuable information for better understanding of the spatial and temporal distribution and trends in rainfall and temperature in the study area, which is critical for managing water resources and ensuring sustainable agricultural production.

Finally, our study relied on in-situ data in the analyses of changes in rainfall and temperature variability for agricultural water management in Ethiopia. The lack of continuous and densely distributed in-situ hydrological data and gauged observations of rainfall makes it difficult to provide robust assessments of drought impacts on water availability for agricultural production. Remote sensing techniques are emerging as important and open access data sources to help

prioritize agricultural water management and address threats to water and food security. However, they are also accurate methods that underpin yield forecasts as well as facilitating our capacity to measure important properties of plants (e.g., morphology, chlorosis, transpiration rates) that underpins the assessment of crop health. The use of satellite-based rainfall, soil moisture and vegetation products provide these services, and serves as important alternatives for assessing agricultural water management in data deficient regions like Ethiopia.

CHAPTER FOUR:

4. UNDERSTANDING HYDROLOGICAL PROCESSES UNDER LAND USE LAND COVER CHANGE IN THE UPPER GENALE RIVER BASIN, ETHIOPIA

Abstract

The expansion of cultivated land in place of natural vegetation has a substantial influence on a hydrologic characteristic of a watershed. However, due to basin characteristics and the nature and intensity of landscape modification, the response varies across basin. This study aims to evaluate the performance of Soil and Water Assessment Tool (SWAT) model and its applicability in assessing the effects of land use land cover (LULC) changes on hydrological processes of the upper Genale river basin. The results of satellite change detection during the past 30 years (between 1986 and 2016) revealed that the landscape of the basin has changed considerably. It showed that settlement, cultivated and bare land areas had increased from 0.16% to 0.28%, 24.4% to 47.1%, and 0.16% to 0.62%, respectively. On the contrary, land cover units like forest, shrubland and grassland reduced from 29.6% to 13.5%, 23.9% to 19.5% and 21.8% to 18.9%, respectively. Based on monthly measured flow data, the model was calibrated and validated in SWAT-CUP using the sequential uncertainty fitting (SUFI-2) algorithm. The result showed that model performed well with Coefficient of Determination (R^2) ≥ 0.74, Nash–Sutcliffe Efficiency (NSE) ≥ 0.72, and Percent Bias (PBIAS) between -5% and 5%, for calibration and validation periods. The hydrological responses of LULC change for the 1986, 2001, and 2016 models showed that, the average annual runoff increased by 13.7% and 7.9% and ground water flow decreased by 2.85% and 2.1% between 1986 to 2001 and 2001 to 2016, respectively. Similarly, the total water yield increased from 324.42 mm to 339.63 mm and from 339.63 mm to 347.32 mm between 1986 to 2001 and 2001 to 2016, respectively. The change in hydrological processes, mainly the rise in runoff and total water yield as well as the reduction of lateral and groundwater flow in the watershed, resulted from LULC changes. This change has broader implications for planning and management of the land use and water resource development.

Keywords: Upper Genale river basin; SWAT model; LULC change

4.1. Introduction

Hydrology is the scientific study of the water cycle and how water moves in relation to the topographical characteristics of a region. These processes have a significant effect on the natural environment and are important for understanding water resource management in any watershed. Precipitation, infiltration, surface runoff, evapotranspiration, groundwater recharge, and flow are all influenced by a variety of factors including land use, topography, soil properties, and vegetation cover. The interaction between land cover and the hydrological cycle is particularly significant, as changes in land use can directly alter water retention, drainage patterns, and overall watershed behavior (Sulamo et al., 2021). For instance, forests function like natural sponges by soaking up rainfall and helping to replenish groundwater. In contrast, impervious surfaces like bare land and urban environments enhance surface runoff, raising the likelihood of flooding and lowering groundwater levels.

Land use and land cover (LULC) changes are dynamic and uninterrupted processes that are often influenced by both anthropogenic and natural factors (Birhanu et al., 2019; Samal & Gedam, 2021). Human activities have been identified as the primary drivers of LULC changes (Betru et al., 2019; Dibaba et al., 2020a). Although humans have been altering land for thousands of years to obtain livelihoods and other necessities, the amount, rate, and severity of LULC modification are significantly larger now than they were previously (Hassan et al., 2016). Population growth, societal development, overgrazing, inappropriate utilization of forest resources, and agricultural land expansion have all contributed to a substantial rise in the rate of LULC changes (Hailu et al., 2020; Mucova et al., 2018; Shawul & Chakma, 2019; Zewdie & Csaplovies, 2015). These human actions lead to simultaneous changes in natural environments and ecosystem services (Alemu, 2015; Obeidat et al., 2019; Woldeyohannes et al., 2018). As a result of its numerous effects on the natural environment, LULC change has emerged as a top priority for the global change research community (Chang et al., 2018).

In developing countries like Ethiopia, whose economies largely depend on agriculture, LULC conditions are considerably changing (Aredo et al., 2021; Berihun et al., 2019). The alteration of grass, shrub, and forest lands into cultivated and settlement areas have been a common experience (Aredo et al., 2021; Hailu et al., 2020; Negese, 2021; Shawul & Chakma, 2019; Yesuph &

Dagnew, 2019). An increasing extent of agricultural land and urbanization at the cost of natural vegetation have significant influence on the hydrologic responses of a basin. Vegetation can have a significant effect on hydrological fluxes due to variations in the physical characteristics of the land surface and soil, such as the roughness, architectural resistance, stomatal conductance, albedo, leaf area index (LAI), root depth, and infiltration capacity (Maza et al., 2020; Srivastava et al., 2020). Vegetation disturbance and the subsequent conversion to other LULC classes are known to have multiple effects on land productivity, streamflow, geomorphological processes, and the socioeconomic status within a catchment. The impacts vary from one basin to the other depending on the extent and intensity of the natural land cover modification and basin characteristics (Samal & Gedam, 2021).

The LULC change also has a significant effect on changing hydrological processes such as runoff volumes, groundwater recharge, and infiltration in Ethiopian river basins (Negese, 2021). The Genale Dawa river basin is one of the largest river basins and is found in a semi-arid, drought prone region in Ethiopia (MoWE, 2007c). The basin's water resource potential has the capacity to satisfy the demand of the current and planned water resource development projects in the basin and downstream water users. However, the resource has been poorly developed for water supply, irrigation, hydropower, and other purposes (MoWE, 2007c). This is due to the lack of an in-depth study with updated information and appropriate methods to understand and quantify the water balance components and surface water potential in the basin. Proper management and development of sustainable water resources necessitate modeling as well as an understanding of hydrological processes (Shukla & Gedam, 2018). Furthermore, understanding the relationship between LULC and hydrologic parameters is crucial for effective and sustainable water resource management and development. However, because of the complex LULC-climate-hydrology nexus, studying watershed hydrologic processes and responses in a river basin is a major challenge (Gyamfi et al., 2016).

Nowadays, to understand and quantify the hydrological characteristics and water resource potential of a basin, several hydrological models have been developed across the world (Johnston & Smakhtin, 2014; Singh, 2018). In Ethiopia, to evaluate the hydrological processes of a watershed, numerous public domain hydrologic models have been used. Among the physically-based, empirical, and conceptual models, soil water assessment tool (SWAT), hydrologic

modeling system (HEC-HMS), Hydrologiska Byråns Vattenbalansavdelning (HBV) model, European Hydrological System Model (MIKE-SHE), and artificial neural network (ANN) are the most commonly used hydrological models (Birhanu et al., 2019; Bizuneh et al., 2021; Dibaba et al., 2020b; Haile et al., 2017; Takele et al., 2022; Tassew et al., 2019; Teklay et al., 2020; Tufa & Sime, 2020; Worqlul et al., 2018; Zelelew & Melesse, 2018). Due to the ability of SWAT model to accurately simulate hydrological processes and its user-friendly interface, it is one of the most extensively used hydrological models worldwide for addressing numerous small and large watershed issues (Khoi & Thom, 2015; Leng et al., 2020; Shukla & Gedam, 2018). Additionally, the model is compatible with ArcGIS for spatial analysis, frequently updated has options for evaluations of hydrologic processes and also capable to subdivide a watershed up to a number of sub watershed levels and further subdivide up to a smaller homogeneous land management unit of HRU (Hydrologic Response Units). These characteristics make the SWAT model more suitable and applicable for modeling hydrological characteristics of a watershed (Chimdessa et al., 2019).

SWAT model has been widely used for water resources management, impacts of LULC and climate change on hydrological parameters of a watersheds. LULC changes have an impact on hydrological processes of a watershed through changing evapotranspiration, groundwater recharge, soil water holding capacity, infiltration, and surface runoff (Alvarenga et al., 2016; Awotwi et al., 2019; da Silva et al., 2018). This change can also result in a significant and long-term impact on surface and subsurface water quantity and quality of a basin (Chishugi et al., 2021; Kumar et al., 2017). Scholars around the world have documented the impacts of LULC changes on watershed hydrologic components of a river basin (Bogale, 2021; Gashaw et al., 2018; Guzha, 2018; Li et al., 2022; Li et al., 2018; Samal & Gedam, 2021; Teklay et al., 2020; Woldesenbet et al., 2018). For instance, a research in India, in the Upper Bhima River basin, showed that the effects of LULC changes on hydrological variables are minimal at the basin level, however at sub-basin level, the observed changes have increased total water yield up to 8% and runoff up to 13.6% (Samal & Gedam, 2021). Another study in the Wei River Basin, China, indicated that the expansion of agricultural land over the last 30 years has contributed significantly to a substantial reduction in annual and dry season river flow (Li et al., 2018). The expansion of agricultural land and the development of settlement areas in place of natural vegetation from 1985 up to 2015 in the Andassa watershed, Ethiopia, resulted in an increase in runoff, wet season flow, water yield, and annual flow by 9.3%, 4.6%, 2.4%, and 2.2%, respectively. The observed land cover changes, on

the other hand, diminished groundwater flow, lateral flow, dry season flow, and evapotranspiration by 7.8%, 5.7%, 2.8%, and 0.3%, respectively (Gashaw et al., 2018). Another study conducted in the Pra River Basin, Ghana, showed that LULC changes increased water yield and surface runoff by 40.13% and 124.51%, while decreasing evapotranspiration and baseflow by 13.25% and 30.08%, respectively (Awotwi et al., 2019).

Although the processes of hydrologic cycle are well understood at the global level, knowledge at the catchment and regional levels is limited. Besides, the effects of LULC changes on the hydrological responses of a watersheds are often not well defined (Aredo et al., 2021). Hence, evaluating and understanding hydrological parameters at the basin and subbasin scales as a result of LULC change is an essential element for implementing effective and sustainable water resource planning, management, and development (Gashaw et al., 2018; Mango et al., 2011). In addition, understanding of the amount of water produced in the river basin through the analysis of appropriate, adequate, and reliable data with relevant spatial and temporal scales is indispensable for managing water resources, providing strategic information needed, as well as decision-making on water related development projects (Adeba et al., 2015; Lv et al., 2020; Takele et al., 2022). Therefore, the importance of assessing the impacts of LULC change on the hydrological characteristics of a watershed is unquestionable.

In the Upper Genale River basin, change in LULC is a common phenomenon. This continuous change in LULC has an impact on the basin's water balance by altering the magnitude and pattern of hydrological variables, thereby exacerbating the water management problem. The lack of enough quantitative information on LULC change and its impacts on hydrological characteristics in the upper Genale river basin is a bottleneck for the promotion of sustainable development. Based on this premise, the upper Genale river basin was purposefully selected as the study watershed. To this end, the importance of having updated information on understanding the impact of LULC change on hydrologic variables of upper Genale river basin in order to design sustainable land use planning and water resource management strategies is becoming critical. Therefore, in this study, an effort has been made to evaluate the effects of LULC change on hydrological components, such as surface runoff, total water yield, groundwater flow, lateral flow, and evapotranspiration at both basin and sub basin scales. In this regard, quantifying, understanding, and addressing the hydrological characteristics are relevant for water resource planners and managers to work on

policy issues in relation to planning of land and water use in the watershed. Therefore, this research aims to improve understanding of hydrological processes under LULC change of the Upper Genale river basin leveraging physically-based, semi-distributed SWAT model.

4.2. Materials and Methods

4.2.1. Description of the study area

The Genale river basin is located in the south-eastern part of Ethiopia. The basin covers a portion of Southern Nations, Nationalities, and Peoples' (SNNP), Oromia, and Somali regional states. It is situated between latitudes of 3^0 30' and 7^0 20' N and longitudes 37^0 05' and 43^0 20' E. The basin area is about 172,713 km^2. It is one of Ethiopia's three widest river basins (Awulachew et al., 2007). Specifically, the upper Genale river basin (study area) is located between latitudes of 6^0 52' and 5^0 20' N and longitudes of 38^0 30' and 39^0 45' E and it lies in the upper central area of the Basin. It has a basin area of about 10,582.19 km^2 (Figure 4-1). Due to topographic and the ITCZ (Inter-Tropical Convergence Zone) effects, the basin experiences bimodal type I (three season type) and bimodal type II (double wet and dry seasons) annual rainfall cycle in northern (highland) and southeastern (lowland) parts, respectively. The northern and highland area characterized by the three wet seasons types, March–May (locally known as *Belg*), June–September (locally known as *Kiremt*) and September–November (locally known as *Meher*) (MoWE, 2007c). The lowland and the southeastern parts of the study area experience two wet season, one from March to May, with the highest in April, and the other from September to November, with the highest in October (Degefu et al., 2021a; MoWE, 2007c)**.** The annual average rainfall varies from 1617.7 mm to 591 mm**.** The annual mean minimum and maximum temperatures range between 6.9 to 16.2 ^oC and 18.9 to 27.7^oC, respectively. The main river, Genale, emanates in the north west from Sidamo Mountains and in the north-east from the Bale Mountains massif (MoWE, 2007c).

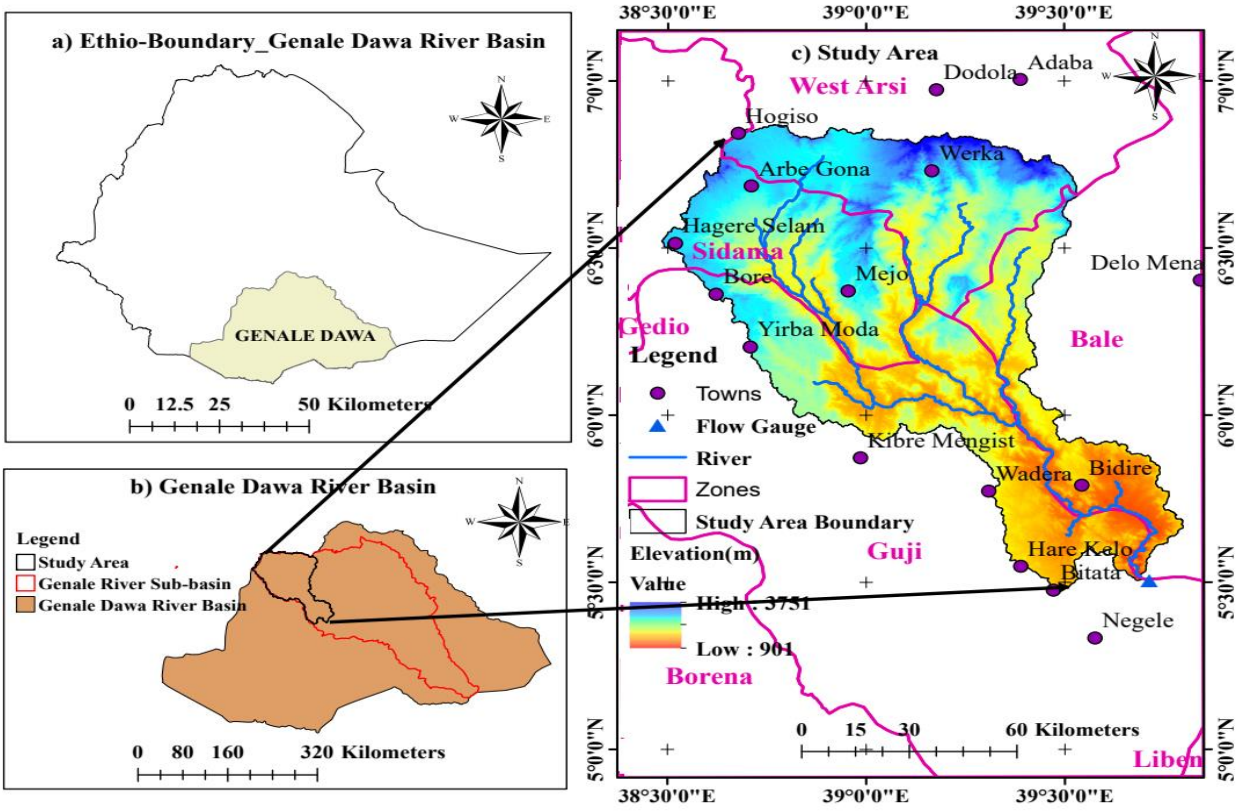

Figure 4-1. Location map of the upper Genale river basin.

4.2.2. SWAT Model input

To evaluate the performance of the SWAT model and to assess the effect of LULC changes on watershed hydrologic characteristics, temporal data such as climate and streamflow data and spatial data such as study area DEM, three different period LULC maps (1986, 2001, and 2016), and a soil map were used (Table 4-1).

Table 4-1. Input data for SWAT model

S.N	Data Type	Source	Resolution
1	DEM	Global Earth Explorer (USGS)	30 m by 30 m
2	Landsat 5 TM and Landsat 8 OLI imagery	Global Earth Explorer (USGS)	30 m by 30 m
3	Soil map	World Food and Agriculture Organization (FAO)	5 km
4	Meteorological data	National Meteorological Service Agency (NMSA) of Ethiopia	Point
5	Streamflow data	Ethiopian Ministry of Water and Energy	Point

4.2.2.1. Study area DEM (Digital Elevation Model)

A DEM of the upper Genale river basin with a horizontal resolution of 30 m shuttle radar topography mission (SRTM) was obtained from the USGS website. It is used to determine the watershed boundary, sub-watershed, and hydrologic response unit. The DEM was additionally used to identify the sub-basin characteristics of the watershed, including elevation, channel slope, slope gradient, reach length, and river network (Figure 4-1).

4.2.2.2. Land use land cover map

LULC is one of the primary factors influencing hydrologic characteristics such as runoff, evapotranspiration, and surface erosion in a watershed, and it is also used in the SWAT model for HRU delineation. To evaluate and understand the hydrological parameters under the effects of LULC changes of the study watershed, the classified LULC maps of 1986, 2001 and 2016 were used separately (For details please see section 4.3.1).

4.2.2.3. Soil map

Soil map of the study basin affecting the hydrological parameters of the basin were used as SWAT model input. The upper Genale river basin soil map was found from Food and Agricultural Organization (FAO, 2002) and extracted using ArcGIS10.5 software. From the SWAT database, the soil's physical and chemical properties, such as its texture, hydrologic group, bulk density, depth, organic matter content, water capacity, erodibility factors, and saturated hydraulic conductivities, were extracted. In addition, the required soil physicochemical properties extracted from the SWAT database were compared and verified with the soil survey reports from the Genale Dawa river basin master plan developed by the Federal Democratic Republic of Ethiopia, Ministry of Water Resource (MoWE, 2007e). Based on the FAO soil classification system, the study basin contains the soil types of Haplic Yermosols, Eutric Nitosols, Eutric Cambisols, Ferric Acrisols, and Calcaric Regosols soils, which covers about 41.4%, 40.3%, 13.1%, 3.7%, and 1.6%, respectively, of the total watershed.

4.2.2.4. Meteorological data

The required daily rainfall and temperature data for 33 years (1984 – 2016) were used to run the SWAT model. Due to the limitation on the availability of the minimum and maximum temperature data in the study basin, five stations (Arbgona, Bidere, Hager Selam, Haroklo, and Nghele) and rainfall data from ten stations (at Arbegona, Bore, Bidere, Hager Selam, Haroklo, Kibre Mengist, Neghele, Talamokentise, Woreka, and Yirba Muda) were collected from the Ethiopian National Meteorological Service Agency (NMA) Data from three locations (Arbegona, Bidere and Harokelo) were extracted from the Enhancing National Climate Services (ENACTS) dataset. It is a 4 x 4 km resolution dataset reconstructed by integrating data sources from records of local meteorological stations and satellite estimates from NASA (the US National Aeronautics and Space Administration) and EUMET-SAT (the European Organization for the Exploitation of Meteorological Satellites) (Dinku et al., 2014, 2016). The performance of ENACTS has been tested at various stations throughout the country and has proven to perform well (Alemayehu & Bewket, 2017; Dinku et al., 2014, 2016).

To make the series for further analyses, the missing values were generated and filled by multiple imputations using Fully Conditional Specification (FCS) implemented by the MICE (Multivariate Imputation by Chained Equations) algorithm as described in van Buuren & Groothuis-Oudshoorn (van Buuren & Groothuis-Oudshoorn, 2011). In addition, weather elements such as relative humidity, solar radiation, and wind speed were produced using ARCSWAT, WGNMarker 4. Then, the weather data were arranged in SWAT model format and used for simulation. The first three years of data, from 1984 to 1986 were used as the model initialization phase. The subsequent data, from 1987 to 2016, were used for SWAT analysis.

4.2.2.5. River flow data

The streamflow data for the periods of 1984 to 2011, measured at the Chenemassa hydrological station located at the watershed's outlet (Figure 4-1), was obtained from the Ministry of Water and Energy (MoWE). The missed values of streamflow data were estimated using the multiple imputation method. It is the best estimation of missing values (Sattari et al., 2017). Then the flow data were arranged according to SWAT requirement data format for model calibration and

validation. Flow data from 1987 to 2002 were used for model calibration, whereas independent data sets from 2003 to 2011 were used for model validation.

4.2.3. LULC analysis

To extract LULC data, cloud free (< 10%) dry season images of Landsat 5 TM (Thematic Mapper) and Landsat 8 OLI (Operational Land Imagery) were used. Landsat images were selected because NASA's Landsat missions provided free and extensive data on global coverage (since 1972) at a moderate to high level of resolution and the data has been widely used for detecting LULC changes (Alam et al., 2019).The Landsat imageries of a resolution of 30 m of 1986, 2001, and 2016 were collected from United State Geological Survey (USGS) Earth explorer available at htpp://EarthExplorer usgs.gov/ (Table 4-2.). To cover the entire area of the watershed, three satellites imageries with path/raw of 167/056, 168/055, and 168/056 were used. The imageries were selected based on historical drought events and availability of Landsat imageries. To minimize errors, due to different seasonal variation in vegetation distribution, in LULC change detection, images of the same annual season were used (Dibaba et al., 2020a; Kindu et al., 2013).

Table 4-2. Description of Landsat imagery.

Dataset	Resolution(m)	Path/raw	Imagery Acquisition Date
Landsat 5 TM imagery	30 m*30 m	167/056, 168/055 and 168/056	Jan 01, 1987; Jan 21, 1986 and Jan 05, 1986
Landsat 5 TM imagery	30 m*30 m	167/056, 168/055 and 168/056	Jan 26, 2002; Mar 03, 2001 and Mar 03, 2001
Landsat 8 OLI imagery	30 m*30 m	167/056, 168/055 and 168/056	Feb 02, 2016; Mar15, 2016 and Mar 15, 2016

Then, the downloaded images were preprocessed in ARC GIS 10.5. Preprocessing such as, georeferencing, geometric correction, compositing /layer stacking, mosaicking and clipping were done prior to image classification (Lillesand et al., 2015). During the pre-processing of satellite images, radiometric and geometric corrections were applied to the raw Landsat images. This approach produces the adjusted satellite images, which are radiometrically and geometrically corrected. Radiometric corrections are generally used to normalize the multi-temporal satellite

imageries for time series comparisons. For better interpretation of the scenes, local enhancement (data scaling and histogram equalization) was carried out (Lillesand et al., 2015). Once the preprocessing and mosaicking of the images were completed, the area of interest was clipped using the inbuilt raster processing tools in Arc GIS 10.5.

Image classification and accuracy assessment

In this LULC change analysis, to generate and classify the LULC maps, unsupervised and supervised techniques of classification were employed (Gashaw et al., 2018). The unsupervised method was done to generate initial information of the spectral characteristics of clustered pixels prior to the supervised classification (Lillesand et al., 2015). The supervised/ maximum likelihood classification technique was conducted to generate the land cover types using the training sites developed from ground truth data, Google earth, and 1975-topo maps of 1:250,000 scale from Ethiopian Geospatial Information Agency (EGIA).

Using the supervised classification Maximum Likelihood algorithm embedded in ARC GIS 10.5 software, images of the years 1986, 2001 and 2016 were classified based on average total of 360 training points gathered from the digital 1975-topo maps of 1:250,000 scale from EGIA, Google Earth, previous LULC maps, and ground based reference points. To determine the sampling points systematic purposive sampling method was used. With this regard, training point from the northern, middle, and southern parts of the study basin were collected. During the field work, at the time of ground truth data collection, in depth discussion with elders from the area, to recall the past land cover information, were conducted.

In the classification approach, seven major LULC classes such as built-up or settlement, cultivated land, shrubland, forest land, grassland, bare land, and waterbody were identified. Settlement or built-up areas, includes urban, road network, and rural residential areas such as villages and rural town; cultivated land, areas used to cultivate annuals rainfed and irrigated crops; shrubland, shrubland embraced shrubs, bush, short mixed dense vegetation, and lower height trees; forestland, land includes areas covered by dense natural forest, trees plantations, coffee and other dense vegetation; grassland, referred to communal and private owned grazing lands and also areas with sparse vegetations dominated with grass; bare land, areas covered with stones with very little

vegetation, exposed rocks and bare soil, and degraded areas found at a lower rivers and steep mountain sides and water body, referred to the main Genale river.

Once the land cover classifications were developed, the LULC maps of 1986, 2001 and 2016 were prepared. Then, by comparing the sample LULC class of the classified layer and the reference layer, the classification accuracy of the resulting LULC maps was assessed. To evaluate accuracy of 1986, 2001, and 2016 LULC maps, overall, producer's, user's accuracy and Kappa coefficient, assessment were computed using equation 1,2,3, and 4, respectively. The details described at Lillesand et al ((Lillesand et al., 2015).

$$\text{Overall accuracy} = \frac{\text{Total correctly classified pixels}}{\text{Total of classified pixels}} * 100 \ldots\ldots\ldots\ldots\ldots\ldots\ldots\ldots\ldots\ldots\ldots\ldots\ldots\ldots\ldots\ldots (1)$$

Overall accuracy is calculated by dividing the total number of correctly classified pixels (i.e., the sum of the major diagonal) by the total number of reference pixels.

$$\text{Producer accuracy} = \frac{\text{Number of correctly classified pixels per class}}{\text{Number of reference totals per class}} * 100 \ldots\ldots\ldots\ldots\ldots\ldots\ldots (2)$$

The value of the producer's accuracy indicates how well test set pixels of the given cover type are classified.

$$\text{User accuracy} = \frac{\text{Number of correctly classified pixels per class}}{\text{Number of classified totals per class}} * 100 \ldots\ldots\ldots\ldots\ldots\ldots\ldots\ldots\ldots\ldots (3)$$

The value of the user's accuracy is a measure of commission error that indicates the probability that a pixel classified into a given category actually represents that category on the ground.

$$\text{Kstat} = \frac{N \sum_{i=1}^{r} Xij - \sum_{i=1}^{r} (X_{RT} * X_{CT})}{N^2 - \sum_{i=1}^{r} (X_{RT} * X_{CT})} \ldots\ldots\ldots\ldots\ldots\ldots\ldots\ldots\ldots\ldots\ldots\ldots\ldots\ldots\ldots\ldots (4)$$

Where: Kstat is Kappa statistics, N is total number of samples, Xij is the product of total number of sample and total diagonal values, X_{RT} is row total, X_{CT} is the column total and r is the number of categories. The statistics or coefficient evaluates the difference between the actual agreement of classified map and chance agreement of random classifier compared to reference data(Minta et al., 2018). Overall LULC classification displayed on Figure 4-2 of the general conceptual framework of the research methodology.

To quantifies the percentage share, gains/ losses, and percentage change of each LULC classes, the areas of the LULC classes, area comparison analysis of LULCC of two classified LC maps (1986 to 2001, 2001 to 2016, and 1986 to 2016), and the percentage of LULC change were computed from the maps. The total gain or loss of LULCC and their percentage between the two periods is computed using Equation 5 and 6 as follows (Minta et al., 2018; Yesuph & Dagnew, 2019):

$$\text{Gain /Loss of LULCC=final year LULC area - initial year LULC area} \tag{5}$$

$$\text{LULCC (\%)} = \frac{(\text{LULC area of the final year - LULC area of the initial year})}{\text{LULC area of the initial year}} * 100 \tag{6}$$

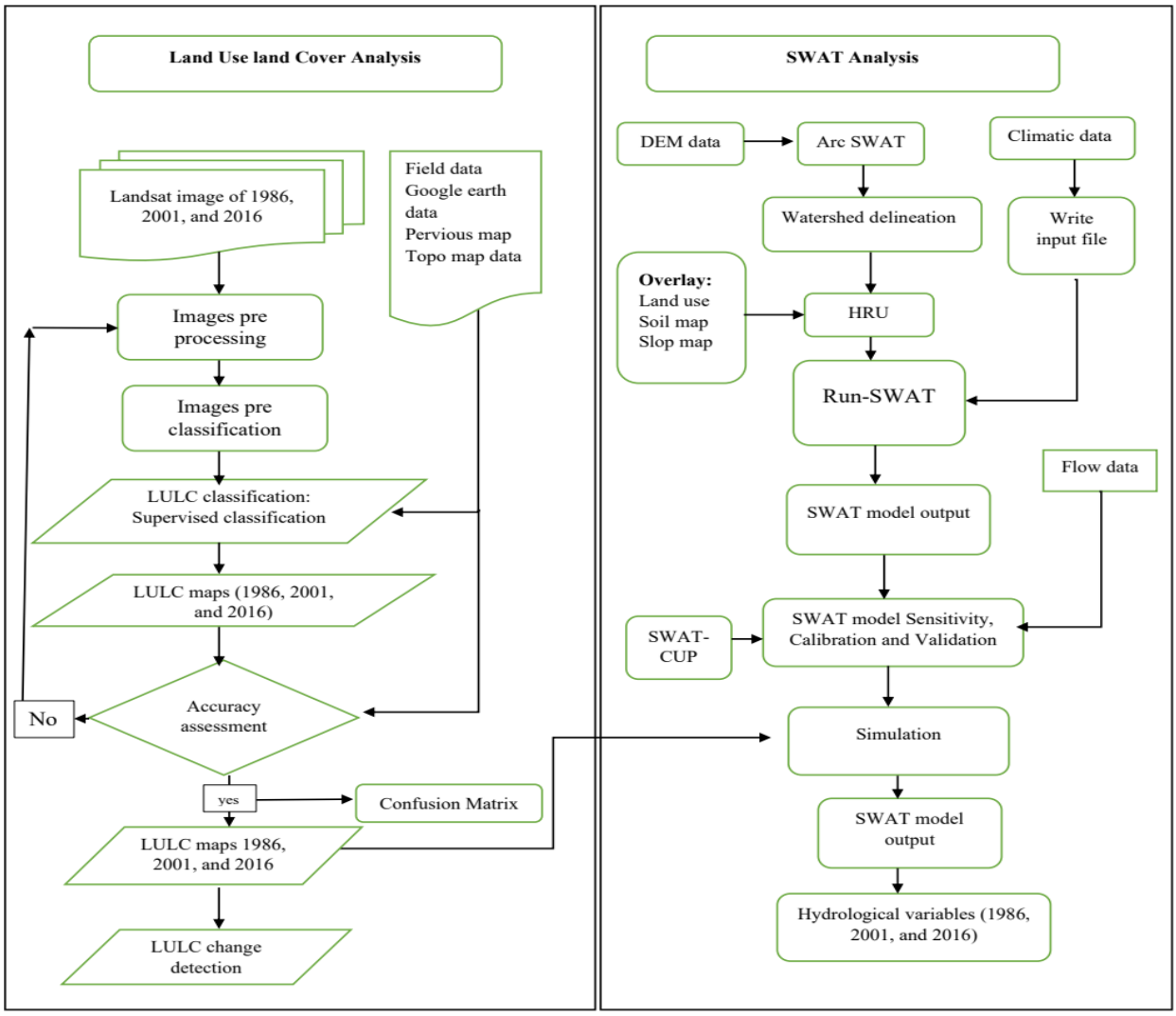

Figure 4-2. Conceptual framework of the research.

4.2.4. Description of the SWAT model set up

The Soil and Water Assessment Tool (SWAT) is a semi-distributed and physically based watershed model that runs at a continuous time-step (Arnold et al., 2012). It is developed to test and predict the impacts of change in land use practices and climate on hydrology, agricultural pollutant, sediment movement of large and complex basins (Arnold et al., 1998; Taylor et al., 2016). The SWAT simulate the hydrologic process of a watershed using two major ways: the land phase and the water or routing phase. The former, regulate the amount of water transported, chemicals, nutrients and sediment loading from the sub-watershed through the channel route, while

the latter controls the flow movement up to the basin outlet. Detailed information of the physical processes modelled within SWAT presented in (Neitsch et al., 2011). To simulate the hydrological processes of the watershed, In the land phase of hydrological cycle, the SWAT used the water balance equation described as follows (Narsimlu et al., 2015; Neitsch et al., 2011):

$$SW_t = SW_o + \sum \left(R_{day} - Q_{surf} - E_a - W_{seep} - Q_{gw}\right) \quad (7)$$

From equation 7, SW_0 and SW_t represents the initial and final soil water content on day i (mm), P_{day}, Q_{surf}, E_a, Q_{gw}, and W_{seep} represents the amount of precipitation, surface runoff, evapotranspiration, return flow, and water entering the vadose zone from the soil profile, respectively, on day i (mm), and t is the time (days).

The SWAT model calculates surface runoff from the watershed using either the USDA Conservation Service Curve Number (SCN-CN) method or Green and Amp method (Neitsch et al., 2011). For this study, to compute surface runoff for each HRU, the SCN-CN method was used (Equation 8) (Arnold & Fohrer, 2005).

$$\text{Rsurf} = \frac{(\text{Pday} - 0.2\text{S})^2}{(\text{Pday} + 0.8\text{S})} \quad (8)$$

Where, R_{surf} is depth of daily accumulated runoff (mm), S is a retention parameter, and Pday is the daily rainfall depth (mm). The above equation indicates that surface runoff in a watershed occurs when the value of the depth of rainfall in a day (Pday) is greater than 0.2S.

In terms of curve number (CN), the parameters S is computed by equation 9. The parameter S is affected by slope, types of soil, and land use management practices.

$$\frac{\text{S}}{25.4} = \left(\frac{1000}{\text{CN}} - 10\right) \quad (9)$$

According to Arnold et al. (Arnold et al., 2012), CN is significant parameter which determines the surface runoff of the catchment during the model calibration.

SWAT model has three option to compute evaporation, Hargreaves, Priestly-Taylor, and Penman-Monteith formulas as cited in Neitsch et al. (2011). The Hargreaves method, due to its simplicity and limited data availability, was used for calculating evapotranspiration.

4.2.5. Watershed delineation

To delineate the study basin, the SWAT model were set-up using the ARCSWAT install of the ARCGIS extension. Using the study area DEM and watershed outlet location point (at Chenemassa gauging station), the watershed, sub watershed, and reaches of the watershed of the upper Genale basin were delineated. With this delineation process, 21 sub-watersheds were defined (Figure 4-3).

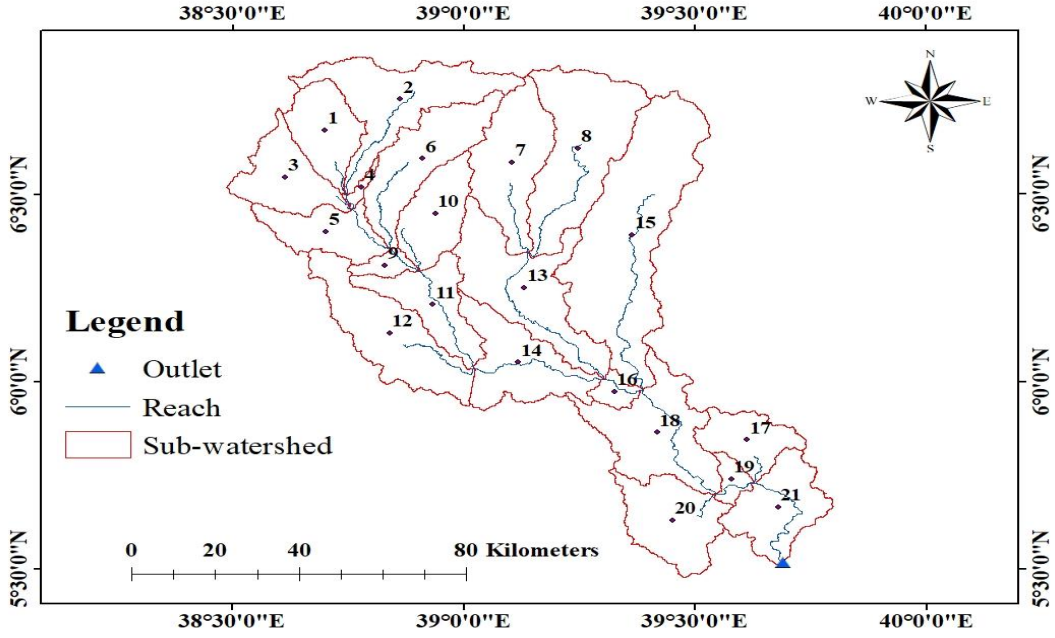

Figure 4-3. Sub-watershed of upper Genale river basin.

Then after watershed and their parameters had been determined, based on a combination of land cover map, soil map, and slope categories with a 10% threshold value, 352, 337 and 350 number of HRUs for the 1986, 2001, and 2016 LULC model, respectively, were created.

4.2.6. Model simulation and sensitivity analysis

The study area watershed hydrological processes were simulated using hydro-climatic data. The climate data from 1984 to 2016 periods were arranged according to the SWAT requirement format. Data from 1984 to 1986 were used to initialize the model, and the subsequent data from 1987 to 2016 were used for parameters sensitivity analysis and model calibration.

The SWAT model has a large number of hydrological parameters that affect streamflow, and calibrating them all is difficult and time-consuming. Therefore, identifying the more sensitive parameters that affect model output is valuable (Chimdessa et al., 2019). The parameter sensitivity analysis helps to detect the most influential flow parameters that are used for calibration and validation in the model (Abbaspour et al., 2018). To differentiate the most influential SWAT flow parameters in this study, twenty-one flow parameters from SWAT-CUP and literature were carefully chosen at the initial phase. Then, using multiple regression methods with Latin hypercube parameters of the objective function, t-stat and p-values, sensitivity of the parameters were determined. The t-stat and p-values indicate the degree and level of sensitivity to flow parameters. Which demonstrates that small absolute t-stat values indicate less sensitivity while large values indicate higher sensitivity. Smaller p-values indicate greater sensitivity, while larger values indicates less sensitivity (Abbaspour, 2015; Narsimlu et al., 2015).

4.2.7. SWAT model calibration and validation

For model calibration and validation, recorded daily river flow data at the Chenemasa hydrological station were used. The daily flow data was changed to monthly flow data and arranged according to the SWAT data format requirement for model calibration and validation. Model calibration was then executed using the monthly flow data series ranging from 1987 to 2002. Following the identification of calibrated flow parameters, validation was carried out using flow data ranging from 2003 to 2011. To execute calibration and validation processes, SUFI-2 (Sequential Uncertainty Fitting) algorithm in SWAT-CUP2012 version 5.1.6 were used (Abbaspour, 2015). SUFI-2 is a popular and extensively used program for model uncertainty, calibration, and validation analysis in different parts of Ethiopia (Abraham & Nadew, 2018; Bekele et al., 2021;

Birhanu et al., 2019; Bogale, 2021; Chimdessa et al., 2019; Dibaba et al., 2020b, 2020a; Gashaw et al., 2018; Takele et al., 2022; Tufa & Sime, 2020).

4.2.8. Model performance evaluation

The SWAT model's performance was evaluated by comparing the fitness of the output of the measured streamflow data to that of simulated model output. The statistical indices assess the closeness between the measured streamflow data and the corresponding simulated output. Hence, for this study, PBIAS (Percent of bias), R^2 (coefficients of determination), and NES (Nash-Sutcliffe efficiency) were used to evaluate the performance of the model.These statistical parameters are the most widely used model performance evaluation (Akoko et al., 2021; Shukla & Gedam, 2018). The performance indices of R^2, NSE, and PBIAS were calculated using equations 10, 11, and 12, respectively.

The regression coefficient (R^2) describe the degree of collinearity between the measured streamflow data and simulated output data (Moriasi et al., 2007). The calculated R^2 varies from 0 to 1. The closer the R^2 value to 1 indicates less error variance i.e., the agreement between the observed flow data and the simulated output is higher. Equation 10 is used to compute R^2.

$$R^2 = \left\{ \frac{\sum_{i=1}^{N}(Oi - \overline{O})(Pi - \overline{P})}{\left[\sum_{i=1}^{N}(Oi - \overline{O})^2\right]^{0.5}\left[\sum_{i=1}^{N}(P - \overline{Pi})^2\right]^{0.5}} \right\}^2 \quad (10)$$

The Nash-Sutcliffe efficiency (NSE) is a statistical index that is used to assess how much the model accurately simulated or to determine how the measured data and the simulated output closely fits in 1:1 line (Moriasi et al., 2007; Nash & Sutcliffe, 1970) and calculated as described in Equation 11.

$$NSE = 1 - \frac{\sum_{i=1}^{N}(Oi - Pi)^2}{\sum_{i=1}^{N}(Oi - \overline{O})^2} \quad (11)$$

The percent of bias (PBIAS) as explained in Moriasi et al.(Moriasi et al., 2007) was employed to determines how much is the simulated output to be smaller or larger than the measured counterparts. According to (Moriasi et al., 2007) the PBIAS was computed using as Equation 12.

$$\text{PBIAS} = \frac{\sum_{i=1}^{N}(oi - pi)}{\sum_{i=1}^{N}(oi)} * 100 \quad (12)$$

Where: Oi and Pi, is the measured and simulated flow value, respectively $\overline{O}$ and $\overline{P}$ is the average measured and simulated flow value, respectively.

According to Moriasi et al. (2007), the performance of the model is acceptable when the values of R^2 and NSE is greater than 0.6 ang 0.5, respectively, and the value of PBIAS is in the ranges of ±25%. The value of R^2 varies from 0 and 1, where R^2 approaches to 1 indicates less error. The value of NSE ranges from -∞ to 1. If NSE closer to one, the model performance is best. On the other hand, the closer the PBIAS value to 0 indicates best simulation. Positive values shows the model underestimates the simulation, where as a negative value shows the model overestimates the simulation (Nasiri et al., 2020).

4.2.9. Impacts of LULC change on hydrological processes

Understanding the hydrologic response of a watershed due to changes in land cover characteristics is imperative for managing water resource measures (Gashaw et al., 2018). To evaluate the hydrological process under the impacts of land cover modifications, the SWAT model was executed for the 1986 LULC, 2001LULC, and 2016LULC scenarios using the same climatic data from 1987-2016 periods. The study was carried out with the "fixing-changing" technique. The method works by changing the land cover input data while fixing the other data in the SWAT model, such as climatic, soil, and DEM data. This approach has been used by various scholars across the world (Awotwi et al., 2019; Gashaw et al., 2018; Gebremicael et al., 2019; Gyamfi et al., 2016). The effect of the LULC change on the basin's hydrologic characteristics and water resources was calculated by comparing SWAT outputs for LULC maps of (1986, 2001, and 2016). The differences in observed outputs represented the impacts of LULC change on hydrologic response and water resources in the catchment.

4.3. Results and Discussions

4.3.1. LULC Change dynamics

Based on spectral characteristics and Landsat image processing, seven land cover types were developed. The areal coverage and the spatial distribution of the 1986, 2001, and 2016 LULC classifications are depicted in Table 4-3 and Figure 4-4, respectively. The expansion of cultivated land and a significant reduction of forest land occurred in the highland area of the catchment. In addition, significant portions of grassland and bushland were found in the lower part of the catchment. Furthermore, the analysis in Table 4-3 and Figure 4-4 showed that in 1986, about 29.6% of the land was covered with forest, followed by cultivated land, shrubland, and grassland, which covered about 24.4%, 23.85%, and 21.8% of the total area, respectively. On the other hand, settlement, bare land, and water body were covered about 0.16%, 0.16%, and 0.06% of the total area, respectively. However, in 2001, cultivated land, settlement, and bare land coverage increased to 36.85%, 0.2%, and 0.3%, while forest, shrubland, and grassland decreased to 20.1%, 23.2%, and 19.3%, respectively. In 2016, settlement, cultivated land, and bare land further increased to 0.28%, 47.08%, and 0.62% while forest, shrubland and grassland decreased to 13.53%, 19.5%, and 18.9%, respectively (Table 4-3).

Table 4-3. LULC of the years 1986, 2001 and 2016.

LULC Type	SWAT code	1986 LULC		2001 LULC		2016LULC	
		Area coverage (ha)	%	Area coverage (ha)	%	Area coverage(ha)	%
Settlements	URBN	1731.78	0.16	2100.42	0.2	2939.4	0.28
Cultivated land	AGRL	257741.9	24.35	389986.3	36.85	498167.6	47.08
Shrubland	SHRB	252403.7	23.85	245208.2	23.17	206725.8	19.53
Forest land	FRST	312945.6	29.57	212807.7	20.11	143124.4	13.53
Grassland	GRAS	230954.8	21.82	204505.7	19.33	199965.2	18.9
Bare land	BARR	1740.06	0.16	2997.27	0.28	6587.37	0.62
Water body	WATR	701.46	0.06	613.62	0.06	709.38	0.067
Total		1058219	100	1058219	100	1058219	100

SWAT code = URBN= settlement, AGRL=cultivated land, SHRB= shrubland, FRST= forest land, GRAS- grassland, BARR= bare land and WATR= water body.

During the last three decades, between 1986 and 2016, the Upper Genale basin experienced a substantial alteration in major LULC. Cultivated land, settlement and bare land had all been

increasing in a continuous manner. In contrast, forest, shrubland, and grassland coverage decreased, possibly as a result of growth in population and increased demand for agricultural production. The finding of this study agrees with the studies by (Aredo et al., 2021; Messele & Moti, 2019) in Genale Dawa basin.

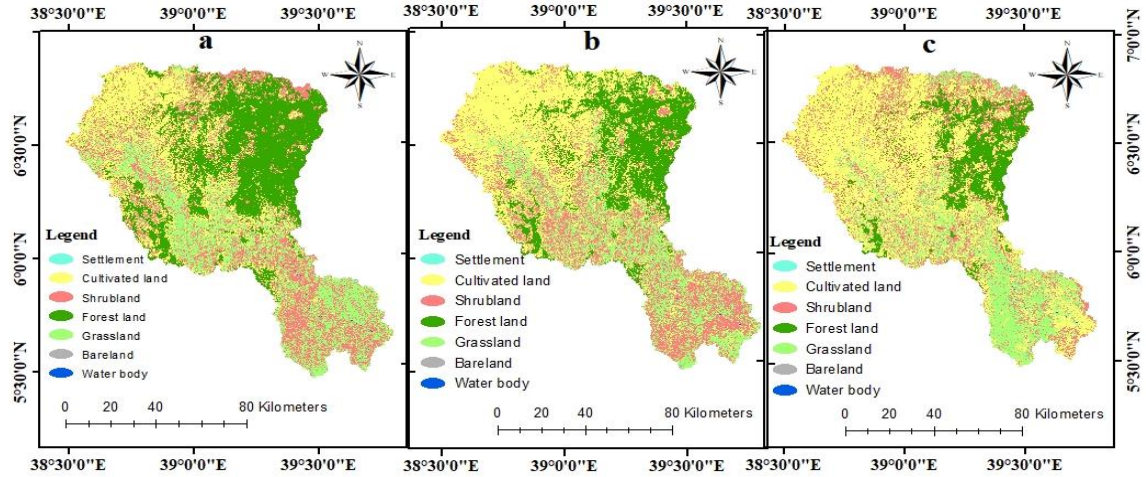

Figure 4-4. LULC of 1986 (a), 2001(b), and 2016 (c) periods of the study basin.

The LULC investigation revealed that the rate and pattern of change varied significantly across land uses and study time periods. Between 1986 and 2001, cultivated land increased by 51.3%, and between 2001 and 2016, it increased by 27.7%. Between 1986 and 2001, and 2001 and 2016, about 132,244.4 ha and 108,181.4 ha of land cover were converted into agricultural land, with annual average rate of 8816.3 ha and 7212.1 ha, respectively. However, between 1986 to 2001, the coverage of forest, grass, and shrublands were reduced by 32%, 11.45%, and 2.85%, respectively. Between 2001 and 2016, forest, grass, and shrublands further decreased by 32.7%, 2.2%, and 15.7%, with rate of 4645.6 ha, 302.7 ha, and 2565.5 ha per year, respectively. Between 1986 to 2001 and 2001 to 2016 study periods, bare land expanded rapidly at a rate of 72.3% and 119.8%, respectively. Throughout the study period (1986 -2016), the area of cultivated land, settlement area, and barren land increased by 93.3%, 69.7%, and 278.6%, respectively. Through these same periods, the coverage of forestland, shrubland, and grassland reduced by 54.3%, 18.1%, and 13.4%, respectively (Table 4-4. and Figure 4-5).

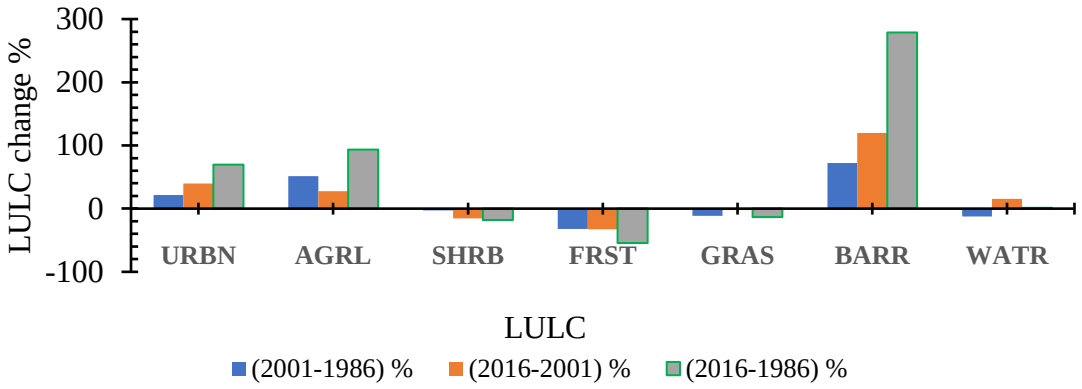

Figure 4-5. Pattern of LULC changes percentage from 1986 to 2016.

Table 4-4. LULC conversion between the study years and corresponding annual rates.

LULC	(2001-1986)			(2016-2001)			(2016-1986)		
	Gain/loss of Area(ha)	%	Annual rate(ha)	Gain/loss of Area(ha)	%	Annual rate(ha)	Gain/loss of Area(ha)	%	Annual rate(ha)
URBN	368.6	21.29	24.6	838.98	39.9	55.9	1207.62	69.7	40.25
AGRL	132244.4	51.31	8816.3	108181.4	27.7	7212.1	240425.7	93.3	8014.19
SHRB	-7195.5	-2.85	-479.7	-38482.4	-15.7	-2565.5	-45677.9	-18.1	-1522.6
FRST	-100137.9	-32.0	-6675.9	-69683.3	-32.7	-4645.6	-169821	-54.3	-5660.71
GRAS	-26449	-11.45	-1763.3	-4540.5	-2.2	-302.7	-30989.5	-13.4	-1032.98
BARR	1257.2	72.25	83.8	3590.1	119.8	239.3	4847.31	278.6	161.58
WATR	-87.8	-12.52	-5.9	95.76	15.6	6.4	7.92	1.1	0.26

LULC = Land Use Land Cover, URBN= settlement, AGRL=cultivated land, SHRB= shrubland, FRST= forest land, GRAS- grassland, BARR= bare land and WATR= water body.

Table 4-5, 4-6, and 4-7 shows the detection of LULC modification and LULC the transitional matrix for each LULC. The totals in the column (Table 4-5) correspond to land cover values in 1986, while the totals in the row relate to land cover classifications in 2001. The proportion of the corresponding land cover that remained under its original cover is represented by the diagonals of the change matrix.

From 1986 to 2001, about 57.2% of the total LULC remained unchanged in 2001, and about 42.8% of the total LULC areas were converted to other types. The transition matrix analysis also revealed that in 2001, approximately 83.6%, 68.5%, 52.3%, 58.8%, 47.4%, 54.1%, and 87.5% of settlement, cultivated land, shrubland, forestland, grassland, bare land, and water bodies remained unchanged. As it can be inferred from Table 4-5, about 36.5% of grassland, 19% of shrub, 25.8% of forest, and 26.3% of bare land were converted into cultivated land between 1986 and 2001.Study by

Babiso et al. (2016), in the Wallecha watershed, in southern Ethiopia indicated that the transformation of forestland, grassland, and shrubland into agricultural land is primarily related with the need for more cropland to fulfill the food demands of an expanding population and the loss of soil productivity due to unsustainable crop farming techniques.

Table 4-5. LULC change matrix between the years 1986 and 2001(ha).

LULC	URBN	AGRL	SHRB	FRST	GRAS	BARR	WATR	Total
URBN	**1437.38**	212.16	257.07	44.11	69.42	80.28	0	2100.42
AGRL	0	**176442**	47956.69	80708.75	84421.64	457.22	0	389986.29
SHRB	194.03	36822.83	**132139**	40941.48	34906.79	169.42	34.3	245208.15
FRST	0	12389.38	15144.22	**184046**	1227.94	0	0	212807.7
GRAS	0	31139.38	56906.34	6911.79	**109457**	91.31	0	204505.74
BARR	100.37	736.04	0.03	293.41	872.05	**941.83**	53.54	2997.27
WATR	0	0	0	0	0	0	**613.62**	613.62
Total	1731.78	257741.91	252403.65	312945.57	230954.76	1740.06	701.46	1058219

LULC= Land Use Land Cover, URBN= settlement, AGRL= cultivated land, SHRB= shrubland, FRST= forest land, GRAS- grassland, BARR= bare land and WATR= water body.

According to the change matrix between 2001 and 2016, about 57.54% of total land cover remained under its original cover in 2016 (Table 4-6). In addition, in 2016, approximately 97.4% of settlements, 78.1% of cultivated land, 33.3% of shrubland, 49.7% of forestland, 55.7% of grassland, 61.7% of bare land, and 100% of water bodies remained unchanged. Furthermore, Table 4-6 also showed that cultivated land expanded significantly, primarily at the cost of shrubland (35.2%), grassland (29%), and forest land (22.3%).

Table 4-6. LULC change matrix between the years 2001 and 2016(ha).

LULC	URBN	AGRL	SHRB	FRST	GRAS	BARR	WATR	Total
URBN	**2046.52**	350	107.6	63.42	288.36	83.5	0	2939.4
AGRL	53.9	**304712.54**	86313.27	47473.17	59306.66	308.1	0	498167.64
SHRB	0	56938.04	**81030.44**	48130.57	20383.99	242.73	0	206725.77
FRST	0	16769.41	10543.95	**105713.8**	10097.23	0	0	143124.39
GRAS	0	8836.4	66206.2	11401.14	**112986.9**	534.6	0	199965.24
BARR	0	2379.9	936.53	0	1442.6	**1828.34**	0	6587.37
WATR	0	0	70.16	25.6	0	0	**613.62**	709.38
Total	2100.42	389986.3	245208.2	212807.7	204505.7	2997.27	613.62	1058219.19

LULC= Land Use Land Cover, URBN= settlement, AGRL= cultivated land, SHRB= shrubland, FRST= forest land, GRAS- grassland, BARR= bare land and WATR= water body.

Table 4-7. LULC change matrix between the years 1986 and 2016(ha).

LULC	URBN	AGRL	SHRB	FRST	GRAS	BARR	WATR	Total
URBN	**1325.65**	447.7	507.56	86.78	546.91	24.77	0	2939.4
AGRL	98.5	**190414.36**	93389.33	114225.2	99856.25	184	0	498167.64
SHRB	129.63	33809.59	**82632.5**	59459.66	30694.39	0	0	206725.77
FRST	0	3443	14617.95	**106401.5**	18661.94	0	0	143124.39
GRAS	0	27496.18	60061.69	32500.95	**79666.4**	240.02	0	199965.24
BARR	178	2131.08	1186.7	271.48	1528.84	**1291.27**	0	6587.37
WATR	0	0	7.92	0	0	0	**701.46**	709.38
Total	1731.78	257741.91	252403.65	312945.57	230954.76	1740.06	701.46	1058219.19

LULC = Land Use Land Cover, URBN= settlement, AGRL=cultivated land, SHRB= shrubland, FRST= forest land, GRAS- grassland, BARR= bare land and WATR= water body.

During the last 30 years (1986–2016), the magnitude and direction of LULC transformation had varied continuously and substantially in the study basin. From 1986 to 2016, about 43.7% (462441.8ha) of the total land cover remained the same as it was in 1986, while the remaining 56.3% (595777.4ha) shifted to another land cover class (Table 4-7). Cultivated land expanded significantly at a rate of 8014.2ha per year during this time period. From the totals covered in 1986, approximately 37.2% (93389.33ha) of shrubland, 43.2% (99856.25ha) of grassland, and 36.5% (114225.2ha) of forest land were shifted to cropland. As a result, it is clear that the most dynamic land cover classes were forest, shrubs, and grass land, which mostly converted to cultivated land. In the same way, settlement and bare land coverage also expanded during the study period. Each of these land cover types are heavily influenced by land form, soils, and climate properties as in the rest of Ethiopia. Natural vegetation cover, particularly forest land, is being heavily encroached by cultivated lands as a result of high population growth, followed by people's and the government's preferences for food and export crops in order to alleviate the prevailing food and employment insecurity (MoWE, 2007d). Various studies in Ethiopia revealed that settlement areas and cultivated lands were replacing forest, shrub, and grass lands (Hassen & Assen, 2018; Mathewos et al., 2019; Meshesha et al., 2016; Shawul & Chakma, 2019). Similarly, LULC changes were also reported by different scholars in different parts of Genale Dawa basin (Aredo et al., 2021; Ayele et al., 2019; Hailemariam et al., 2016; Messele & Moti, 2019). For instance, Hailemariam et al. (2016) reported a total loss of 123,751 ha forests and an expansion of cultivated land by 292.294 ha in 30 years period at Bale mountains eco-region. The increasing demand of land for built-up and cultivation, the demand for fuel wood and fodder, institutional and policy

changes regarding land resource management, an absence of adequate technology to enhance farming practices for socioeconomic purposes and income generation all contributed to land use conversion, primarily the destruction of natural vegetation (Dibaba et al., 2020a; Hassen & Assen, 2018). According to (Hailu et al., 2020) and (Betru et al., 2019), the main reasons for land cover changes mainly the conversion of forestland, shrubland, grassland into settlement, cultivated, and bare land are poverty, population growth, unemployment, lack of off-farm employment, institutional and policy changes, low level of awareness on natural resource conservation and managements, lack of proper execution of legal and institutional frameworks related to natural resources managements. The Genale Dawa master plan report (MoWE, 2007d) showed that LULC changes in the basin mainly influenced with fast growth rate of population, occurrence of recurrent drought, shortage of cultivated land, illegal utilization forest resources, and inclination of the government policy to implement different land and water resource development activities.

4.3.2. Accuracy assessment of LULC images

The accuracy of the 1986, 2001, and 2016 classified images assessed by calculating the kappa coefficients, the user's, producer's, and overall accuracy. Table 4-8 displays the summarized LULC classification accuracy of the 1986, 2001, 2016 periods. Based on the error matrix, the overall accuracy of the classified images of the 1986, 2001, and 2016 were 85.3%, 87%, and 90.05%, respectively. The findings revealed that the overall accuracy found from the classified images exceeded the minimum recommended accuracy of 85% (Anderson et al., 1976).

Table 4-8. Accuracy assessment of the 1986, 2001 and 2016 classified images.

Classified Data (1986)	Reference Data								
	URBN	AGRL	SHRB	FRST	GRAS	BARR	WATR	Total	User accuracy (%)
URBN	**22**	2	0	0	0	0	0	24	91.7
AGRL	3	**52**	1	0	6	5	0	67	77.6
SHRB	0	3	**49**	4	2	0	1	59	83.1
FRST	0	0	7	**61**	0	0	0	68	89.7
GRAS	0	7	1	0	**47**	2	0	57	82.5
BARR	3	2	0	0	2	**25**	**0**	32	78.1
WATR	0	0	0	0	0	0	**39**	39	100
Total	28	66	58	65	57	32	40	**346**	
Producer accuracy (%)	78.6	78.8	84.5	93.8	82.5	78.1	97.5		
Overall accuracy = 85.3%; Kappa statics=82.5%									
Classified Data (2001)									
URBN	**41**	0	0	0	2	1	0	46	89.1
AGRL	2	**48**	3	0	5	3	0	59	78.7
SHRB	0	3	**42**	3	4	0	0	51	80.8
FRST	0	0	8	**59**	0	0	0	68	88.1
GRAS	1	5	0	0	**45**	1	0	52	86.5
BARR	1	2	0	0	2	**43**	0	48	89.6
WATR	0	0	1	0	0	0	**36**	37	97.3
Total	45	58	54	62	58	48	36	**361**	
Producer accuracy (%)	91.1	82.8	77.8	95.2	77.6	89.6	100		
Overall accuracy = 87%; Kappa statics=84.7%									
Classified Data (2016)									
URBN	**46**	1	0	0	0	2	0	49	93.9
AGRL	2	**53**	1	0	9	2	0	67	79.1
SHRB	0	1	**44**	0	1	0	0	46	95.7
FRST	0	0	5	**59**	0	0	0	64	90.8
GRAS	0	7	0	0	**54**	0	0	61	88.5
BARR	5	0	0	0	1	**41**	0	47	87.2
WATR	0	0	0	0	0	0	**38**	38	100
Total	53	62	50	59	65	45	38	**372**	
Producer accuracy (%)	86.8	85.5	88	100	83.1	91.1	100		
Overall accuracy = 90.05%; Kappa statics=88.3%									

URBN= settlement, AGRL=cultivated land, SHRB= shrubland, FRST= forest land, GRAS-grassland, BARR= bare land and WATR= water body.

These results show that about 85%, 87%, and 90% of the LULC classes were precisely classified. For the 1986, 2001, and 2016 periods, the kappa statics were 82.5%, 84.7%, and 88.3%, respectively; indicating that the agreement between the identified LULC classes and the

geographical data is strong. According to (Viera & Garrett, 2005), kappa value higher than 0.8 represents a strong agreement, whereas values ranging from 0.61 to 0.8 indicates a very good agreement. The user accuracy of individual classes for 1986, 2001, and 2016 ranges from 77.6% for cultivated land and 100% for water body. In these same years, the producer accuracy ranging from 77.6% for grass land and 100% for forest land and water body.

4.3.3. Sensitivity analysis

For model calibration and validation, the key parameters that affect the streamflow in the SWAT model were identified using sensitivity analysis (Arnold et al., 2012). Throughout the simulation period, the SWAT-CUP software, SUFI-2 algorithms were used to determine the most significant flow parameters. The sensitivity of the stream flow was calculated using average monthly streamflow data for 25 years (1987–2011) recorded at the Chenemassa hydrological station. During the initial phase of the process, twenty-one flow parameters were carefully selected from the SWAT-CUP and the literature. Out of these initially selected parameters, ten sensitive flow parameters were identified based on the t-stat value (ranging from 7.86 to 0.65) and the p-value (ranging from 0 to 0.5) (Table 4-9).

Table 4-9. Identified sensitive flow parameters of the study area.

Parameter Name	Description	Ranking	t-Stat	P-Value
ALPHA_BF.gw	Baseflow alpha factor (days)	1	7.86	0
CN2.mgt	SCS runoff curve number	2	-3.15	0
CANMX.hru	Maximum canopy storage (mm H2O)	3	2.68	0.01
GWQMN.gw	Threshold depth of shallow water aquifer	4	-1.25	0.21
CH_K2.rte	Effective hydraulic conductivity (mm/h)	5	-1.14	0.25
REVAPMN.gw	Threshold depth of water in the shallow aquifer for “revap” to occur (mm)	6	-0.99	0.32
SOL_AWC(..).sol	Available water capacity of the soil	7	-0.92	0.36
RCHRG_DP.gw	Deep aquifer percolation fraction	8	-0.78	0.44
ESCO.hru	Soil evaporation compensation factor	9	-0.7	0.49
GW_DELAY.gw	Groundwater delay (days)	10	-0.65	0.51

Among the identified parameters, the ALPHA_BF.gw, the runoff SCS curve number, CN2.mgt and CANMX.hru were found to be the three most sensitive parameters with respect to streamflow.

CN2,mgt is the most influential flow parameter in most Ethiopian watersheds (Tufa & Sime, 2020).

4.3.4. Model calibration and validation

The SWAT model was calibrated and validated using the identified key sensitive flow parameters (shown in Table 4-9) on the measured streamflow data at Chenemassa station. During the process, the monthly streamflow data from 1987 to 2002 and from 2003 to 2011 were used for model calibration and validation, respectively. To improve the performance of the model during calibration, the selected parameters were changed iteratively within a realistic range until a reasonable agreement between observed and simulated streamflow output was obtained (Table 4-10). Then, after obtaining a reasonable result, the validation was performed using the same set of calibrated flow parameters. During the processes, multiples calibration runs had been caried out and finally the calibration range and their corresponding best fitted values were obtained and presented in Table 4-10.

Table 4-10. Final calibration parameters and their fitted value for the SWAT model.

	Min Value	**Max Value**	**Calibrated Value**
ALPHA_BF.gw	0	1	0.74
CN2.mgt	-0.2	0.2	0.0136
CANMX.hru	0	50	15.3
GWQMN.gw	1250	2150	1755.13
CH_K2.rte	0.01	100	58.7
REVAPMN.gw	0	250	1.875
SOL_AWC(..).sol	0	1	0.0325
RCHRG_DP.gw	0	1	0.0075
ESCO.hru	0	1	0.277
GW_DELAY.gw	30	450	52.05

4.3.5. Performance evaluation

The statistical indices of the performance of model calibration and validation results are summarized and presented in Table 4-11. In this table, the two indices, the P-factor and the R-factor, are expressed. Together they show the model calibration's strength as well as the uncertainty

assessment of the simulation results (Abraham & Nadew, 2018). The percentage of observation bracketed by the 95% prediction uncertainty (95PPU) was 88% for calibration and 81% for validation periods. The R-factor is a measure of the width of the 95PPU band that is determined by dividing the 95PPU average thickness by the measured variable of the standard deviation (Abbaspour et al., 2018). The calculated R-factor showed that 1.02, and 0.87 during the calibration and the validation periods, respectively. According to (Abbaspour, 2015), the closeness of the P-factor and the R-factor is used to assess the goodness of calibration and prediction uncertainty. The value of P-factor should ideally be 1, representing 100% bracketing of the measured data, hence capturing or accounting for all the correct processes, while R-factor value should ideally be close to 0, hence matching with the measured data (Abbaspour, 2015).

Furthermore, Table 4-11 also shows additional information on the statistical valuation results of the model calibration and validation periods for mean monthly flow. The result demonstrated that the statistical indices of R^2, NSE, and PBIAS of the SWAT model performed well. Accordingly, the SWAT model result showed a good match between observed and simulated monthly flow with NSE of 0.73 and 0.72 for model calibration and validation periods, respectively. The R^2 result also showed that the model has good agreements between observed and simulated streamflow, with values of 0.78 and 0.74 during the calibration and validation period, respectively.

Table 4-11. Summary of statistical values of calibration, validation and uncertainty of streamflow modeling.

Statistical Parameters	Calibration	Validation
P-factor	0.88	0.81
R-factor	1.02	0.87
R^2	0.78	0.74
NSE	0.73	0.72
PBIAS	-3.2	3.9
Mean Observed discharge (m3/s)	101.63	98.42
Mean Simulated discharge (m3/s)	104.95	94.59

The PBIAS value for the model was -3.2% for the calibration periods, and 3.9% for the validation periods, respectively. The result indicated that the flow during calibration with reference to the observed flow slightly over estimated. On the other hand, during the validation period, the value of the PBIAS indicated that the SWAT model underestimated the simulated flow.

The simulated and observed streamflow hydrographs of the calibrated model displayed that the SWAT model underestimated the peak streamflow of August 1993 and 1996, November, 1997, and July, September and October, 1998 in the calibration period, while on the validation period, the model underestimated most of the simulated streamflow (Figure 4-6).

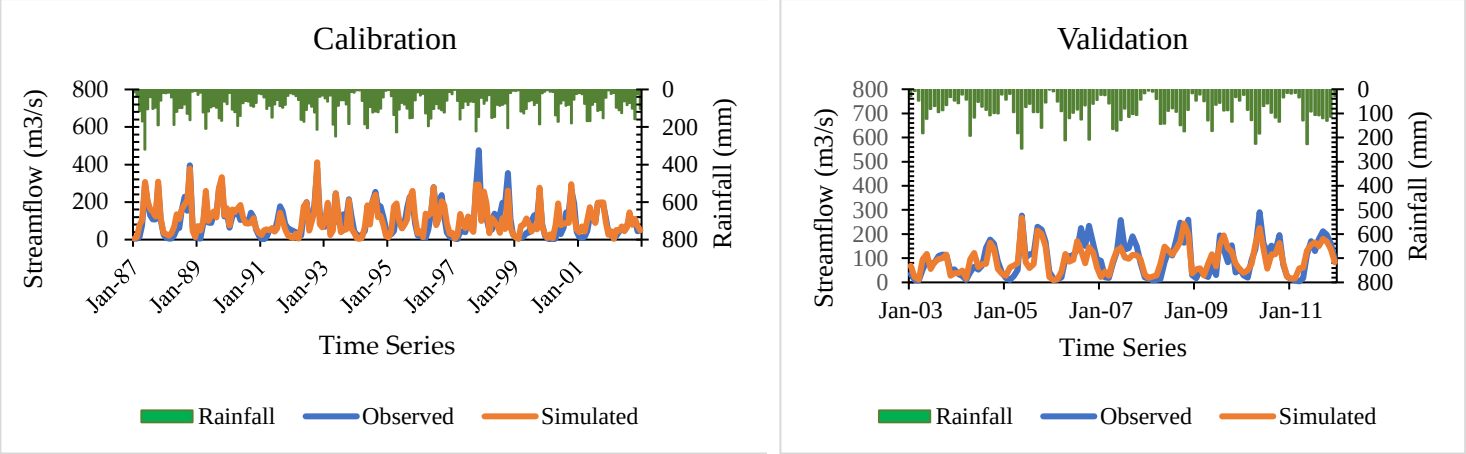

Figure 4-6. Streamflow hydrograph of observed and simulated model's calibration and validation.

Figure 4-7 depicts the scattered plot of the linear regression of measured and simulated flow of model calibration and validation. The result revealed that the coefficients of determination (R^2) for the calibration and validation periods were 0.78 and 0.74, respectively. This indicates a good relationship between the observed and simulated streamflow graphs (Figure 4-6).

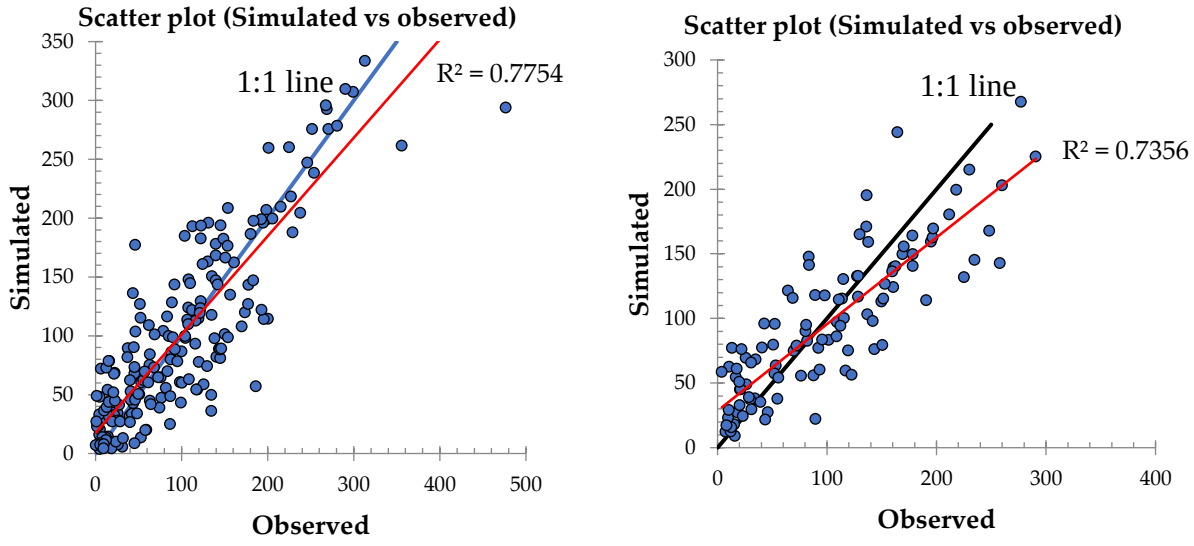

Figure 4-7. Scatter plot of measured and simulated streamflow; left panel shows the calibration period and right panel shows validation period.

Overall, based on the statistical metrics of R^2, NSE, and PBIAS, the SWAT model findings indicated that the measured and simulated monthly streamflow were in a good agreement in the study area river basin. Previous research conducted in the Genale Dawa and the surrounding river basin showed that the calibrated and validated SWAT model values of R^2 and NSE statistical indices ranged from 0.6 to 0.90 and from 0.55 to 0.90, respectively (Belihu et al., 2020; Negewo & Sarma, 2021; Roba et al., 2021; Shawul et al., 2013). For instance, research conducted by (Negewo & Sarma, 2021) in the Genale Dawa basin showed that during calibration and validation, the value of NSE was 0.81 and 0.78, and the value R^2 was 0.87 and 0.85, respectively. As a result, the SWAT model is appropriate for further application in understanding the hydrological component and quantifying the potential impacts of LULC change on water resource in the study watershed.

4.3.6. Effect of land use land cover change on hydrological process

Based on the simulated precipitation, runoff, evapotranspiration, lateral flow, ground water flow, and water yield of the SWAT models, the hydrological responses to the 1986, 2001, and 2016 LULC models were examined and presented in Table 4-12.

Table 4-12. Average annual water balances components for 1986, 2001 and 2016 LULC periods.

Hydrological fluxes	**1986 LULC**	**2001LULC**	**2016 LULC**	**Percent change (%)**		
	(mm)	**(mm)**	**(mm)**	**1986-2001**	**2001-2016**	**1986-2016**
Precipitation	1060.25	1060.25	1060.25			
Surface Runoff	139.87	159.03	171.57	13.7	7.9	22.7
Lateral Flow	38.68	37.92	36.08	-1.96	-4.85	-6.72
Ground Water flow	145.46	141.31	138.34	-2.85	-2.10	-4.89
Evapotranspiration	692.49	676.76	670.34	-2.27	-0.95	-3.20
Potential Evapotranspiration	1699.68	1699.68	1699.68			
Total Water Yield	324.42	339.63	347.32	4.69	2.26	7.06

The results during the 1986 to 2001 periods showed the annual average runoff in the watershed increased from 139.87 mm to 159.03 mm, and in 2016 it further increased to 171.57 mm, which indicated that there was a 13.7% and 7.9% increment of surface runoff between 1986 to 2001 and 2001 to 2016. The model output also showed that between 1986 and 2016, surface runoff increased

by about 31.7 mm, which shows 22.7% increment. Similarly, during the 1986 to 2001 periods, the annual total water yield of the study basin has raised from 324.42 mm to 339.63 mm, and to 347.32 mm in 2016. Evidently, this is related to the expansion of settlement, agriculture, and bare land area and the diminishing of forestland, bushland and grassland throughout the study period, which has a direct influence on total water yield and runoff. In comparison to a degraded land and cultivated land, the presence of vegetation on a given landscape allows to increases infiltration depth and initial abstraction, this allows for more recharge in a given watershed (Aredo et al., 2021).

A number of studies in various parts of Ethiopia have witnessed the same results as this one (Aredo et al., 2021; Belihu et al., 2020; Gashaw et al., 2018; Haregeweyn et al., 2015; Messele & Moti, 2019). For example, study by (Aredo et al., 2021) in the Genale Dawa basin, in the Shaye Catchment, showed that the increase in cultivated land and built-up areas, as well as a continuous depletion of natural vegetations contributed to the production of higher runoff in the watershed. Similarly, another study by (Messele & Moti, 2019), in the Weib catchement, in the Genale Dawa river basin, concluded that the rapid alteration of vegetation cover such as grass, shrubs, and forestland to agricultural and settlement areas resulted in more runoff. Another study in the Lake Ziway watershed by (Abraham & Nadew, 2018) showed that the change in land cover from 1996 to 2014 increased annual runoff from 67.5 mm to 129.1 mm and from 40.6 mm to 59.6 mm in the Katar and Meki river basins, respectively. The finding indicated that the land use alteration are the primary causes to increased surface runoff in both watersheds.

Furthermore, the analysis result showed that, during 1986, 2001 and 2016 LULC model, 13.2%, 14.99%, and 16.2% of the basin precipitation converted to surface runoff, while 692.49 mm, 676.76 mm, and 670.34 mm of the precipitation is lost by ET, which is about 65.3%, 63.8%, and 63.2% of precipitation, respectively. These results indicated that the reduction in ET in the watershed was related to the reduction of forest coverage. Moreover, ground water and lateral flow have declined from 145.46 and 38.68 mm in 1986 to 141.31 and 37.92 mm in 2001, and then to 138.34 and 36.08 mm in 2016, respectively. On the other hand, compared to the earlier historical LULC data of 1986 and 2001, the recent land cover of 2016 yields higher runoff and water yield and lower ground water and lateral flow. During the entire period (1986 to 2016), ground water flow reduced from 145.46 mm to 138.34 mm.

In general, the occurrence of LULC change over the last 30 years (1986–2016) resulted to increase mean annual runoff and total water yield, as well as a reduction in groundwater flow, lateral flow, and evapotranspiration in the watershed. However, the rate of increase and decrease of hydrological components were associated with the rate of LULC changes. For instance, the rate of vegetation reduction (forest, shrub, and grassland) and agricultural expansion during 1986–2001 were higher than 2001–2016. Consequently, the rate of increase in surface runoff and total water yield was higher during the 1986–2001 period compared to the 2001–2016 periods. The reduction of groundwater recharge and the increase in surface runoff are linked with the expansion of agricultural land as well as a significant reduction in vegetation cover. The reduction of forest cover reduced the soil infiltration capacity, which resulted in a large portion of rainfall being converted to runoff, which caused a decline in groundwater and lateral flow. Furthermore, the reduction of evapotranspiration is related to the decline of forest cover and a shortage of soil moisture (Dibaba et al., 2020b).

The monthly distribution of simulated precipitation, runoff, evapotranspiration and water yield in Figure (4-8), showed that, the highest values of monthly average surface runoff, evapotranspiration, and water yield were noted during the two main rainy seasons, which run during March, April, and May and September, October, and November. The larger values of runoff, evapotranspiration, and water yield found during these seasons were associated with the substantial amounts and rainfall patterns during the rainy season. Study by (Bekele et al., 2021) confirmed that the amount and pattern of rainfall is the most influential aspect in the hydrologic process.

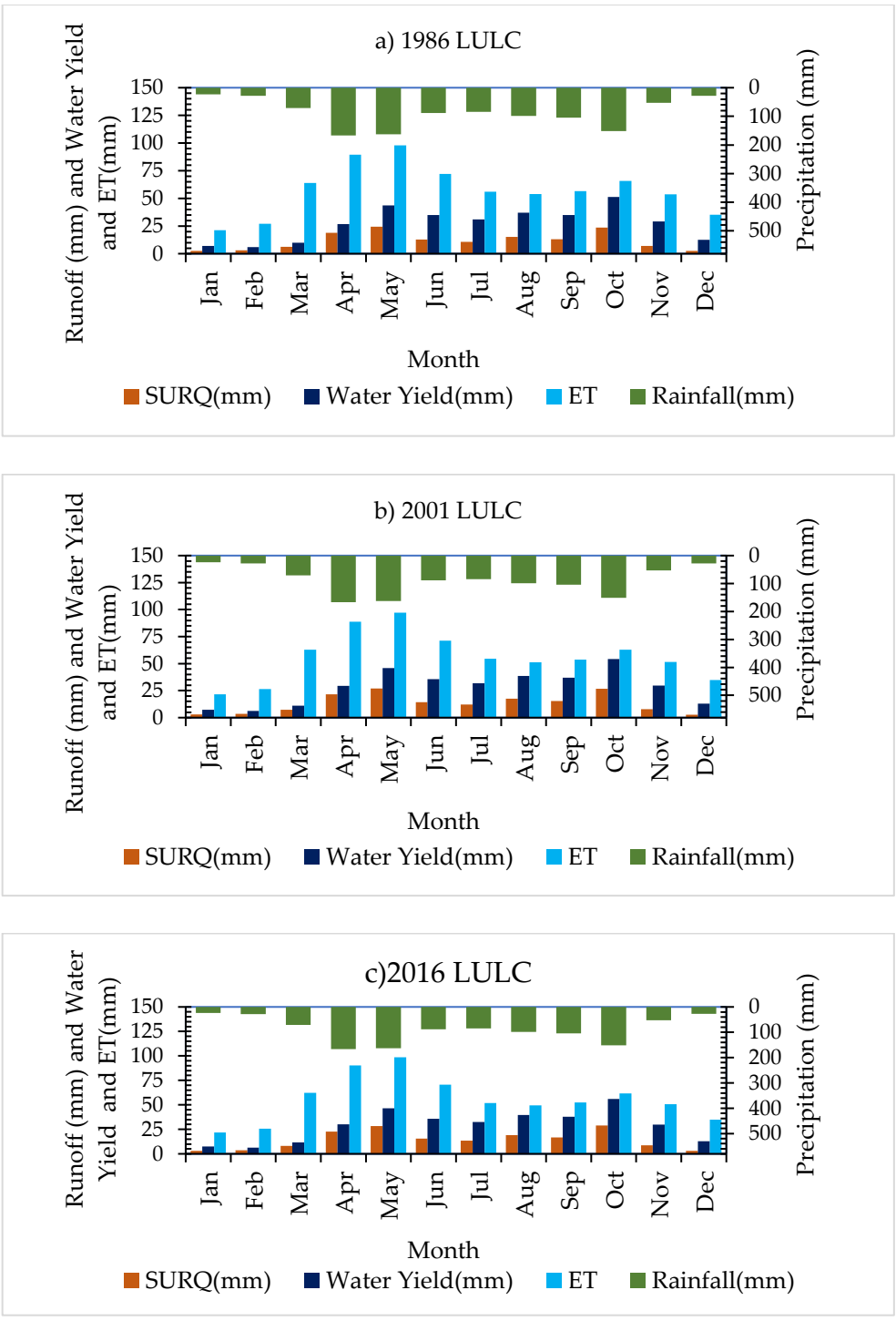

Figure 4-8. Monthly distribution of simulated precipitation, runoff, evapotranspiration, and water yield of LULC for (a) 1986, (b) 2001, and (c) 2016.

The spatial distribution of the water-balance components for 1986, 2001, and 2016 LULC models at sub basin scale presented in (Figure 4-9 – 4-11). The illustrations help in understanding the hydrologic components of the watershed. At the sub basin scale, during 1986, 2001, and 2016 LULC model, the annual average runoff in the Upper Genale River basin varied from 7.75 mm to 427.51 mm, 7.53 mm to 443.09 mm, and 9.72 mm to 476.65 mm, respectively (Figure 4-9). The Figures also depicted, sub basin 20 contribute the least amount of runoff whereas sub basin 5 produced the highest amount of runoff. In the 1986, 2001, and 2016 LULC model, annual mean surface runoff increased in the majority of the sub basins. The observed land cover change over the past 30 years has resulted in changes in runoff and other hydrological components.

The annual evapotranspiration of the sub basin varied 581.06 mm to 968.37 mm, 563.61 mm to 895 mm, and 582.21 mm to 856.14 mm, during 1986 LULC, 2001 LULC, and 2016 LULC models (Figure 4-10). The Figure also further depicted that, sub basin 15 contributed the height amount of evapotranspiration, this is due to the fact that sub basin 15 covered with significant amount of vegetation. A study by (Nicholls et al., 2019) confirmed the rate of evapotranspiration was highest in areas covered with forest than in other land covers. Furthermore, the annual average water yield at the sub basin level varied from 11.35 mm to 985.77 mm, 11.3 mm to 986.89 mm, and 13.93 mm to 983.99 mm during 1986, 2001, and 2016 LULC model, respectively (Figure 4-11).

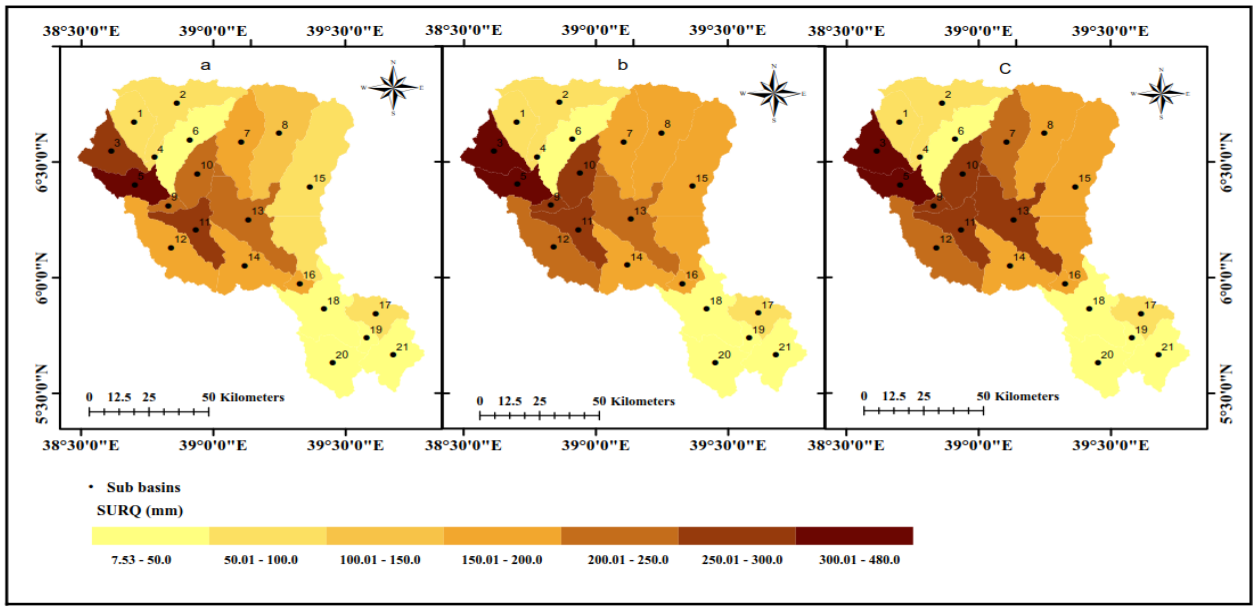

Figure 4-9. Simulated spatial distribution of runoff for (a) 1986, (b) 2001, and (c) 2016 LULC scenario.

.

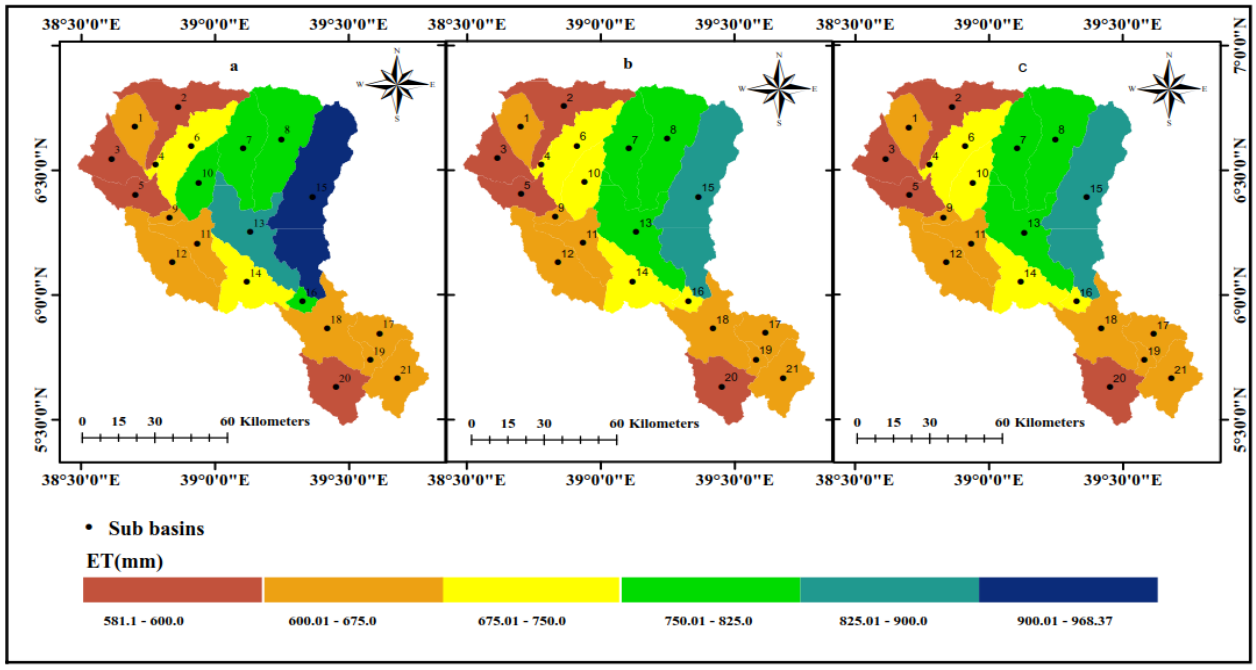

Figure 4-10. Simulated spatial distribution of evapotranspiration for (a) 1986, (b) 2001, and (c) 2016 LULC scenario.

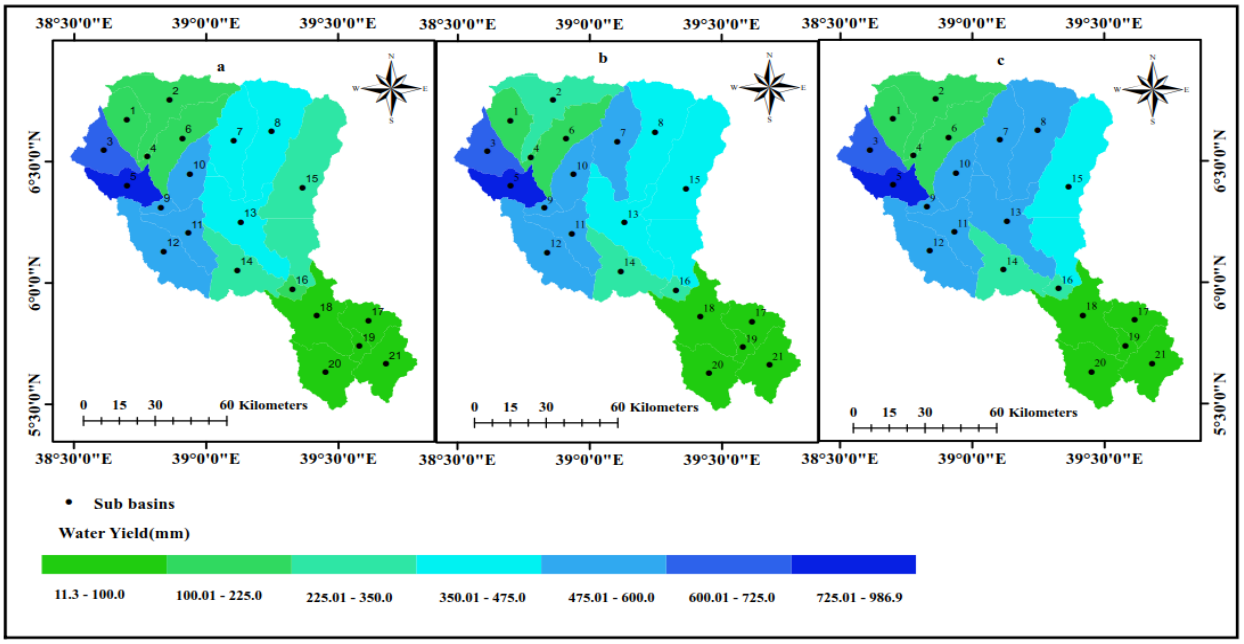

Figure 4-11. Simulated spatial distribution of water yield for (a) 1986, (b) 2001 and (c) 2016 LULC.

Overall, the reduction of vegetation cover in the land scape, as well as an increase in cultivated land, settlement area, and barren land, have a substantial impact on the hydrologic processes in the study basin. A research review by Negese (2021) indicated that in Ethiopia during the last forty years, due to the alteration of natural vegetation (grassland, forestland, and shrubland) into built-up area and agricultural land, the mean annual streamflow, surface runoff, sediment yield, soil erosion rate has increased. On the contrary, the observed changes have decreased the ground water recharge, ground waterflow, and evapotranspiration.

4.4. Summary and Conclusion

A physically, continuous, semi-distributed SWAT model was used to understand the hydrological processes of the Upper Genale river basin over three different LULC periods (1986, 2001, and 2016). The SUFI-2 algorithm in the SWAT-CUP2012 software was executed for model calibration, validation, and sensitivity analysis. The performance of the model calibration and validation were evaluated using R^2, NSE, and PBIAS statistical parameters and monthly measured streamflow data. Flow data from 1987 to 2002 and 2003 to 2011 were used for calibration and validation, respectively.

During the sensitivity analysis, it was discovered that the ground water and hydrologic response parameters were the most sensitive to streamflow than other parameters. During the calibration period, the performance indicators of R^2, NSE, and PBIAS were 0.78, 0.73, and -3.2%, respectively, while during the validation period, the values of R^2, NSE, and PBIAS were 0.74, 0.72, and 3.9%, respectively. The performance of the model calibration and validation showed that the evaluation results were acceptable. Hence, the SWAT model performed well and is applicable to simulating hydrological processes in the study basin.

The image analyses during the 1986, 2001, 2016 period in the upper Genale river basin showed that the extent of settlement, cultivated land, and barren land area significantly increased by 93.3%, 69.7%, and 278.6%, respectively. On the contrary, forestland, shrubland, and grassland diminished by 54.3%, 18.1%, and 13.4%, respectively. These continuous and dynamic modifications of LULC had a substantial effect on the watershed hydrology of the study area The expansion of settlement, cultivated, and bare land and the reduction of vegetation cover (grassland, shrubland, and

forestland) during the 1986 to 2016 periods caused an increase in the annual runoff and water yield. On the other hand, the observed land cover changes decreased groundwater and lateral flow. The hydrological responses of LULC for the 1986, 2001, and 2016 models showed that the average annual runoff increased by 13.7% and 7.9% between 1981 to 2001 and 2001 to 2016. Similarly, between 1986 to 2001 and 2001 to 2016, the annual total water yield increased by 4.69% and 2.26% in the study watershed, respectively. The model output also exhibited that between 1986 and 2016, surface runoff increased by about 31.7 mm, which is a 22.7% increment. Moreover, during the 1986, 2001 and 2016 LULC models, about 43.2%, 47.01%, and 49.6% of runoff contributed to the total flow. The model also showed that ground water and lateral flow contributions were reduced through the entire study period. Evidently, this result is clearly associated with the declining vegetation cover, as well as the expansion of settlement/built-up, agriculture, and degraded land in the watershed, which have had a direct influence on hydrological processes. Additionally, forest ecosystems play important roles in hydrological processes, especially in providing controls to groundwater recharge. The large decrease in forest cover observed in the region could alter changes in the patterns of recharge. The increase in total water yield and surface runoff along with the declining of groundwater and lateral flow due to land use and land cover changes has broader implications for managing and developing water resource and the environment. In this respect, assessing and understanding of watershed hydrologic characteristics are significantly important for water resource planners and managers. Furthermore, it will assist them in establishing decision support systems connected to land and water use spatial planning for sustainable development in the watershed and working on policy concerns. Therefore, understanding the hydrologic characteristics of a basin under the influence of LULC changes is crucial to develop and apply a land and water resource development plan and management strategies for those areas.

Besides the aforementioned facts, the result of this study confirmed the SWAT model's applicability for modeling hydrological characteristics of a river basin. Hence, the findings of this research help to improve the understanding of the available water resource potential as well as plan, manage, and develop the water resources for current and future development projects across the study area. In general, the study results indicated that the impact of LULC modification on hydrological variables is significant. As a result, natural resource managers, policymakers, and stakeholders will be better able to design and implement effective and sustainable land use

planning and water resource management. Furthermore, the results and approach of this study can be used in the future as a guide for the Genale-Dawa River basin and other regions that have similar land use and climatic conditions. To improve the result, we recommend further studies in the study basin to generate more detailed information for modeling work by taking into account different hydrological models, high-quality hydro-meteorological data, and soil management.

CHAPTER FIVE:

5. ASSESSING THE IMPACTS OF CLIMATE CHANGE ON HYDROLOGICAL PROCESSES IN THE UPPER GENALE RIVER BASIN, ETHIOPIA

Abstract

The aim of this research is to assess the impact of future climate change on hydrological parameters (e.g., precipitation, temperature, etc.) in Ethiopia's upper Genale river basin. Future climate scenarios for the 2021–2050 and 2051–2080 periods were developed from four different GCM–RCM combinations of CORDEX-Africa projections using the RCP 4.5 and RCP 8.5 (Representative Concentration Pathways). These climate models were bias corrected and used as input to the Soil and Water Assessment Tool (SWAT) model. During the 2030s (2021–2050) and 2060s (2051–2080) under the two RCPs, the projected precipitation in the annual and seasonal periods tends to decrease while temperatures increase. The simulated result revealed a significant change in hydrological components (e.g., During the 2060s), under the RCP4.5 scenario, CNRM-CM5 climate model runoff, ground water flow, and total water yield increased by 24.4%, 27.98%, and 28.56%, respectively. On the contrary, during the 2060s under the MIROC5 climate model, runoff, ground water flow, and total water yield reduced by 20.84%, 34.34%, and 25.8%, respectively. The annual hydrological components of the study area under MPI-ESM-LR, EC-EARTH, and MIROC5 showed a decrease in total water yield, surface runoff, ground waterflow, and lateral flow. However, due to a rise in temperature, evapotranspiration showed an increase up to 8.1% under all climate models (MPI-ESM-LR, EC-EARTH, CNRM-CM5, and MIROC5). The reduction in rainfall, which coincides with rising temperatures, is expected to reduce annual water yield, surface runoff, ground waterflow, and lateral flow by up to 39.8%, 39%, 50%, and 40.1%, respectively, across MPI-ESM-LR, EC-EARTH, and MIROC5 scenarios for the entire study basin in future projections. Our study helps to give a better insight into understanding climate change in watershed and can benefit the planning of water resources by strengthening adaptation strategies against the impacts of future climate change.

Keywords: Upper Genale river basin, Climate change, Regional climate models, Hydrological processes, SWAT model.

5.1. Introduction

Emissions of greenhouse gases (GHGs) into the atmosphere have increased since the pre-industrial era, primarily due to the expansion of intensive agriculture, industrialization, the utilization of fossil fuels, and urbanization (Hussain et al., 2018; IPCC., 2014; S. Shrestha, 2014). Changes in GHG concentrations in the atmosphere primarily tend to raise the temperature (Syukuro, 2019). The change in climate has caused the mean temperature to rise across the globe. Since the 1900s, it has risen by about 0.8 °C, and by the end of the 21st century, it is expected to rise by 1.4–2.0 °C (IPCC, 2013). A warmer climate accelerates and changes the hydrological cycle, causing long term changes in evapotranspiration, rainfall, and runoff volume and timing, and resulting in negative impacts on natural water resources in a catchment (Dariane & Pouryafar, 2021; Ketema & Dwarakish, 2021b).

Climate change has also had an effect on natural and human systems all over the world (IPCC., 2014). The extent of the adverse impacts, however, varies substantially across continents, countries, and socioeconomic strata, due to the adverse direct impacts on national GDP growth, food security, and low adaptive and high exposure capacity to climate change. The impacts are far more severe for African countries in general, and Ethiopia in particular (Asfaw et al., 2018; Bewket et al., 2015; Dosio et al., 2022; EPCC, 2015; Girvetz et al., 2019; IPCC., 2014; Serdeczny et al., 2017).

Climate change has negatively affected Africa in several ways (Godfrey & Tunhuma, 2020; Welborn, 2018). This includes increased frequency and severity of natural disasters, decreased rainfall amount and distribution, and exacerbated existing water stress. All of these have significant impact on the functional operation of existing water resource development projects, ecological systems, and agricultural development (Chaemiso et al., 2016; Emiru et al., 2022). Moreover, frequent occurrences of hydrological extremes and high rainfall variability, along with rapidly growing populations and alarmingly increasing food and water demands, have an effect on the health and livelihoods of Africans (Dibaba et al., 2019).

Throughout the world numerous studies on the impact of climate change on hydrological responses have been undertaken (Awotwi et al., 2021; Bekele et al., 2019; Bekele et al., 2021; Birkinshaw et al., 2017; Eisner et al., 2017; Galata et al., 2021; Lotfirad et al., 2021; Mengistu et al., 2020;

Näschen et al., 2019; Takele et al., 2022; Tessema et al., 2021; Worku et al., 2021; Worqlul et al., 2018; Zhang et al., 2018). Many of these studies found that climate change influenced and will continue to negatively affect the hydrologic characteristics of a catchment. For instance, Näschen et al. (2019) analyzed the impacts of climate change on water resources in Tanzania's Kilombero Catchment. They reported that the mean annual water yield and surface runoff increased by 61.6% and 67.8%, respectively. Studies undertaken in other regions (e.g., Yangtze basin of China), which used the Representative Concentration Pathways (RCP 8.5) scenario revealed that the annual basin discharge changes from -29.8 to +16.0% (Birkinshaw et al., 2017). Changes in the magnitude and pattern of temperature, rainfall, and climate on both local and global scales affect the rate and occurrence of hydrological characteristics in a basin (Daba & You, 2020).

Climate change is also having a negative effect on water resources in Ethiopia, a largely rain-fed agricultural region in Africa. The impact is primarily caused by shifting rainfall patterns, rising temperatures, and increased atmospheric water demand (Bewket,et al., 2015). Temperature rise as well as alterations in precipitation patterns are two of the most important climate change variables that have a direct impact on almost all other hydrologic processes (Daba & You, 2020; Ketema & Dwarakish, 2021b; Musie et al., 2020; Tessema et al., 2021). A study by Daba and You (2020) in Ethiopia's upper Awash basin revealed that changes in temperature and rainfall under both RCP4.5 and RCP8.5 scenarios for all future periods (2020s, 2050s, and 2080s) are expected to affect surface runoff, streamflow, and total water yield within the basin. Climate change also has an impact on water resource planning and management through changes in the amount and seasonal patterns of flows in streams (Musie et al., 2020). Hence, assessing the effect of climate change on water resources at the small and large watershed scales by combining climate and hydrological models is essential for understanding climate change vulnerability and designing ecologically sound water resource management strategies.

Even though various studies of the impact of climate change on hydrologic analysis have recently been carried out in various parts of Ethiopia using high-resolution ensembles of regional climate predictions generated by Coordinated Regional Climate Downscaling Experiment (CORDEX) (Bekele et al., 2021; Daba & You, 2020; Eromo et al., 2016; Galata et al., 2021; Ketema & Dwarakish, 2021b; Mengistu et al., 2020; Tessema et al., 2021; Worqlul et al., 2018), in depth scientific studies on the quantitative impact of climate change on water resources based on the

RCP have not been conducted in the study basin. Furthermore, studying climate change impact on hydrological variables, particularly total water yield, surface runoff, groundwater flow, and evapotranspiration, by using hydrological models and downscaled climatic data are crucial for arid and semi-arid regions. Water resources mainly runoff and streamflow, are extremely impacted by climate change. A minor change in climate variables can cause significant changes in hydrological components and, as a result, changes in regional water resources (Daba & You, 2020). Moreover, hydrological characteristics vary by location, and the effects of climate change on hydrology vary greatly across regions (Abeysingha et al., 2020); hence, it is vital to conduct such study in arid and semi-arid regions in order to develop and implement sustainable management of scarce water resources and appropriate climate change adaptation and mitigation strategies (Galata et al., 2021; Musie et al., 2020; Worqlul et al., 2018).

Therefore, this study was mainly designed to evaluate climate change impact on hydrological processes over the study area of the upper Genale river basin. The Genale River is a multi-purpose river on which different water-based projects have been implemented. The projects include many proposed and existing hydropower power plants, small- and large-scale irrigation schemes, and fish farming at the different parts of the river. The basin is characterized by a variety of topographic and climatic regimes. Knowledge of the impact of climate change on hydrological characteristics in a river basin is important for planning prospective climate change adaptation as well as mitigation actions. Additionally, the results of this research may be used to develop and execute new strategies for efficient water resource management, utilization, and development in order to prevent water scarcity in the area. Therefore, this study was undertaken with the aim of evaluating the hydrological characteristics of the upper Genale river basin under the effect of climate change using the SWAT model and the CORDEX-Africa Regional Climate Model (RCM) under RCP4.5 and RCP8.5 climate scenarios.

5.2. Materials and Methods

5.2.1. Study area description

The Genale Dawa basin is located in Ethiopia's southern region and includes parts of the regional states of Oromia, Somali, and Southern Nations, Nationalities, and Peoples' (SNNP) (Figure 5-1).

The basin has an approximate area of 172,713 km^2. Geographically, it lies North of 3°30' - 7° 20' latitude and East of 37° 05' - 43° 20' longitude (Awulachew et al., 2007; MoWE, 2007c)(Figure 5.1). The upper Genale River, the study basin, is found in the upper central area of the Genale Dawa river basin. It has an area of approximately 10,582.19 km^2 and is situated between North of 6° 52' and 5° 28' latitude and East of 38° 30' and 39° 45' longitude (Figure 5-1).

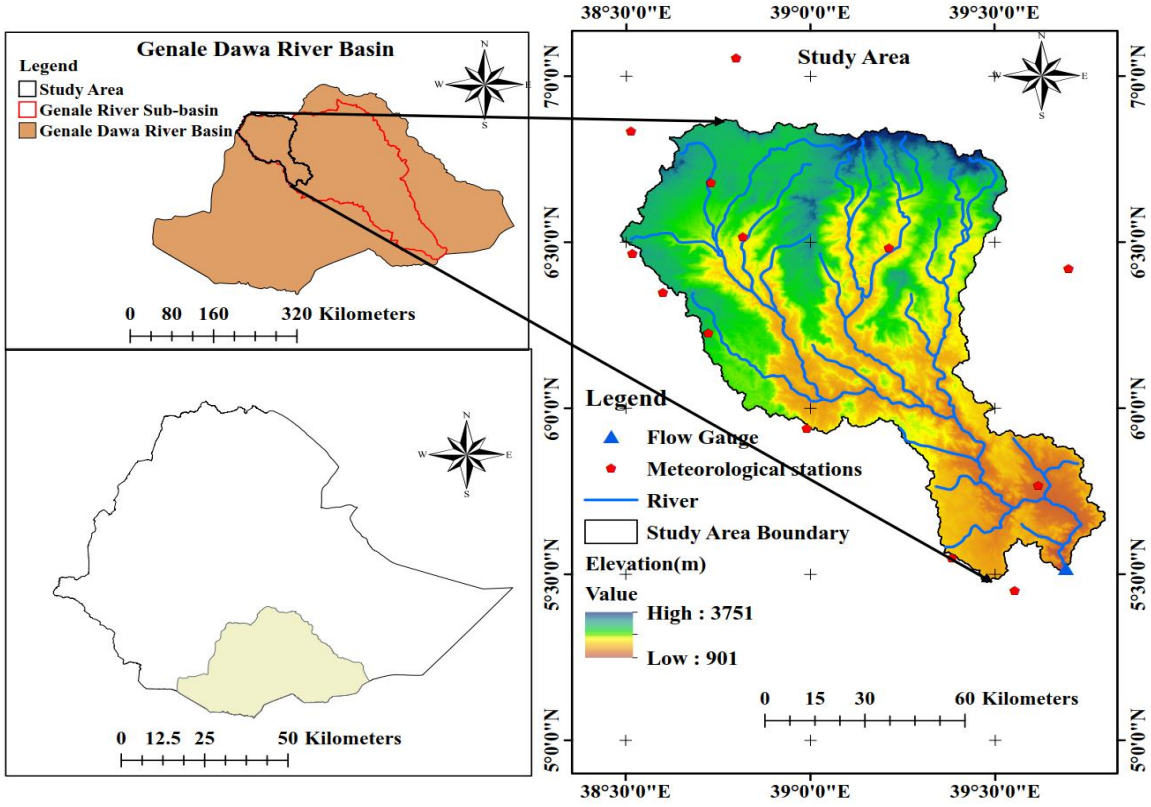

Figure 5-1. Study area Map

The basin has a three-season type I bimodal annual rainfall cycle in the highlands (northern parts) and a double dry and wet season type II in the lowlands (southeastern). The three wet seasons are known locally as *Belg* (March, April, and May), *Kiremt* (June-September), and *Meher* (September, October, and November)(MoWE, 2007c). The double wet season in the southern and southeastern parts is from March to May and from September to November (Degefu et al., 2021; MoWE, 2007)**.** The annual mean rainfall, minimum and maximum temperatures range from 1617.7 mm to 591 mm, 6.9 to 16.2 ^{o}C, and 18.9 to 27.7^{o}C, respectively (Shigute et al., 2023).

5.2.2. Input data

Input Data for SWAT Model

To assess the SWAT model performance and the effect of climate change on the hydrologic characteristics of the watershed, spatial and temporal data were used.

5.2.2.1. Spatial data

A digital elevation model (DEM) was used to determine the basin boundary, sub-basins, sub-basin characteristics of the watershed (e.g., elevation, slope gradient, river network, reach length, and channel slope), and the hydrologic response unit. The USGS website was used to obtain the Shuttle Radar Topography Mission (SRTM) DEM of the study basin with a 30m horizontal resolution. The elevation band of the processed DEM ranges from 901 to 3751 m (Figure 5-1).

Land Use Land Cover

LULC is one of the factors that have the greatest impact on hydrological variables in a river basin, and it is used in the SWAT model to determine HRUs and hydrologic characteristics. To assess the hydrological components of the study basin under the effects climate changes, the classified LULC map of the study watershed was obtained from Shigute et al., (2022). The details of image analysis and classification results at (Shigute et al., 2022), showed that the dominant categories are cultivated land (47%), shrubland (19.53%), forest land (13.53%) and grassland (18.9%) of the watershed. The settlement, bare land and water body areas covered a smaller portion of the watershed.

Soil data

A soil map of the Upper Genale river basin affecting the hydrologic characteristics of the watershed was obtained from FAO and extracted using ARCGIS 10.5 software. The SWAT database was used to extract soil physicochemical properties such as hydrologic group, texture, depth, bulk density, erodibility, hydraulic conductivity, and organic matter content. Furthermore,

the soil survey report of the Genale Dawa river basin master plan developed by Ethiopia's Ministry of Water Resources was used to verify and compare the necessary soil physical and chemical properties extracted from the SWAT database (MoWE, 2007e). The soil types in the study area includes Calcaric Regosols (1.6%), Ferric Acrisols (3.7%), Eutric Cambisols (13.1%), Eutric Nitosols (40.3%), and Haplic Yermosols (41.4%).

5.2.2.2. Temporal data

Climate data

To run the SWAT model, daily rainfall data (1984–2016) for ten stations and minimum and maximum temperature data for five stations were used (Table 5-1). Due to the limitation of climate data in the study area, ten stations of rainfall data and five stations of minimum and maximum temperature data (Negehle, Harokelo, Hager Selam, Bidere, and Arbgona) were obtained from the National Meteorological Agency of Ethiopia (NMA). Data for the Harokelo, Bidere, and Arbegona locations were extracted from the ENACTS dataset. The dataset, which has a resolution of 4 x 4 km, was constructed by combining data from satellite estimates from NASA (the US National Aeronautics and Space Administration) and EUMET-SAT (the European Organization for the Exploitation of Meteorological Satellites) with station records from nearby locations (Dinku et al., 2014, 2016). The effectiveness of ENACTS has been evaluated at numerous stations across the nation, and it has turned out to be effective (Alemayehu & Bewket, 2017; Dinku et al., 2014, 2016).

The Multivariate Imputation by Chained Equations (MICE) algorithm as explained in van Buuren & Groothuis-Oudshoorn, (2011) was used to generate and fill the missing values, and then the data was used for further analyses. To ensure the data's quality and reliability, homogeneity tests were performed. The standard normal homogeneity test (SNHT) (Alexandersson, 1986), the Buishand range test (Buishand, 1982), the Von Neumann ratio test (von Neumann, 1941), and the Pettitt test (Pettitt, 1979) were the four absolute statistical homogeneity tests used. The details of the analysis results in Shigute et al. (2023) showed that the data were homogeneous and could be used for further analyses.

In addition, the ARCSWAT weather generator (WGNMarker 4) was used to generate weather elements such as wind speed, relative humidity, and solar radiation. The model was then initialized

using weather data from 1984 to 1986. The SWAT analysis was then performed on data from 1987 to 2016.

Table 5-1. Summary of the study area meteorological stations and their geographical locations.

Name of Stations	Latitude (N°)	Longitude (E°)	Altitude (m)	Rainfall Period	Temperature Periods
Telamokentise	6°50'1"	38°30'38"	1911	1990-2016	
Yirba Muda	6°13'17"	39°35'43"	2560	1987-2016	
Woreka	6°30'6"	39°12'45"	2450	1987-2016	
Bore	6°20'30"	38°38'29"	2712	1984-2016	
Kibre Mengist	5°53'46"	38°58'1"	1680	1984-2016	
Bidere	5°46'19"	39°36'46"	1400	1984-2016	1984-2016
Arbegona	6°40'48"	38°43'30"	2600	1984-2016	1984-2016
Harokelo	5°33'19"	39°23'17"	1600	1984-2016	1984-2016
Hager Selam	6°30'47"	38°31'18"	2809	1984-2016	1984-2016
Neghele	5°26'1"	39°35'43"	1544	1984-2016	1984-2016

Flow data

For model calibration and validation, the daily stream flow data recorded at Chenemassa gauging station from 1984 to 2011 was collected from the Ethiopian Ministry of Water and Energy (MoWE). To estimate missing values, multiple imputation was used, which is the best method for estimating missing values in flow data (Sattari et al., 2017).

5.2.3. GCM-RCM and scenario selection

To assess future climate change impacts on the hydrologic characteristics of the study watershed, future precipitation and temperature data from CORDEX Africa RCMs were obtained from the ESGF website (https://esgdn1.nsc.liu.se/esgf). For this study, three different RCMs (KNMI Regional Atmospheric Climate Model, version 22 (RAMO22 T), Rossby Center regional atmospheric model (RCA4), and Regional Climate Limited-area modeling (CCLM)) and four downscaled GCM driving models (EC-EARTH, CNRM-CM5, MIROC5, and MPI-ESM-LR) of CMIP5 (Climate Model Inter-comparison Project Phase 5) were used in combination. These resulted in four GCM-RCM combinations of CORDEX-Africa projections under two RCPs (4.5 and 8.5) (Table 5-2), which were used for impact assessment. The details of the two RCPs

scenarios are explained by the IPCC (IPCC, 2014).The choice of the GCM-RCM model was made in consideration of other studies of the effects of climate change on east Africa, particularly in various regions of the Ethiopia river basin, as well as how well the climate models represent past and present climate, their resolution, and other related factors (Adera & Alfredsen, 2020; Adugna et al., 2021; Bekele et al., 2021; Ketema & Dwarakish, 2021b; Mengistu et al., 2020; Musie et al., 2020; Tessema et al., 2021; Worku et al., 2020b).

The spatial resolution of the CORDEX-Africa domain is 0.44° by 0.44°, which is about 50 km by 50 km. The data covers from the years 1951 to 2100, with a historical time frame from 1951 to 2005 and a future projection from 2006 to 2100 (Musie et al., 2020). In this study, to assess the change in patterns of climate data, the baseline scenario period (1987-2016) and the future scenario period (2021-2100) were used. The future scenarios were divided into two different periods of time with 30-year intervals, such as 2021-2050 (the 2030s) and 2051-2080 (2060s).

Table 5-2. Descriptions of selected GCM - RCM climate models

GCM Name	RCM	INSTITUTION
CNRM-CM5	CCLM4-8-17-V1	Climate Limited-area Modelling Community
EC-EARTH	RACMO22T_v1	Royal Netherlands Meteorological Institute
MIROC5	SMHI-RCA4_V1	Swedish Meteorological and Hydrological Institute
MPI-ESM-LP	CCLM4-8-17-V1	Climate Limited-area Modelling Community

5.2.4. Bias correction

To assess the likely effect of climate change on the watershed's hydrological aspects using the SWAT model, bias-corrected RCM data under RCP4.5 and RCP8.5 scenarios were used. The process of bias correction involves adjusting the raw output of a climate model using a transformation algorithm, under the presumption that the algorithm used to parametrize and correct the current climate will also be applicable to future scenarios (Yeboah et al., 2022).

For this study, to bias-correct and extract data from the RCM model, CMhyd tool was used (Rathjens et al., 2016). To correct the maximum and minimum temperature and precipitation data, the linear scaling method was selected from the available bias correction techniques in the CMhyd software. Because of its simplicity, accuracy, and ease of application, this method has been widely used to correct GCM-RCMs in various parts of the world (Abera & Gebeyehu, 2023; Azman et

al., 2022; Galata et al., 2021; Mahmood et al., 2018; Mahmood & Babel, 2013; Mahmood & Jia, 2017; Shrestha et al., 2017; Takele et al., 2022). Furthermore, the method works well for climate change-related water resource research (Takele et al., 2022).

To adjust the RCM simulation of temperature and rainfall, the linear scaling method employs additive and multiplicative factors, respectively. The factors are produced by comparing the measured data to the corresponding historical RCM simulations (Worku et al., 2020). The detailed description of the method is available on the previous work of Luo et al. (2018) and Teutschbein & Seibert (2012).

5.2.5. SWAT model description and set up

The SWAT is a semi-distributed, physically based hydrologic model that operates on a continuous time-step (Arnold et al., 2012). The model is developed to simulate the climate change effects on hydrology, land management, and movement of agricultural chemicals and sediment of a wide and complex basin(Arnold et al., 1998; Taylor et al., 2016). The hydrology is simulated in two major ways: The Land Phase, which controls the nutrient, pesticide, sediment loaded, and water transport to each channel from sub-watersheds, and the Water or Routing Phase that controls the movement of flow up to the basin outlet. The SWAT model simulates the hydrologic phenomena of the land phase using the water balance equation shown as follows (Narsimlu et al., 2015; Neitsch et al., 2011):

$$SW_t = SW_o + \sum_{i=1}^{t}\left(P_{day} - Q_{surf} - E_a - Q_{gw} - W_{seep}\right) \quad (1)$$

where SW_t and SWo represent the final and initial soil water content on day i (mm), W_{seep}, Q_{gw}, E_a, $Q_{surf,}$ and P_{day} represent the amount of water entering the vadose zone from the soil profile, return flow, evapotranspiration, surface runoff, and precipitation, respectively on day i (mm), and t is time (days).

The SWAT model uses either the USDA Conservation Service Curve Number (SCN-CN) or the Green and Amp method for calculating surface runoff produced in the watershed (Neitsch et al.,

2011). For this study, the SCN-CN technique (Equation 2) was applied to estimate runoff for each HRU (Arnold & Fohrer, 2005).

$$Qsurf = \frac{(Pday - 0.2S)^2}{(Pday + 0.8S)} \quad (2)$$

Where, Q_{surf}, *Pday*, and *S* represent, daily depth of accumulated surface runoff (mm), the daily rainfall (mm), and retention parameter, respectively. Based on equation 2, runoff happens in a watershed when *Pday > 0.2S*.

In relation to the CN, the parameter *S* is calculated using Equation 3. The retention parameter, *S*, is affected by slope, soil type, and land management practices.

$$S = \frac{254(100 - \mathrm{CN})}{\mathrm{CN}} \quad (3)$$

Where, *CN* is the curve number for the day. During model calibration process, *CN* is the main parameter that determine the catchment runoff (Arnold et al., 2012).

The SWAT model has three different approaches for calculating evaporation: the Hargreaves, Priestly-Taylor, or Penman-Monteith methods (Neitsch et al., 2011). For this study, because of the limited availability of data and the simplicity of the method, the Hargraves method was applied.

5.2.6. Sensitivity analysis

Hydro-climatic parameters from 1984 to 2016 were used to simulate the hydrological characteristics of the study watershed. Climate data from the first three years (1984-1986) were used to initialize the SWAT model, and data afterwards from 1987-2016 were employed to perform model sensitivity and calibration analysis.

Because the SWAT model contains a large number of flow parameters, identifying the parameters that are most sensitive to streamflow that can be used in model calibration and validation is critical (Abbaspour et al., 2018; Chimdessa et al., 2019). For this study, to differentiate the most sensitive parameters, initially twenty-one flow parameters were meticulously chosen from the literature and the SWAT-CUP. Then, by using the objective function, *P*-values and *t*-stat, multiple regression

methods with Latin hypercube method, sensitivities of parameters were determined. The *p*-values and *t*-stat show the level and degree of sensitivity to flow parameters, respectively. The larger *p*-values indicating less sensitivity and smaller values indicating greater sensitivity. Small absolute *t*-stat values imply lower sensitivity, while large values reveal higher sensitivity (Abbaspour, 2015; Narsimlu et al., 2015).

5.2.7. Calibration and validation of SWAT model

Streamflow data from the Chenemasa gauging station was used to calibrate and validate the SWAT model. Calibration and validation were performed using streamflow data from 1987 to 2002 and 2003 to 2011, respectively. To calibrate and validate the model, the SWAT-CUP2012 software's sequential uncertainty fitting (SUFI-2) algorithm was used (Abbaspour, 2015). SUFI-2, is the most widely applied program in Ethiopia for model calibration, validation, and sensitivity analysis (Abraham & Nadew, 2018; Bekele et al., 2021; Belihu et al., 2020; Bizuneh et al., 2021; Bogale, 2021; Mengistu et al., 2020; Takele et al., 2022; Teklay et al., 2020; Tessema et al., 2021).

5.2.8. Evaluation of SWAT model performance

The performance of the SWAT model was evaluated in order to compare observed data and model simulation outputs. Hence, in this study, the statistical parameter values of Nash-Sutcliffe efficiency (NSE), coefficients of determination (R^2), and percent bias (PBIAS) were used to assess the performance of the SWAT model. These statistical units are the most commonly used parameters to assess the performance of models (Akoko et al., 2021; Shukla & Gedam, 2018). Statistical indices of *PBIAS*, R^2, and *NSE* were calculated using Equations 4, 5, and 6 respectively

The amount of the total variance in the observed data that the model can explain is indicated by the regression coefficient (R^2). The greater the agreement between the observed and the simulated flow, the closer the value of R^2 is to 1. Equation 4 is used to calculate R^2 as shown below:

$$R^2 = \left\{ \frac{\sum_{i=1}^{N}(Oi - \bar{O})(Pi - \bar{P})}{\left[\sum_{i=1}^{N}(Oi - \bar{O})^2\right]^{0.5}\left[\sum_{i=1}^{N}(P - \bar{P}\imath)^2\right]^{0.5}} \right\}^2 \quad (4)$$

Nash-Sutcliffe coefficient (Nash & Sutcliffe, 1970) described in Equation 5 was used to determine how the observed data and simulated output closely fit in 1:1 line.

$$NSE = 1 - \frac{\sum_{i=1}^{N}(Oi - Pi)^2}{\sum_{i=1}^{N}(Oi - \bar{O})^2} \quad (5)$$

According to Moriasi et al. (2007), the percent of bias (PBIAS) was used to estimate how much the measured values would differ from the values of the simulated output of counterparts. To calculate PBIAS equation 6 was used.

$$PBIAS = \frac{\sum_{i=1}^{N}(oi\text{-}pi)}{\sum_{i=1}^{N}(oi)} * 100 \quad (6)$$

Where $\bar{P}$ and $\bar{O}$ represent mean simulated and measured data; Pi and Oi represent simulated and measured data; and N represents the number of compared values.

Moriasi et al. (2007) state that the model's performance is acceptable when the value *R2* is exceeds 0.6, NSE is higher than 0.5, and PBIAS falls within ±25% range. The value of the *NSE* varies from -∞ to 1, and where the *NSE* is close to 1, the model performs best. The value of R^2 ranges between 0 to 1, where R^2 close to 1 specifies less error. On the other hand, the model simulation works best when *PBIAS* is close to 0. The model under- and overestimates the simulation, respectively, as indicated by the positive and negative PBIAS values (Nasiri et al., 2020).

5.2.9. Analysis of future climate characteristics

To analyze the RCM simulations of climate characteristics, seasonal and annual future temperature and precipitation time series data from the selected GSM were used. A few techniques have been developed to analyse climate characteristics. For this study, trend analysis using MK test and Sen's slope estimator were used.

5.2.9.1. Trends

Sen's slope estimator and the Mann-Kendall (MK) test were used to identify and measure potential trends in seasonal and annual temperature and precipitation time series data. The trend is

determined by comparing the previous and subsequent data values. If a data value from a previous time is less than a data value from a later time, the *S* statistic is increased by one. *S*, on the other hand, is decremented by one if the data value from an earlier time is greater than the data value sampled at a later time. The final *S* value is the net result of all decrements and increments. Equation 7 shows the MK statistic *S* of the series x. (Kendall, 1975; Mann, 1945):

$$S = \sum_{i=1}^{n-1} \sum_{j=i=1}^{n} sgn(xj - xi) \tag{7}$$

Where, the sequential value of the time series data in the years i and j (j>i) are represented by the letters xi and xj, respectively, and N is the length of the time series. S is the Mann-Kendal's test statistics. An S value that is positive or negative denotes an upward or downward trend in the data series. *S* is computed by Equation 8.

$$sgn = (Xj - Xi) = \begin{cases} +1 \; if (Xj - Xi) > 0 \\ 0 \; if (Xj - Xi) = \quad 0 \\ -1 \; if (Xj - Xi) < 0 \end{cases} \tag{8}$$

According to Kendall (1975) and Mann (1945), the 'S' statistic is approximately normally distributed with the mean, and E(S) becomes 0 when the number of observations exceeds 10. In this case, Equation 9 computes the $Var\ (S)$ (variance statistic) as:

$$Var\ (S) = \frac{1}{18}\left[N(N-1)(2N+5) - \sum_{p=1}^{q} tp(tp-1)(2tp+5)\right] \tag{9}$$

Where, *N* represents the number of data points and *tp* and *q* represent the number of data points in the i[th] tied group and the number of tied groups in the data set, respectively.

When the sample size is greater than ten, Equation 10 is used to compute the MK standardized test statistic, ZMK (Kendall, 1975; Mann, 1945).

$$Z_{MK} = \begin{cases} \frac{S-1}{\sqrt{Var(S)}} \; if \; S > 0 \\ 0 \; if \; S = 0 \\ \frac{S+1}{\sqrt{Var(S)}} \; if \; S < 0 \end{cases} \tag{10}$$

The standardized test statistic, ZMK, was applied to assess whether or not there was a statistically significant trend. The alternate hypothesis (Ha ≠ μ) and the null hypothesis (Ho = μ = μo) in this trend test state that there is a monotonic (upward or downward) trend or no monotonic trend observed in the dataset over time, respectively.

Estimating the Magnitude of the Trend

Sen's slope estimator was used to compute the slope of seasonal and annual rainfall and temperature changes. Theil (1950) and Sen (1968) developed Sen's slope method to estimate the magnitude of a linear trend in a time series. As a result, the linear model, *f (t)*, can be expressed as Equation 11:

$$f(t) = Qt + \beta \tag{11}$$

Where *Q* and *β* indicate the slope and the intercept of the trend line.

To determine the slope estimate, *Q*, the slopes of all data value pairs are calculated as follows:

$$Q_i = \frac{Y_j - Y_i}{X_j - X_i} \qquad i = 1, 2, \ldots . N, j > i. \tag{12}$$

where, Xi and Yi represent the i^{th} observation's time and its value of the rainfall variable, respectively. The median of these *N* values of *Qi* is Sen's estimator of slope. Equation 13 is used to calculate the Sen's estimator, which ranks the *N* values of *Qi* from the smallest to the largest:

$$Q_{med} = \begin{cases} Q * \left[\frac{(N+1)}{2}\right], if\ N\ is\ odd \\ \frac{Q * \left[\frac{N}{2}\right] + Q * \left[\frac{(N+2)}{2}\right]}{2}, if\ N\ is\ even \end{cases} \tag{13}$$

The sign in Equation 13, indicate the direction of the trend. A time series' trend that is decreasing or increasing is indicated by a negative or positive value of Qmed, respectively (Mulu et al., 2018).

5.2.10. Estimating the impact of climate change on hydrology

To assess the climate change impact on the hydrology of the study catchment, simulations from four GCM-RCM combinations of climate models were used. Furthermore, for each climate model,

two different RCPs scenarios, i.e., RCP 4.5 and RCP 8.5, were used as inputs to the calibrated SWAT model to simulate and evaluate the anticipated hydrological variables in the 2030s (2021–2050) and 2060s (2051–2080) of the century. Simulation results of hydrological variables, namely precipitation, evapotranspiration, surface runoff, total water yield, lateral, and ground water flow for the baseline period (1987 to 2016) were compared with the future time periods of the 2030s and the 2060s simulation. The differences in simulation outputs between the observed baseline and the future time indicates climate change impacts on the watershed's hydrologic response.

5.3. Results and Discussion

5.3.1. Calibration and validation of SWAT model

The SWAT-CUP software's SUFI-2 algorithms were utilized for sensitivity analysis to identify key flow parameters influencing streamflow in the SWAT model's calibration and validation. Initially, twenty-one flow parameters underwent sensitivity analysis, and following that, ten sensitive flow parameters namely ALPHA_BF.gw, CN2.mgt, CANMX.hru, GWQMN.gw, CH_K2.rte, REVAPMN.gw, SOL_AWC(..).sol, RCHRG_DP.gw, ESCO.hru, and GW_DELAY.gw, were selected based on p-value (ranging from 0 to 0.5) and t-stat (ranging from 7.86 to 0.65). The details of the analysis presented at Shigute et al. (2022).

The SWAT model was calibrated and validated using Chenemassa station's streamflow data from 1987 to 2002 for calibration and from 2003 to 2011 for validation. Results showed good performance with R^2, PBIAS, and NSE values of 0.78, -3.2%, and 0.73 during calibration, and 0.74, 3.9%, and 0.72 during validation. Additional information on model calibration, validation, performance evaluation, and streamflow hydrograph are available in prior studies (e.g., Shigute et al., 2022).

5.3.2. Bias correction of precipitation and temperature of RCMs

To enhance the forecasting ability of climate models, it is critical to correct the uncertainties and discrepancies between the measured and GCM/RCM data, which serve as inputs to the climate change impact assessment. For this study, to adjust the overestimation and underestimation of the raw output of the RCMs simulations of rainfall and temperature, the linear scaling bias correction technique was employed, and the discrepancy of the RCM's simulation of rainfall and temperature was adequately corrected with the measured rainfall and temperature data of the study basin.

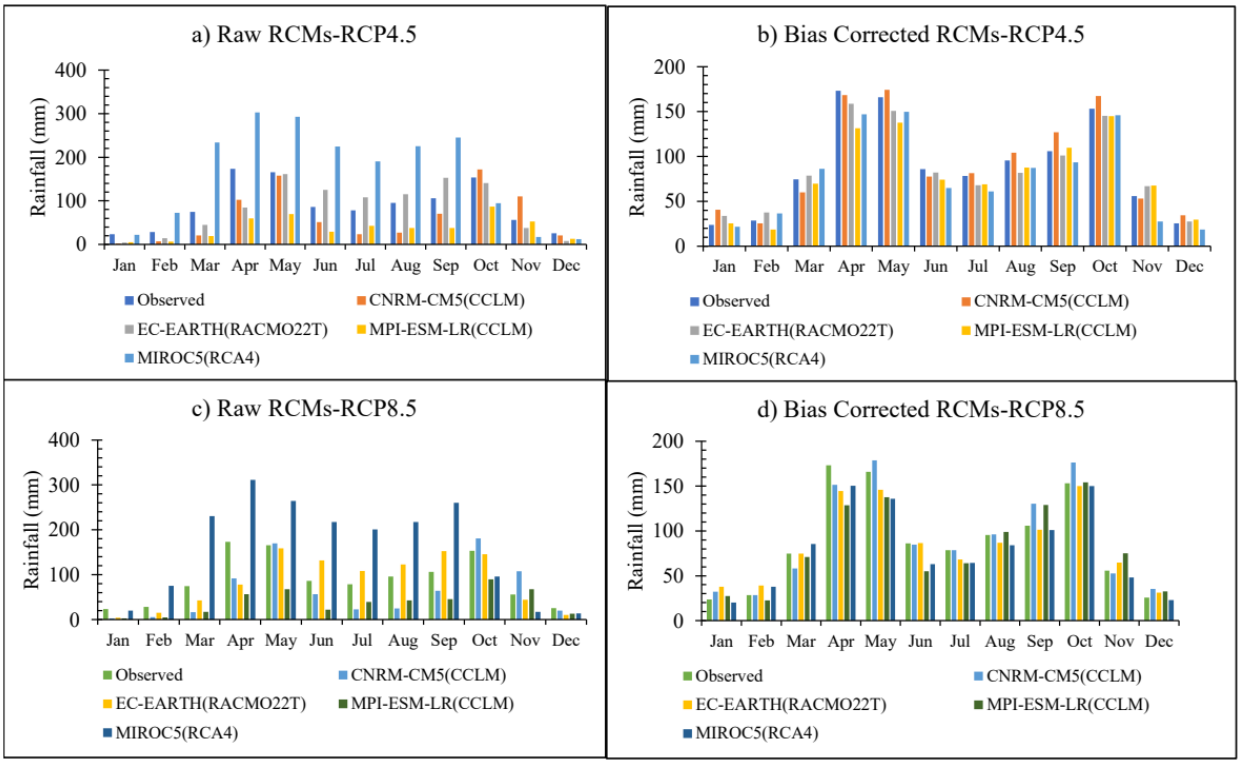

Figure 5-2. Performance of RCP 4.5 and RCP8.5 mean rainfall data before and after bias correction. a) and c) represent Raw RCM of RCP 4.5 and 8.5 before bias correction and b) and d) RCM of RCP4.5 and 8.5 after bias correction.

The bias correction procedures effectively corrected the initial overestimation in the raw RCMs simulation of monthly rainfall. This was observed from February to September for MIROC5 and from June to September for EC-EARTH, as shown in Figure 5-2a and c. The correction, illustrated in Figure 5-2 b and d, significantly improved the discrepancies between the observed and RCM's simulation of average monthly rainfall under RCP4.5 and RCP8.5.

Moreover, the initial underestimation in the RCM simulations of CNRM-CM5 and MPI-ESM-LR from January to September, and EC-EARTH from January to May, October, and November under RCP4.5 and 8.5 was successfully corrected. This is also depicted in Figures 5-2b and d, which also show the long-term average monthly rainfall after bias correction for the selected climate models.

In this regard, the linear scaling method has effectively adjusted both the monthly rainfall distribution and the extreme rainfall values.

Figure 5-3 shows that RCMs simulation of RCP 4.5 of TMAX and TMIN appears to be overestimated. The overestimation of climate models ranges from 0.22 to 8.01°C for the TMAX and 0.88 to 5.3°C for the TMIN during the RCP4.5 scenario (Figs. 5-3, a and c).

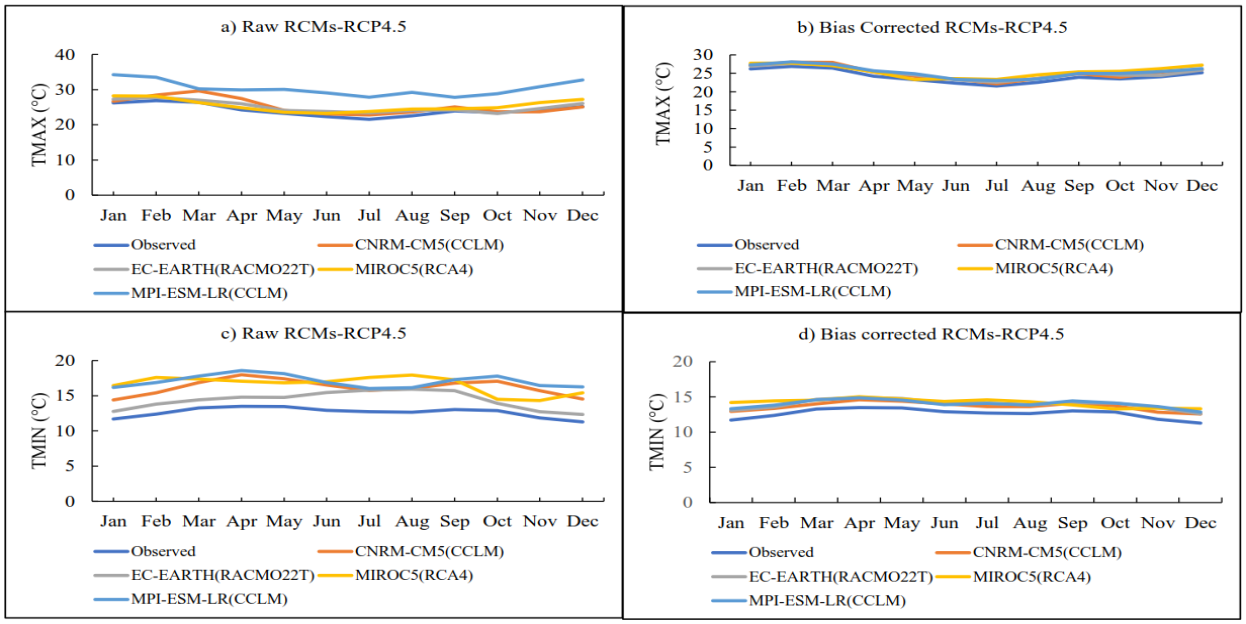

Figure 5-3. RCMs simulation of RCP 4.5 monthly average TMAX (°C) and TMIN (°C); raw (a and c) and bias corrected (b and d).

In the case of RCP8.5 scenario as shown in Figure 5- 4 (a and c), the overestimation values of TMAX and TMIN range from 0.3 to 8.56°C and from 1.88 up to 6.2°C, respectively.

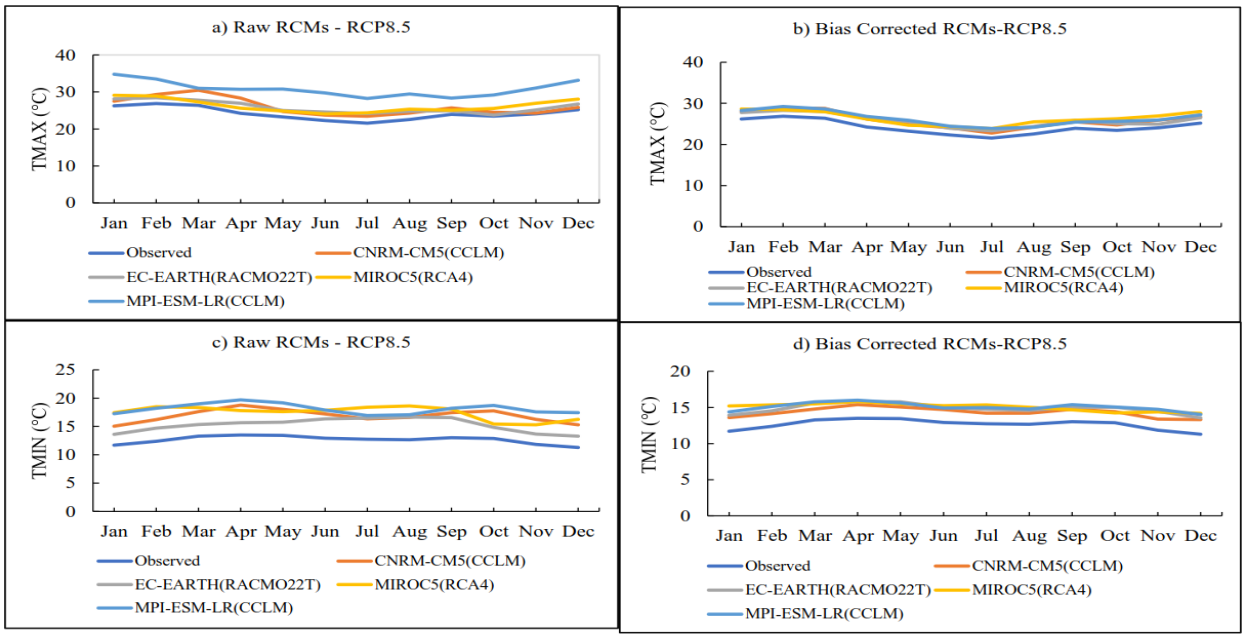

Figure 5-4. RCMs simulation of RCP 8.5 monthly average TMAX (°C) and TMIN (°C); raw (a and c) and bias corrected (b and d).

By using bias correction, the RCMs' overestimation of TMAX and TMIN was successfully corrected with measured mean monthly TMAX and TMIN. The adjusted TMAX and TMIN the climate models after the application of bias correction for RCP4.5 and RCP8.5 is showed on Figure 5-3, (b and d) and Figure 5-4, (b and d), respectively.

5.3.3. Forecasted change in rainfall and temperature

5.3.3.1. Future rainfall projection

The annual and seasonal change in projected rainfall for the 2030s (2021–2050) and 2060s (2051–2080) scenarios for the selected GCM-RCM models for RCP 4.5 and 8.5 emission scenarios are presented in Figure 5-5.

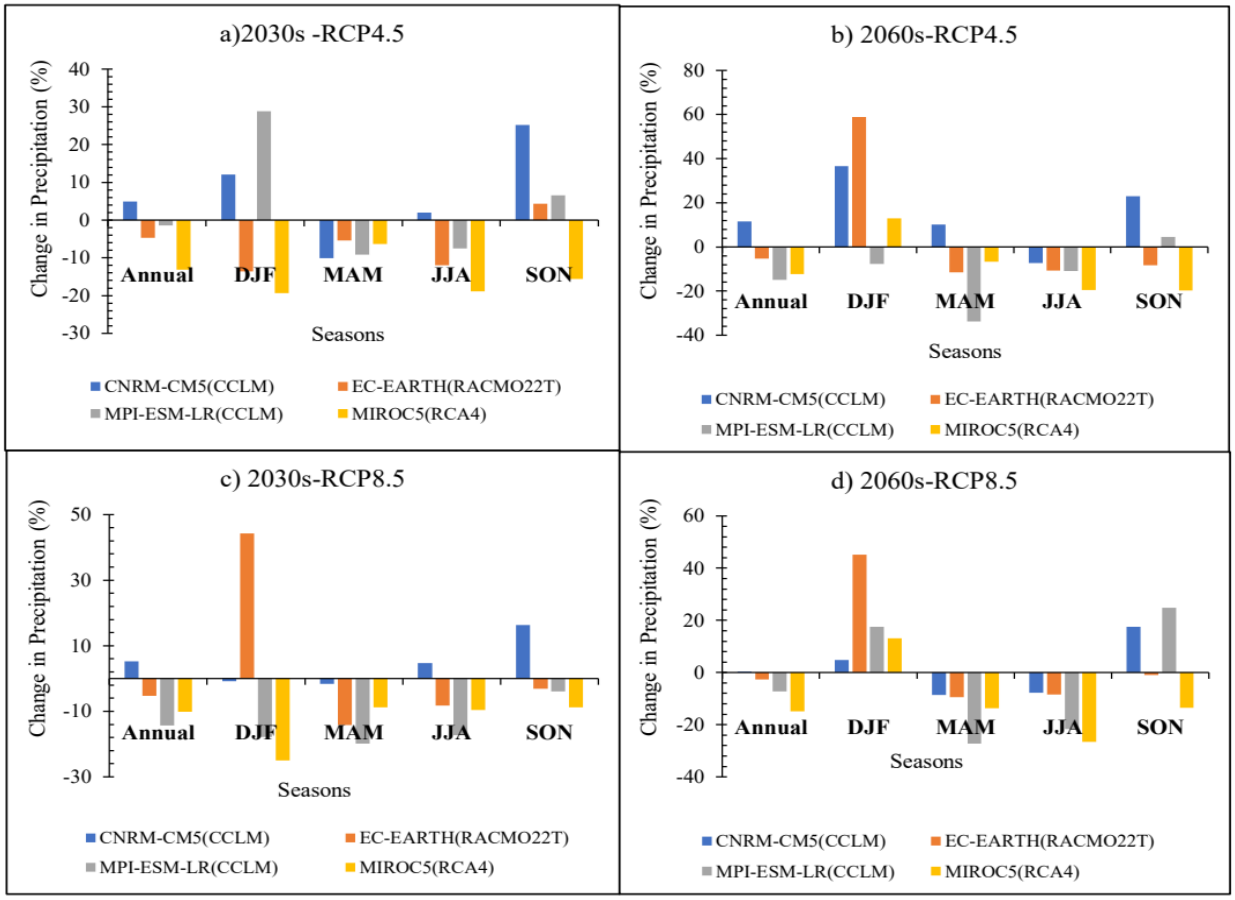

Figure 5-5. The future annual and seasonal projected change of rainfall of climate models, a) 2030s under RCP4.5, b) 2060s under RCP4.5, c) 2030s under RCP8.5, and d) 2060s under RCP8.5.

The analysis revealed that future rainfall projections in the study area show a range of magnitudes of changes compared to the observed rainfall. For RCP 4.5 and RCP 8.5 emission scenarios, the change in annual and seasonal projected rainfall ranges from -33.79 to + 58.95% for the 2030s and 2060s time periods. In both RCP emission scenarios, during the 2030s and 2060s, the projected annual rainfall of the EC-EARTH, MPI-ESM-LR, and MIROC5 models showed likely reductions ranging from 1.36 to 14.96%, whereas the CNRM-CM5 model displayed a likely increase ranging from 1.43 to 11.6% (Figures 5-5 a-d). However, under the RCP 4.5 and RCP 8.5 scenarios, annual mean rainfall will likely be reduced by up to 13.1% and 14.36%, respectively, in the 2030s, compared to observed rainfall. Similarly, under RCP4.5 and RCP8.5 emission scenarios, during the 2060s, annual rainfall is likely to decrease by up to 14.96% and 14.84%, respectively. This result is consistent with the findings of other studies conducted in various parts of Ethiopia, which

reported a likely increase and decrease in future annual rainfall in various parts of Ethiopia (Balcha et al., 2023; Kuma et al., 2021; Takele et al., 2022). For instance, the study undertaken by Takele et al., (2022) in the upper blue Nile basin showed that during 2030s and 2050s in the two RCPs scenarios, the projected annual average rainfall is likely to change from -13 to 6%.

Under the RCP4.5 emission scenario, the seasonal rainfall projections for DJF, MAM, JJA, and SON decreased by up to 19.36%, 10.1%, 18.9%, and 15.6%, respectively, during the 2030s (Figure 5-5, a). However, in the same future period and scenario (in the 2030s of RCP 4.5), CNRM-CM5 during DJF, JJA, and SON, EC-EARTH during SON, and MPI-ESM-LR during DJF and SON seasons showed an increasing rainfall (Figure 5-5, a). Similarly, in RCP 4.5 scenario, seasonal rainfall decreased relative to observed rainfall during the 2060s. The reduction of rainfall reached up to 7.65% during DJF, 33.8% during MAM, 19.6% during JJA, and 19.8% during SON seasons (Figure 5-5, b). During the 2030s in RCP 8.5, the seasonal rainfall is anticipated to be reduced by up to 25%, 19%, 17%, and 9% during the DJF, MAM, JJA, and SON seasons, respectively (Figure 5-5, c). In the RCP 8.5 scenario, rainfall in the MAM, JJA, and SON seasons, will likely decrease by up to 27.3%, 26.6%, and 13.5%, respectively, during the 2060s (Figure 5-5, d). On the other hand, during the 2030s of RCP8.5, the CNRM-CM5 climate model in DJF, MAM, and SON seasons, MPI-ESM-LR in SON, and EC-EARTH and MIROC5 in DJF season, as well as the MPI-ESM-LR, EC-EARTH, CNRM-CM5, and MIROC5 climate models in the DJF season, and MPI-ESM-LR and CNRM-CM5 in the SON season in the 2060s of RCP8.5 emission, showed likely increasing rainfall. During 2030s and 2060s under both RCP scenarios, the change in projected increasing rainfall expected to reach up to 58.95%. On the other hand, for the same time periods in both RCP emission scenarios, most of the evaluated models indicate a decrease in projected rainfall during the MAM and JJA seasons. This finding agrees with the result of Daniel & Abate, (2022) and Kuma et al., (2021). They found that projected rainfall is expected to increase during DJF and reduce during the wet seasons of MAM and JJA. In the southern, southeastern, eastern lowland and highland of Ethiopia, the MAM season used to cultivate crops and agro-pastoral activities (Bekele-Biratu et al., 2018). A reduction or delay in the MAM and JJA seasons, combined with future temperature increases, may result in severe drought and a reduction in water resources, posing a threat to Ethiopia's agricultural development.

In general, in the study basin, the annual and seasonal projected rainfall has not shown any systematic increasing or decreasing trend. This indicates that climate models do not agree on the magnitude and direction of future changes in annual and seasonal rainfall amounts for future time periods. These variations in forecasting future changes are most probably a result of the use of different climate models and subsequent parameterizations (Bekele et al., 2021).

5.3.3.2. Temperature change projection

The expected changes in maximum and minimum temperatures of the selected climate models for the RCP 4.5 and RCP 8.5 scenarios for the 2030s and 2060s are summarized in Table 5-3. The result displayed that during the 2030s, in the RCP 4.5 scenario, minimum and maximum temperatures are expected to rise up to 1.3 ℃ and 1.2 ℃, respectively. During the 2060s, in this same emission scenario, the minimum and maximum temperatures would increase to 1.82 ℃ and 1.74 ℃, respectively. Similarly, during 2030s in RCP 8.5 scenarios, the minimum and maximum temperature is expected to rise up to 1.6 ℃ and 1.36 ℃, respectively. During 2060s in RCP 8.5 scenario, the minimum and maximum temperature may raise up to 3.02 ℃ and 2.85 ℃, respectively. The analysis result also displayed that the change in temperature during 2060s expected to be higher than 2030s in both the RCPs. Furthermore, in both RCP scenarios, during 2030s and 2060s, the rate of change in minimum temperature would be higher than the maximum temperature.

Table 5-3. Future mean annual minimum and maximum temperatures change under both RCP scenarios.

GCM - RCM	2030s (2021-2050)				2060s (2051-2080)			
	RCP 4.5		RCP 8.5		RCP 4.5		RCP 8.5	
	TMAX (℃)	TMIN (℃)	TMAX (℃)	TMIN (℃)	TMAX (℃)	TMIN (℃)	TMAX (℃)	TMIN (℃)
CNRM-CM5(CCLM)	0.61	0.65	0.89	0.87	1.22	1.28	2.18	2.09
EC-EARTH(RACMO22T)	0.67	0.98	0.78	1.19	1.38	1.73	2.19	2.77
MIROC5(RCA4)	1.2	1.3	1.36	1.59	1.7	1.82	2.85	2.91
MPI-ESM-LR(CCLM)	0.76	1.04	1.26	1.31	1.74	1.78	2.52	3.02
Average	0.81	0.99	1.07	1.24	1.51	1.65	2.44	2.7

In general, the analysis results revealed that under the RCP 8.5 scenario, the expected change in the minimum and maximum temperatures of the individual and average climate models would be higher than the RCP 4.5 scenario. This is because RCP8.5 has a higher emission scenario than RCP4.5. Furthermore, the results of all climate and average models showed that the change in minimum temperature would be more significant than the change in maximum temperature in both the 2030s and 2060s. This finding is consistent with the results (Bekele et al., 2019; Bekele et al., 2021; Moges & Bhat, 2021; Takele et al., 2022; Tessema et al., 2021; Worku et al., 2021). They showed that the expected change in minimum and maximum temperature is higher in RCP 8.5 than RCP 4.5. Furthermore, they found that the increase in minimum temperature were higher than the increase in maximum temperature in different parts of Ethiopia.

5.3.4. Analysis of future annual and seasonal rainfall trends

The annual and seasonal projected rainfall trend analysis results are displayed in Table 5-4. The MK trend test in the RCP 4.5 and RCP 8.5 emission scenarios revealed both positive and negative trends for annual and seasonal rainfall in the 2030s and 2060s, indicating the existence of variations in climate models for predicting climate in terms of magnitude and direction. The decreasing and increasing trends in all RCMs and future time periods (2030s and 2060s) under the two RCP scenarios range from -0.05 to -7.43 mm per year and + 0.03 to +7.01 mm per year, respectively. During the 2030s in RCP 4.5 and RCP 8.5, the MK test for MAM and annual future rainfall data indicated an insignificant trend, but it showed a decreasing tendency with rates ranging from 0.97 to 6.16 mm per year for the MPI-ESM-LR, EC-EARTH, and CNRM-CM5 climate models. However, the RCP 8.5 of the 2060s of the RCM of MIROC5 and MPI-ESM-LR model showed statistically significant increasing and decreasing trend at 95% confidence level, with a rate of 3.34 and 7.43 mm per year, respectively. On the other hand, most of the RCMs showed an insignificant increasing trend during the JJA season. However, the detected trends were significant for EC-EARTH of the RCP 8.5 in the 2030s. During the SON season, most RCMs show a decreasing trend, with rates ranging from 0.27 to 3.62 mm per year in the 2030s and 2060s scenarios.

Table 5-4. Trends of seasonal and annual projected rainfall under RCP4.5 and RCP8.5

GCM-RCM	RCPs	Periods	DJF		MAM		JJA		SON		Annual-RF	
			P-value	Sen's slope	P-value	Sen's slope	P-value	Sen's slope	P-value	Sen's slope	P-value	Sen's slope
CNRM-CM5 (CCLM)	RCP4.5	2030s	0.38	0.58	0.24	-3.53	1.00	0.00	0.97	-0.27	0.92	-0.97
		2060s	0.60	-0.82	0.70	1.88	0.08	3.77	0.78	-1.37	1.00	0.03
	RCP8.5	2030s	0.70	0.32	0.09	-5.22	0.17	2.16	0.97	0.11	0.55	-4.60
		2060s	0.94	-0.12	0.34	2.16	0.21	2.49	0.44	2.89	0.17	7.01
EC-EARTH (RACMO22T)	RCP4.5	2030s	1.00	-0.07	0.06	-4.11	0.83	-0.11	0.70	0.69	0.36	-3.17
		2060s	0.67	0.75	0.42	1.46	0.97	-0.06	0.11	-2.27	0.83	-0.64
	RCP8.5	2030s	0.75	0.52	0.06	-3.99	**0.03***	1.41	0.09	-2.17	0.19	-3.96
		2060s	0.80	0.29	0.48	1.59	0.27	-0.86	0.09	2.76	0.11	4.40
MIROC5 (RCA4)	RCP4.5	2030s	0.26	1.20	0.55	1.19	0.57	0.50	**0.04***	2.04	0.08	3.99
		2060s	0.97	0.11	1.00	0.07	0.94	0.22	0.08	-1.92	0.80	-1.14
	RCP8.5	2030s	0.23	0.94	0.67	0.59	0.65	-0.39	0.50	1.72	1.00	-0.05
		2060s	0.86	-0.32	**0.01***	3.34	0.72	0.35	0.19	1.82	0.10	4.86
MPI-ESM-LR (CCLM)	RCP4.5	2030s	0.19	1.56	0.27	-5.43	0.40	1.50	0.40	-3.62	0.44	-5.13
		2060s	0.60	-0.32	0.60	1.36	0.80	-0.53	0.80	-1.63	0.92	-0.28
	RCP8.5	2030s	0.50	0.42	0.21	-3.67	0.97	0.24	0.50	-2.16	0.32	-6.16
		2060s	0.80	0.31	**0.048***	-7.43	0.14	2.96	0.65	2.53	0.75	-2.70
Ensemble Mean	RCP4.5	2030s	0.17	1.31	0.11	-2.80	0.44	0.68	0.67	-0.65	0.50	-1.84
		2060s	0.48	0.38	0.27	2.00	0.36	0.86	0.19	-1.65	0.97	-0.12
	RCP8.5	2030s	0.21	0.95	0.17	-2.59	0.21	0.80	0.50	-0.62	0.38	-2.67
		2060s	0.94	0.10	0.55	-1.14	0.06	1.62	0.08	3.01	0.48	2.17

DJF is from December to February, MAM is from March to May, JJA is from June to August, and SON is from September to November; * Indicate significance at $\alpha = 0.05$.

The mean seasonal and annual projected rainfall trends analysis in Table 5-4 indicated that the annual rainfall projection in both RCPs showed an insignificant decreasing trend during the 2030s and 2060s. Similarly, except for the 2060s of RCP 4.5 and RCP 8.5, the MAM and SON seasons displayed a decreasing trend. On the contrary, DJF and JJA seasons during the 2030s and 2060s in both RCPs, as well as RCP 4.5 of the 2060s of MAM and RCP 8.5 of the 2060s of SON, showed a positive trend.

5.3.5. Seasonal and annual projected temperature trend

The annual, seasonal, and an ensemble mean of maximum and minimum temperature trends for 2030s and 2060s under RCP 4.5 and RCP 8.5 emission scenarios are presented in Tables 5-5 and 5-6. During the 2030s and 2060s in the RCP 4.5 scenario, the MK analysis result of the seasonal

and annual minimum and maximum temperatures exhibited an increasing trend. However, during the 2030s in the RCP 4.5scenario, most of the seasonal and annual maximum and minimum temperatures of the RCM of the MPI-ESM-LR, CNRM-CM5, and EC-EARTH showed a significantly increasing trend at 1% and 5% levels of confidence. On seasonal basis, during the 2030s in the RCP4.5, climate model of CNRM-CM5 (in MAM, JJA, and SON), EC-EARTH (in DJF, MAM, JJA, and SON), MPI-ESM-LR (in MAM, SON, and JJA), and MIROC5 (in DJF and JJA) seasons showed statistically significant increasing trend at 1% and 5% level of confidence. Similarly, the annual and seasonal ensemble means of minimum and maximum temperatures during the 2030s and 2060s in RCP4.5 emission showed a significant increasing trend at the 1% and 5% levels of confidence.

Table 5-6 displays projected temperature trends for RCP8.5 in the 2030s and 2060s for all RCM models. The trend results show that there is an increasing trend in seasonal, annual, and ensemble mean minimum and maximum temperatures. Specifically, most of the seasons in the CNRM-CM5 and EC-EARTH models show a significant increase in seasonal temperatures at 1% and 5% confidence levels. Additionally, the ensemble mean of maximum and minimum temperatures in the 2030s and 2060s, as well as the MPI-ESM-LR and MIROC5 models in the 2060s under RCP8.5, exhibit statistically significant trends at both 1% and 5% confidence levels.

The Sen's slope of seasonal and annual temperature in the future periods under both the RCPs emission scenarios is summarized in Table 5-5 and 5-6. Accordingly, during 2030s and 2060s in both RCPs, the annual, seasonal and an ensemble mean of the slope of change of minimum temperature was higher than the slope of change of the annual, seasonal and an ensemble mean maximum temperature in most of RCMs model. The rate of slope change in minimum temperature during the 2030s and 2060s forecast period varies from 0.004 °C to 0.059 °C per annual, whereas in case of maximum temperature, the rate of slope changes varies from -0.007 °C to 0.61°C per annual. On the other hand, the rate of slope of change varies from 0.003 to 0.071°C for minimum temperature and from 0.004 °C to 0.096 °C for the maximum temperature in the 2030s and 2060s of the RCP8.5 emission scenario. This finding is in line with a study by Takele et al., (2022) in the Upper Blue Nile basin and Worku et al., (2021) in the Jemma sub-basin. They found out that, in the near and long term of 21st century most of the evaluated RCM models showed statistically significant increasing trend of maximum and minimum temperature at 1% and 5% significance

level. In addition, they discovered that the rate of slope change in the minimum temperature is higher than that of maximum temperature. According to the IPCC report, anthropogenic forcing are likely to have contributed significantly to surface temperature increases across all continents (IPCC., 2014).

In general, the observed potential increase in maximum and minimum temperature in the 2030s and 2060s in the two RCP scenarios during the MAM, JJA, and SON seasons may result in dryer conditions at the start of the rainy season, increasing the rate of evapotranspiration and delaying the onset of rainy seasons in the area. This has a significant impact on rainfed agriculture practices, particularly for crops with longer growing seasons. Furthermore, due to decreased water supply and increased water demands, irrigation water requirements are likely to increase, potentially reducing crop yield. Future temperature increases in the study watershed could have an impact on the hydrologic cycle, water resource system, hydropower, and water use.

Table 5-5. Summary of trends in seasonal and annual projected maximum and minimum temperature under RCP4.5.

GCM-RCM	RCP-4.5	Parameters	DJF		MAM		JJA		SON		Annual	
			Tmax(°C)	Tmin (°C)	Tmax(°C)	Tmin (°C)	Tmax(°C)	Tmin (°C)	Tmax(°C)	Tmin (°C)	Tmax(°C)	Tmin (°C)
CNRM-CM5 (CCLM)	2030s	P-Value	0.457	0.087	0.087	**0.008****	**0.02***	**0.0007****	0.214	**0.001****	**0.007****	**< 0.0001****
		Sen's slope	0.008	0.028	0.031	0.019	0.04	0.027	0.014	0.026	0.023	0.027
	2060s	P-Value	**0.037***	0.101	0.166	0.101	0.888	0.058	0.101	0.242	**0.026***	**0.012***
		Sen's slope	0.028	0.023	0.036	0.021	-0.004	0.02	0.034	0.009	0.024	0.016
EC-EARTH (RACMO22T)	2030s	P-Value	0.288	**0.0001****	**0.024***	**0.016***	0.094	**0.0001****	0.832	**0.019***	0.009	**0.0003****
		Sen's slope	0.015	0.046	0.045	0.019	0.019	0.029	0.003	0.017	0.02	0.023
	2060s	P-Value	0.646	**0.004****	0.832	0.272	0.416	0.256	0.069	0.081	0.054	**0.006****
		Sen's slope	0.009	0.035	-0.005	0.007	0.013	0.01	0.024	0.008	0.016	0.017
MIROC5 (RCA4)	2030s	P-Value	**0.041***	0.117	0.805	0.724	0.081	**0.012***	0.548	0.189	0.480	0.075
		Sen's slope	0.028	0.059	-0.007	0.006	0.036	0.024	0.01	0.022	0.009	0.03
	2060s	P-Value	0.087	0.256	0.888	0.646	0.750	0.117	0.166	0.256	0.166	0.135
		Sen's slope	0.026	0.028	0.001	0.006	0.007	0.018	0.023	0.026	0.017	0.022
MPI-ESM-LR (CCLM)	2030s	P-Value	0.069	0.075	**0.035***	**0.03***	0.177	**0.029***	**0.004****	0.135	**0.004****	**0.0065****
		Sen's slope	0.027	0.031	0.041	0.046	0.035	0.029	0.061	0.022	0.045	0.024
	2060s	P-Value	0.646	0.087	0.339	0.075	0.457	0.724	0.502	0.214	0.972	0.069
		Sen's slope	0.009	0.023	0.017	0.017	-0.019	0.004	0.014	0.015	0.0008	0.016
Ensemble Mean	2030s	P-Value	**0.0037****	**0.00045****	**0.0084****	**0.0073****	**0.037***	**< 0.0001****	**0.0042****	**0.0004****	**0.0073****	**0.00068****
		Sen's slope	0.021	0.043	0.033	0.020	0.021	0.023	0.027	0.019	0.018	0.019
	2060s	P-Value	**0.00043****	**0.001****	0.304	**0.02***	0.860	**0.016***	**0.011***	**0.026****	**0.024***	**0.019***
		Sen's slope	0.023	0.030	0.014	0.014	0.002	0.015	0.021	0.013	0.014	0.016

DJF is from December to February, MAM is from March to May, JJA is from June to August, and SON is from September to November; ∗∗ and ∗ show significance at α = 0.01 and 0.05, respectively

Table 5-6. Summary of trends in seasonal and annual projected maximum and minimum temperature under RCP8.5.

GCM-RCM	RCP-8.5	Parameters	DJF		MAM		JJA		SON		Annual	
			Tmax(°C)	Tmin (°C)	Tmax(°C)	Tmin (°C)	Tmax(°C)	Tmin (°C)	Tmax(°C)	Tmin (°C)	Tmax(°C)	Tmin (°C)
CNRM-CM5 (CCLM)	2030s	P-Value	**0.004****	**0.049***	**0.001****	**0.022***	**0.0002****	**0.0002****	**0.0075****	**< 0.0001****	**0.0013****	**0.0017****
		Sen's slope	0.031	0.036	0.063	0.024	0.021	0.034	0.043	0.031	0.037	0.033
	2060s	P-Value	**0.0003****	**0.0037****	**0.012***	**< 0.0001****	**< 0.0001****	**< 0.0001****	**0.008****	**0.0003****	**< 0.0001****	**< 0.0001****
		Sen's slope	0.051	0.06	0.053	0.066	0.049	0.061	0.033	0.031	0.061	0.071
EC-EARTH (RACMO22T)	2030s	P-Value	0.109	**0.0005****	**0.0002****	**< 0.0001****	**0.0047****	**< 0.0001****	**0.0075****	**< 0.0001****	**<0.0004****	**< 0.0001****
		Sen's slope	0.026	0.049	0.036	0.042	0.04	0.051	0.041	0.045	0.042	0.030
	2060s	P-Value	0.081	**< 0.0001****	**0.016***	**< 0.0001****	**0.0003****	**< 0.0001****	0.109	**< 0.0001****	**< 0.0001****	**< 0.0001****
		Sen's slope	0.032	0.056	0.047	0.054	0.06	0.056	0.03	0.041	0.041	0.05
MIROC5 (RCA4)	2030s	P-Value	**0.024***	0.054	0.621	0.256	0.321	**0.018***	0.081	0.832	0.075	**0.038***
		Sen's slope	0.033	0.054	0.004	0.016	0.022	0.028	0.023	0.003	0.02	0.03
	2060s	P-Value	**0.0002****	**0.012***	0.101	**0.01****	0.155	0.069	**0.038***	0.77	**0.0006****	**0.0008****
		Sen's slope	0.059	0.054	0.028	0.029	0.031	0.016	0.04	0.070	0.041	0.039
MPI-ESM-LR (CCLM)	2030s	P-Value	**0.0053****	**0.004****	0.256	0.081	0.457	0.201	**0.026***	**0.008****	**0.013***	**0.016***
		Sen's slope	0.032	0.053	0.021	0.028	0.010	0.01	0.039	0.026	0.026	0.023
	2060s	P-Value	**0.0023****	**0.0002****	**< 0.0001**	**0.0003****	0.28	**0.028***	**0.0075****	**< 0.0001****	**0.0032****	**< 0.0001****
		Sen's slope	0.049	0.06	0.096	0.064	0.033	0.030	0.05	0.065	0.029	0.056
Ensemble Mean	2030s	P-Value	**< 0.0001****	**< 0.0001****	**< 0.0001****	**< 0.0001****	**< 0.0001****	**< 0.0001****	**< 0.0001****	**0.0001****	**< 0.0001****	**< 0.0001****
		Sen's slope	0.028	0.050	0.034	0.035	0.041	0.046	0.035	0.021	0.03	0.034
	2060s	P-Value	**< 0.0001****	**< 0.0001****	**< 0.0001****	**< 0.0001****	**0.0006****	**< 0.0001****	**0.0001****	**<0.0012****	**< 0.0001****	**< 0.0001****
		Sen's slope	0.049	0.063	0.048	0.053	0.037	0.037	0.04	0.018	0.037	0.046

DJF is from December to February, MAM is from March to May, JJA is from June to August, and SON is from September to November; ∗∗ and ∗ show significance at α = 0.01 and 0.05, respectively

5.3.6. Climate change impact on the hydrological processes

To forecast the potential impacts of climate change on the hydrological components under RCP4.5 and RCP8.5 scenarios, future rainfall and temperature in the 2030s (2021–2050) and 2060s (2051–2080) periods and a previously calibrated and validated SWAT model, were used. The simulated hydrological response of the base period (1987-2016) and the future periods (2030s and 2060s) were then compared to evaluate the change in the watershed's future hydrological components.

The result of the impact of future climate change on the hydrological components based on the simulated precipitation, total water yield, surface runoff, ET, groundwater flow, and lateral flow of the SWAT models is presented in Table 5-7. The result displayed that, during 2030s and 2060s under RCP 4.5 and RCP 8.5 scenario, the surface runoff changes from -33.47% to 24.47% and -39.3% to 5.29%, respectively. The highest increment of surface runoff, which is 24.47%, was observed during 2060s under RCP4.5 scenario. In contrast, the highest reduction of surface runoff, which is 39.03% was observed during 2030s under RCP8.5 scenario. The climate model of MPI-ESM-LR and CNRM-CM5 showed the highest negative and positive change in surface runoff, respectively. In addition to this, Table 5-7 showed that, except for the CNRM-CM climate model, all the models show a likely decrease in surface runoff in the future periods in both RCP scenarios.

Furthermore, the analysis results indicate that, under the two Representative Concentration Pathways (RCPs), the anticipated hydrological components, specifically surface runoff, water yield, lateral flow, and groundwater flow, are expected to experience significant decreases in the 2030s and 2060s. The projected reductions are estimated to reach up to 39.3%, 39.8%, 40.08%, and 50.06%, respectively, in comparison to the 1987–2016 base period for all climate models except the CNRM-CM5. Under CNRM -CM5 model, annual runoff, total water yield, ground waterflow, lateral flow, and are likely to increase by up to 24.47%, 28.56%, 27.98%, and 23.26%, respectively. However, during the 2030s and 2060s under the two RCPs, the annual ET may increase across the basin in all climate model. The rise in ET is triggered mainly by a consistent rise in temperature. The expected change in increase of annual ET varies from 0.94% to 8.11% in all scenarios. The reduction or increase of future annual total water yield, runoff, lateral, and ground waterflow associated with the decrease or increase of future periods simulated precipitation in the study basin. For instance, a 2.88% increase in mean annal rainfall during 2030s under

RCP4.5 scenario resulted in an increasing surface runoff, ground waterflow, lateral flow, and total water yield by 8.78%, 4.32%, 7.67%, and 9.17% for the CNRM-CM5 model. On the other hand, a 15.8% reduction of annual average rainfall during 2060s under RCP8.5 for MIRCOS models will lead to 31.89%, 27.68%, 40.59%, and 29.37% reduction of total water yield, runoff, ground waterflow, and lateral flow, respectively. This study's findings are consistent with those of other studies conducted in Ethiopia (Daniel & Abate, 2022; Merga et al., 2022; Takele et al., 2022; Worku et al., 2021). For example, a study conducted by Worku et al. (2021) in the Jemma sub-basin, Ethiopia, showed that under RCP4.5 and RCP8.5 scenarios, the impact of climate change may result in reduced runoff, water yield, groundwater, lateral flow, and an increase in evapotranspiration during the near- and long-term (2021–2050 and 2071–2100) periods.

In general, decreasing surface water under the scenarios will have a significant impact on agricultural activities. Reductions in rainfall along with increasing temperatures are expected to have a significant effect on the main economic sectors, such as agriculture and water resource sectors, of the study watershed. Moreover, the dominant rain-fed, non-input-intensive way of agricultural practices, together with the economic dependency of most people's livelihoods on agriculture production, make the area susceptible to climate change and variability. If extreme weather events and the effects of climate change continue in the future, subsistence and smallholder farmers' vulnerability may worsen, triggering further economic loss (Miheretu, 2020).

Table 5-7. Baseline and future climate models' mean annual water balance components under RCP4.5 and RCP8.5.

GCM-RCM	RCP	Period	PRECIPmm	% Change	ETmm	% Change	SURQmm	% Change	GW_Qmm	% Change	LAT_Qmm	% Change	WYLDmm	% Change
	Baseline	1987-2016	1060.25		676.76		159.03		141.31		37.92		339.63	
CNRM-CM5 (CCLM)	RCP4.5	2030s	1090.74	2.88	683.13	0.94	173.00	8.78	147.42	4.32	40.83	7.67	370.77	9.17
		2060s	1164.48	9.83	692.26	2.29	197.95	24.47	180.85	27.98	46.74	23.26	436.63	28.56
	RCP8.5	2030s	1089.72	2.78	698.44	3.20	167.44	5.29	148.21	4.88	40.42	6.58	365.37	7.58
		2060s	1049.61	-1.00	706.95	4.46	156.47	-1.61	133.66	-5.42	37.28	-1.70	336.15	-1.03
EC-EARTH (RACMO22T)	RCP4.5	2030s	1001.41	-5.55	698.05	3.15	147.14	-7.48	116.95	-17.24	31.56	-16.78	301.88	-11.12
		2060s	988.26	-6.79	700.59	3.52	142.65	-10.30	107.89	-23.65	29.83	-21.34	286.08	-15.77
	RCP8.5	2030s	991.32	-6.50	702.86	3.86	146.35	-7.97	113.40	-19.75	31.15	-17.86	297.64	-12.36
		2060s	1019.60	-3.83	708.63	4.71	150.13	-5.60	123.82	-12.38	31.99	-15.64	313.16	-7.80
MIROC5 (RCA4)	RCP4.5	2030s	915.47	-13.66	695.19	2.72	119.16	-25.07	95.35	-32.53	27.35	-27.88	248.07	-26.96
		2060s	923.87	-12.86	716.79	5.92	125.89	-20.84	92.78	-34.34	27.17	-28.36	251.99	-25.80
	RCP8.5	2030s	946.86	-10.69	706.87	4.45	124.90	-21.46	107.19	-24.15	28.14	-25.81	267.16	-21.34
		2060s	892.47	-15.82	726.40	7.33	115.01	-27.68	83.95	-40.59	26.79	-29.37	231.33	-31.89
MPI-ESM-LR (CCLM)	RCP4.5	2030s	1026.19	-3.21	703.16	3.90	151.62	-4.66	124.80	-11.69	33.61	-11.37	318.32	-6.27
		2060s	881.71	-16.84	717.53	6.02	105.81	-33.47	76.71	-45.72	26.85	-29.20	214.86	-36.74
	RCP8.5	2030s	877.02	-17.28	710.29	4.95	96.53	-39.30	70.57	-50.06	22.73	-40.08	204.47	-39.80
		2060s	956.51	-9.78	731.62	8.11	128.75	-19.04	104.16	-26.29	30.06	-20.73	278.57	-17.98

PRECIPmm, Precipitation in millimeter; ETmm, Evapotranspiration in millimeter; SURQmm, Surface runoff in millimeter; GW_Qmm, Ground waterflow in millimeter; LAT_Qmm, Lateral flow in millimeter; WYLDmm, Total water yield in millimeter.

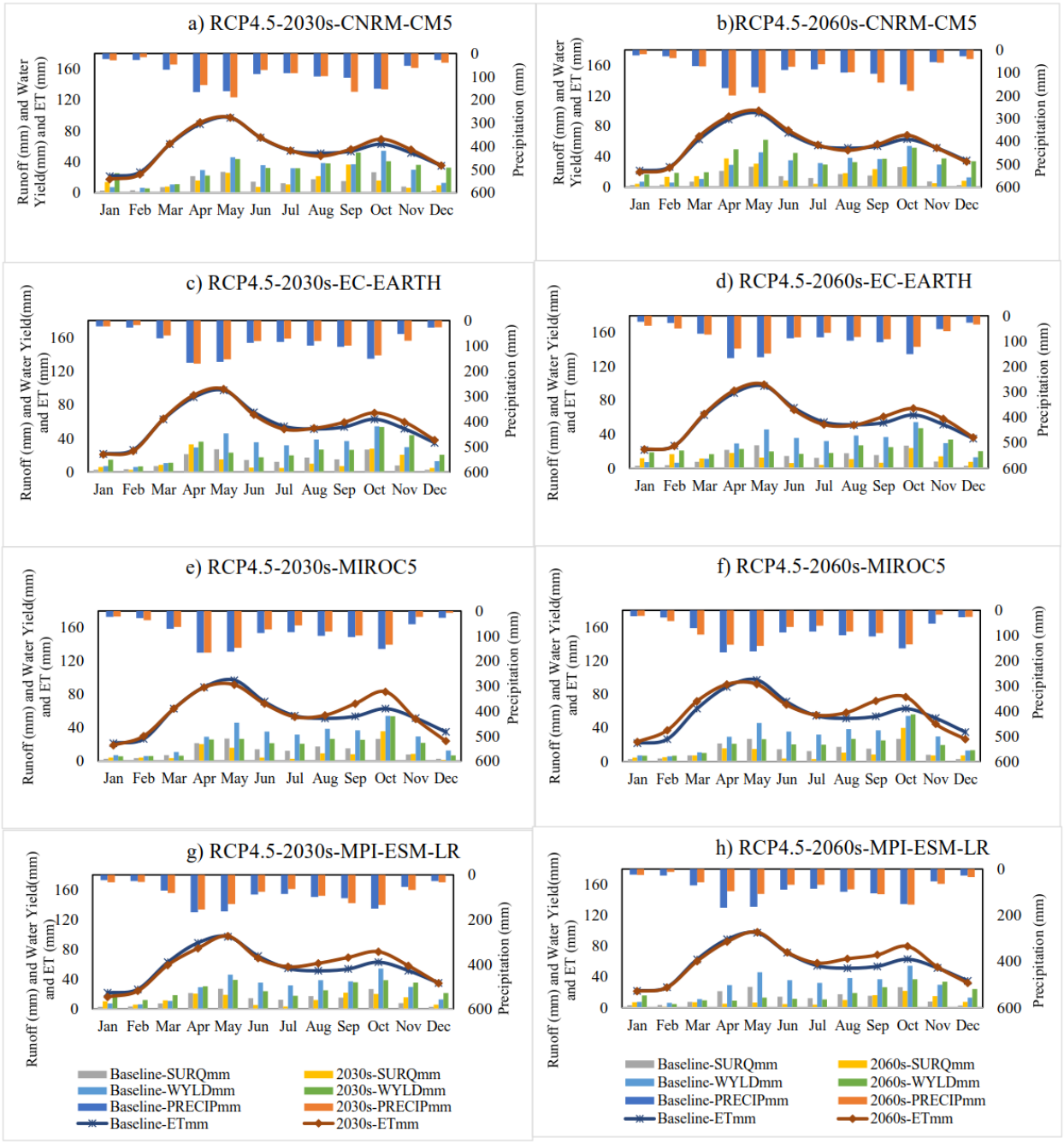

Figure 5-6. Represent the average monthly simulated precipitation, evapotranspiration, surface runoff, and water yield for different climate models and time periods (2030s and 2060s) under RCP4.5 scenario. Models include CNRM-CM5, EC-EARTH, MIROC5, and MPI-ESM-LR.

The simulated mean monthly hydrological components of the baseline and the future climate model under the two RCPs during 2030s and 2060s in the Figure 5-6 and 5-7 a-h shows that highest value of average monthly water yield, runoff, and ET were observed during the spring (MAM) and autumn (SON) seasons. Furthermore, except the CNRM-CM5 model, during 2030s and 2060s

under RCP4.5, the climate models EC-EARTH, MIROC5, and MPI-ESM-LR showed likely reduction of water yield and surface runoff in most months from April to October (Figure 5-6 c-h). Similarly, Figure 5-7 (a - h) during the future period under RCP8.5, in most month from April to September for EC-EARTH, March to September for MIROC5, and March to October for MPI-ESM-LR climate models reduction of water yield and surface runoff is anticipated. During the future time (2030s and 2060s) under the two RCP, from March to August up to 68% runoff and 57% water yield reduction expected for EC-EARTH model. Similarly, for MIROC5 up to 62% of water yield and 88% surface runoff and for MPI-ESM-LR up to 72% of water yield and 86% surface runoff reduction is anticipated. The result for MPI-ESM-LR, MIROC5, and EC-EARTH models also showed that the simulated rainfall in most months from March to October, is likely to be reduced during the 2030s and 2060s under the two emission scenarios. In contrast to other hydrological parameters such as runoff, water yield, groundwater flow, and lateral flow, evapotranspiration is expected to increase in all climate models during most months in the 2030s and 2060s under the two emission scenarios. This is due to an increasing future temperature in all climate models. The likely reduction of total water yield and runoff in the future period may be due to reduction of rainfall, increasing of temperature and increasing of evapotranspiration in the study basin. Different research in different parts of Ethiopia stated that reduction of hydrological parameters mainly total water yield, surface runoff, and ground waterflow linked with an increasing of evapotranspiration and temperature and reduction of rainfall (Daniel & Abate, 2022; Takele et al., 2022; Tessema et al., 2021; Worku et al., 2021).

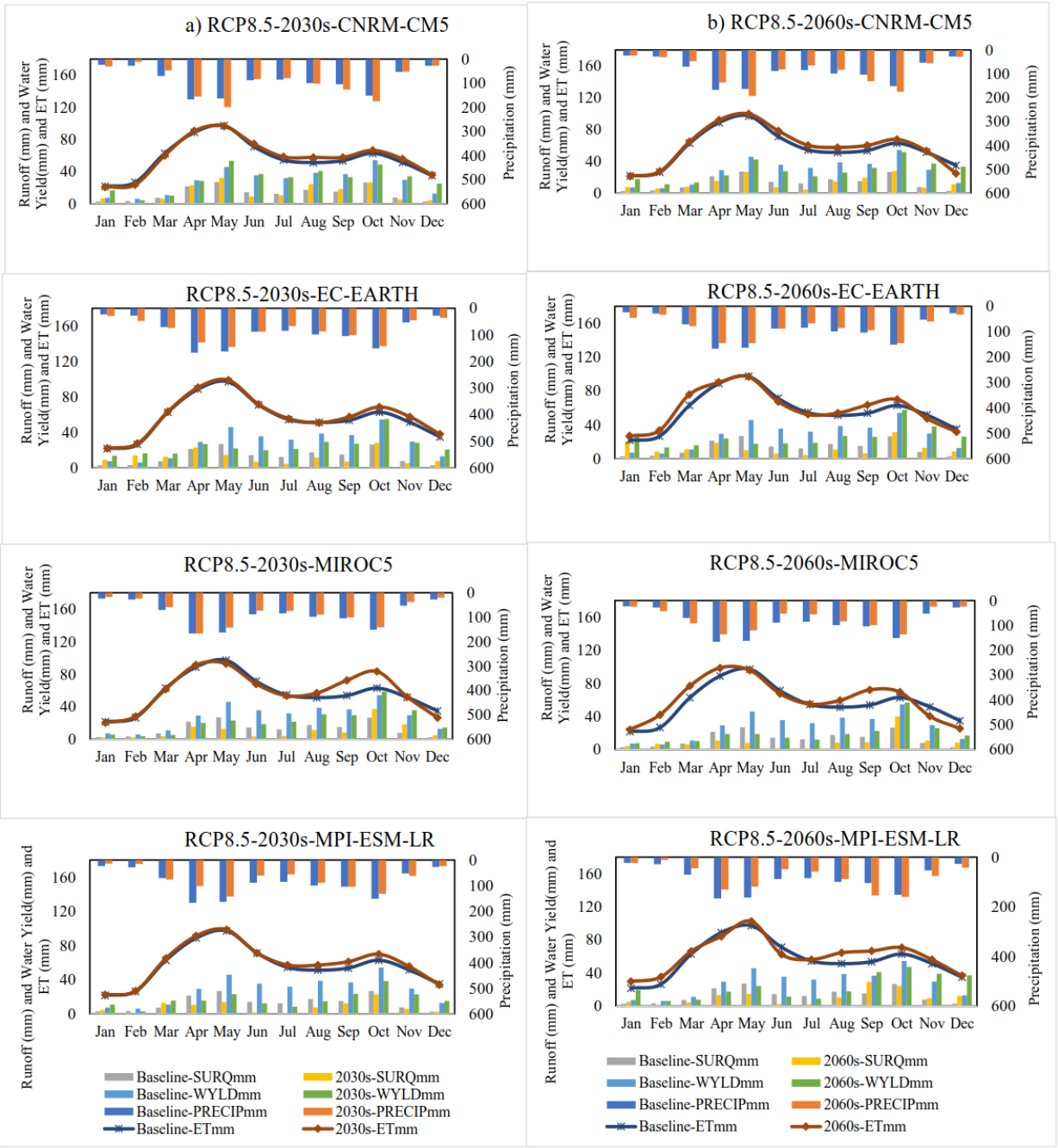

Figure 5-7. Shows mean monthly simulated precipitation, surface runoff, water yield and evapotranspiration for different climate models (i.e., CNRM-CM5, EC-EARTH, MIROC5, and MPI-ESM-LR) and time periods (2030s and 2060s) under RCP8.5 scenario.

Overall, the impact of climate change due to an increasing temperature and a reduction of rainfall that is likely to occur in the future time under the RCP4.5 and RCP8.5 scenarios significantly affect the water resource of the upper Genale river basin. The likely reduction of runoff, ground

waterflow, lateral flow, and total water yield as well as an increase of ET in the study basin may result in a water stress. Water stress, especially due to the reduction of total water yield, runoff, and groundwater flow during the rainy season may cause extensive impact on water supply for domestic and livestock, agricultural activities, and ecosystem service in the study basin. A change in rainfall and temperature could have significantly reduced agricultural yield and, in the worst cases, causes complete crop failure, leading to famine and deaths of both humans and animal (Shigute et al., 2023). Therefore, to deal with the expected negative effects of climate change on agricultural development and other sectors due to future warming of temperature and decrease of rainfall amount and distribution, it is essential to design and implement watershed management practices, develop management and adaptation measure, and water allocation system in the study basin.

5.4. Summary and Conclusion

Climate change affects the water resource of the river basin. To assess the likely impacts of climate change on the hydrological components and water resource potential of the upper Genale river basin during 2030s and 2060s under RCP4.5 and RCP8.5, bias corrected future temperature and precipitation data from CORDEX Africa RCMs (EC-EARTH, CNRM-CM5, MIROC5, and MPI-ESM-LR) were applied in to calibrated SWAT model.

The result shows that except for the CNRM-CM5 climate model, the predicted climate shows a rise in temperature and a decrease in rainfall in all future times (in the 2030s and 2060s) under the two RCPs. The change in future temperature and rainfall in comparison with the baseline period could significantly affect the hydrological components. Under both RCPs, rising temperatures and decreasing precipitation during the 2030s and 2060s are projected to significantly reduce the annual hydrological components of the entire study basin. Total water yield, runoff, ground waterflow, and lateral flow are all expected to decline within a range of 1.03% to 39.8%, 1.61% to 39%, 5.42% to 50%, and 1.7% to 40.1%, respectively. However, evapotranspiration is projected to increase significantly in these future scenarios. The observed change in hydrological parameters such as reduction of water yield, runoff, lateral flow, ground waterflow flow as well as a rise in evapotranspiration in the study watershed evidently associated with the future change in

temperature and rainfall. The reduction of water resources, especially during the rainy seasons can cause extensive impact on agriculture and ecosystem service of the basin.

The declining of runoff, total water yield, and ground waterflow along with an increasing evapotranspiration due to future impact of climate change has boarder implication for developing and managing water resource. In this regard, designing and implementing water resource management strategies is indispensable for minimizing the potential impact of climate change on water resources in the study basin. To develop an efficient and long-lasting water resource management strategy in the watershed, it is critical to incorporate projected and simulated climate and hydrologic variables into adaptation decision analysis. In line with this, it is crucial to implement policies and strategies that enhance the water resource systems in the study basin in order to increase the capacity for dealing with the anticipated impact of climate change and variability on hydrological variables. An increase in climate change related research and designing and implementing effective water resource management strategies to provide optimal benefits to adapt and mitigate the impact of climate change and maintaining the water resources availability, would be one approach.

As a result, the current research has provided valuable insight into the expected rainfall and temperature trends, as well as the future impact of climate change on hydrological elements in the study basin, which is essential for managing water resources and maintaining sustainable agricultural production. As a result, the results of this study contribute to a better understanding of the available water resource potential, as well as to water resource planning, management, and development for current and future development projects in the study basin. Moreover, the study's findings and methodology can be used to develop guidelines for other regions and the Genale Dawa River basin in the future. To further enhance the results, we propose additional research in the study watershed that provides more detailed and accurate information for modeling work that takes into account high-quality climatic data, different climate models as well as different bias correction approaches, the use of different hydrologic models, and the combined effect of socioeconomic, climate, and land use change in the study watershed.

CHAPTER SIX:

6. EVALUATING STREAMFLOW POTENTIAL AND DEMAND OF THE UPPER GENALE RIVER BASIN UNDER CURRENT AND FUTURE DEVELOPMENT PLAN, ETHIOPIA

Abstract

The management of water in river basins depends on accurate assessment and efficient distribution of limited water resources. This study investigates the water resource potential, demand, and allocation in the upper Genale River basin under various future scenarios. SWAT to generate streamflow data and WEAP models to optimally allocate water demands for the period 2020-2050 have been used. Scenarios considered population growth, improved water consumption, irrigation expansion, and climate change (RCP4.5 and RCP8.5). Results indicate the livestock sector as the current primary water user, followed by domestic and commercial sectors, with irrigation having the lowest consumption. The reference scenario projects a significant increase in total water demand (79.99 MCM in 2020 to 330.91 MCM in 2050) due to population and livestock growth. Scenarios with high population growth and improved consumption or irrigation development showed substantial demand increases, highlighting the pressure these factors exert. Additionally, the study highlights a significant risk of water scarcity, especially in scenarios with a combination of high population growth, increased irrigation development, and climate change. This research emphasizes the critical need for proactive water management policies to tackle these challenges. Such policies should ensure effective transboundary water management and promote sustainable water allocation for future generations. Furthermore, the study highlights the need for diversifying energy sources beyond hydropower due to potential water limitations. This research significantly improves understanding of water availability, demand, and allocation, informing effective planning and development of water resources in the upper Genale River basin.

Keywords: Upper Genale River Basin, SWAT model, WEAP model, Future Scenarios, Climate change

6.1. Introduction

Fresh water sources around the world are depleting, resulting in a water shortage in the domestic and agricultural sectors. This is a major global issue because it has an impact on water resources as well as the availability of safe drinking water for the population (Liu et al., 2017). Because of ever-increasing demands from urban water supply, industry, energy, and agriculture production, competition for available water resources is increasing rapidly in many developing countries (Gedefaw et al., 2019; Xu et al., 2018). Growing urbanization, and increasing standards of living and water consumption rate all have a strong correlation, putting extra pressure on the available water resources (Amin et al., 2018; Bao & He, 2015). These pressures reduce per capita water availability of the limited fresh water resources in a basins (Al Radif, 1999).

In addition to the aforementioned factors, climate change has a significant impact on water resources and the hydrologic cycle process. The availability and properties of natural water resources will be significantly affected by climate change (IPCC, 2014). Climate change, economic activity, and population growth all contribute to water scarcity, a condition in which water supply is insufficient to meet demand due to scarcity and inadequate water management infrastructure. Water allocation fall short to satisfy the intended demand when demand exceeds available supply, resulting in a reduction in availability of per capita water (Amin et al., 2018). Increasing living standards, rapid urbanization, and severe weather conditions are all contributing to heightened water demand, further exacerbating the existing problem (Abraha et al., 2022).

Freshwater availability is critical to economic growth and social development in Sub-Saharan Africa. These freshwater supplies, however, are unevenly distributed and fall on the earth at varying times, locations, and magnitudes. Water insecurity and a lack of access to safe water are major challenges in Sub-Saharan Africa. Extreme weather events and climate change have exacerbated the problems, as have poor infrastructure, inadequate funding, and unsustainable governance (Eludoyin & Olanrewaju, 2020).

The Genale Dawa is one of 12 river basin of Ethiopia; however, surface water use in the basin is currently low. The use is restricted to water supply to large townships and a few small to medium-sized irrigation areas (MoWE, 2007b). Water demand, however, is rising as a result of urbanization, population growth, agricultural land expansion, climate change, and the potential

construction of several medium- to large-scale irrigation plans, water supplies, and hydropower plants. Future changes in the utilization situation will also have a significant impact on the use of natural resources, particularly water and land (MoWE, 2007b). In this situation, competition for water among different water sectors jeopardizes the sustainability of the water resources, resulting in conflicts (Divakar et al., 2011; Gedefaw et al., 2019; Goshime et al., 2021). During dry periods, water demand is likely to exceed supply, potentially leading to reduced water availability for the Genale Dawa hydropower plant (GD3) and shortages in lower basin schemes due to upstream abstractions. Hence, in order to balance the supply and demand of water resources based on economic development, efficient and optimal analyses of water resource demand and allocation is very important (Divakar et al., 2011).

Nowadays, water resources are now modeled using a variety of models, including water resource allocation and simulation model (WAS) (Yan et al., 2018), MODSIM (Berhe et al., 2013), Cooperative Water Allocation Model (CWAM) (Wang et al., 2008), Multi-objective Evolutionary Algorithms (MOEA) (Yan et al., 2017), Soil and Water Assessment Tool (SWAT) (Kuma et al., 2023; Marin et al., 2022), and the Water Evaluation And Planning (WEAP) model (Gedefaw et al., 2019) (Goshime et al., 2021; Yan et al., 2018). This study chose the SWAT and Water Evaluation and Planning (WEAP) models because of their ability to address various hydrological components in areas with limited data. Furthermore, the model's simplicity, flexibility, and ability to assess water resource potential, the effects of climate change on water resources, and analyze water demand and allocation using a scenario-based approach were important factors in its selection. When compared to other allocation models, the WEAP model also simulated domestic, irrigation, and ecological water consumption in time and space. The WEAP model provides a set of objects and procedures that can be used to apply to river basins, watersheds, and reservoirs through the use of a scenario-based system and solve problems faced by water resource managers and planners (Gedefaw et al., 2019).

Previously, the WEAP model was used to assess and analyze the existing balance and expected future water resource management scenarios in various Ethiopian watersheds (Abera Abdi & Ayenew, 2021; Adgolign et al., 2016; Gedefaw et al., 2019; Goshime et al., 2021; Hamza & Getahun, 2022; Kifle Arsiso et al., 2017; Orkodjo et al., 2022). Although numerous studies have explored water resource assessment, demand, and allocation in different regions of Ethiopia, a

comprehensive scientific analysis of water potential, demand, and allocation under various scenarios has been lacking for the upper Genale river basin. Additionally, the majority of studies conducted in Ethiopia to date have not reached definitive conclusions and fail to accurately model the basin's water resources to effectively allocate and address water resource development scenarios. This highlights the need for further investigation in the upper Genale basin.

Therefore, this study evaluated the basin's water potential, demand, and allocation under population growth, irrigation expansion, and climate change scenarios to ensure the sustainable availability of water in the study basin in the future. The basin encompasses varying topographic and climatic regimes. The main river, the Genale, is a multi-purpose river that has been used for a variety of water-related projects, and additionally, the federal government of Ethiopia has designed huge development plans to develop the water resources of the river basin (MoWE, 2007b). Hence, knowledge of water potential, demand, allocation under different scenarios in a river basin is essential to attain sustainable social, economic and environmental benefits and to plan possible climate change adaptation and mitigation measures. In addition, the output of this study may be utilized to design and implement effective water resources development and management in the area.

6.2. Materials And Methods

6.2.1. Description of the Study Area

The Genale river basin lies in the southern part of Ethiopia, covering parts of Oromia, Southern Nations, Nationalities, and Peoples', and Somali regions. Geographically located between 3^0 30' and 7^0 20' North latitude and 37^0 05' and 43^0 20' East longitude. The basin covers an area of about 172,713km^2. It is one of the three largest river basins in Ethiopia. Adjacent river basins are the Wabi-Shebelle to the north and east, the Rift Valley basin to the west (Awulachew et al., 2007). Specifically, the upper Genale Sub-River basin (study area) is located between 6^0 52’ and 5^0 20’ North latitude and 38^0 30' and 39^0 45' East longitude and lies in the upper central area of the Basin. It has a basin area of about 10,582.19 km^2 (Figure 6-1). Due to the north-south oscillation of the Inter-Tropical Convergence Zone (ITCZ) and effects of topography, the basin experiences bimodal type I (three season type) and bimodal type II (double wet and dry seasons) annual rainfall cycle

in northern (highland) and southeastern (lowland) parts, respectively. The northern and highland area characterized by the three wet seasons types, March–May (locally known as *Belg*), June–September (locally known as *Kiremt*) and September–November (locally known as *Meher*) (MoWE, 2007c). The lowland and the southeastern parts of the study area characterized by double wet season, the first wet season runs from March to May with a peak on April, and the second from September to November, with a peak on October (Degefu et al., 2021; MoWE, 2007)**.** The mean annual rainfall ranges from 1617.7 mm to 591mm**.** The mean annual minimum and maximum temperatures range between 18.9 to 27.7^{o}C and 6.9 to 16.2 ^{o}C, respectively. The Genale River originates from the southern slopes of the Bale Mountains massif in the north-east and from the Sidamo Mountains in the north-west (MoWE, 2007c).

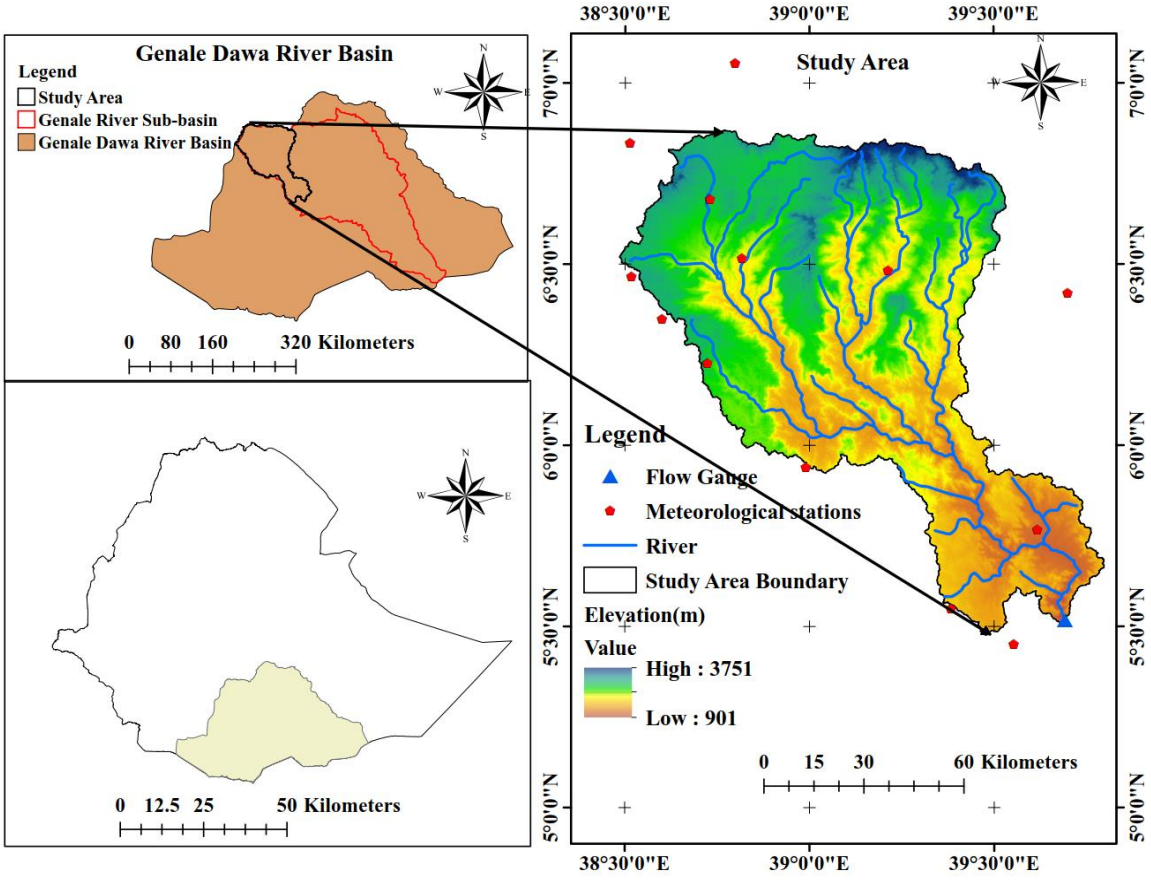

Figure 6-1. Location of the study area

6.2.2. Data collection

6.2.2.1. Climate Data

The basic data required for this study were collected from different sources. Daily rainfall data (1984–2016) for ten stations and minimum and maximum temperature data for five stations were used (Table 6-1). Due to the limitation of climate data in the study area, ten stations of rainfall data and five stations of minimum and maximum temperature data (Negehle, Harokelo, Hager Selam, Bidere, and Arbgona) were obtained from the National Meteorological Agency of Ethiopia (NMA). Data for the Harokelo, Bidere, and Arbegona locations were extracted from the ENACTS dataset. The dataset, which has a resolution of 4 x 4 km, was constructed by combining data from satellite estimates from NASA (the US National Aeronautics and Space Administration) and EUMET-SAT (the European Organization for the Exploitation of Meteorological Satellites) with station records from nearby locations (Dinku et al., 2014, 2016). The effectiveness of ENACTS has been evaluated at numerous stations across the nation, and it has turned out to be effective (Alemayehu & Bewket, 2017; Dinku et al., 2014, 2016).

Table 6-1. Summary of the study area meteorological stations and their geographical locations.

Name of Stations	Latitude	Longitude	Altitude	Rainfall	Temperature
	(N°)	(E°)	(m)	Period	Periods
Telamokentise	6°50'1"	38°30'38"	1911	1990-2016	
Yirba Muda	6°13'17"	39°35'43"	2560	1987-2016	
Woreka	6°30'6"	39°12'45"	2450	1987-2016	
Bore	6°20'30"	38°38'29"	2712	1984-2016	
Kibre Mengist	5°53'46"	38°58'1"	1680	1984-2016	
Bidere	5°46'19"	39°36'46"	1400	1984-2016	1984-2016
Arbegona	6°40'48"	38°43'30"	2600	1984-2016	1984-2016
Harokelo	5°33'19"	39°23'17"	1600	1984-2016	1984-2016
Hager Selam	6°30'47"	38°31'18"	2809	1984-2016	1984-2016
Neghele	5°26'1"	39°35'43"	1544	1984-2016	1984-2016

The Multivariate Imputation by Chained Equations (MICE) algorithm as explained in van Buuren & Groothuis-Oudshoorn, (2011) was used to generate and fill the missing values, and then the data was used for further analyses. To ensure the data's quality and reliability, homogeneity tests were

performed. The standard normal homogeneity test (SNHT) (Alexandersson, 1986), the Buishand range test (Buishand, 1982), the Von Neumann ratio test (von Neumann, 1941), and the Pettitt test (Pettitt, 1979) were the four absolute statistical homogeneity tests used. The details of the analysis results in Shigute et al. (2023) showed that the data were homogeneous and could be used for further analyses.

6.2.2.2. GCM-RCM and scenario selection

To assess future climate change impacts scenario on the water demand of the study watershed, future precipitation and temperature data from CORDEX Africa RCMs were obtained from the ESGF website (https://esgdn1.nsc.liu.se/esgf). For this study, three different RCMs (KNMI Regional Atmospheric Climate Model, version 22 (RAMO22 T), Rossby Center regional atmospheric model (RCA4), and Regional Climate Limited-area modeling (CCLM)) and four downscaled GCM driving models (EC-EARTH, CNRM-CM5, MIROC5, and MPI-ESM-LR) of CMIP5 (Climate Model Inter-comparison Project Phase 5) were used in combination. These resulted in four GCM-RCM combinations of CORDEX-Africa projections under two RCPs (4.5 and 8.5) (Table 6-2), which were used for impact assessment. The details of the two RCPs scenarios are explained by the IPCC (IPCC, 2014).The choice of the GCM-RCM model was made in consideration of other studies of the effects of climate change on east Africa, particularly in various regions of the Ethiopia river basin, as well as how well the climate models represent past and present climate, their resolution, and other related factors (Adera & Alfredsen, 2020; Adugna et al., 2021; Bekele et al., 2021; Ketema & Dwarakish, 2021; Mengistu et al., 2020; Musie et al., 2020; Tessema et al., 2021; Worku et al., 2020).

The CORDEX-Africa data has a spatial resolution of approximately 50 km by 50 km, which is equivalent to 0.44 degrees by 0.44 degrees. The data covers from the years 1951 to 2100, with a historical time frame from 1951 to 2005 and a future projection from 2006 to 2100 (Musie et al., 2020). In this study, to assess the change in patterns of climate data, the baseline scenario period (1987-2016) and the future scenario period (2021-2100) were used. The future scenarios were divided into two different periods of time with 30-year intervals, such as 2021-2050 (the 2030s) and 2051-2080 (2060s).

Table 6-2. Descriptions of selected GCM - RCM climate models

GCM Name	RCM	INSTITUTION
CNRM-CM5	CCLM4-8-17-V1	Climate Limited-area Modelling Community
EC-EARTH	RACMO22T_v1	Royal Netherlands Meteorological Institute
MIROC5	SMHI-RCA4_V1	Swedish Meteorological and Hydrological Institute
MPI-ESM-LP	CCLM4-8-17-V1	Climate Limited-area Modelling Community

6.2.2.2.1. Bias correction

The RCM climate data outputs in CORDEX-Africa under emission scenarios RCP 4.5 and 8.5 were bias corrected for application for climate change impact studies in the study basin. The process of bias correction involves adjusting the raw output of a climate model using a transformation algorithm, under the presumption that the algorithm used to parametrize and correct the current climate will also be applicable to future scenarios (Yeboah et al., 2022). For this study, to bias-correct and extract data from the RCM model, CMhyd tool was used (Rathjens et al., 2016). To correct the maximum and minimum temperature and precipitation data, the linear scaling method was selected from the available bias correction techniques in the CMhyd software. Because of its simplicity, accuracy, and ease of application, this method has been widely used to correct GCM-RCMs in various parts of the world (Abera & Gebeyehu, 2023; Azman et al., 2022; Galata et al., 2021; Mahmood et al., 2018; Mahmood & Babel, 2013; Mahmood & Jia, 2017; Shrestha et al., 2017; Takele et al., 2022). Furthermore, the method works well for climate change-related water resource research (Takele et al., 2022).

6.2.2.3. Streamflow data

The daily streamflow data recorded at Chenemassa gauging station from 1984 to 2011 was collected from the Ethiopian Ministry of Water and Energy (MoWE). To estimate missing values, multiple imputation was used, which is the best method for estimating missing values in flow data (Sattari et al., 2017). Then, for model calibration and validation, the streamflow data from 1987 to 2002 and from 2003 to 2011 were used, respectively.

6.2.2.4. Spatial data

SWAT model utilizes spatial data such as the Digital Elevation Model (DEM), Land Use Land Cover (LULC), and soil map.

DEM data

A digital elevation model (DEM) was used to determine the basin boundary, sub-basins, sub-basin characteristics of the watershed (e.g., elevation, slope gradient, river network, reach length, and channel slope), and the hydrologic response unit. The USGS website was used to obtain the Shuttle Radar Topography Mission (SRTM) DEM of the study basin with a 30m horizontal resolution. The elevation band of the processed DEM ranges from 901 to 3751 m (Figure 6-1).

Land Use Land Cover

LULC is one of the factors that have the greatest impact on hydrological variables in a river basin, and it is used in the SWAT model to determine HRUs and hydrologic characteristics. To assess the hydrological components of the study basin under the effects climate changes, the classified LULC map of the study watershed was obtained from Shigute et al., (2022). The details of image analysis and classification results at (Shigute et al., 2022), showed that the dominant categories are cultivated land (47%), shrubland (19.53%), forest land (13.53%) and grassland (18.9 %) of the watershed. The settlement, bare land and water body areas covered a smaller portion of the watershed.

Soil data

A soil map of the Upper Genale river basin affecting the hydrologic characteristics of the watershed was obtained from FAO and extracted using ARCGIS 10.5 software. The SWAT database was used to extract soil physicochemical properties such as hydrologic group, texture, depth, bulk density, erodibility, hydraulic conductivity, and organic matter content. Furthermore, the soil survey report of the Genale Dawa river basin master plan developed by Ethiopia's Ministry

of Water Resources was used to verify and compare the necessary soil physical and chemical properties extracted from the SWAT database (MoWE, 2007e). The soil types in the study area includes Calcaric Regosols (1.6%), Ferric Acrisols (3.7%), Eutric Cambisols (13.1%), Eutric Nitosols (40.3%), and Haplic Yermosols (41.4%).

6.2.2.5. Socio-economic data

Important socio-economic information such as agriculture, domestic water supply, demographic surveys and water-use were collected from different governmental offices in the regions. Population data were obtained from CSA. Location of irrigation site including command areas and Livestock population were obtained from Oromia and Sidama irrigation development, and Agriculture bureaus. Details of the data used in this study are presented in Appendix Table 12 – 16.

6.2.3. SWAT model description and set up

The SWAT is a semi-distributed, physically based hydrologic model that operates on a continuous time-step (Arnold et al., 2012). The model is developed to simulate the climate change effects on hydrology, land management, and movement of agricultural chemicals and sediment of a wide and complex basin(Arnold et al., 1998; Taylor et al., 2016). The hydrology is simulated in two major ways: The Land Phase, which controls the nutrient, pesticide, sediment loaded, and water transport to each channel from sub-watersheds, and the Water or Routing Phase that controls the movement of flow up to the basin outlet. The SWAT model simulates the hydrologic phenomena of the land phase using the water balance equation shown as follows (Narsimlu et al., 2015; Neitsch et al., 2011):

$$SW_t = SW_o + \sum_{i=1}^{t}\left(P_{day} - Q_{surf} - E_a - Q_{gw} - W_{seep}\right) \quad (1)$$

where SW_t and SWo represent the final and initial soil water content on day i (mm), W_{seep}, Q_{gw}, E_a, $Q_{surf,}$ and P_{day} represent the amount of water entering the vadose zone from the soil profile,

return flow, evapotranspiration, surface runoff, and precipitation, respectively on day i(mm), and t is time (days).

The SWAT model uses either the USDA Conservation Service Curve Number (SCN-CN) or the Green and Amp method for calculating surface runoff produced in the watershed (Neitsch et al., 2011). For this study, the SCN-CN technique (Equation 2) was applied to estimate runoff for each HRU (Arnold & Fohrer, 2005).

$$Qsurf = \frac{(Pday - 0.2S)^2}{(Pday + 0.8S)} \quad (2)$$

Where, Q_{surf}, $Pday$, and S represent, daily depth of accumulated surface runoff (mm), the daily rainfall (mm), and retention parameter, respectively. Based on equation 2, runoff happens in a watershed when $Pday > 0.2S$.

In relation to the CN, the parameter S is calculated using Equation 3. The retention parameter, S, is affected by slope, soil type, and land management practices.

$$S = \frac{254(100 - \mathrm{CN})}{\mathrm{CN}} \quad (3)$$

Where, *CN* is the curve number for the day. During model calibration process, *CN* is the main parameter that determine the catchment runoff (Arnold et al., 2012).

The SWAT model has three different approaches for calculating evaporation: the Hargreaves, Priestly-Taylor, or Penman-Monteith methods (Neitsch et al., 2011). For this study, because of the limited availability of data and the simplicity of the method, the Hargraves method was applied.

6.2.4. Sensitivity analysis

Hydro-climatic parameters from 1984 to 2016 were used to simulate the hydrological characteristics of the study watershed. Climate data from the first three years (1984-1986) were used to initialize the SWAT model, and data afterwards from 1987-2016 were employed to perform model sensitivity and calibration analysis.

Because the SWAT model contains a large number of flow parameters, identifying the parameters that are most sensitive to streamflow that can be used in model calibration and validation is critical (Abbaspour et al., 2018; Chimdessa et al., 2019). For this study, to differentiate the most sensitive parameters, initially twenty-one flow parameters were meticulously chosen from the literature and the SWAT-CUP. Then, by using the objective function, *P*-values and *t*-stat, multiple regression methods with Latin hypercube method, sensitivities of parameters were determined. The *p*-values and *t*-stat show the level and degree of sensitivity to flow parameters, respectively. The larger *p*-values indicating less sensitivity and smaller values indicating greater sensitivity. Small absolute *t*-stat values imply lower sensitivity, while large values reveal higher sensitivity (Abbaspour, 2015; Narsimlu et al., 2015).

6.2.5. Calibration and Validation of SWAT Model

Streamflow data from the Chenemasa gauging station was used to calibrate and validate the SWAT model. Calibration and validation were performed using streamflow data from 1987 to 2002 and 2003 to 2011, respectively. To calibrate and validate the model, the SWAT-CUP2012 software's sequential uncertainty fitting (SUFI-2) algorithm was used (Abbaspour, 2015). SUFI-2, is the most widely applied program in Ethiopia for model calibration, validation, and sensitivity analysis (Abraham & Nadew, 2018; Bekele et al., 2021; Belihu et al., 2020; Bizuneh et al., 2021; Bogale, 2021; Mengistu et al., 2020; Takele et al., 2022; Teklay et al., 2020; Tessema et al., 2021).

6.2.6. Evaluation of SWAT model performance

The performance of the SWAT model was evaluated in order to compare observed data and model simulation outputs. Hence, in this study, the statistical parameter values of Nash-Sutcliffe efficiency (NSE), coefficients of determination (R^2), and percent bias (PBIAS) were used to assess the performance of the SWAT model. These statistical units are the most commonly used parameters to assess the performance of models (Akoko et al., 2021; Shukla & Gedam, 2018). Statistical indices of *PBIAS*, R^2, and *NSE were* calculated using Equations 4, 5, and 6 respectively.

The amount of the total variance in the observed data that the model can explain is indicated by the regression coefficient (R^2). The greater the agreement between the observed and the simulated flow, the closer the value of R^2 is to 1. Equation 4 is used to calculate R^2 as shown below:

$$R^2 = \left\{ \frac{\sum_{i=1}^{N}(Oi - \bar{O})(Pi - \bar{P})}{\left[\sum_{i=1}^{N}(Oi - \bar{O})^2\right]^{0.5}\left[\sum_{i=1}^{N}(P - \bar{P}\imath)^2\right]^{0.5}} \right\}^2 \quad (4)$$

Nash-Sutcliffe coefficient (Nash & Sutcliffe, 1970) described in Equation 5 was used to determine how the observed data and simulated output and closely fit in 1:1 line.

$$NSE = 1 - \frac{\sum_{i=1}^{N}(Oi - Pi)^2}{\sum_{i=1}^{N}\left(Oi - \bar{O}\right)^2} \quad (5)$$

According to Moriasi et al., (2007), the percent of bias (PBIAS) was used to estimate how much the measured values would differ from the values of the simulated output of counterparts. To calculate PBIAS equation 6 was used.

$$PBIAS = \frac{\sum_{i=1}^{N}(\text{oi-pi})}{\sum_{i=1}^{N}(\text{oi})} * 100 \quad (6)$$

Where $\bar{P}$ and $\bar{O}$ represent mean simulated and measured data; Pi and Oi represent simulated and measured data; and N represents the number of compared values.

Moriasi et al., (2007) state that the model's performance is acceptable when the value R^2 is exceeds 0.6, NSE is higher than 0.5, and PBIAS falls within ±25% range. The value of the *NSE* varies from -∞ to 1, and where the *NSE* is close to 1, the model performs best. The value of R^2 ranges between 0 to 1, where R^2 close to 1 specifies less error. On the other hand, the model simulation works best when *PBIAS* is close to 0. The model under- and overestimates the simulation, respectively, as indicated by the positive and negative PBIAS values (Nasiri et al., 2020).

6.2.7. WEAP model Set up

WEAP is a user-friendly and powerful tool for managing water resources. WEAP is designed to consider all aspects of water management, and it's known for being efficient, easy to use, and

accessible to water professionals. It's also flexible, allowing users to adjust the data and complexity to fit their specific needs. This makes WEAP valuable for water managers, especially in areas with limited data. The software was used to simulate various future water management and development situations. These simulations were defined by specific time periods, areas, and water system components (Hussen et al., 2018).

In WEAP model the simulation began in a phase known as "current accounts," which was distinguished by the availability of all or nearly all relevant data. For this study, the year 2020 was designated as the current accounting, while 2050 was the scenario's final year. At the beginning of the evaluation processes, the water system's spatial location was defined by the study area's borders. The demand sites were represented in the schematic view by nodes that were placed in relative positions. Nodes were connected to the river via transmission and return flow links. Transmission links provide a pathway for water to flow from supply systems to demand sites, while return flow links channel water back from demand sites to the river.

The SWAT sub-basin map and the upper Genale River shapefiles were imported into the WEAP model. The streamflow output data from the SWAT model, which simulated the hydrology, served as the water supply source for the WEAP model. According to Adgolign et al.(2016), Hussen et al. (2018), and Touseef et al. (2021), the mean monthly stream output flows from the SWAT model were used as the river head flows in the WEAP model.

6.2.8. Water demand in the study basin

The study considered all the water needs within the area, including domestic, commercial and institutional, livestock, irrigation, hydropower, and environmental flow.

To understand how much water is needed for different purposes, the WEAP model looked at each use separately (disaggregated approach). For livestock, domestic, and agriculture, they considered various social and economic factors. In the simplest scenario, they assumed a certain number of people, animals, or land area and multiplied it by a standard amount of water used per person, animal, or land area. The methods used to determine these demands are discussed below.

6.2.8.1. Water demand for consumptive use

6.2.8.1.1. Domestic Water demand

The amount of domestic water needed is primarily determined by gathering data on the number of people residing in the watershed and their average daily water consumption. The national GTP-2 plan provided a framework for domestic water needs. This plan established a new water supply standard, setting a daily per capita allocation of 25 liters for rural areas and 40-100 liters for urban areas (NPC, 2016). As this research focuses on a rural and small-town area, these recommended values of 25 liters per capita per day for rural areas and 40 liters per capita per day for small towns was adopted to ensure sufficient water supply for the local population.

The method for projecting the population for the upcoming period was selected based on an analysis of the community's growth between recent censuses. Geometric approaches are generally suitable for determining projected population using the geometric increase method of equation 7 and population data for the study area collected from the CSA for the year 2020. To determine the water demand, the total population was multiplied by the per capita water demand.

$$P_n = P_i(1 + G_r)^n \quad (7)$$

Where P_n is population after n years, P_i initial population, and G_r is Growth rate in percentage.

6.2.8.1.2. Livestock water consumption

The total water consumption by livestock in the basin is estimated by multiplying the average daily water requirement per animal by the total livestock population. To determine these requirements, studies by Sileshi et al. (2003) on standard water demands in Sub-Saharan Africa, particularly Ethiopia, Vijayan et al. (2022) in Yergalem Tula Kebele, Ethiopia, and Adeba et al. (2015) in the Awash basin, Ethiopia, were considered. These studies suggest varying daily water intake: Sileshi et al. (2003) reported 25-60 liters for cattle, 30-45 liters for horses, and 5-15 liters for goats/sheep. Vijayan et al. (2022) recommends 50 liters for cattle, 10 liters for goats/sheep, and 0.2 liters for poultry, while Adeba et al. (2015) provides specific figures for different livestock: 54 liters for cattle, 7.14 liters for sheep, 45.6 liters for equines, 55.6 liters for camels, and 0.4 liters for poultry.

Based on these studies and the specific context of this basin, the following daily water requirements (Table 6-3) were adopted for this study: 50 liters for cattle, 45 liters for horses/donkeys/mules, 10 liters for goats/sheep, and 0.4 liters for poultry.

Table 6-3. Daily water requirement for different animals

Livestock class	Daily water demand (Liters/day)
Cattle	50
Sheep and Goats	10
Horse/Donkys/Mules	45
Camel	43
Chickens	0.4

Adapted from (Sileshi et al., 2003).

6.2.8.1.3. Demand for agriculture

To determine the required irrigation water in the study area, data was collected from various sources, including the Ethiopian Ministry of Water and Energy (MoWE), the Oromia and Sidama regional bureaus of irrigation development and prefeasibility study, and existing irrigation projects. Subsequently, the irrigation demands were calculated using Irrigation Demands only (simplified coefficient method) developed by SEI (Sieber & Purkey, 2015) using (Equation 8 and 9). The Irrigation Demands Only method is a simplified approach to estimating irrigation water needs in the Water Evaluation and Planning System (WEAP) model. The model developed to simulate the observed seasonal pattern of irrigation with different cropping seasons. Irrigation water demand is influenced by various factors such as crop type, climate, growing calendar, and irrigation technology. Estimates were made based on representative crop types commonly found in the study basin. Meteorological data was utilized to assess net evaporation from the catchment area and interannual variations in irrigation demand.

To calculate the crop water requirements (CWR) for both individual fields and the entire irrigation project, the WEAP model was employed. The determination of the CWR by this model depends on the determination of the reference evapotranspiration values using the available climatic data.

The reference evapotranspiration values for each irrigation sites were extracted from SWAT output results.

$$I_g = \sum_{i-1}^{c}(CWR * A) \quad (8)$$

Where I_g is total irrigation requirement; c is total number of individual areas or fields being considered for irrigation, CWR is crop water requirement per unit area, and A is he area (ha) of each individual field being considered for irrigation.

Irrigation Demand (ETc) = ET_o x Kc x Efficiency Factor (9)

Where ETc = Crop water requirement, Kc = Crop coefficient, ETo = reference evapotranspiration.

Irrigation demand for water is a function of acreage, crop type, growing cycles (crop coefficients), reference evapotranspiration, and effective precipitation within the irrigated area. Irrigation water demand varied inter annually based on annual rainfall; during wet years the irrigation demand would decrease and during dry years it would increase accordingly (FAO, 1998).

6.2.8.1.4. Commercial and Institutional Water Demand (CIWD)

Apart from domestic water consumption, urban water demand encompasses the collective water needs of the community for various public facilities, including schools, offices, hotels, restaurants, hospitals, and clinics. The water demand for commercial and institutional purposes typically exhibits a direct correlation with the population size. The Genale Dawa master plan study utilized 5% of the domestic water demand to estimate the demand for commercial and institutional purposes (MoWE, 2007b). However, to account for the recent improvements and growth of commercial institutions in the country, this study employs a 10% allowance to estimate commercial and institutional water demand.

6.2.8.2. non-Consumptive use

6.2.8.2.1. Hydropower Water Demand Modeling in WEAP

To analyze the water demand of a hydropower facility, GD3, with a significant energy production output of 1,640 Gigawatt-hours (GWh) annually. Specific parameters such as total storage capacity, monthly net evaporation, and operational characteristics are important to evaluate hydropower water demand. The report of Genale-Dawa River Basin Integrated Resources Development Master Plan (MoWE, 2007a) shows the hydropower facility GD3 possesses a total storage capacity of 2570 million cubic meters (MCM), with a monthly net evaporation rate of 83.67 millimeters (mm). Additionally, key attributes include a top conservation level of 2,310 MCM, a top of inactive volume at 260 MCM, and a maximum turbine flow of 216 cubic meters per second (CMS). These factors, along with a plant factor of 72%, tailwater elevation of 840 meters above sea level (asl), and full supply level of 1,120 meters asl, collectively inform the analysis of water demand within the WEAP model.

In WEAP, the hydropower facility is represented through a reservoir element, utilizing data on storage capacity, conservation levels, and inactive storage volume to delineate usable storage for power generation. Evaporation losses are specified as a monthly rate, while the maximum turbine flow and plant factor determine the rate of water withdrawal for power generation. Furthermore, tailwater elevation and full supply level information are employed to establish reservoir operation rules within WEAP, which influence water releases and power generation dynamics. Through simulation of water inflows and outflows based on these parameters, WEAP estimates the water demand necessary for the hydropower facility to achieve the specified average annual energy production (Sieber & Purkey, 2015).

6.2.8.2.2. Environmental flow requirement

Environmental flow refers to the volume of water necessary to support the health of a stream's ecosystem and maintain ecological equilibrium downstream. However, in the absence of specific regulations and guidelines for determining the required flow to safeguard aquatic ecosystems in the research area, the environmental flow recommendation proposed by Tennant (1976) was

adopted. According to Tennant (1976), maintaining the ecological balance downstream necessitates approximately 15-20% of the average annual flow. For this investigation, to ensure the well-being of aquatic ecosystems and the functions they offer, an environmental flow equivalent to 20% of the mean annual streamflow was designated.

6.2.9. Scenario development

Water supply and demand are impacted by a number of factors. Population growth, urban expansion, changes in climate, and advancements in irrigation infrastructure all contribute to demand. Conversely, natural climate fluctuations, such as changes in rainfall and temperature, significantly affect water availability. To evaluate how these elements will influence future water resources, diverse scenarios have been formulated. These scenarios allow exploration of various hypothetical situations, including shifts in population growth trends and changes in water consumption rates, the development of potential irrigation projects, and the potential impact of climate change on water supply dynamics.

For this study, the following scenarios were adopted:

6.2.9.1. Baseline water demand

Water use in the study area was estimated based on current data for domestic demand (including CIWD), livestock, and irrigation, reflecting the current state of the watershed. Baseline is the year in which the most complete and reliable data on water use are available, and it serves as the starting point for the analysis (Sieber & Purkey, 2015). As a result, for this study, the 2020 year was designated as the current account year, and the year 2050 was designated as the final year of scenarios.

6.2.9.2. Reference scenarios (2021-2050)

Based on current data and watershed conditions, the current water demand for domestic, livestock, and irrigation purposes was determined. Scenarios are developed to explore potential future changes to the system beyond the Current Accounts year. A default scenario, known as the

"reference" or "business-as-usual" scenario, maintains the current accounts data throughout the specified project period, serving as a benchmark for evaluating other scenarios in which system data is modified (Ougougdal et al., 2020). In this scenario, the changes are primarily caused by population and livestock growth rates. The annual population and livestock growth rates were taken from FDRE Population Census Commision, (2008) and Fantu et al. (2018), respectively.

6.2.9.3. Scenario I: High Population Growth with Increased Water Consumption Rate

This scenario looks at how high population growth and increased water consumption rate will affect future domestic water requirements. It assumes that population growth will be the sole factor influencing water demand between 2021 and 2050. In accordance with the Genale Dawa River Basin Integrated Development Master Plan (MoWE, 2007b), high population growth rate of 3.2%, is considered. In addition, to ensure basic water needs and health concerns, the World Health Organization's (WHO) recommendation of 100 liters of water per person per day was considered. In this scenario, the demand for irrigation and livestock water was supposed to be constant.

6.2.9.4. Scenario II: Potential Irrigation development

What if the potential irrigation fully developed: This scenario examines the potential effects of fully developing the irrigation areas identified in the Genale Dawa River Basin master plan between 2021 and 2050. The plan identifies about 31774 ha of irrigation area suitable for development (MoWE, 2007f). This scenario assesses the impact on water demand if these irrigation areas were fully developed. In this scenario, the demand for livestock, domestic and CIWD water was supposed to be the same as reference scenario.

6.2.9.5. Scenario III: High Population Growth with Improved Water Consumption Rate and Potential Irrigation Development

Scenario III combines the factors from both Scenario I and Scenario II to provide a comprehensive outlook on future water demand in the upper Genale river basin.

Firstly, similar to Scenario One, Scenario Three considers the high population growth rate of 3.2% as outlined in the Genale Dawa River Basin Integrated Development Master Plan (MoWE, 2007b).

This high population growth is expected to be a primary driver of increased domestic water requirements from 2021 to 2050.

Secondly, in alignment with Scenario Two, Scenario Three examines the potential impact of fully developing the identified irrigation areas in the master plan. With approximately 31,774 hectares of irrigation area identified for development (MoWE, 2007f), this scenario delves into the implications of maximizing irrigation capacity within the basin.

By integrating these elements, Scenario Three offers' insights into the combined effects of population growth and irrigation expansion on future water demand. This scenario acknowledges the necessity of addressing both domestic water needs and agricultural water usage to ensure sustainable water management in the region.

6.2.9.6. Scenario IV: Potential Irrigation Development, High Population Growth Rate with Improved Water Consumption, and Climate Change Impact

Scenario IV was formulated to assess the collective impacts of potential irrigation expansion, high population growth rates accompanied by increased water consumption, and the influence of climate change, specifically focusing on RCP 4.5 and RCP 8.5 projections during the 2030s. The primary objective of this scenario is to gain a comprehensive understanding of the future water demand dynamics within the upper Genale River basin.

Utilizing the Soil and Water Assessment Tool (SWAT) model, projected surface water resources under climate change scenarios RCP 4.5 and RCP 8.5 are seamlessly integrated into the Water Evaluation and Planning (WEAP) model. The WEAP model serves as a platform for simulating water demand, supply, and distribution across diverse sectors, encompassing domestic, livestock, agricultural, and hydropower domains.

By comparing WEAP model simulations under present conditions (reference scenario) with those of Scenario Four (encompassing potential irrigation development, high population growth rates with increased water consumption, and climate change scenarios RCP 4.5 and RCP 8.5), it becomes feasible to assess the potential impacts on water consumption across various demand sites. This comprehensive analysis sheds light on the intricate interactions between irrigation expansion, high population growth, improved water usage patterns, and climate change, aiding in informed water resource management and planning strategies for the study river basin.

6.3. Result and Discussion

6.3.1. Calibration and validation of SWAT model.

An analysis was conducted using SWAT-CUP software's SUFI-2 algorithm to find important factors affecting streamflow in the SWAT model calibration and validation process. They examined 21 flow parameters initially and then narrowed it down to 10 key ones. These key parameters include ALPHA_BF.gw, CN2.mgt, and CANMX.hru, GWQMN.gw, CH_K2.rte, REVAPMN.gw, SOL_AWC(..).sol, RCHRG_DP.gw, ESCO.hru, and GW_DELAY.gw. They used a p-value between 0 and 0.5 and a t-statistic ranging from 0.65 to 7.86 to identify these important parameters as described in Shigute et al. (2022).

The SWAT model was calibrated and validated using streamflow data collected at Chenemassa station. Data from 1987 to 2002 were used to adjust the model, and its performance was assessed using data from 2003 to 2011. The adjusted model achieved good results in both phases. Details information on model calibration, validation, performance evaluation, and streamflow hydrography is available in prior study of Shigute et al. (2022).

6.3.2. Streamflow under the effect of climate change

Figure 6-2 a and b displays the mean monthly simulated streamflow for the Upper Genale River, along with projected streamflow for the 2030s under two climate change scenarios (RCP4.5 and RCP8.5) generated by four climate models and their ensemble mean using the SWAT model. The simulated monthly flows range from 22.6 CMS in February to 143.94 CMS in October, with the minimum flow occurring in February and the maximum in October.

The Figure 6-2 also shows the monthly impact of climate change on projected streamflow under RCP4.5 and RCP8.5 for the 2030s. Compared to the simulated baseline flow, the ensemble projected streamflow is expected to increase by up to 69.56% from January to March, November, and December. However, from April to October, the projected ensemble mean flow is expected to decrease. Overall, the annual ensemble mean flow is projected to decrease by 10.1% under RCP4.5 (Figure 6-2 a).

Under the RCP8.5 scenario, the projected ensemble mean flow is expected to increase by 36.7% (January), 2.64% (March), 5.5% (November), and 25.87% (December) compared to the simulated baseline flow. However, for other months, the flow is likely to decrease by up to 40.2%. On an annual basis, the ensemble mean flow is projected to decrease by 15.06% (Figure 6-2 b). The projected increase and decrease in streamflow during the dry and wet seasons under RCP4.5 and RCP8.5 are attributed to the likely increase and decrease in rainfall amounts during these respective periods. A study by Worqlul et al. (2018) supports this finding, suggesting potential increases in dry season streamflow of up to 64% and decreases in wet season streamflow of up to 19% for future periods.

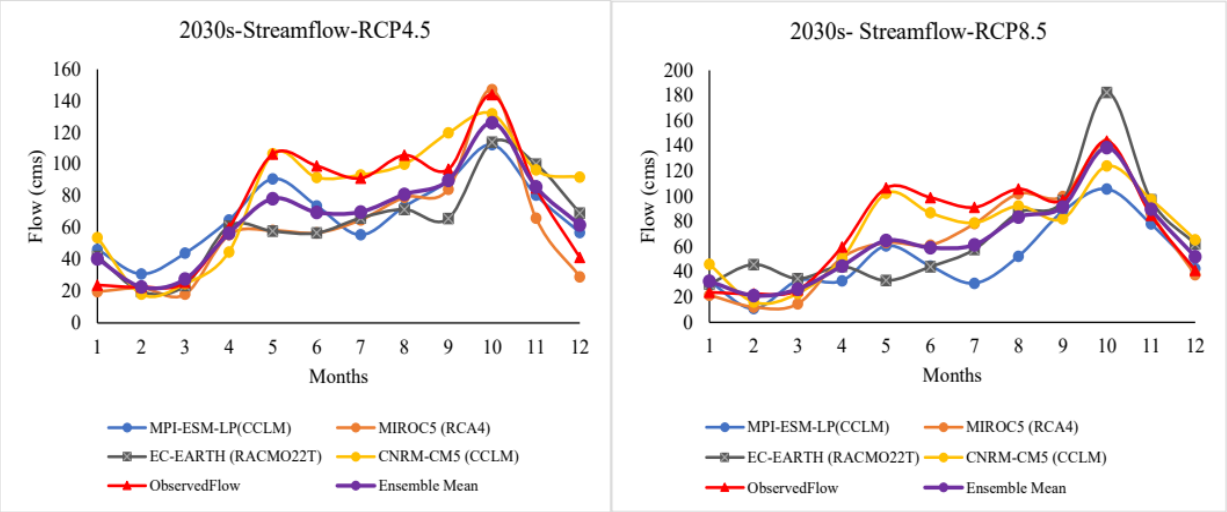

Figure 6-2. Mean Monthly streamflow under the effect of climate change (right panel under RCP4.5, left panel under RCP8.5).

6.3.3. Baseline Water demand

The primary sectors examined for water usage were domestic (including commercial/institutional), livestock, and irrigation. For the current account, the livestock sector utilized 45.79 million cubic meters (MCM) of water, followed by domestic and commercial/institutional sectors at 24.84 MCM. Irrigation had the lowest consumption at 9.37 MCM (Figure 6-3). This indicates a total estimated water consumption of approximately 79.99 MCM across these sectors in the watershed, representing around 3.4% of the available water supply in the basin.

Limited development of irrigation structures in the study area contributes to lower irrigation water consumption. Data from the Ethiopian Ministry of Water Resources and regional irrigation authorities in Oromia and Sidama regions confirm this, with a total small-scale irrigated area of only approximately 1,023.79 hectares.

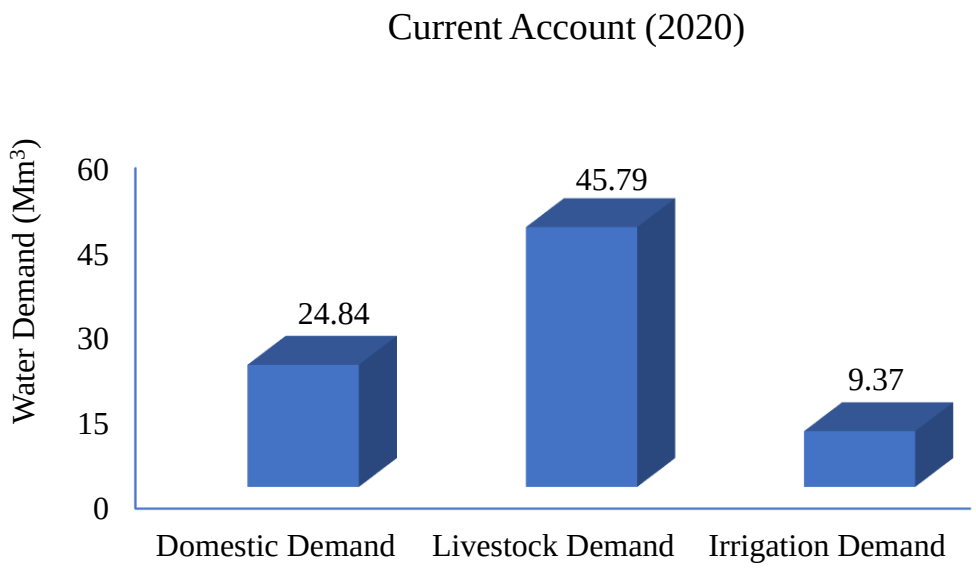

Figure 6-3. Water demand for different sectors for current account year

6.3.4. Reference Scenario

The reference scenario, also known as the business-as-usual scenario, assumes that there will be no improvements in the demand and water supply systems compared to the current accounting year. The changes in this scenario are solely due to population and livestock growth rates. The annual population and livestock growth rate were adopted from different sources. The annual population growth rate for Sidama and Oromia of 2.9% was obtained from the FDRE Population Census Commision, (2008), while the livestock growth rate of 6% came from Fantu et al. (2018), Figure 6-4 illustrates the simulation results of the reference scenario. According to this scenario, the water demand in the study basin is expected to increase from 79.99 MCM in 2020 to approximately 330.91 MCM in 2050, primarily due to changes in population and livestock numbers. This indicates that water consumption from the basin's water supply would increase from 3.4% of the current account to about 14.24% in the final year of the reference scenario.

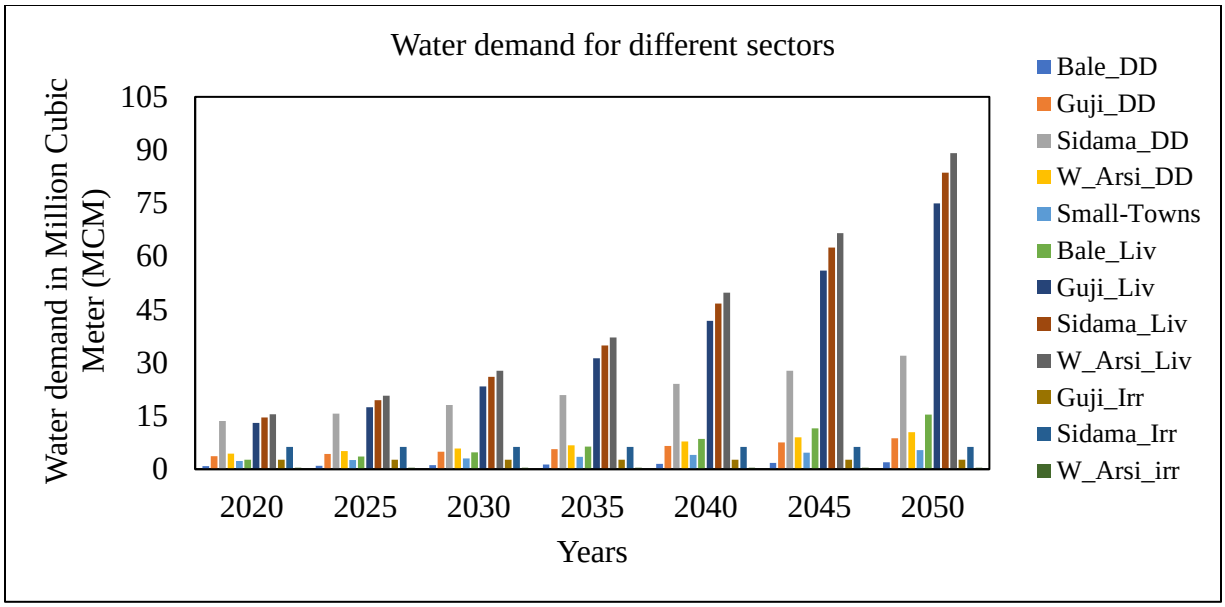

Figure 6-4.Water demand for different sectors under reference scenario for selected years

Based on the results shown in Table 6-4, it is estimated that domestic and CIWD (Commercial and Institutional water demand) water consumption will increase as follows: 24.85 MCM in 2020, 33.05 MCM in 2030, 44 MCM in 2040, and 58.56 MCM in 2050. The demand for livestock water consumption is projected to rise from 45.79 MCM in 2020 to 82 MCM in 2030, 146.85 MCM in 2040, and 262.99 MCM in 2050. It is important to note that the demand for irrigation water will remain constant over the years due to the business-as-usual scenario. Under the reference scenario, the water availability in the basin is sufficient to meet the required demands.

Table 6-4. The current account (2020) and projected reference scenarios (2021 – 2050) water demand (MCM) for each sector

Year	Domestic and CIWD	Livestock Demand	Irrigation Demand	Total Water Demand
2020	24.85	45.79	9.37	79.99
2025	28.67	61.28	9.37	99.31
2030	33.05	82.00	9.37	124.4
2025	38.13	109.74	9.37	157.22
2040	44.00	146.85	9.37	200.21
2045	50.76	196.52	9.37	256.64
2050	58.56	262.99	9.37	330.91

6.3.5. Scenario One: High Population Growth with Increased Water Consumption Rate

Scenario one was created to investigate the potential situation within the water demand evaluation model. This scenario examined how changes in population growth and water consumption rates might affect the basin. As shown in Table 6-5 and Figure 6-5, the model projected total water demand based on a high population growth rate (3.2%) and improved water rate (consuming 40.15 cubic meters per person per year). Compared to the reference scenario, domestic water use was projected to increase significantly. For example, in 2025, domestic consumption could reach 112.26 million cubic meters (MCM) compared to the reference scenario's 28.67 MCM. This trend continued throughout the projection period, with total water demand in the basin rising substantially. By 2050, domestic demand could reach 246.73 MCM under scenario one, compared to 58.56 MCM in the reference scenario (Table 6-5).

Table 6-5. Water demand projections (in million cubic meters) for various sectors under both the reference and high population growth rate (Scenario one)

Year	Reference Scenario				Scenario One			
	Domestic & CIWD (MCM)	Livestock (MCM)	Irrigation (MCM)	Total Water Demand(MCM)	Domestic & CIWD (MCM)	Livestock (MCM)	Irrigation (MCM)	Total Water Demand(MCM)
2020	24.85	45.79	9.37	79.99	24.84	45.79	9.37	79.99
2025	28.67	61.28	9.37	99.31	112.26	61.28	9.37	182.90
2030	33.05	82.00	9.37	124.42	131.41	82.00	9.37	222.78
2035	38.13	109.74	9.37	157.23	153.82	109.74	9.37	272.92
2040	44.00	146.85	9.37	200.22	180.06	146.85	9.37	336.28
2045	50.76	196.52	9.37	256.64	210.78	196.52	9.37	416.66
2050	58.56	262.99	9.37	330.91	246.73	262.99	9.37	519.08

Figure 6-5 shows, the total water demand for the basin is predicted to increase significantly in scenario one when compared to the reference scenario. By 2025, demand is expected to rise from 99.31 million cubic meters (MCM) to 182.90 MCM, an increase of 83.59 MCM. The observed upward trajectory in water demand persists throughout the modeling timeframe (2021 to 2050). By 2050, total water demand under scenario one could reach 519.08 MCM, a substantial increase of 188.17 MCM compared to the reference scenario's 330.91 MCM (Figure 6-5).

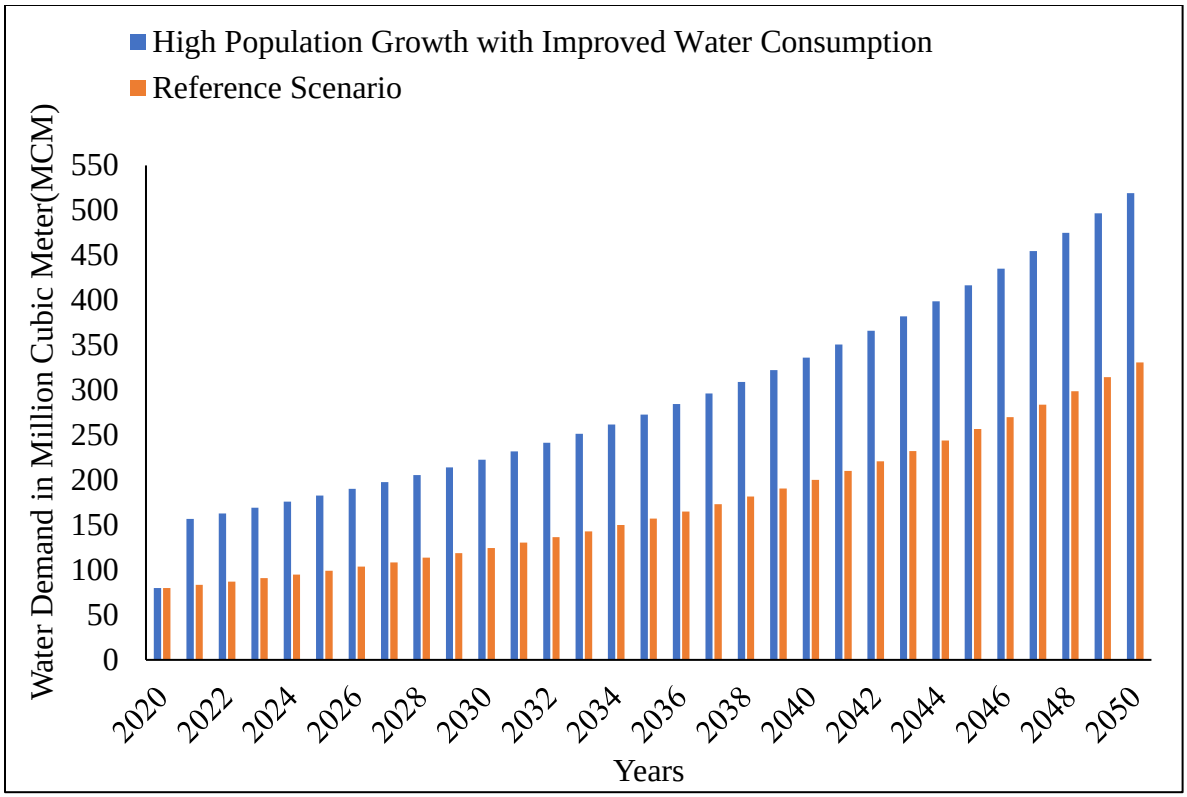

Figure 6-5.Water demand for current and high population growth scenario (scenario one), from 2021 to 2050

6.3.6. Scenario Two: Potential Irrigation Development

The Genale Dawa Basin is well-suited for irrigation development because it receives rain twice a year (a bimodal rainfall pattern). This rainfall pattern conveniently coincides with the planting seasons, ensuring there's also a good flow of water in the rivers during these crucial times. The basin has a mix of small and large perennial and seasonal rivers suitable for irrigation development. Despite the basin's abundant water and land resources, currently development of water resources remains limited across the study areas.

The Ethiopian Ministry of Water Resources, along with irrigation authorities in the Oromia and Sidama regions (which cover the basin's entire irrigable area), is identifying potential irrigation development sites. Their analysis identified approximately 31,774 hectares of land suitable for irrigation. This scenario investigates what would happen if the identified suitable irrigation area will fully develop between 2021 and 2050. Figure 6-6 illustrates the projected total water demand

in the basin. Compared to the reference scenario, water consumption is expected to significantly increase throughout the period. By 2050, the difference in water usage could reach as high as 276.48 million cubic meters (Mm3) annually. Here's a breakdown of the projected increase shown in Figure 6-6.

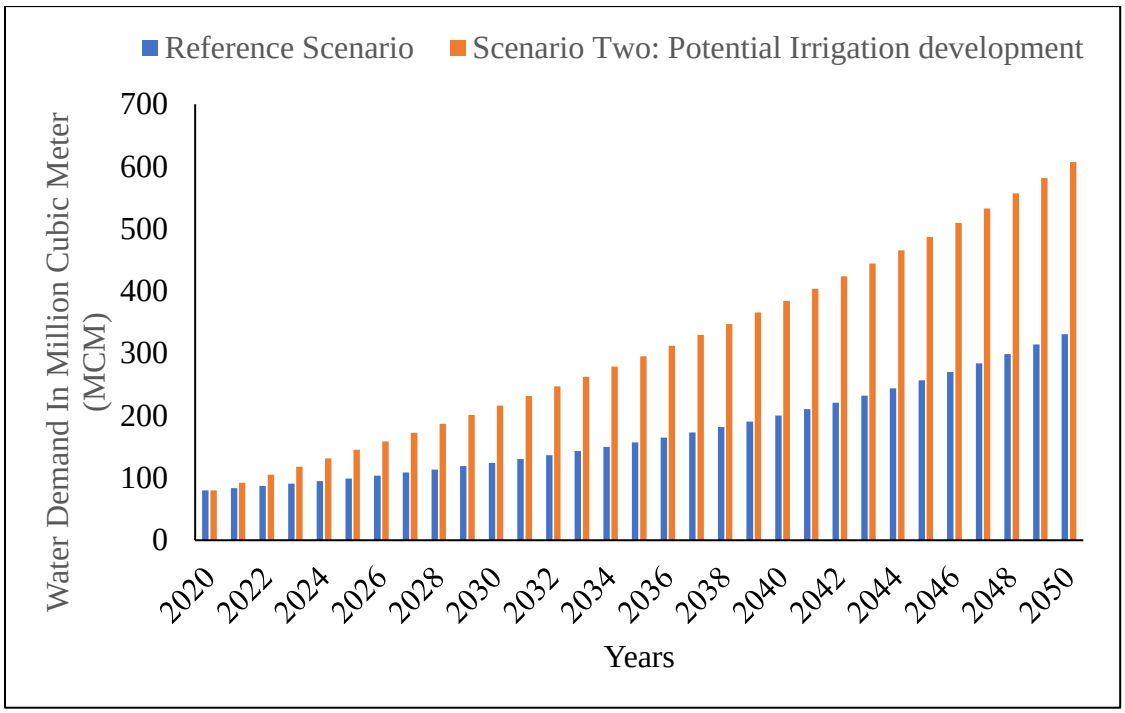

Figure 6-6. Water demand for current and potential irrigation expansion scenario (scenario two), from 2021 to 2050

The analysis results also indicate a significant increase in water consumption for future irrigation development within the basin. In comparison to the reference scenario, Scenario Two demonstrates a significant rise in water demand. For instance, over the duration of the reference scenario period, annual water consumption is projected to be 9.37 million cubic meters (MCM). However, under Scenario Two, irrigation water usage experiences a substantial increase. For instance, by the year 2025, consumption is anticipated to rise from 9.37 MCM to 55.10 MCM. Furthermore, by 2050, water consumption in Scenario Two is estimated to reach 285.86 MCM, a significant leap from the 9.37 MCM recorded in the reference scenario (Table 6-6).

Table 6-6. Water demand projections (in million cubic meters) for various sectors under both the reference and potential irrigation expansion (Scenario two)

Year	Reference Scenario				Scenario Two			
	Domestic & CIWD (MCM)	Livestock (MCM)	Irrigation (MCM)	Total Water Demand(MCM)	Domestic & CIWD (MCM)	Livestock (MCM)	Irrigation (MCM)	Total Water Demand(MCM)
2020	24.85	45.79	9.37	79.99	24.85	45.79	9.37	79.99
2025	28.67	61.28	9.37	99.31	28.67	61.28	55.10	145.05
2030	33.05	82.00	9.37	124.42	33.05	82.00	101.25	216.30
2035	38.13	109.74	9.37	157.23	38.13	109.74	147.40	295.27
2040	44.00	146.85	9.37	200.22	44.00	146.85	193.56	384.41
2045	50.76	196.52	9.37	256.64	50.76	196.52	239.71	486.99
2050	58.56	262.99	9.37	330.91	58.56	262.99	285.86	607.40

6.3.7. Scenario Three: High Population Growth with Improved Water Consumption Rate and Potential Irrigation Development

The scenario was formulated to examine the impact of potential irrigation development, coupled with high population growth and improved water consumption, on water demand within the study basin. Table 6-7 provides a detailed breakdown of water consumption across the demand sites. Contrasting with the reference scenario, there is a notable increase in water consumption observed at domestic and irrigation sites, escalating from 28.67 and 9.37 million cubic meters (MCM) to 112.26 and 55.1 MCM respectively by the year 2025. By 2035, consumption at domestic and irrigation sites sees a substantial surge, surging from 38.13 and 9.37 MCM in the reference scenario to 153.82 and 147.4 MCM under scenario three. These trends persist and intensify, reaching 246.73 and 285.86 MCM for domestic and irrigation consumption by the year 2050. The finding confirms that the potential growing of irrigation and a larger population are key drivers behind the rising water needs in the basin over time. This study further emphasizes that expanding irrigation areas, population increases, and changes in how people use water all significantly contribute to the increasing water demand across the entire basin.

Table 6-7 reflects this growing need at different locations over time. Grasping these trends is vital for managing water resources effectively and planning for sustainable use as demands rise. The projected sharp increase in water consumption underscores the need for proactive actions to meet future water needs and ensure the basin's water security.

Table 6-7. Water demand projections (million cubic meters) by sector for two scenarios: reference and high population growth with irrigation expansion (Scenario Three).

Year	Reference Scenario				Scenario Three			
	Domestic & CIWD (MCM)	Livestock (MCM)	Irrigation (MCM)	Total Water Demand(MCM)	Domestic & CIWD (MCM)	Livestock (MCM)	Irrigation (MCM)	Total Water Demand(MCM)
2020	24.85	45.79	9.37	79.99	24.84	45.79	9.37	79.99
2025	28.67	61.28	9.37	99.31	112.26	61.28	55.10	228.64
2030	33.05	82.00	9.37	124.42	131.41	82.00	101.25	314.66
2035	38.13	109.74	9.37	157.23	153.82	109.74	147.40	410.96
2040	44.00	146.85	9.37	200.22	180.06	146.85	193.56	520.47
2045	50.76	196.52	9.37	256.64	210.78	196.52	239.71	647.00
2050	58.56	262.99	9.37	330.91	246.73	262.99	285.86	795.57

Figure 6-7 also illustrates the total water demand for both the reference scenario and scenario three throughout the analysis period spanning from 2021 to 2050. The total water consumption experienced a notable increase attributed to potential expansion of irrigation, high population growth, and enhanced water consumption practices. In 2021, the total water demand in the basin was projected to shift from 83.46 to 165.69 MCM, while in 2025, it was expected to rise from 99.3 to 228.64 MCM. By 2035, the total water demand was estimated to surge from 157.24 to 410.96 MCM between the reference scenario and scenario three, respectively.

The trend of escalating total water demand persisted, leading up in an estimated amount of 795.57 MCM by 2050 in scenario three. These findings underscore the significant impact of various factors on the overall water demand within the basin over the specified time horizon. The data presented in Figure 6-7 provides a clear visualization of the increasing water requirements driven by factors such as expansion of irrigation, population growth, and changing consumption patterns. Understanding these dynamics is crucial for effective water resource management and planning to ensure sustainable water supply and meet the growing demands in the study area.

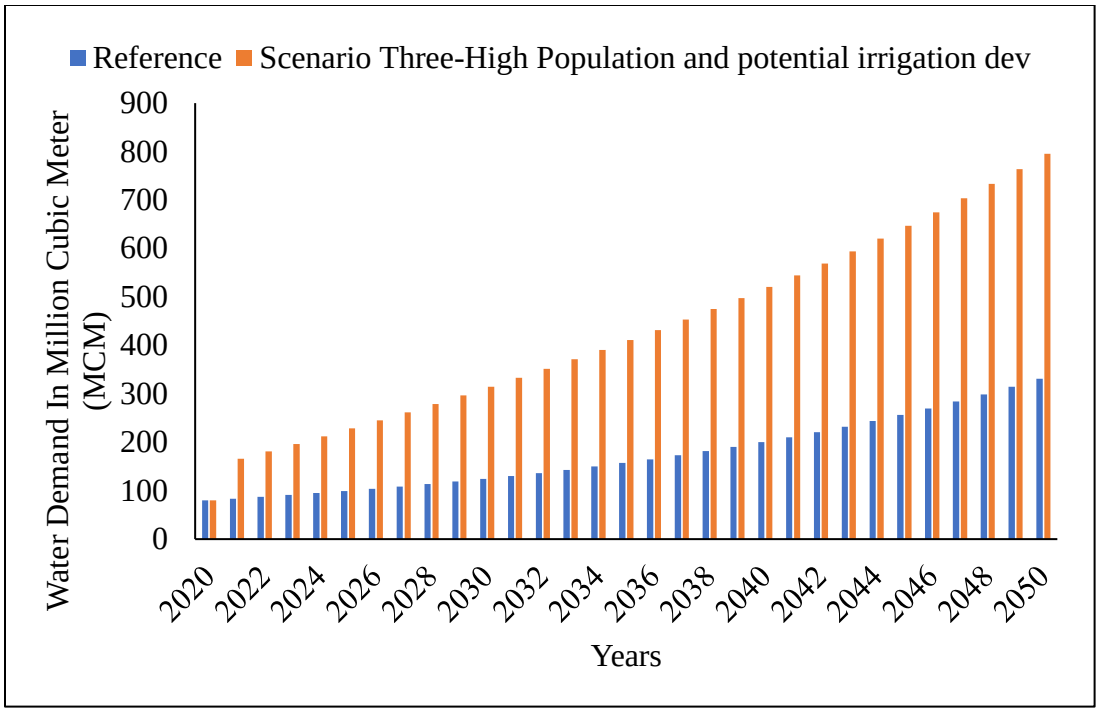

Figure 6-7. Water demand for current and high population growth and potential irrigation development scenario (scenario three), from 2021 to 2050

6.3.8. Scenario Four: Potential Irrigation Development, High Population Growth Rate with Improved Water Consumption, and Climate Change Impact

Climate change is exerting adverse effects on water resources in Ethiopia, primarily driven by shifting rainfall patterns, rising temperatures, and heightened atmospheric water demand (Bewket et al., 2015). The increase in temperature, alongside changes in precipitation patterns, stands out as crucial climate change variables significantly affecting various hydrological processes, particularly streamflow and evapotranspiration. These alterations can lead to fluctuations in water demand across different sectors, including agriculture, domestic use, livestock rearing, hydropower generation, and institutional needs within the region.

The potential expansion of irrigation, coupled with a high population growth rate and increased water consumption, along with the impacts of climate change, may exacerbate stress on water resources across different sectors. To examine this, scenario four was formulated to explore the potential impact on water consumption due to the projected expansion of irrigation, population growth with enhanced water usage, and the influence of climate change, focusing specifically on

RCP 4.5 and RCP 8.5 projections for the 2030s. Table 6-8 show details water consumption across various demand sites. Compared to the reference scenario, domestic and irrigation consumption under RCP4.5 by 2025 are projected to reach 112.26 million cubic meters (MCM) and 77.54 MCM, respectively (up from 28.68 MCM and 9.37 MCM). Similarly, under RCP8.5, these values are expected to be 112.26 MCM and 79.04 MCM by 2025. By 2050, significant increases in consumption are expected at both domestic and irrigation sites. Under RCP4.5, these values are projected to reach 246.73 MCM and 399.87 MCM, respectively (up from 58.56 MCM and 9.37 MCM in the reference scenario). Under RCP8.5, domestic consumption remains at 246.73 MCM, while irrigation consumption rises further to 407.61 MCM.

The Table 6-8 highlights a key finding: irrigation water demand within the basin is projected to rise significantly due to climate change, with variations between RCP scenarios. RCP8.5 shows a slightly higher irrigation demand compared to RCP4.5 throughout the period (2025-2050). This data underscores the importance of considering climate change impacts when managing water resources within the basin.

Table 6-8. Water use projections (irrigation) by sector under Scenario Four: high population growth rate, irrigation expansion, and climate change (RCP4.5 and RCP8.5).

Year	Scenario Four under RCP4.5				Scenario Four under RCP8.5			
	Domestic & CIWD (MCM)	Livestock (MCM)	Irrigation (MCM)	Total Water Demand(MCM)	Domestic & CIWD (MCM)	Livestock (MCM)	Irrigation (MCM)	Total Water Demand(MCM)
2020	24.85	45.79	9.37	79.99	24.84	45.79	9.37	79.99
2025	112.26	61.28	77.54	251.08	112.26	61.28	79.04	252.58
2030	131.41	82.00	142.00	355.41	131.41	82.00	144.75	358.16
2035	153.82	109.74	206.47	470.03	153.82	109.74	210.47	474.03
2040	180.06	146.85	270.93	597.84	180.06	146.85	276.18	603.09
2045	210.78	196.52	335.40	742.70	210.78	196.52	341.89	749.18
2050	246.73	262.99	399.87	909.59	246.73	262.99	407.61	917.32

In Figure 6-8, with the consideration of potential irrigation expansion, rapid population growth, heightened water usage, and the impact of climate change under RCP 4.5 and RCP 8.5 scenarios for the 2030s, a substantial increase in total water demand across various sectors is anticipated. By 2025, total water consumption is forecasted to surge from 99.31 million cubic meters (MCM) to 251.08 MCM in scenario four under RCP4.5, and to 252.58 MCM in scenario four under RCP8.5. This escalating trend is projected to persist, potentially reaching up to 909.59 MCM for RCP4.5 and 917.32 MCM for RCP8.5 by the year 2050. The data emphasizes the pressing need for strategic

plans for managing water resources in order to address the increasing demands resulting from a number of factors, such as population growth, increased agricultural practices, an increase in livestock numbers, and climate change. This emphasizes how important it is to plan ahead in order to ensure sustainable water availability and use in the future.

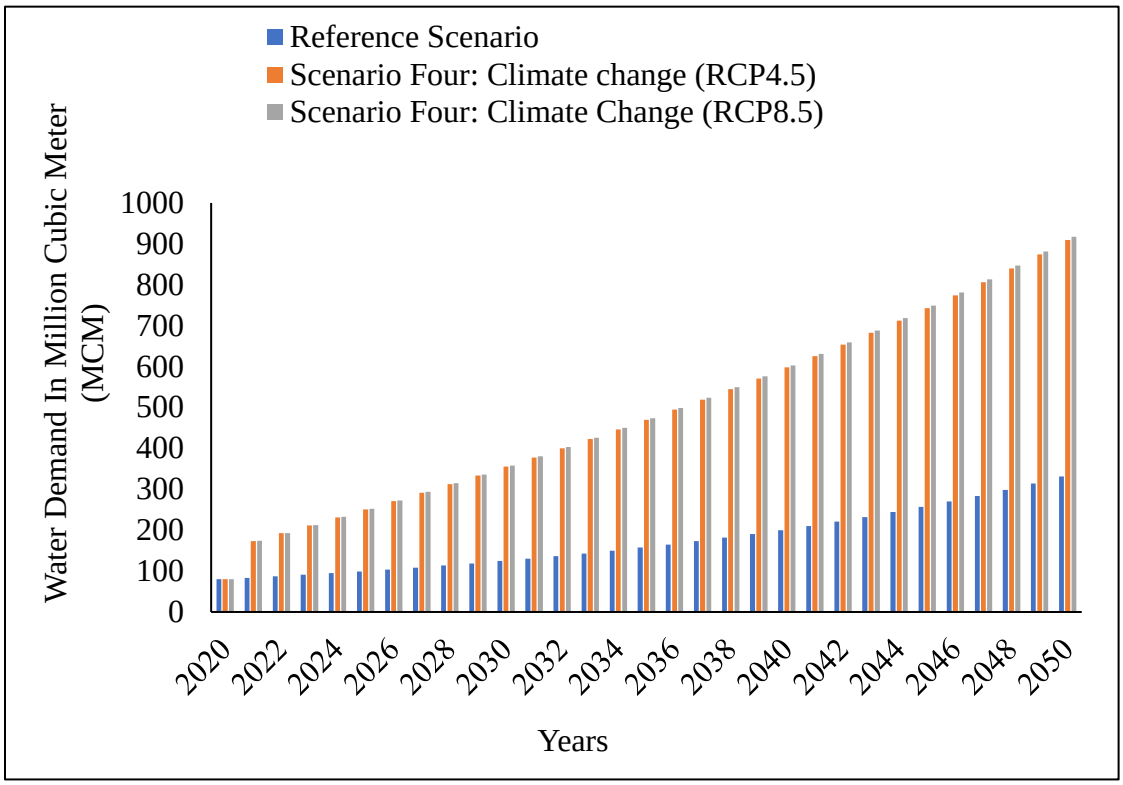

Figure 6-8. Water demand for current and high population growth, potential irrigation development, and climate change under RCP4.5 and RCP8.5 scenario (scenario three), from 2021 to 2050.

6.3.9. Unmet demand for different Sectors

This analysis focuses on evaluating the difference between supply delivered and demand across various locations under different future scenarios, as outlined in Table 6-9 and 6-10. Unmet demand, a critical metric examined herein, refers to situations where the amount of supplied water falls short of the required quantity.

In the reference scenario, there appears to be a balance between supply and demand, with adequate water allocations for domestic (39.88 MCM), livestock (127.91 MCM), and irrigation (9.37 MCM)

sectors. However, projections into future scenarios indicate potential challenges, particularly concerning irrigation, where water shortages may emerge.

Table 6-9. Supply delivered for different scenarios (2021-2050)

Scenarios	Supply Delivered (MCM)			
	Domestic & CIWD (MCM)	Livestock (MCM)	Irrigation (MCM)	Total Water Delivered (MCM)
Reference	39.88	127.91	9.37	177.15
Scenario One	162.09	127.87	9.25	299.21
Scenario Two	39.88	127.91	136.47	304.25
Scenario Three	162.09	127.87	126.91	416.86
Scenario Four-Under RCP4.5	162.14	127.91	192.76	482.80
Scenario Four-Under RCP8.5	161.77	127.61	182.43	471.80

Several factors contribute to the escalation of unmet demand in future scenarios. High population growth scenarios, with increased demand for domestic water (162.14 MCM), strain available resources, intensifying competition and potential shortages. Moreover, scenarios involving irrigation expansion further exacerbate water demands for agricultural purposes, posing a significant challenge to water resource management.

Table 6-10. Mean annual unmet demand for different scenarios (2021 – 2050)

Scenarios	Annual Unmet Demand (2021 - 2050)			
	Domestic & CIWD (MCM)	Livestock (MCM)	Irrigation (MCM)	Total Unmet Demand (MCM)
Reference	0.00	0.00	0.00	0.00
Scenario One	0.05	0.04	0.11	0.20
Scenario Two	0.00	0.00	15.55	15.55
Scenario Three	0.05	0.04	25.11	25.20
Scenario Four-Under RCP4.5	0.00	0.00	20.16	20.16
Scenario Four-Under RCP8.5	0.37	0.30	34.60	35.28

The impact of climate change, particularly under the RCP8.5 scenario, presents a compounded challenge. Elevated temperatures, leading to higher evaporation rates, coupled with altered precipitation patterns, may exacerbate water scarcity issues, particularly in regions reliant on irrigation. The culmination of these factors, especially under the most extreme scenario, underscores the pressing need for proactive water management strategies to mitigate potential

future shortages, emphasizing the significance of sustainable resource allocation and conservation efforts.

This analysis examines water availability compared to projected demand across different scenarios from 2021 to 2050. As shown in Table 6-11 and Figure 6-9, up to 2030, supplied water seems sufficient to meet demand requirements across various sectors. However, a concerning trend emerges after 2030, with a significant risk of water scarcity.

The data reveals a significant increase in unmet demand across various scenarios after 2030. For example, by 2035, scenarios involving high population growth, potential irrigation expansion, and climate change variations (RCP4.5 and RCP8.5) show unmet demand ranging from 4.19 to 15.28 million cubic meters (MCM) per year. This trend continues to worsen by 2040, with unmet demand reaching even higher levels across all scenarios. Notably, the scenario with potential irrigation development alone could face an unmet demand of 15.81 MCM by 2040.

Table 6-11. Unmet demand for different scenarios for selected years

Scenarios	Unmet Demand (2021 - 2050)					
	2025	2030	2035	2040	2045	2050
Reference	0.00	0.00	0.00	0.00	0.00	0.00
Scenario One	0.00	0.00	0.00	0.00	0.00	4.24
Scenario Two	0.00	0.00	0.00	15.81	37.42	69.13
Scenario Three	0.00	0.00	7.24	31.44	58.35	96.15
Scenario Four-Under RCP4.5	0.00	0.00	4.19	25.06	46.87	80.85
Scenario Four-Under RCP8.5	0.00	0.00	15.28	42.84	77.80	135.48

Figure 6-9 further highlights the projected rise in unmet demand. By 2050, the potential shortfall reaches significant levels. Even under the scenarios of irrigation expansion, the annual shortfall is expected to exceed 69 million cubic meters (MCM). However, when other factors considered, the situation become even more worsens. Under the RCP8.5 climate change scenario, irrigation expansion coupled with high population growth could result in potential unmet demand surpassing 135.48MCM annually by 2050.

These findings highlight the growing risk of water scarcity in the coming decades. Proactive measures are crucial to address this challenge and ensure sustainable water management for future generations.

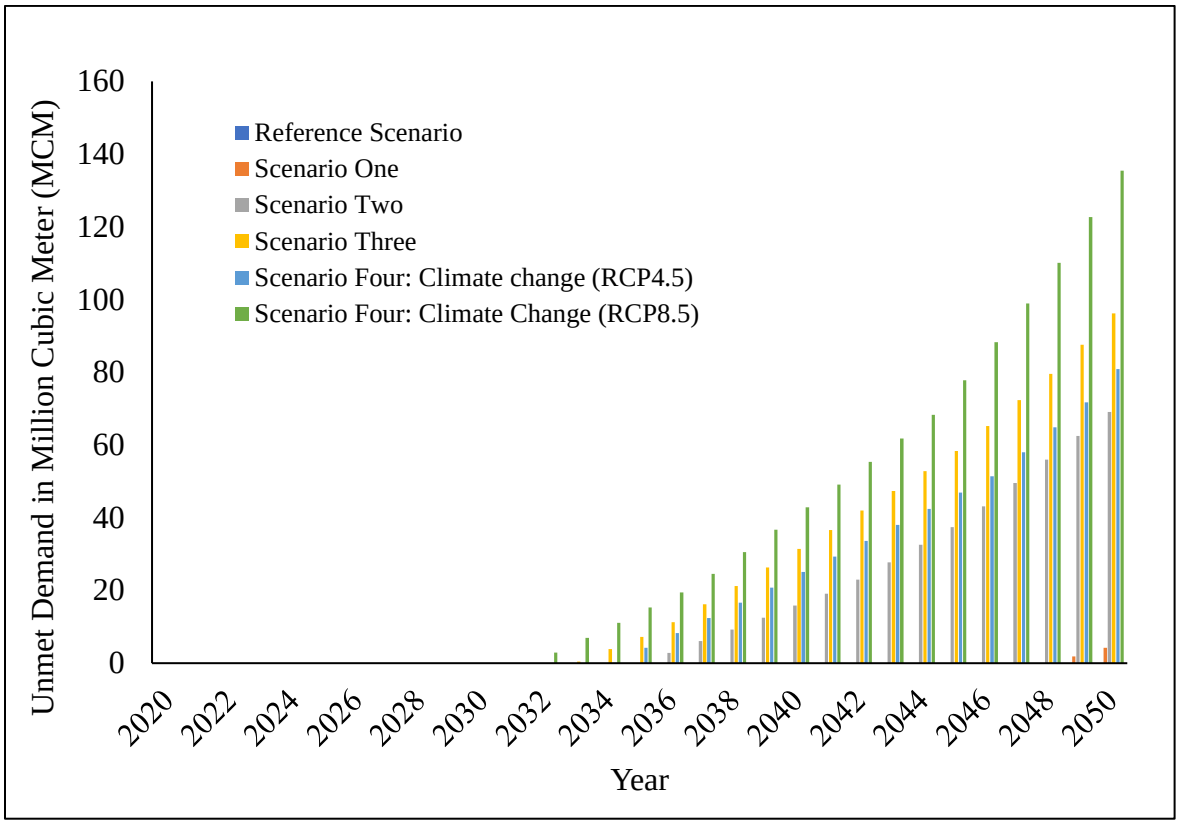

Figure 6-9. Unmet demand for different scenarios during 2021 to 2050

6.3.10. Water Demand for non-consumptive use

6.3.10.1. Instream flow requirement

When estimating water resource availability, it is crucial to account for environmental flow requirements to preserve river ecosystems, fulfill downstream user obligations, and maintain streamflow levels. In this study, the environmental flow for the watershed was set at 20% of the river flow to meet downstream needs.

Utilizing the WEAP model, the minimum monthly water flow essential for sustaining water quality, wildlife habitats, navigation, recreation, and other downstream uses was assessed across

various scenarios. The analysis spanned each month, indicating fluctuating required flow rates: January: 6.93 million cubic meters per month (MCM), February: 4.93 MCM, March: 7.38 MCM, April: 16.98 MCM, May: 27.29 MCM, June: 22.51 MCM, July: 20.65 MCM, August: 24.98 MCM, September: 24.94 MCM, October: 36.55 MCM, November: 22.00 MCM, and December: 11.40 MCM. These findings demonstrate seasonal variations in demands, with higher flow requirements during spring (April-May) and potentially in autumn (October) to adequately meet both environmental and human needs. The pattern aligns with the natural changes in river flow throughout the year (monthly streamflow).

6.3.10.2. Hydropower demand and unmet demand

The results of a WEAP model for hydropower under evaluated scenarios: a reference scenario, scenario one, scenario two, scenario three, and scenario four for the evaluation periods of 2021 – 2050 presented. Hydropower Demand (Energy) refers to the amount of electrical energy desired or required from a specific hydropower source, such as a reservoir or a run-of-river hydropower node (Sieber & Purkey, 2015). The annual hydropower energy demand for all scenarios shows identical demand of 1640.33 GWh. This suggests that the demand for hydropower energy is not influenced by the factors included in the scenarios. Hydropower Demand (Flow)" refers to the amount of water flow needed to generate the desired amount of electrical energy ("Hydropower Demand (Energy)") from a hydropower source (Sieber & Purkey, 2015). It essentially translates the electricity demand into a water flow requirement. The mean annual hydropower flow demand for reference is 2279.54 MCM, scenario one (high population growth scenario) is 2285.98 MCM, scenario two (irrigation expansion scenario) is 2286.30 MCM, scenario three (high population growth and irrigation expansion) is 2293 MCM, scenario four (climate change under RCP 4.5, high population growth, and irrigation expansion) and scenario four (climate change under RCP 8.5, high population growth, and irrigation expansion) is 2313.85 MCM and 2322.13MCM, respectively (Table 6-12). The scenarios (high population growth, irrigation expansion, climate change) likely impact the available water or how efficiently it can be used. For instance, altered precipitation patterns or increased evaporation rates, due to climate change might reduce the amount of water available, requiring more flow to generate the same amount of electricity.

Table 6-12. Mean monthly hydropower water demand (MCM) and hydropower energy demand (GWh) for different scenarios

Scenarios	Hydropower Water Demand (MCM)												Total
	Jan	Feb	Mar	Apr	May	Jun	Jul	Aug	Sep	Oct	Nov	Dec	
Reference	189.09	189.90	190.68	191.33	191.44	190.81	190.39	190.07	189.57	189.28	188.45	188.52	2279.54
Scenario One	189.56	190.40	191.19	191.87	191.99	191.36	190.96	190.65	190.15	189.87	188.97	189.01	2285.98
Scenario Two	189.77	190.61	191.34	191.95	192.01	191.33	191.00	190.64	190.08	189.75	188.81	189.00	2286.30
Scenario Three	190.27	191.11	191.88	192.54	192.61	191.90	191.57	191.21	190.67	190.34	189.36	189.54	2293.00
Scenario Four: Climate change (RCP4.5)	191.80	192.39	193.12	193.71	193.75	193.46	193.60	193.42	193.02	192.56	191.51	191.50	2313.85
Climate Change (RCP8.5)	192.27	192.93	193.66	194.25	194.47	194.35	194.60	194.50	193.94	193.33	191.97	191.87	2322.13
For all Scenario	Hydropwer Demand (Energy) (GWh)												
	136.69	136.69	136.69	136.69	136.69	136.69	136.69	136.69	136.69	136.69	136.69	136.69	1640.3

The monthly and the annual average hydropower generation shows in Table 6-13 The mean annual hydropower generation for reference stands at 1528.4 GWh. In scenario one, which involves high population growth, the generation reduces to 1441.57 GWh. Scenario two, focusing on irrigation expansion, further decreases the generation to 1439.47 GWh. In scenario three, a combination of high population growth and irrigation expansion brings the generation down to 1359.68 GWh. Finally, scenario four, considering climate change under RCP 4.5 along with high population growth and irrigation expansion, yields 1142.03 GWh. Another variant of scenario four, involving climate change under RCP 8.5 with similar conditions, results in 1065.98 GWh. This reduction is likely due to decreased water availability for power generation, resulting from the increased hydropower water demand and other climate change impacts affecting river flow and reservoir levels.

Table 6-13. Mean monthly hydropower generation (GWh) for different scenarios

Scenarios (2021-2050)	Hydropower Generation (GWh)												Total
	Jan	Feb	Mar	Apr	May	Jun	Jul	Aug	Sep	Oct	Nov	Dec	
Reference	125.20	116.72	109.69	108.46	115.40	119.86	123.29	128.86	132.00	158.56	152.42	137.95	1528.40
Scenario One	119.82	111.20	103.96	102.64	109.34	113.72	117.02	122.43	125.48	146.37	141.36	128.23	1441.57
Scenario Two	117.44	109.59	103.15	102.52	109.68	113.30	117.21	123.23	126.83	148.29	141.48	126.74	1439.47
Scenario Three	112.03	104.08	97.40	96.69	103.75	107.21	110.98	116.88	120.39	137.76	132.42	120.09	1359.68
Scenario Four: Climate change (RCP4.5)	99.35	92.41	86.94	86.55	89.15	88.04	89.57	93.22	97.54	107.93	108.10	103.23	1142.03
Climate Change (RCP8.5)	94.12	87.48	82.22	80.33	81.32	79.30	80.07	84.89	90.24	103.23	104.30	98.48	1065.98

The WEAP evaluation results of unmet demand, presented in Table 6-14, show the annual average for 2021-2050. In the reference scenario, the unmet demand is 153.88 GWh. However, in scenario one (high population growth), it increases to 218.17 GWh. In scenario two (irrigation expansion), it rises further to 223.49 GWh. Scenario three (high population growth and irrigation expansion)

experiences a larger unmet demand of 291.66 GWh. Notably, scenario four, which includes climate change under RCP 4.5 alongside high population growth and irrigation expansion, records a significant unmet demand of 498.31 GWh. Similarly, scenario four with climate change under RCP 8.5 and the same conditions presents the highest unmet demand at 574.35 GWh. This substantial increase in unmet demand in the climate change scenarios indicates that higher water demand combined with insufficient water availability for hydropower generation leads to significant energy shortfalls, with critical implications for energy security and reliability.

Table 6-14. Mean monthly hydropower unmet demand (GWh) for different scenarios

Scenarios (2021-2050)	Hydropower Unmet Demand (GWh)												Total
	Jan	Feb	Mar	Apr	May	Jun	Jul	Aug	Sep	Oct	Nov	Dec	
Reference	11.50	19.98	27.00	28.23	21.30	16.83	13.40	7.84	4.70	0.05	0.06	2.99	153.88
Scenario One	16.87	25.50	32.74	34.05	27.36	22.97	19.67	14.26	11.21	2.50	2.56	8.47	218.17
Scenario Two	19.25	27.10	33.55	34.17	27.01	23.40	19.48	13.47	9.86	2.02	3.29	10.88	223.49
Scenario Three	24.66	32.62	39.29	40.00	32.94	29.48	25.72	19.81	16.31	6.30	7.92	16.61	291.66
Scenario Four: Climate change (RCP4.5)	37.34	44.29	49.75	50.15	47.54	48.66	47.12	43.48	39.16	28.76	28.60	33.46	498.31
Climate Change (RCP8.5)	42.57	49.21	54.47	56.36	55.37	57.40	56.63	51.80	46.45	33.47	32.40	38.21	574.35

In general, population growth, irrigation expansion, and climate change all contribute to the variation in hydropower generation and the rise in unmet demand. These factors highlight the challenges of maintaining a reliable electricity supply solely through hydropower, especially considering future population growth and the impacts of climate change.

6.4. Summary and Conclusion

The upper Genale river basin's water resource potential, demand, and allocation were simulated using various scenarios, including high population growth rate, improved consumption, potential irrigation development, and climate change under RCP4.5 and RCP8.5 for the 2030s (2021 to 2050). The study integrated calibrated SWAT output simulated streamflow data into the WEAP model to assess the current water demand (2020) and future scenarios (2021 to 2050) in the study area. The scenarios considered were: scenario one, high population growth along with improved consumption; scenario two, potential irrigation expansion; scenario three, a combination of high population growth along with improved consumption and potential irrigation expansion; scenario

four, high population growth along with improved consumption, potential irrigation expansion, and climate change under RCP4.5 and RCP8.5.

The results showed that the livestock sector utilized 45.79 million cubic meters (MCM) of water, followed by domestic and commercial/institutional sectors at 24.84 MCM, with irrigation having the lowest consumption at 9.37 MCM. Under the reference scenario, the water demand in the study basin is expected to increase from 79.99 MCM in 2020 to approximately 330.91 MCM in 2050, primarily due to changes in population and livestock numbers. High population growth with improved water consumption rate scenario, compared to the reference scenario, domestic water use was projected to increase significantly, with the total demand reaching up to 519.08 MCM at 2050. Under potential irrigation development scenario, the total demand increased by 276.48 MCM by 2050. For high population growth with improved water consumption rate and potential irrigation development by 2050, consumption at domestic and irrigation sites sees a substantial increase, rising from 58.56 and 9.37 MCM in the reference scenario to 246.73 and 285.86 MCM under scenario three. This data underscores the significant impact of both irrigation development and population growth on the escalating water demands within the basin over time.

The study highlights the significant impact of irrigation expansion, population growth, and shifting water use habits on the escalating water demand across the basin. The potential expansion of irrigation, coupled with a high population growth rate and increased water consumption, along with the impacts of climate change, may exacerbate stress on water resources across different sectors. The unmet demand for water is expected to increase significantly in future scenarios, particularly concerning irrigation, where water shortages may emerge. The study emphasizes the growing risk of water scarcity in the coming decades, particularly in the context of high population growth rate, potential irrigation development, and climate change. Proactive measures are crucial to address this challenge and ensure sustainable water management for future generations.

The study also highlights the importance of accounting for environmental flow requirements to preserve river ecosystems, fulfill downstream user obligations, and maintain streamflow levels. The variation between annual hydropower energy demand and generation leads to unmet demand, which increases substantially in the climate change scenario compared to the reference scenario. This indicates that despite the higher water demand, there is insufficient water available for

hydropower generation, leading to unmet energy needs. The study emphasizes the challenges of maintaining a reliable electricity supply solely through hydropower, especially considering future population growth and the impacts of climate change.

Therefore, to safeguard a long-lasting sustainable water resource, it is crucial to devise more effective policies for water resource management in the basin. These policies should include measures to address the growing demand for water, preserve river ecosystems, ensure downstream user obligations, and maintain streamflow levels. This research significantly improves our understanding of water availability, demand, and allocation. This information is essential for effective planning and development of water resources for current and future projects across the study area. The study also emphasizes diversifying energy sources as a crucial strategy for ensuring reliable and secure energy in a future marked by climate change and increasing water pressure.

CHAPTER SEVEN:

7. SUMMARY, CONCLUSIONS, AND RECOMMENDATIONS

This section wraps up the key findings of the study on the Upper Genale River Basin's surface water potential and future demands, considering the influences of climate change and land use alterations. It presents the study's summary, conclusions, and recommendations for future actions.

7.1. Summary and Conclusions

The Genale Dawa river basin is one of the largest river basins in Ethiopia. The use of surface water in the basin is low at the moment due to low irrigation or agricultural activity, low population pressure, and absence of water storage infrastructure. However, population growth and changes in land use land cover due to urbanization and agricultural land expansion, as well as climate change and the potential implementation of several medium- to large-scale irrigation schemes, water supplies, and hydropower plants, cause an increase in water demand. Therefore, understanding and analyzing the interaction of water systems, LULC, climate change, as well as the associated impacts on water resources and the basin's current and future water potential and demand through the integration of various climate and hydrologic models is essential in the basin for strategic decision-making on water resource-related development projects and for comprehensive understanding of hydrological processes.

To this end, this dissertation was conducted with aims to assess long-term changes in annual and seasonal rainfall and temperature for agricultural water management, the effects of LULC change and future climate change on hydrological parameters, as well as to evaluate the water demand and allocation under different scenarios in the upper Genale River basin, Ethiopia.

To assess the current and future climate conditions and their effects on hydrology of the study basin, a wide-ranging study was conducted employing climate data over 30 years from the National Meteorological Service Agency (ENMA) alongside projected climate data derived from four distinct GCM-RCM combinations under the RCP 4.5 and RCP 8.5 scenarios for the time periods of 2021-2050 and 2051-2080 sourced from CORDEX-Africa. The analysis also involved examining the dynamics of LULC changes and their impact on the hydrological characteristics of

the watershed, employing 30 m-resolution Landsat imageries (1986, 2001, 2016). Additionally, an evaluation of the basin's water potential, demand, and allocation was carried out by developing scenarios such as potential irrigation development, population growth, and climate change. To provide a comprehensive understanding of the region's hydrological dynamics, SWAT and WEAP models were employed. This integrated approach allows for a holistic assessment of the interactions between climate, land use, and water resources management, enabling informed decision-making for sustainable water resource utilization in the basin.

The observed climate characteristics and the trend and magnitude of changes in rainfall and temperature were analyzed by the Coefficient of Variation (CV), Standard Rainfall Anomaly (SRA), and Precipitation Concentration Index (PCI), as well as the Mann-Kendall test and Sen's slope estimator. The result showed that the winter, summer, autumn, spring, and annual rainfall variability was high with CV of 89%, 45%, 32%, 30%, and 20%, respectively. The standardized rainfall anomalies revealed that the basin experienced a drier season than a wet season. The average length of the growing season in *Belg* and *Kiremt* was 43 to 79 days and 38 to 170 days, respectively. During the annual, summer, and autumn rainfall seasons, most rainfall stations showed no significant trend, but during spring season, rainfall except for Bore, Bensadaye, Yirba Muda, and Telamokentise, all station showed insignificant decreasing trend. In the past 30 years, most of the stations minimum and maximum annual and seasonal temperatures have recorded a warming trend. The increasing trend of temperature and the decreasing trend of rainfall were the major threat to the agricultural sector. Hence, during spring and autumn season supplementary irrigation is crucial to prevent lower crop yields and crop failure. In these seasons, sorghum and maize varieties require up to 252 mm and 202 mm supplementary irrigation, respectively.

The hydrological characteristics of the watershed due to LULC and climate change analyzed using the Soil and Water Assessment Tool (SWAT) model. Based on monthly measured flow data, the model was calibrated and validated using streamflow data in SWAT-CUP using the sequential uncertainty fitting (SUFI-2) algorithm. The result showed that the Percent Bias (PBIAS) between -5% and 5%, Nash–Sutcliffe Efficiency (NSE) ≥ 0.72, and Coefficient of Determination (R^2) ≥ 0.74, for calibration and validation periods. These results confirmed that model performed well and used for hydrological impact assessment. The LULC change dynamics during the past 30 years (1986- 2016) reveled that land cover units such as shrubland, forest land, and grassland reduced

from 23.9% to 19.5%, 29.6% to 13.5%, and 21.8% to 18.9%, respectively. Conversely, cultivated, bare land, and settlement areas expanded from 24.4% to 47.1%, 0.16% to 0.62%, and 0.16% to 0.28%, respectively. The hydrological response of the watershed to changes in LULC during 1986, 2001, and 2016 indicated that alterations in LULC within the watershed have impacted the hydrological cycle. The impact has led to an increase in total water yield and surface runoff, while there has been a reduction in lateral and groundwater flow. The transition in LULC from 1986 to 2001 and from 2001 to 2016 resulted in an increase in total water yield from 324.42 mm to 339.63 mm and then to 347.32 mm. Similarly, surface runoff also increased from 139.87 mm to 159.03 mm and further to 171.57 mm during these periods. In contrast, groundwater flow decreased by 2.85% between 1986 and 2001, and by 2.1% between 2001 and 2016. Land use changes significantly impacted the watershed's hydrology, primarily by increasing surface runoff and total water yield while decreasing lateral and groundwater flow. These findings highlight the crucial link between land use and water resources. By understanding these connections, stakeholders, natural resource managers, and policymakers, can design effective and sustainable plans for land and water management in the region.

The potential impact of climate change on the basin's water resources in the coming decades (2030s and 2060s) were evaluated using climate models from CORDEX Africa (EC-EARTH, CNRM-CM5, MIROC5, and MPI-ESM-LR). These models predicted rising temperatures and decreasing rainfall across two future scenarios with varying levels of greenhouse gas emissions (RCP4.5 and RCP8.5). To understand how these changes would affect the basin's water availability, the bias-corrected climate data applied to a calibrated SWAT hydrological model. The findings indicate significant reductions in annual water resources, with total water yield, runoff, groundwater flow, and lateral flow all expected to decline within a range of 1% to nearly 40% depending on the specific hydrological component (water yield: 1.03% to 39.8%, runoff: 1.61% to 39%, groundwater flow: 5.42% to 50%, and lateral flow: 1.7% to 40.1%). Conversely, evapotranspiration is projected to increase. The observed link between these changes in hydrological parameters and the predicted rise in temperature and decrease in rainfall suggests a strong dependence of the basin's water resources on future climate conditions. This potential decrease in water availability, particularly during rainy seasons, poses a significant threat to agricultural activities and the overall health of the basin's ecosystem.

The WEAP water resources management model to simulate future water demand and allocation scenarios considered various factors including population growth, improved water consumption rates, potential irrigation development, and the effects of climate change under emission scenarios (RCP4.5 and RCP8.5) for the 2030s (2021-2050). The findings indicate a significant rise in overall water demand across various sectors, primarily driven by population growth and the potential for expanded irrigation. By 2050, the basin's water demand is projected to increase from 79.99 million cubic meters (MCM) to 330.91 MCM under the reference scenario. Under the high population growth scenario with improved consumption, domestic water use is projected to nearly double by 2050. Similarly, potential irrigation development could increase total water demand by more than 276 MCM by 2050. The irrigation development coupled with high population growth and increased water consumption could exacerbate water scarcity, especially for irrigation purposes, leading to unmet water needs. The combined effects of these factors, along with the potential decrease in water availability due to climate change, are expected to further exacerbate water scarcity challenges, particularly for irrigation. To address these challenges, it is crucial to implement proactive water management strategies including accounting for environmental flow needs and diversifying energy sources beyond hydropower to ensure sustainable water resource management for future generations. Overall, this research provides valuable insights into the future water demands and allocation within the basin, informing effective water resource planning and development efforts.

7.2. Recommendations

The dissertation highlights the challenges of water resource management in the upper Genale River basin, Ethiopia, due to factors like variable rainfall, land-use changes, and climate change. Here are some recommendations based on the findings:

- The implementation of appropriate integrated watershed management practices, such as afforestation and soil and water conservation, is crucial in the watershed to minimize the effects of water scarcity and land degradation on the local community, which are caused by reduced groundwater recharge and increased surface runoff.

- Smallholder farmers should be actively involved in forest management to improve water resources. Their participation can help protect and restore forests, which are essential for water infiltration, reducing runoff, and replenishing groundwater.
- To improve water resource management in the area, it is essential to enhance the quality of hydro-climatic data readings and strengthen the hydrological and meteorological network by installing additional climate and streamflow stations within the watershed.
- Develop adaptation strategies to cope with the projected decrease in rainfall and increase in temperature. This could involve introducing drought-resistant crop varieties, developing early warning systems for extreme weather events, and implementing efficient irrigation systems.
- Implement training programs for agricultural experts and farmers to raise awareness about annual and seasonal rainfall variability, which will enhance decision-making and improve agricultural planning.
- To alleviate pressure on the Genale River, sustainable water management strategies should be adopted, such as rainwater harvesting, improved irrigation techniques, and promoting water-efficient agriculture. Additionally, exploring alternative sources like groundwater development and wastewater treatment for reuse is crucial
- Reliance solely on hydropower for electricity generation is risky in the face of climate change and increasing water demands. Explore and invest in alternative energy sources like solar or wind to ensure a more reliable and sustainable electricity supply
- Engage stakeholders, including policymakers, farmers, and local communities, in developing and implementing water management strategies to ensure practical, equitable, and sustainable solutions.

To further refine the water resource assessment and support long-term sustainability, the study additionally recommends additional research encompassing: 1) high-quality climate data and diverse climate models for more precise simulations, 2) investigations into the combined effects of socioeconomic factors, climate change, and land use changes on water resources, and 3) evaluations of various water management strategies under different future scenarios. This detailed analysis will provide a clearer picture of the basin's water resources, resulting in better decision-making and sustainable water management practices. By implementing these recommendations, the upper Genale River basin can achieve a more sustainable and resilient water management

system that meets the needs of the population, agriculture, and the environment under changing climatic conditions.

REFERENCES

Abbaspour, K. C. (2015). *SWAT-CUP: SWAT calibration and uncertainty programs—a user manual. Eawag: Dübendorf, Switzerland, 16-70.*

Abbaspour, K. C., Vaghefi, S. A., & Srinivasan, R. (2018). A Guideline for Successful Calibration and Uncertainty Analysis for Soil and Water Assessment : A Review of Papers from the 2016 International SWAT Conference. *Water*, *10*(6). https://doi.org/10.3390/w10010006

Abdulkareem, J. H., Pradhan, B., Sulaiman, W. N. A., & Jamil, N. R. (2018). Review of studies on hydrological modelling in Malaysia. *Modeling Earth Systems and Environment*, *4*(4), 1577–1605. https://doi.org/10.1007/s40808-018-0509-y

Abebe, B. W., Mana, T. T., & Hatiye, S. D. (2024). Assessment of meteorological drought and its association with global climate drivers in Genale Dawa River Basin, South-East of Ethiopia. *Modeling Earth Systems and Environment*, *10*(4), 5027–5042. https://doi.org/10.1007/s40808-024-02048-6

Abegaz, W. B., & Mekoya, A. (2020). Rainfall Variability and Trends over Central Ethiopia. *International Journal of Environmental Science and Natural Resources*, *24*(4). https://doi.org/10.19080/IJESNR.2020.24.556144

Abera Abdi, D., & Ayenew, T. (2021). Evaluation of the WEAP model in simulating subbasin hydrology in the Central Rift Valley basin, Ethiopia. *Ecological Processes*, *10*(1), 41. https://doi.org/10.1186/s13717-021-00305-5

Abera, K., & Gebeyehu, A. (2023). Hydrological drought forecasting and monitoring system development using artificial neural network (ANN) in Ethiopia. *Heliyon*, *9*(2), e13287. https://doi.org/10.1016/j.heliyon.2023.e13287

Abeysingha, N. S., Islam, A., & Singh, M. (2020). *Assessment of climate change impact on fl ow regimes over the Gomti River basin under IPCC AR5 climate change scenarios*. 303–326. https://doi.org/10.2166/wcc.2018.039

Abraha, T., Tibebu, A., & Ephrem, G. (2022). Rapid Urbanization and the Growing Water Risk Challenges in Ethiopia: The Need for Water Sensitive Thinking. *Frontiers in Water*, *4*(June), 1–19. https://doi.org/10.3389/frwa.2022.890229

Abraham, T., & Nadew, B. (2018). Impact of Land Use Land Cover Dynamics on Water Balance , Lake Ziway Watershed, Ethiopia. *Hydrology: Current Research*, *9*(4), 309.

Addisu, S., Selassie, Y. G., Fissha, G., & Gedif, B. (2015). Time series trend analysis of temperature and rainfall in lake Tana Sub-basin, Ethiopia. *Environmental Systems Research*, *4*(25). https://doi.org/10.1186/s40068-015-0051-0

Adeba, D., Kansal, M. L., & Sen, S. (2015). Assessment of water scarcity and its impacts on sustainable development in Awash basin, Ethiopia. *Sustainable Water Resources Management*, *1*(1), 71–87. https://doi.org/10.1007/s40899-015-0006-7

Ademe, F., Kibret, K., Beyene, S., Mitike, G., & Getinet, M. (2020). Rainfall analysis for rain-

fed farming in the great rift valley basins of Ethiopia. *Journal of Water and Climate Change*, *11*(3), 1–17. https://doi.org/10.2166/wcc.2019.242

Adera, A. G., & Alfredsen, K. T. (2020). *Climate change and hydrological analysis of Tekeze river basin Ethiopia : implication for potential hydropower production*. 744–759. https://doi.org/10.2166/wcc.2019.203

Adgolign, T. B., Rao, G. S., & Abbulu, Y. (2016). WEAP modeling of surface water resources allocation in Didessa Sub-Basin, West Ethiopia. *Sustainable Water Resources Management*, *2*(1), 55–70. https://doi.org/10.1007/s40899-015-0041-4

Adugna, M., Boru, N., & Debele, A. (2021). Impact of climate change on potential evapotranspiration and crop water requirement in Upper Wabe Bridge watershed , Wabe Shebele River. *Journal of African Earth Sciences*, *180*(2021), 104223. https://doi.org/10.1016/j.jafrearsci.2021.104223

Akoko, G., Le, T. H., Gomi, T., & Kato, T. (2021). A Review of SWAT Model Application in Africa. *Water*, *13*(9), 1313. https://doi.org/10.3390/ w13091313

Al Radif, A. (1999). Integrated water resources management (IWRM): an approach to face the challenges of the next century and to avert future crises. *Desalination*, *124*(1), 145–153. https://doi.org/https://doi.org/10.1016/S0011-9164(99)00099-5

Alam, A., Bhat, M. S., & Maheen, M. (2019). Using Landsat satellite data for assessing the land use and land cover change in Kashmir valley. *GeoJournal*, *85*, 1529–1543. https://doi.org/10.1007/s10708-019-10037-x

Alemayehu, A., & Bewket, W. (2016). Local climate variability and crop production in the central highlands of Ethiopia. *Environmental Development*, *19*, 36–48. https://doi.org/10.1016/j.envdev.2016.06.002

Alemayehu, A., & Bewket, W. (2017). Local spatiotemporal variability and trends in rainfall and temperature in the central highlands of Ethiopia. *Geografiska Annaler, Series A: Physical Geography*, *99*(2), 85–101. https://doi.org/10.1080/04353676.2017.1289460

Alemayehu, F., Taha, N., Nyssen, J., Girma, A., Zenebe, A., Behailu, M., Deckers, S., & Poesen, J. (2009). The impacts of watershed management on land use and land cover dynamics in Eastern Tigray (Ethiopia). *Resources, Conservation and Recycling*, *53*(4), 192–198. https://doi.org/10.1016/j.resconrec.2008.11.007

Alemayehu, T., Mccartney, M., & Kebede, S. (2010). The water resource implications of planned development in the lake Tana catchment, Ethiopia. *Ecohydrology and Hydrobiology*, *10*(2–4), 211–221. https://doi.org/10.2478/v10104-011-0023-6

Alemayehu, Z., & Kabite Wedajo, G. (2023). Spatiotemporal climate and vegetation trends, and their relationship: A case of Genale Dawa basin, Ethiopia. *Remote Sensing Applications: Society and Environment*, *32*, 101070. https://doi.org/https://doi.org/10.1016/j.rsase.2023.101070

Alemu, B. (2015). The Effect of Land Use Land Cover Change on Land Degradation in the Highlands of Ethiopia. *Journal of Environment and Earth Science*, *5*(1), 1–13. https://core.ac.uk/download/pdf/234663949.pdf

Alemu, B., Garedew, E., Eshetu, Z., & Kassa, H. (2015). Land use and land cover changes and associated driving forces in north western lowlands of Ethiopia. *International Research Journal of Agricultural Science and Soil Science*, *5*(1), 28–44.

Alemu, M. M., & Bawoke, G. T. (2019). Analysis of spatial variability and temporal trends of rainfall in Amhara Region, Ethiopia. *Journal of Water and Climate Change*, *11*(4), 1–16. https://doi.org/10.2166/wcc.2019.084

Alemu, T., & Mengistu, A. (2019). *Impacts of Climate Change on Food Security in Ethiopia: Adaptation and Mitigation Options: A Review. In: Castro P., Azul A., Leal Filho W., Azeiteiro U. (eds) Climate Change-Resilient Agriculture and Agroforestry. Climate Change Management. Springer, Cham*. https://doi.org/10.1007/978-3-319-75004-0-23

Alexandersson, H. (1986). A homogeneity test applied to precipitation data. *Journal of Climatology*, *6*(6), 661–675. https://doi.org/10.1002/joc.3370060607

Alhamshry, A., Fenta, A. A., Yasuda, H., Kimura, R., & Shimizu, K. (2019). Seasonal Rainfall Variability in Ethiopia and Its Long-Term Link to Global Sea Surface Temperatures. *Water*, *12*(1), p.55. https://doi.org/doi:10.3390/w12010055

Allen, R. G., Pereira, L. S., Raes, D., Smith, M., & Ab, W. (1998). *Crop evapotranspiration - Guidelines for computing crop water requirements - FAO Irrigation and drainage paper 56 . FAO, Rome, Vol. 300, No. 9, P*. 1–15.

Alvarenga, L. A., Mello, C. R. De, Colombo, A., Cuartas, L. A., & Bowling, L. C. (2016). Assessment of land cover change on the hydrology of a Brazilian head- water watershed using the Distributed Hydrology-Soil-Vegetation Model. *Catena*, *143*, 7–17. https://doi.org/10.1016/j.catena.2016.04.001

Amin, A., Iqbal, J., Asghar, A., & Ribbe, L. (2018). Analysis of current and futurewater demands in the Upper Indus Basin under IPCC climate and socio-economic scenarios using a hydro-economic WEAP Model. *Water (Switzerland)*, *10*(5). https://doi.org/10.3390/w10050537

Anderson, J. R., Hardy, E. E., & Roach, J. T. (1976). *A Land Use and Land Cover Classification System for Use with Remote Sensor Data* (Vol. 964). US Government Printing Office.

Anose, F. A., Beketie, K. T., Terefe Zeleke, T., Yayeh Ayal, D., & Legese Feyisa, G. (2021). Spatio-temporal hydro-climate variability in Omo-Gibe river Basin, Ethiopia. *Climate Services*, *24*, 100277. https://doi.org/10.1016/j.cliser.2021.100277

Aredo, M. R., Hatiye, S. D., & Pingale, S. M. (2021). Impact of Land Use / Land Cover Change on Stream Flow in the Shaya Catchment of Ethiopia using the MIKE SHE Model. *Arabian Journal of Geosciences*, *14*(2), 1–15. https://doi.org/10.1007/s12517-021-06447-2

Arnold, J. G., & Fohrer, N. (2005). SWAT2000 : Current Capabilities and Research Opportunities in Applied watershed Modelling. *Hydrological Processes*, *19*, 563–572. https://doi.org/10.1002/hyp.5611

Arnold, J. G., Moriasi, D. N., Gassman, P. W., Abbaspour, K. C., White, M. J., Srinivasan, R., Santhi, C., Harmel, R. D., Griensven, A. Van, Van Liew, M. W., Kannan, N., & Jha, M. K. (2012). SWAT: Model Use, Calibration, and Validation. *Transactions of the American*

Society of Agricultural and Biological Engineers, *55*(4), 1491–1508.

Arnold, J. G., Srinivasan, R., Muttiah, R. S., & Williams, J. R. (1998). Large area hydrologic modeling and assessment: Part I. Model development. *Journal of the American Water Resources Association*, *34*(1), 73–89.

Arnold, J. G., & Williams, J. R. (1987). Validation of SWRRB—simulator for water resources in rural basins. *Journal of Water Resources Planning and Management*, *113*(2), 243–256.

Asfaw, A., Simane, B., Hassen, A., & Bantider, A. (2018). Variability and time series trend analysis of rainfall and temperature in northcentral Ethiopia: A case study in Woleka sub-basin. *Weather and Climate Extremes*, *19*(2018), 29–41. https://doi.org/10.1016/j.wace.2017.12.002

Awotwi, A., Annor, T., Anornu, G. K., Quaye-Ballard, J. A., Agyekum, J., Ampadu, B., Nti, I. K., Gyampo, M. A., & Boakye, E. (2021). Climate change impact on streamflow in a tropical basin of Ghana, West Africa. *Journal of Hydrology: Regional Studies*, *34*(September 2020), 100805. https://doi.org/10.1016/j.ejrh.2021.100805

Awotwi, A., Kwame, G., Quaye-ballard, J. A., Annor, T., Kwabena, E., Harris, E., Agyekum, J., & Lawer, J. (2019). Water balance responses to land-use / land-cover changes in the Pra River Basin of Ghana , 1986 – 2025. *Catena*, *182*, 104129. https://doi.org/10.1016/j.catena.2019.104129

Awulachew, S. B., Erkossa, T., & Namara, R. E. (2010). Irrigation potential in Ethiopia: Constraints and opportunities for enhancing the system. Research Report, International Water Management Institute, Addis Ababa. *International Water Management Institute*, *July*, 1–59.

Awulachew, S. B., Yilma, A. D., Loiskandl, W., Ayana, M., & Alamirew, T. (2007). Water resources and irrigation development in Ethiopia. Colombo, Sri Lanka: International Water Management Institute (IWMI) 66p. In *[IWMI Working Paper 123]*.

Ayalew, D., Tesfaye, K., Mamo, G., Yitaferu, B., & Bayu, W. (2012). Variability of rainfall and its current trend in Amhara region , Ethiopia. *African Journal of Agricultural Research*, *7*(10), 1475–1486. https://doi.org/10.5897/AJAR11.698

Ayalew, D. W. (2018). Theoretical and Empirical Review of Ethiopian Water Resource Potentials , Challenges and Future Development Opportunities. *International Journal of Waste Resources*, *8*(4). https://doi.org/10.4172/2252-5211.1000353

Ayele, G., Hayicho, H., & Alemu, M. (2019). Land Use Land Cover Change Detection and Deforestation Modeling: In Delomena District of Bale Zone, Ethiopia. *Journal of Environmental Protection*, *10*(04), 532–561. https://doi.org/10.4236/jep.2019.104031

Azman, A. H., Tukimat, N. N. A., & Malek, M. A. (2022). Analysis of Linear Scaling Method in Downscaling Precipitation and Temperature. *Water Resources Management*, *36*(1), 171–179. https://doi.org/10.1007/s11269-021-03020-0

Babel, M. S., Gupta, A. Das, & Nayak, D. K. (2005). A Model for Optimal Allocation of Water to Competing Demands. *Water Resources Management*, *19*(6), 693–712. https://doi.org/10.1007/s11269-005-3282-4

Babiso, B., Toma, S., & Bajigo, A. (2016). Land use / Land Cover Dynamics and its Implication on Sustainable Land Management in Wallecha Watershed , Southern Ethiopia. *Global Journal of Science Frontier Research: H Environment & Earth Science*, *16*(4), 49–53.

Balcha, S. K., Awass, A. A., Hulluka, T. A., Bantider, A., & Ayele, G. T. (2023). Assessment of future climate change impact on water balance components in Central Rift Valley Lakes Basin, Ethiopia. *Journal of Water and Climate Change*, *14*(1), 175–199. https://doi.org/10.2166/wcc.2022.249

Bao, C., & He, D. (2015). The causal relationship between urbanization, economic growth and water use change in provincial China. *Sustainability (Switzerland)*, *7*(12), 16076–16085. https://doi.org/10.3390/su71215803

Bekele-Biratu, E., Thiaw, W. M., & Korecha, D. (2018). Sub-seasonal variability of the Belg rains in Ethiopia. *International Journal of Climatology*, *38*(7), 2940–2953. https://doi.org/10.1002/joc.5474

Bekele, D., Alamirew, T., Kebede, A., Zeleke, G., Assefa, M., & Bekele, D. (2021). Modeling the impacts of land use and land cover dynamics on hydrological processes of the Keleta watershed , Ethiopia. *Sustainable Environment*, *7*(1), 0–14. https://doi.org/10.1080/27658511.2021.1947632

Bekele, D., Alamirew, T., Kebede, A., Zeleke, G., & Melese, A. M. (2017). Analysis of rainfall trend and variability for agricultural water management in awash river Basin, Ethiopia. *Journal of Water and Climate Change*, *8*(1), 127–141. https://doi.org/10.2166/wcc.2016.044

Bekele, D., Alamirew, T., Kebede, A., Zeleke, G., & Melesse, A. M. (2019). Modeling Climate Change Impact on the Hydrology of Keleta Watershed in the Awash River Basin , Ethiopia. *Environmental Modeling & Assessment*, *24*, 95–107. 10.1007/s10666-018-9619-1

Bekele, F., Mosisa, N., & Tereefe, D. (2017). Analysis of Current Rainfall Variability and Trends over Bale-Zone, South Eastern Highland of Ethiopia. *SciFed Journal of Global Warming*, *1*(2), 1–7. https://doi.org/https://doi.org/10.23959/sfjgw-1000007

Bekele, W. T., Haile, A. T., & Rientjes, T. (2021). Impact of Climate Change on the Streamflow of the Arjo-Didessa catchment Under RCP Scenarios. *Journal of Water and Climate Change*, 1–13. https://doi.org/10.2166/wcc.2021.307

Belay, A., Demissie, T., Recha, J. W., Oludhe, C., Osano, P. M., Olaka, L. A., Solomon, D., & Berhane, Z. (2021). Analysis of climate variability and trends in Southern Ethiopia. *Climate*, *9*(6), 1–17. https://doi.org/10.3390/cli9060096

Belihu, M., Tekleab, S., Abate, B., & Bewket, W. (2020). Hydrologic response to land use land cover change in the Upper Gidabo Watershed, Rift Valley Lakes Basin, Ethiopia. *HydroResearch*, *3*, 85–94. https://doi.org/10.1016/j.hydres.2020.07.001

Berhanu, B., Seleshi, Y., & Melesse, A. M. (2014). *Surface Water and Groundwater Resources of Ethiopia: Potentials and Challenges of Water Resources Development* (A. M. Melesse, W. Abtew, & S. G. Setegn (Eds.); pp. 97–117). Springer International Publishing. https://doi.org/10.1007/978-3-319-02720-3_6

Berhe, F. T., Melesse, A. M., Hailu, D., & Sileshi, Y. (2013). MODSIM-based water allocation modeling of Awash River Basin, Ethiopia. *CATENA*, *109*, 118–128. https://doi.org/https://doi.org/10.1016/j.catena.2013.04.007

Berihun, M. L., Tsunekawa, A., Haregeweyn, N., Meshesha, D. T., Adgo, E., Tsubo, M., Masunaga, T., Fenta, A. A., Sultan, D., & Yibeltal, M. (2019). Exploring land use/land cover changes, drivers and their implications in contrasting agro-ecological environments of Ethiopia. *Land Use Policy*, *87*, 104052. https://doi.org/10.1016/j.landusepol.2019.104052

Berihun, M. L., Tsunekawa, A., Haregeweyn, N., Tsubo, M., Yasuda, H., Fenta, A. A., Dile, Y. T., Bayabil, H. K., & Tilahun, S. A. (2023). Examining the past 120 years' climate dynamics of Ethiopia. In *Theoretical and Applied Climatology* (Vol. 154, Issues 1–2). Springer Vienna. https://doi.org/10.1007/s00704-023-04572-4

Betru, T., Tolera, M., Sahle, K., & Kassa, H. (2019). Trends and drivers of land use/land cover change in Western Ethiopia. *Applied Geography*, *104*, 83–93. https://doi.org/10.1016/j.apgeog.2019.02.007

Bewket, W. (2012). Climate change perceptions and adaptive responses of smallholder farmers in central highlands of Ethiopia. *International Journal of Environmental Studies*, *69*(3), 507–523. https://doi.org/10.1080/00207233.2012.683328

Bewket, W., & Conway, D. (2007). A note on the temporal and spatial variability of rainfall in the drought-prone Amhara region of Ethiopia. *International Journal of Climatology*, *27*, 1467–1477. https://doi.org/10.1002/joc.1481 A

Bewket, W., Radeny, M., & Mungai, C. (2015). Agricultural Adaptation and Institutional Responses to Climate Change Vulnerability in Ethiopia. *CCAFS Working Paper No. 106. CGIAR Research Program on Climate Change, Agriculture and Food Security (CCAFS). Copenhagen, Denmark.* www.ccafs.cgiar.org

Beyene, A. N. (2016). *Precipitation and Temperature Trend Analysis in Mekelle city , Northern Ethiopia , the Case of Illala Meteorological Station*. *7*(1), 1–6. https://doi.org/10.4172/2157-7617.1000324

Bianucci, P., Sordo-Ward, A., Lama-Pedrosa, B., & Garrote, L. (2024). How do environmental flows impact on water availability under climate change scenarios in European basins? *Science of the Total Environment*, *911*(November 2023), 168566. https://doi.org/10.1016/j.scitotenv.2023.168566

Birhanu, A., Masih, I., Zaag, P. Van Der, Nyssen, J., & Cai, X. (2019). Impacts of land use and land cover changes on hydrology of the Gumara catchment , Ethiopia. *Physics and Chemistry of the Earth*, *112*, 165–174. https://doi.org/10.1016/j.pce.2019.01.006

Birkinshaw, S. J., Guerreiro, S. B., Nicholson, A., Liang, Q., Quinn, P., Zhang, L., He, B., Yin, J., & Fowler, H. J. (2017). Climate change impacts on Yangtze River discharge at the Three Gorges Dam. *Hydrology and Earth System Sciences*, *21*(4), 1911–1927. https://doi.org/10.5194/hess-21-1911-2017

Biru, W. D., Zeller, M., & Loos, T. K. (2020). The Impact of Agricultural Technologies on Poverty and Vulnerability of Smallholders in Ethiopia: A Panel Data Analysis. *Social*

Indicators Research, *147*(2), 517–544. https://doi.org/10.1007/s11205-019-02166-0

Bishaw, B. (2001). Deforestation and land degradation in the Ethiopian highlands: a strategy for physical recovery. *Northeast African Studies*, 7–25.

Bizuneh, B. B., Moges, M. A., Sinshaw, B. G., & Kerebih, M. S. (2021). SWAT and HBV models ' response to streamflow estimation in the upper Blue Nile Basin , Ethiopia. *Water-Energy Nexus*, *4*, 41–53. https://doi.org/10.1016/j.wen.2021.03.001

Bogale, S. (2021). Hydrological Response to Land Use and Land Cover Changes of Ribb Watershed , Ethiopia. *Hydrology*, *9*(1), 1–12. https://doi.org/10.11648/j.hyd.20210901.11

Bufebo, B., & Elias, E. (2021). Land Use/Land Cover Change and Its Driving Forces in Shenkolla Watershed, South Central Ethiopia. *Scientific World Journal*, *2021*. https://doi.org/10.1155/2021/9470918

Buishand, T. . (1982). Some Methods for Testing the Homogeneity of Rainfall Records. *Journal of Hydrology*, *58*(1–2), 11–27. https://doi.org/doi:10.1016/0022-1694(82)90066-x

Cai, X., & Rosegrant, M. W. (2002). Global Water Demand and Supply Projections: Part 1. A Modeling Approach. *Water International*, *27*(2), 159–169. https://doi.org/10.1080/02508060208686989

Chaemiso, S. E., Abebe, A., & Pingale, S. M. (2016). Assessment of the impact of climate change on surface hydrological processes using SWAT: a case study of Omo-Gibe river basin, Ethiopia. *Modeling Earth Systems and Environment*, *2*(4), 1–15. https://doi.org/10.1007/s40808-016-0257-9

Chakilu, G. G., & Moges, M. A. (2017). Assessing the Land Use/Cover Dynamics and its Impact on the Low Flow of Gumara Watershed, Upper Blue Nile Basin, Ethiopia. *Hydrology: Current Research*, *08*(01). https://doi.org/10.4172/2157-7587.1000268

Chang, C. K., Ghani, A. A., & Othman, M. A. (2017). Homogeneity Testing and Trends Analysis in Long Term Rainfall Data for Sungai Pahang River Basin Over 40 Years Records. *Proceedings of the 37th IAHR World Congress*, *August*, 4197–4203.

Chang, Y., Hou, K., Li, X., Zhang, Y., & Chen, P. (2018). Review of Land Use and Land Cover Change research progress. *IOP Conference Series: Earth and Environmental Science*, *113*(1), 012087. https://doi.org/10.1088/1755-1315/113/1/012087

Chapman, S., E Birch, C., Pope, E., Sallu, S., Bradshaw, C., Davie, J., & H Marsham, J. (2020). Impact of climate change on crop suitability in sub-Saharan Africa in parameterized and convection-permitting regional climate models. *Environmental Research Letters*, *15*(9). https://doi.org/10.1088/1748-9326/ab9daf

Chiew, F. H. S., Zheng, H., & Potter, N. J. (2018). Rainfall-Runoff modelling considerations to predict streamflow characteristics in ungauged catchments and under climate change. *Water (Switzerland)*, *10*(10), 7–9. https://doi.org/10.3390/w10101319

Chimdessa, K., Quraishi, S., Kebede, A., & Alamirew, T. (2019). Effect of land use land cover and climate change on river flow and soil loss in Didessa River Basin, South West Blue Nile, Ethiopia. *Hydrology*, *6*(2), 1–20. https://doi.org/10.3390/hydrology6010002

Chishugi, D. U., Sonwa, D. J., Kahindo, J.-M., Itunda, D., Chishugi, J. B., Félix, F. L., & Sahan, M. (2021). How Climate Change and Land Use/Land Cover Change Affect Domestic Water Vulnerability in Yangambi Watersheds (D. R. Congo). *Land*, *10*(165). https://doi.org/10.3390/land10020165

Chokkavarapu, N., & Mandla, V. R. (2019). Comparative study of GCMs, RCMs, downscaling and hydrological models: a review toward future climate change impact estimation. *SN Applied Sciences*, *1*(12), 1698. https://doi.org/10.1007/s42452-019-1764-x

da Silva, V. de P. R., Silva, M. T., Singh, V. P., de Souza, E. P., Braga, C. C., de Holanda, R. M., Almeida, R. S. R., de Assis Salviano de Sousa, F., & Braga, A. C. R. (2018). Simulation of stream flow and hydrological response to land-cover changes in a tropical river basin. *Catena*, *162*, 166–176. https://doi.org/10.1016/j.catena.2017.11.024

Daba, M. H., & You, S. (2020). Assessment of climate change impacts on river flow regimes in the upstream of awash basin, ethiopia: Based on ipcc fifth assessment report (ar5) climate change scenarios. *Hydrology*, *7*(4), 1–22. https://doi.org/10.3390/hydrology7040098

Dananto, M., Aga, A. O., Yohannes, P., & Shura, L. (2022). Assessing the Water-Resources Potential and Soil Erosion Hotspot Areas for Sustainable Land Management in the Gidabo Watershed, Rift Valley Lake Basin of Ethiopia. *Sustainability (Switzerland)*, *14*(9). https://doi.org/10.3390/su14095262

Dandesa, T., Korecha, D., Nigatu, L., & Br, C. (2017). Assessment of Climatic Variability and Development of Localized Climate Prediction Method for Livestock Production in Borana Area , Southern Ethiopia. *Environ Sci Ind J.*, *13*(3), 1–30.

Daniel, E. B., Camp, J. V, Leboeuf, E. J., Penrod, J. R., Dobbins, J. P., & Abkowitz, M. D. (2011). Watershed Modeling and its Applications : A State-of-the-Art Review. *The Open Hydrology Journal*, 26–50.

Daniel, H., & Abate, B. (2022). Effect of climate change on stream fl ow in the Gelana watershed , Rift valley basin, Ethiopia. *Journal of Water & Climate Change*, *13*(5), 2205–2232. https://doi.org/10.2166/wcc.2022.059

Dariane, A. B., & Pouryafar, E. (2021). Quantifying and projection of the relative impacts of climate change and direct human activities on streamflow fluctuations. *Climatic Change (2021)*, *165*(34). https://doi.org/10.1007/s10584-021-03060-w

de Fraiture, C., & Wichelns, D. (2010). Satisfying future water demands for agriculture. *Agricultural Water Management*, *97*(4), 502–511. https://doi.org/10.1016/j.agwat.2009.08.008

De Luis, M., González-Hidalgo, J. C., Brunetti, M., & Longares, L. A. (2011). Precipitation concentration changes in Spain 1946-2005. *Natural Hazards and Earth System Science*, *11*(5), 1259–1265. https://doi.org/10.5194/nhess-11-1259-2011

Dechasa, A., Aga, A. O., & Dufera, T. (2022). Erosion Risk Assessment for Prioritization of Conservation Measures in the Watershed of Genale Dawa-3 Hydropower Dam, Ethiopia. *Quaternary*, *5*(4). https://doi.org/10.3390/quat5040039

Degefu, M. A., Tadesse, Y., & Bewket, W. (2021a). Observed changes in rainfall amount and

extreme events in southeastern Ethiopia, 1955–2015. *Theoretical and Applied Climatology*, *144*(3–4), 967–983. https://doi.org/10.1007/s00704-021-03573-5

Degefu, M. A., Tadesse, Y., & Bewket, W. (2021b). Spatiotemporal variability and trends of drought episode in southeastern Ethiopia. *Physical Geography*, 1–28. https://doi.org/10.1080/02723646.2021.1930654

Devia, G. K., Ganasri, B. P., & Dwarakish, G. S. (2015). A Review on Hydrological Models. *Aquatic Procedia*, *4*(Icwrcoe), 1001–1007. https://doi.org/10.1016/j.aqpro.2015.02.126

Devries, J. J., & Hromadka, T. V. (1993). Computer models for surface water. *Handbook of Hydrology*, 21.

Dibaba, W. T., Demissie, T. A., & Miegel, K. (2020a). Drivers and Implications of Land Use/Land Cover Dynamics in Finchaa Catchment, Northwestern Ethiopia. *Land*, *9*(113), 1–20. https://doi.org/doi:10.3390/land9040113

Dibaba, W. T., Demissie, T. A., & Miegel, K. (2020b). Watershed Hydrological Response to Combined Land Use / Land Cover and Climate Change in Highland Ethiopia: Finchaa Catchment. *Water*, *12*(4), 1801. https://doi.org/doi:10.3390/w12061801

Dibaba, W. T., Miegel, K., & Demissie, T. A. (2019). Evaluation of the CORDEX regional climate models performance in simulating climate conditions of two catchments in Upper Blue Nile Basin. *Dynamics of Atmospheres and Oceans*, *87*(August), 101104. https://doi.org/10.1016/j.dynatmoce.2019.101104

Dickinson, R. E., Errico, R. M., Giorgi, F., & Bates, G. T. (1989). A regional climate model for the western United States. *Climatic Change*, *15*(3), 383–422. https://doi.org/10.1007/BF00240465

Dinku, T., Cousin, R., Corral, J., Ceccato, P., Thomson, M. C., Faniriantsoa, R., Khomyakov, I., & Vadillo, A. (2016). The ENACTS Approach: Transforming climate services in Africa one country at a time. *World Policy Papers*, 1–24.

Dinku, T., Hailemariam, K., Maidment, R., Tarnavsky, E., & Connor, S. (2014). Combined use of satellite estimates and rain gauge observations to generate high-quality historical rainfall time series over Ethiopia. *International Journal of Climatology*, *34*(7), 2489–2504. https://doi.org/10.1002/joc.3855

Dinsa, H. T., & Nurhusein, M. M. (2023). Integrated water resources management stumbling blocks: Prioritization for better implementation under ethiopian context. *Heliyon*, *9*(8), e18785. https://doi.org/10.1016/j.heliyon.2023.e18785

Divakar, L., Babel, M. S., Perret, S. R., & Gupta, A. Das. (2011). Optimal allocation of bulk water supplies to competing use sectors based on economic criterion – An application to the Chao Phraya River Basin, Thailand. *Journal of Hydrology*, *401*(1), 22–35. https://doi.org/https://doi.org/10.1016/j.jhydrol.2011.02.003

Dolan, F., Lamontagne, J., Link, R., Hejazi, M., Reed, P., & Edmonds, J. (2021). Evaluating the economic impact of water scarcity in a changing world. *Nature Communications*, *12*(1), 1–10. https://doi.org/10.1038/s41467-021-22194-0

Dosio, A., Lennard, C., & Spinoni, J. (2022). Projections of indices of daily temperature and precipitation based on bias - adjusted CORDEX - Africa regional climate model simulations. *Climatic Change*, 1–24. https://doi.org/10.1007/s10584-022-03307-0

Dubale, P. (2002). Present and future trends in natural resources management in agriculture: An overview. *Integrated Water and Land Management Research and Capacity Building Priorities for Ethiopia*, *29*.

Eisner, S., Flörke, M., Chamorro, A., Daggupati, P., Donnelly, C., Huang, J., Hundecha, Y., Koch, H., Kalugin, A., Krylenko, I., Mishra, V., Piniewski, M., Samaniego, L., Seidou, O., Wallner, M., & Krysanova, V. (2017). An ensemble analysis of climate change impacts on streamflow seasonality across 11 large river basins. *Climatic Change*, *141*(3), 401–417. https://doi.org/10.1007/s10584-016-1844-5

Eludoyin, A. O., & Olanrewaju, O. E. (2020). *Water Supply and Quality in the Sub-Saharan Africa BT - Clean Water and Sanitation* (W. Leal Filho, A. M. Azul, L. Brandli, A. Lange Salvia, & T. Wall (Eds.); pp. 1–17). Springer International Publishing. https://doi.org/10.1007/978-3-319-70061-8_166-1

Emiru, N. C., Recha, J. W., Thompson, J. R., Belay, A., Aynekulu, E., Manyevere, A., Demissie, T. D., Osano, P. M., Hussein, J., Molla, M. B., Mengistu, G. M., & Solomon, D. (2022). Impact of Climate Change on the Hydrology of the Upper Awash River Basin , Ethiopia. *Hydrology*, *9*, 3. https://doi.org/10.3390/hydrology9010003

Engdaw, K. (2016). *Assessment on Surface Water Potential and Demands of Wabishebele Basin in Ethiopia. Addis Ababa: Unpublished.*

EPCC. (2015). Ethiopian Panel on Climate Change: First Assessment Reoport, Working Group II Biodiversisty and Ecosystems. *Ethiopian Academy of Sciences. Addis Ababa, Ethiopia*.

Ermias, M. (2019). „Surface water and groundwater resources of Rift Valley Lakes Basin of Ethiopia: A review of potentials, challenges and future development perspectives". *International Journal of Recent Development in Engineering and Technology*, *8*(6), 4–10.

Eromo, S., Adane, C., Santosh, A., & Pingale, M. (2016). Assessment of the impact of climate change on surface hydrological processes using SWAT : a case study of Omo-Gibe river basin , Ethiopia. *Modeling Earth Systems and Environment*, *2*(4), 1–15. https://doi.org/10.1007/s40808-016-0257-9

Eshete, S., Asefa, T., & Mekonnen, H. (2024). Hydrological responses to historical and predicted land use / land cover changes in the Welmel watershed , Genale Dawa Basin , Ethiopia : Implications for water resource management. *Journal of Hydrology: Regional Studies*, *52*(October 2023), 101709. https://doi.org/10.1016/j.ejrh.2024.101709

Eshetu, G., Johansson, T., & Garedew, W. (2016). Rainfall trend and variability analysis in Setema-Gatira area of Jimma , Southwestern Ethiopia. *African Journal of Agricultural Research*, *11*(32), 3037–3045. https://doi.org/10.5897/AJAR2015.10160

Fantu, B., Bart, M., Fanaye, T., & Taffesse, A. S. (2018). The evolving livestock sector in Ethiopia: growth by heads, not by productivity. *ESSP Working Paper-Ethiopia Strategy Support Program*, *122*.

FAO. (2002). *(Food and Agricultural Organization). Major Soils of the World Land and Water Digital Media Series ; CD-ROM; Food and Agricultural Organization of the United Nations: Rome, Italy, 2002.*

Fasika, A., Motuma, T., & Gizaw, T. (2019). Land Use Land Cover Change Trend and Its Drivers in Somodo Watershed South Western, Ethiopia. *African Journal of Agricultural Research*, *14*(2), 102–117. https://doi.org/10.5897/ajar2018.13672

FDRE Population Census Commision. (2008). *Summary and statistical report of the 2007 population and housing census: population size by age and sex*. Federal Democratic Republic of Ethiopia, Population Census Commission. https://www.ethiopianreview.com/pdf/001/Cen2007_firstdraft(1).pdf

Fentaw, F., Melesse, A., Asfaw, D., & Nigussie, A. (2018). *Impacts of Climate Changes on the Water Resources of Tekeze River Basin part of Eastern Nile , Ethiopia*. *20*, 3102.

Fita, T., & Abate, B. (2022). Impact of climate change on streamflow of Melka Wakena catchment, Upper Wabi Shebelle sub-basin, south-eastern Ethiopia. *Journal of Water and Climate Change*, *13*(5), 1995–2010. https://doi.org/10.2166/wcc.2022.191

Fowler, H. J., Blenkinsop, S., & Tebaldi, C. (2007). Linking climate change modelling to impacts studies: recent advances in downscaling techniques for hydrological modelling. *International Journal of Climatology: A Journal of the Royal Meteorological Society*, *27*(12), 1547–1578.

Galata, A. W., Tullu, K. T., & Guder, A. C. (2021). Evaluating watershed hydrological responses to climate changes at Hangar Watershed, Ethiopia. *Journal of Water and Climate Change*, *12*(6), 2271–2287. https://doi.org/10.2166/wcc.2021.229

Gashaw, T., Tulu, T., Argaw, M., & Worqlul, A. W. (2018). Modeling the hydrological impacts of land use / land cover changes in the Andassa watershed , Blue Nile Basin , Ethiopia. *Science of the Total Environment*, *619–620*, 1394–1408. https://doi.org/10.1016/j.scitotenv.2017.11.191

Gebrechorkos, S. H., Hülsmann, S., & Bernhofer, C. (2019). Statistically downscaled climate dataset for East Africa. *Scientific Data*, *6*(1), 31. https://doi.org/10.1038/s41597-019-0038-1

Gebremicael, T. G., Mohamed, Y. A., & Van der Zaag, P. (2019). Attributing the hydrological impact of different land use types and their long-term dynamics through combining parsimonious hydrological modelling , alteration analysis and PLSR analysis. *Science of the Total Environment*, *660*, 1155–1167. https://doi.org/10.1016/j.scitotenv.2019.01.085

Gedefaw, M., Denghua, Y., & Girma, A. (2023). Assessing the Impacts of Land Use/Land Cover Changes on Water Resources of the Nile River Basin, Ethiopia. *Atmosphere*, *14*(4). https://doi.org/10.3390/atmos14040749

Gedefaw, M., Wang, H., Yan, D., Qin, T., Wang, K., Girma, A., Batsuren, D., & Abiyu, A. (2019). Water resources allocation systems under irrigation expansion and climate change scenario in Awash River Basin of Ethiopia. *Water (Switzerland)*, *11*(10), 1–15. https://doi.org/10.3390/w11101966

Gedefaw, M., Wang, H., Yan, D., Song, X., Yan, D., Dong, G., Wang, J., Girma, A., Ali, B. A.,

Batsuren, D., Abiyu, A., & Qin, T. (2018). Trend Analysis of Climatic and Hydrological Variables in the Awash River Basin , Ethiopia. *Water*, *10*(11), 1–14. https://doi.org/10.3390/w10111554

Genjebo, M. G., Kemal, A., & Nannawo, A. S. (2023). Assessment of surface water resource and allocation optimization for diverse demands in Ethiopia's upper Bilate Watershed. *Heliyon*, *9*(10), e20298. https://doi.org/10.1016/j.heliyon.2023.e20298

Geremew, G. M., Mini, S., & Abegaz, A. (2020). Spatiotemporal variability and trends in rainfall extremes in Enebsie Sar Midir district , northwest Ethiopia. *Modeling Earth Systems and Environment*, *6*, 1177–1187. https://doi.org/10.1007/s40808-020-00749-2

Getachew, B. (2018). Trend analysis of temperature and rainfall in south Gonder zone , Ethiopia. *Journal of Degraded and Mining Lands Management*, *5*(2), 1111–1125. https://doi.org/10.15243/jdmlm.2018.052.1111

Getaneh, Y., Abera, W., Abegaz, A., & Tamene, L. (2022). A systematic review of studies on freshwater lakes of Ethiopia. *Journal of Hydrology: Regional Studies*, *44*(October), 101250. https://doi.org/10.1016/j.ejrh.2022.101250

Gezie, M. (2019). Farmer's response to climate change and variability in Ethiopia: A review. *Cogent Food & Agriculture*, *5*(1). https://doi.org/10.1080/23311932.2019.1613770

Giorgi, F., Hewitson, B., Christensen, J., Hulme, M., Von Storch, H., Whetton, P., Jones, R., Mearns, L., & Fu, C. (2001). Regional Climate Information Evaluation and Projections. *Climate Change 2001: The Scientific Basis. Contribution of Working Group I to the Third Assessment Report of the Intergovernmental Panel on Climate Change*.

Girvetz, E., Ramirez-Villegas, J., Claessens, L., Lamanna, C., Navaroo-Racines, C., Nowak, A., & Thornton, P. (2019). *Future climate projections in Africa: where are we headed?. in The Climate-Smart Agriculture Papers* (T. S. Rosenstock, A. Nowak, & E. Girvetz (Eds.)). Springer, Cham. https://doi.org/10.1007/978-3-319-92798-5

Gissila, T., Black, E., Grimes, D. I. F., & Slingo, J. M. (2004). Seasonal forecasting of the ethiopian summer rains. *International Journal of Climatology*, *24*, 1345–1358. https://doi.org/10.1002/joc.1078

Godfrey, S., & Tunhuma, F. A. (2020). The Climate Crisis: Climate Change Impacts, trend and Vulnerabilities of Children inSub Sahara Africa. *United Nations Children's Fund and Esatern and Southern Africa Regional Office. Nairobi*, 1–72. https://doi.org/10.2307/j.ctvmd85w3.12

Goshime, D. W., Haile, A. T., Rientjes, T., Absi, R., Ledésert, B., & Siegfried, T. (2021). Implications of water abstraction on the interconnected Central Rift Valley Lakes sub-basin of Ethiopia using WEAP. *Journal of Hydrology: Regional Studies*, *38*, 100969. https://doi.org/https://doi.org/10.1016/j.ejrh.2021.100969

Guida-Johnson, B., & Zuleta, G. A. (2013). Land-use land-cover change and ecosystem loss in the Espinal ecoregion, Argentina. *Agriculture, Ecosystems & Environment*, *181*, 31–40. https://doi.org/https://doi.org/10.1016/j.agee.2013.09.002

Gummadi, S., Rao, K. P. C., Seid, J., Legesse, G., Kadiyala, M. D. M., Takele, R., Amede, T., &

Whitbread, A. (2018). Spatio-temporal variability and trends of precipitation and extreme rainfall events in Ethiopia in 1980–2010. *Theoretical and Applied Climatology*, *134*(3–4), 1315–1328. https://doi.org/10.1007/s00704-017-2340-1

Guug, S. S., Abdul-ganiyu, S., & Kasei, R. A. (2020). Application of SWAT hydrological model for assessing water availability at the Sherigu catchment of Ghana and Southern Burkina Faso. *HydroResearch*, *3*, 124–133. https://doi.org/10.1016/j.hydres.2020.10.002

Guzha, A. C. (2018). Impacts of land use and land cover change on surface runoff , discharge and low flows : Evidence from East Africa. *Journal of Hydrology: Regional Studies*, *15*, 49–67. https://doi.org/10.1016/j.ejrh.2017.11.005

Gyamfi, C., Ndambuki, J. M., & Salim, R. W. (2016). Hydrological Responses to Land Use / Cover Changes in the Olifants Basin , South Africa. *Water*, *8*(12), 588. https://doi.org/10.3390/w8120588

Hadgu, G., Tesfaye, K., Mamo, G., & Kassa, B. (2013). Trend and variability of rainfall in Tigray , Northern Ethiopia : Analysis of meteorological data and farmers ' perception. *Academia Journal of Agricultural Research*, *1*(6), 88–100. https://doi.org/10.15413/ajar.2013.0117

Hagosa, F., Makombe, G., Namara, R., & Awulachew, S. (2009). *Importance of Irrigated Agriculture to the Ethiopian Economy: Capturing the direct net benefits of irrigation. Colombo, Sri Lanka: International Water Management Institute. 37p. (IWMI Research Report 128)* (Vol. 32, Issue 1). https://doi.org/10.4314/ejdr.v32i1.68597

Haile, A. T., Akawka, A. L., & Berhanu, B. (2017). Changes in water availability in the Upper Blue Nile basin under the representative concentration pathways scenario. *Hydrological Sciences Journal*, *62*(13), 2139–2149. https://doi.org/10.1080/02626667.2017.1365149

Haile, T. (1988). Causes and characteristics of drought in Ethiopia. *Ethiopian Journal of Agricultural Sciences*, *10*, 85–97.

Hailemariam, S. N., Soromessa, T., & Teketay, D. (2016). Land use and land cover change in the bale mountain eco-region of Ethiopia during 1985 to 2015. *Land*, *5*(4). https://doi.org/10.3390/land5040041

Hailu, A., Mammo, S., & Kidane, M. (2020). Dynamics of land use , land cover change trend and its drivers in Jimma Geneti District , Western Ethiopia. *Land Use Policy*, *99*, 105011. https://doi.org/10.1016/j.landusepol.2020.105011

Hamza, A. A., & Getahun, B. A. (2022). Assessment of water resource and forecasting water demand using WEAP model in Beles river, Abbay river basin, Ethiopia. *Sustainable Water Resources Management*, *8*(1), 22. https://doi.org/10.1007/s40899-022-00615-2

Hamza, I. A., & Iyela, A. (2012). Land use pattern, climate change, and its implication for food security in Ethiopia: A review. *Ethiopian Journal of Environmental Studies and Management*, *5*(1), 26–31.

Hare, W. (2003). Assessment of Knowledge on Impacts of Climate Change–Contribution. *Arctic*, *100*(6).

Haregeweyn, N., Tesfaye, S., Tsunekawa, A., Tsubo, M., Meshesha, D. T., Adgo, E., & Elias, A. (2015). Dynamics of land use and land cover and its effects on hydrologic responses: case study of the Gilgel Tekeze catchment in the highlands of Northern Ethiopia. *Environmental Monitoring and Assessment*, *187*(4090). https://doi.org/10.1007/s10661-014-4090-1

Harka, A. E., Jilo, N. B., & Behulu, F. (2021). Spatial-temporal rainfall trend and variability assessment in the Upper Wabe Shebelle River Basin, Ethiopia: Application of innovative trend analysis method. *Journal of Hydrology: Regional Studies*, *37*, 100915. https://doi.org/10.1016/j.ejrh.2021.100915

Hartmann, D. L. (2016). *Chapter 11 - Global Climate Models* (D. L. B. T.-G. P. C. (Second E. Hartmann (Ed.); pp. 325–360). Elsevier. https://doi.org/https://doi.org/10.1016/B978-0-12-328531-7.00011-6

Harvey, C. A., Saborio-Rodríguez, M., Martinez-Rodríguez, M. R., Viguera, B., Chain-Guadarrama, A., Vignola, R., & Alpizar, F. (2018). Climate change impacts and adaptation among smallholder farmers in Central America. *Agriculture and Food Security*, *7*(1), 1–20. https://doi.org/10.1186/s40066-018-0209-x

Hassan, Z., Shabbir, R., Ahmad, S. S., Malik, A. H., Aziz, N., Butt, A., & Erum, S. (2016). Dynamics of land use and land cover change (LULCC) using geospatial techniques: a case study of Islamabad Pakistan. *SpringerPlus*, *5*(812). https://doi.org/10.1186/s40064-016-2414-z

Hassen, E. E., & Assen, M. (2018). Land use/cover dynamics and its drivers in Gelda catchment, Lake Tana watershed, Ethiopia. *Environmental Systems Research*, *6*(1), 1–13. https://doi.org/10.1186/s40068-017-0081-x

Hatmoko, W., Levina, L., Radhika, R., Amirwandi, A., & Rendy, R. (2020). Quantification of Environmental Flow Requirement for some Rivers in West Java. *E3S Web of Conferences*, *148*. https://doi.org/10.1051/e3sconf/202014807003

Howard, G., Bartram, J., William, A., Overbo, A., Fuente, D., & Geere, J.-A. (2020). Domestic Water Quantity , Service Level and Health, second edition, Geneva: In *World Health Organization. Licence: CC BY-NC-SA 3.0 IGO*.

Hurni, H., Tato, K., & Zeleke, G. (2005). The implications of changes in population, land use, and land management for surface runoff in the upper Nile basin area of Ethiopia. *Mountain Research and Development*, *25*(2), 147–154.

Hussain, M., Liu, G., Yousaf, B., Ahmed, R., Uzma, F., Ali, M. U., Ullah, H., & Butt, A. R. (2018). Regional and sectoral assessment on climate-change in Pakistan: Social norms and indigenous perceptions on climate-change adaptation and mitigation in relation to global context. *Journal of Cleaner Production*, *200*, 791–808. https://doi.org/10.1016/j.jclepro.2018.07.272

Hussen, B., Mekonnen, A., & Pingale, S. M. (2018). Integrated water resources management under climate change scenarios in the sub-basin of Abaya-Chamo, Ethiopia. *Modeling Earth Systems and Environment*, *4*(1), 221–240. https://doi.org/10.1007/s40808-018-0438-9

Ibe, G. ., & Amikuzuno, J. (2019). Climate Change in Sub-Saharan Africa : A menace to

Agricultural productivity and Ecological protection. *Journal of Applied Sciences and Environmental*, *23*(2), 329–335. https://doi.org/https://dx.doi.org/10.4314/jasem.v23i2.20 Copyright:

Insan, S., & Kuntiyawichai, K. (2022). Assessment of Agricultural Water Sufficiency under Climate and Land Use Changes in the Lam Takong River Basin. *Water*, *14*(18), 1–18. https://doi.org/10.3390/w14182794

IPCC. (2014). *Synthesis Report. Contribution of Working Groups I, II and III to the Fifth Assessment Report of the Intergovernmental Panel on Climate Chang [Core Writing Team, R.K. Pachauri and L.A. Meyer (eds.)].IPCC, Geneva, Switzerland, 151 pp.* https://www.ipcc.ch/report/ar5/syr/

IPCC. (2013). *T. F. Stocker, D. Qin, G. K. Plattner, M. Tignor, S. K. Allen, J. Boschung, A. Nauels, Y. Xia, V. Bex & P. M. Midgley (Eds.). Climate Change 2013 The Physical Science Basis. Cambridge University Press*.

IPCC (Ed.). (2014). Evaluation of Climate Models. In *Climate Change 2013 – The Physical Science Basis: Working Group I Contribution to the Fifth Assessment Report of the Intergovernmental Panel on Climate Change* (pp. 741–866). Cambridge University Press. https://doi.org/DOI: 10.1017/CBO9781107415324.020

Izaurralde, R. C., Williams, J. R., McGill, W. B., Rosenberg, N. J., & Jakas, M. C. Q. (2006). Simulating soil C dynamics with EPIC: Model description and testing against long-term data. *Ecological Modelling*, *192*(3–4), 362–384.

Jilo, N. B., Gebremariam, B., Harka, A. E., & Woldemariam, G. W. (2019). Evaluation of the Impacts of Climate Change on Sediment Yield from the Logiya Watershed , Lower Awash Basin, Ethiopia. *Hydrology*, *6*(81). https://doi.org/10.3390/hydrology6030081

Johnston, R., & Smakhtin, V. (2014). Hydrological Modeling of Large river Basins: How Much is Enough? *Water Resources Management*, *28*(10), 2695–2730. https://doi.org/10.1007/s11269-014-0637-8

Kang, H. M., & Yusof, F. (2012). Homogeneity Tests on Daily Rainfall Series in Peninsular Malaysia. *Int. J. Contemp. Math. Scie.*, *7*(1), 9–22.

Kankam-Yeboah, K., Obuobie, E., Amisigo, B., & Opoku-Ankomah, Y. (2013). Impact of climate change on streamflow in selected river basins in Ghana. *Hydrological Sciences Journal*, *58*(4), 773–788. https://doi.org/10.1080/02626667.2013.782101

Kassie, B. T., Rötter, R. P., Hengsdijk, H., Asseng, S., Ittersum, M. K., Kahiluto, H., & Van Keulen, H. (2014). Climate variability and change in the Central Rift Valley of Ethiopia : challenges for rainfed crop production. *Journal of Agricultural Science*, *152*, 58–74. https://doi.org/10.1017/S0021859612000986

Keller, A. A., Garner, K. L., Rao, N., Knipping, E., & Thomas, J. (2022). Downscaling approaches of climate change projections for watershed modeling: Review of theoretical and practical considerations. *PLOS Water*, *1*(9), e0000046. https://doi.org/10.1371/journal.pwat.0000046

Kemal, B., & Adeba, D. (2021). Surface Water Potential Assessment and Water Demand

Evaluation (A Case of Dabus Watershed, Blue Nile Basin). *Computational Water, Energy, and Environmental Engineering*, *10*(04), 155–168. https://doi.org/10.4236/cweee.2021.104012

Kendall, M. G. (1975). *Rank Correlation Methods* (4th ed.). Charles Griffin, London.

Ketema, A., & Dwarakish, G. S. (2021a). *Climate Change Impacts on Water Resources in Ethiopia BT - Climate Change Impacts on Water Resources: Hydraulics, Water Resources and Coastal Engineering* (R. Jha, V. P. Singh, V. Singh, L. B. Roy, & R. Thendiyath (Eds.); pp. 47–58). Springer International Publishing. https://doi.org/10.1007/978-3-030-64202-0_5

Ketema, A., & Dwarakish, G. S. (2021b). Hydro-meteorological impact assessment of climate change on Tikur Wuha watershed in Ethiopia. *Sustainable Water Resources Management*, *7*(4), 1–20. https://doi.org/10.1007/s40899-021-00547-3

Khoi, D. N., & Thom, V. T. (2015). Parameter uncertainty analysis for simulating streamflow in a river catchment of Vietnam. *Global Ecology and Conservation*, *4*, 538–548. https://doi.org/10.1016/j.gecco.2015.10.007

Kibret, K. S., Marohn, C., & Cadisch, G. (2016). Assessment of land use and land cover change in South Central Ethiopia during four decades based on integrated analysis of multi-temporal images and geospatial vector data. *Remote Sensing Applications: Society and Environment*, *3*, 1–19.

Kifle Arsiso, B., Mengistu Tsidu, G., Stoffberg, G. H., & Tadesse, T. (2017). Climate change and population growth impacts on surface water supply and demand of Addis Ababa, Ethiopia. *Climate Risk Management*, *18*(August 2017), 21–33. https://doi.org/10.1016/j.crm.2017.08.004

Kindu, M., Schneider, T., Teketay, D., & Knoke, T. (2013). Land use/land cover change analysis using object-based classification approach in Munessa-Shashemene landscape of the ethiopian highlands. *Remote Sensing*, *5*(5), 2411–2435. https://doi.org/10.3390/rs5052411

Kiparsky, M., Joyce, B., Purkey, D., & Young, C. (2014). Potential impacts of climate warming on water supply reliability in the Tuolumne and Merced River Basins, California. *PloS One*, *9*(1), e84946. https://doi.org/10.1371/journal.pone.0084946

Knisel, W. G. (1980). *CREAMS: A field scale model for chemicals, runoff, and erosion from agricultural management systems* (Issue 26). Department of Agriculture, Science and Education Administration.

Knutti, R. (2008). Should we believe model predictions of future climate change? *Philosophical Transactions of the Royal Society A: Mathematical, Physical and Engineering Sciences*, *366*(1885), 4647–4664. https://doi.org/10.1098/rsta.2008.0169

Kotir, J. H. (2011). Climate change and variability in Sub-Saharan Africa: A review of current and future trends and impacts on agriculture and food security. *Environment, Development and Sustainability*, *13*(3), 587–605. https://doi.org/10.1007/s10668-010-9278-0

Kuma, H. G., Feyessa, F. F., & Demissie, T. A. (2021). Hydrologic responses to climate and land-use / land-cover changes in the Bilate. *Journal of Water & Climate Change*, *12*(8), 3750–3769. https://doi.org/10.2166/wcc.2021.281

Kuma, H. G., Feyessa, F. F., & Demissie, T. A. (2023). Assessing the impacts of land use/land cover changes on hydrological processes in Southern Ethiopia: The SWAT model approach. *Cogent Engineering*, *10*(1). https://doi.org/10.1080/23311916.2023.2199508

Kumar, N., Tischbein, B., Kusche, J., Beg, M. K., & Bogardi, J. J. (2017). Impact of land-use change on the water resources of the Upper Kharun Catchment, Chhattisgarh, India. *Regional Environmental Change*, *17*(8), 2373–2385. https://doi.org/10.1007/s10113-017-1165-x

Kundzewicz, Z. W. (2008). Climate change impacts on the hydrological cycle. *Ecohydrology & Hydrobiology*, *8*(2), 195–203. https://doi.org/https://doi.org/10.2478/v10104-009-0015-y

Lambin, E. F., Geist, H. J., & Lepers, E. (2003). Dynamics of land-use and land-cover change in tropical regions. *Annual Review of Environment and Resources*, *28*, 205–241. https://doi.org/10.1146/annurev.energy.28.050302.105459

Legese, W., Korecha, D., & Ture, K. (2019). Impact of Climate Change on Seasonal Rainfall Patterns over Bale Highlands, Southeastern Ethiopia. *International Journal of Environmental Chemistry*, *3*(2), 84–91. https://doi.org/10.11648/j.ijec.20190302.15

Legese, W., Koricha, D., & Ture, K. (2018). Characteristics of Seasonal Rainfall and its Distribution Over Bale Highland, Southeastern Ethiopia. *Journal of Earth Science & Climatic Change*, *9*(2). https://doi.org/10.4172/2157-7617.1000443

Leitzke, B., & Adamatti, D. (2021). Multiagent system and rainfall-runoff model in hydrological problems: A systematic literature review. *Water (Switzerland)*, *13*(24). https://doi.org/10.3390/w13243643

Lemi, T., & Hailu, F. (2019). Effects of Climate Change Variability on Agricultural Productivity. *International Journal of Environmental Sciences & Natural Resources*, *17*(1). https://doi.org/10.19080/ijesnr.2019.17.555953

Leng, M., Yu, Y., Wang, S., & Zhang, Z. (2020). Simulating the Hydrological Processes of a Meso-Scale Watershed on the Loess Plateau, China. *Water*, *12*(3), 878. https://doi.org/10.3390/w12030878

Leonard, R. A., Knisel, W. G., & Still, D. A. (1987). GLEAMS: Groundwater loading effects of agricultural management systems. *Transactions of the ASAE*, *30*(5), 1403–1418.

Li, H., Yu, C., Qin, B., Li, Y., Jin, J., Luo, L., Wu, Z., Shi, K., & Zhu, G. (2022). Modeling the Effects of Climate Change and Land Use/Land Cover Change on Sediment Yield in a Large Reservoir Basin in the East Asian Monsoonal Region. *Water (Switzerland)*, *14*(15), 1–19. https://doi.org/10.3390/w14152346

Li, Y., Chang, J., Luo, L., Wang, Y., Guo, A., Ma, F., & Fan, J. (2018). Spatiotemporal impacts of land use land cover changes on hydrology from the mechanism perspective using SWAT model with time-varying parameters. *Hydrology Research*, *50*(1), 244–261. https://doi.org/10.2166/nh.2018.006

Lillesand, T. M., Kiefer, R. W., & Chipman, J. W. (2015). *Remote Sensing and Image Interpretation* (7th ed.). Wiley, New York.

Liu, J., Wang, Y., Yu, Z., Cao, X., Tian, L., Sun, S., & Wu, P. (2017). A comprehensive analysis of blue water scarcity from the production, consumption, and water transfer perspectives. *Ecological Indicators*, *72*, 870–880. https://doi.org/https://doi.org/10.1016/j.ecolind.2016.09.021

Lotfirad, M., Adib, A., Salehpoor, J., Ashrafzadeh, A., & Kisi, O. (2021). Simulation of the impact of climate change on runoff and drought in an arid and semiarid basin (the Hablehroud, Iran). *Applied Water Science*, *11*(10), 1–24. https://doi.org/10.1007/s13201-021-01494-2

Loucks, D. P., & van Beek, E. (2017). *Water Resources Planning and Management: An Overview BT - Water Resource Systems Planning and Management: An Introduction to Methods, Models, and Applications* (D. P. Loucks & E. van Beek (Eds.); pp. 1–49). Springer International Publishing. https://doi.org/10.1007/978-3-319-44234-1_1

Lund, J. R., Scheierling, S. M., & Milne, G. (2010). *Modeling for Watershed Management*.

Luo, M., Liu, T., & Meng, F. (2018). Comparing Bias Correction Methods Used in Downscaling Precipitation and Temperature from Regional Climate Models : A Case Study from the Kaidu River Basin in Western China. *Water*, *10*(1046). https://doi.org/10.3390/w10081046

Lv, Z., Zuo, J., & Rodriguez, D. (2020). Predicting of Runoff Using an Optimized SWAT-ANN : A Case Study. *Journal of Hydrology : Regional Studies*, *29*. https://doi.org/10.1016/j.ejrh.2020.100688

Mahmood, R., & Babel, M. S. (2013). Evaluation of SDSM developed by annual and monthly sub-models for downscaling temperature and precipitation in the Jhelum basin, Pakistan and India. *Theoretical and Applied Climatology*, *113*(1–2), 27–44. https://doi.org/10.1007/s00704-012-0765-0

Mahmood, R., & Jia, S. (2017). An extended linear scaling method for downscaling temperature and its implication in the Jhelum River basin, Pakistan, and India, using CMIP5 GCMs. *Theoretical and Applied Climatology*, *130*(3–4), 725–734. https://doi.org/10.1007/s00704-016-1918-3

Mahmood, R., Jia, S., Tripathi, N. K., & Shrestha, S. (2018). Precipitation extended linear scaling method for correcting GCM precipitation and its evaluation and implication in the transboundary Jhelum River basin. *Atmosphere*, *9*(5). https://doi.org/10.3390/atmos9050160

Mango, L. M., Melesse, A. M., Mcclain, M. E., Gann, D., & Setegn, S. G. (2011). Land use and climate change impacts on the hydrology of the upper Mara River Basin , Kenya : results of a modeling study to support better resource management. *Hydrology and Earth System Sciences*, *15*, 2245–2258. https://doi.org/10.5194/hess-15-2245-2011

Mann, H. B. (1945). Nonparametric Tests Against Trend. *Econometrica*, *13*(3), 245–259. https://doi.org/10.2307/1907187

Marahatta, S., Devkota, L. P., & Aryal, D. (2021). Application of swat in hydrological simulation of complex mountainous river basin (Part i: Model development). *Water (Switzerland)*, *13*(11). https://doi.org/10.3390/w13111546

Marin, M., Clinciu, I., Tudose, N. C., Ungurean, C., Mihalache, A. L., Martoiu, N. E., & Tudose,

O. N. (2022). Assessment of Seasonal Surface Runoff under Climate and Land Use Change Scenarios for a Small Forested Watershed: Upper Tarlung Watershed (Romania). *Water (Switzerland)*, *14*(18). https://doi.org/10.3390/w14182860

Mathewos, M., Dananto, M., Erkossa, T., & Mulugeta, G. (2019). Land Use Land Cover Dynamics at Bilate Alaba Sub-watershed , Southern Ethiopia. *Journal of Applied Sciences and Environmental Management*, *28*(8), 1521–1528.

Maza, M., Srivastava, A., Bisht, D. S., Raghuwanshi, N. S., Bandyopadhyay, A., Chatterjee, C., & Bhadra, A. (2020). Simulating hydrological response of a monsoon dominated reservoir catchment and command with heterogeneous cropping pattern using VIC model. *Journal of Earth System Science*, *129*(1). https://doi.org/10.1007/s12040-020-01468-z

Megersa, T., Nedaw, D., & Argaw, M. (2019). Combined effect of land use/cover types and slope gradient in sediment and nutrient losses in Chancho and Sorga sub watersheds, East Wollega Zone, Oromia, Ethiopia. *Environmental Systems Research*, *8*(1). https://doi.org/10.1186/s40068-019-0151-3

Mekonen, A. A., & Berlie, A. B. (2020). Spatiotemporal variability and trends of rainfall and temperature in the Northeastern Highlands of Ethiopia. *Modeling Earth Systems and Environment*, *6*(1), 285–300. https://doi.org/10.1007/s40808-019-00678-9

Mendez, M., Maathuis, B., Hein-Griggs, D., & Alvarado-Gamboa, L.-F. (2020). Performance Evaluation of Bias Correction Methods for Climate Change Monthly Precipitation Projections over Costa Rica. *Water*, *12*, 482. https://doi.org/10.3390/w12020482

Mengistu, A. G., Woldesenbet, T. A., Dile, Y. T., Bayabil, H. K., & Tefera, G. W. (2023). Modeling impacts of projected land use and climate changes on the water balance in the Baro basin, Ethiopia. *Heliyon*, *9*(3), e13965. https://doi.org/10.1016/j.heliyon.2023.e13965

Mengistu, D., Bewket, W., Dosio, A., & Panitz, H. (2020). Climate change impacts on water resources in the Upper Blue Nile (Abay) River Basin, Ethiopia. *Journal of Hydrology*. https://doi.org/10.1016/j.jhydrol.2020.125614

Mengistu, D., Bewket, W., & Lal, R. (2014). Recent spatiotemporal temperature and rainfall variability and trends over the Upper Blue Nile River Basin, Ethiopia. *International Journal of Climatology*, *34*(7), 2278–2292. https://doi.org/10.1002/joc.3837

Mengistu, T. D., Feyissa, T. A., Chung, I., Chang, S. W., Yesuf, M. B., & Alemayehu, E. (2022). Regional Flood Frequency Analysis for Sustainable Water Resources Management of Genale – Dawa River Basin, Ethiopia. *Water*, *14*, 1–18. https://doi.org/10.3390/w14040637

Mera, G. A. (2018). Drought and its impacts in Ethiopia. *Weather and Climate Extremes*, *22*, 24–35. https://doi.org/10.1016/j.wace.2018.10.002

Merga, D. D., Adeba, D., Regasa, M. S., & Leta, M. K. (2022). Evaluation of Surface Water Resource Availability under the Impact of Climate Change in the Dhidhessa Sub-Basin , Ethiopia. *Atmosphere*, *13*, 1296. https://doi.org/10.3390/ atmos13081296 Academic

Meshesha, T. W., Tripathi, S. K., & Khare, D. (2016). Analyses of land use and land cover change dynamics using GIS and remote sensing during 1984 and 2015 in the Beressa Watershed Northern Central Highland of Ethiopia. *Modeling Earth Systems and*

Environment, *2*(168), 1–12. https://doi.org/10.1007/s40808-016-0233-4

Messele, T. A., & Moti, D. T. (2019). Modeling change of land use on hydrological response of river by remedial measures using arc SWAT: Case of weib catchment, Ethiopia. *International Journal of Innovative Technology and Exploring Engineering*, *8*(11), 2381–2390. https://doi.org/10.35940/ijitee.J9531.0981119

Miheretu, B. A. (2020). Temporal variability and trend analysis of temperature and rainfall in the Northern highlands of Ethiopia. *Physical Geography*, *00*(00), 1–18. https://doi.org/10.1080/02723646.2020.1806674

Minta, M., Kibret, K., Thorne, P., Nigussie, T., & Nigatu, L. (2018). Land use and land cover dynamics in Dendi-Jeldu hilly-mountainous areas in the central Ethiopian highlands. *Geoderma*, *314*(June), 27–36. https://doi.org/10.1016/j.geoderma.2017.10.035

Mitiku, A. B., Meresa, G. A., Mulu, T., & Woldemichael, A. T. (2023). Examining the impacts of climate variabilities and land use change on hydrological responses of Awash River basin, Ethiopia. *HydroResearch*, *6*, 16–28. https://doi.org/10.1016/j.hydres.2022.12.002

Moges, D. M., & Bhat, H. G. (2021). Climate change and its implications for rainfed agriculture in Ethiopia. *Journal of Water and Climate Change*, *12*(4), 1229–1244. https://doi.org/10.2166/wcc.2020.058

Moriasi, D. N., Arnold, J. G., Liew, M. W. Van, Bingner, R. L., Harmel, R. D., & Veith, T. L. (2007). Model evaluation guidelines for systematic quantification of accuracy in watershed simulations. *Transactions of the American Society of Agricultural and Biological Engineers*, *50*(3), 885–900.

MoWE. (2007a). *Genale-Dawa River Basin Integrated Resources Development Master Plan Study, Main Report; Volume II, Genale (GD-3) Multipurpose Hydropower Project Feasibility Study; Lahmeyer International GmbH, Germany in association with Yeshi-Ber Consult: Addis Ababa, E*.

MoWE. (2007b). *Genale-Dawa River Basin Integrated Resources Development Master Plan Study, Main Report. Volume I, Lahmeyer International GmbH, Germany in association with Yeshi-Ber Consult: Addis Ababa, Ethiopia: Vol. I*.

MoWE. (2007c). *Genale-Dawa River Basin Integrated Resources Development Master Plan Study, Sector Report; Volume II, A. Hydrology and Climate; Lahmeyer International GmbH, Germany in association with Yeshi-Ber Consult: Addis Ababa, Ethiopia Addis Ababa, Ethiopia*.

MoWE. (2007d). *Genale-Dawa River Basin Integrated Resources Development Master Plan Study, Sector Report; Volume II, E. Land Cover and Land Use and; Lahmeyer International GmbH, Germany in association with Yeshi-Ber Consult: Addis Ababa, Ethiopia Addis Ababa, Ethiopia: Vol. I*.

MoWE. (2007e). *Genale-Dawa River Basin Integrated Resources Development Master Plan Study, Sector Report; Volume II, F. Soil Survey; Lahmeyer International GmbH, Germany in association with Yeshi-Ber Consult: Addis Ababa, Ethiopia*.

MoWE. (2007f). *Genale-Dawa River Basin Integrated Resources Development Master Plan*

Study, Sector Report; Volume II, H, Irrigation and drainage; Lahmeyer International GmbH, Germany in association with Yeshi-Ber Consult: Addis Ababa, Ethiopia.

MoWE. (2007g). *Genale-Dawa River Basin Integrated Resources Development Master Plan Study, Sector Report; Volume II, K . Crop Production: Lahmeyer International GmbH, Germany in association with Yeshi-Ber Consult: Addis Ababa, Ethiopia*.

MoWR. (2001). *the Federal Democratic Republic of Ethiopia Ministry of Water Resources: ETHIOPIAN WATER SECTOR POLICY*. 1–40.

Mucova, S. A. R., Filho, W. L., Azeiteiro, U. M., & Pereira, M. J. (2018). Assessment of land use and land cover changes from 1979 to 2017 and biodiversity & land management approach in Quirimbas National Park, Northern Mozambique, Africa. *Global Ecology and Conservation*, *16*. https://doi.org/10.1016/j.gecco.2018.e00447

Mulu, A., Fasnamol, T. M., & Dwarakish, G. S. (2018). *Estimation of Changes in Annual Peak Flows in Netravathi River Basin, Karnataka, India BT - Climate Change Impacts* (V. P. Singh, S. Yadav, & R. N. Yadava (Eds.); pp. 193–199). Springer Singapore.

Musie, M., Sen, S., & Srivastava, P. (2020). Application of CORDEX-AFRICA and NEX-GDDP datasets for hydrologic projections under climate change in Lake Ziway sub- basin , Ethiopia. *Journal of Hydrology: Regional Studies*, *31*, 100721. https://doi.org/10.1016/j.ejrh.2020.100721

Narsimlu, B., Gosain, A. K., & Chahar, B. R. (2015). SWAT Model Calibration and Uncertainty Analysis for Streamflow Prediction in the Kunwari River Basin , India , Using Sequential Uncertainty Fitting. *Environmental Process*, *2*(1), 79–95. https://doi.org/10.1007/s40710-015-0064-8

Näschen, K., Diekkrüger, B., Leemhuis, C., Seregina, L. S., & van der Linden, R. (2019). Impact of climate change on water resources in the Kilombero Catchment in Tanzania. *Water (Switzerland)*, *11*(4). https://doi.org/10.3390/w11040859

Nash, J., & Sutcliffe, J. (1970). River flow forecasting through conceptual models: part I—a discussion of principles. *Journal of Hydrology*, *10*, 282–290.

Nasiri, S., Ansari, H., & Ziaei, A. N. (2020). Simulation of water balance equation components using SWAT model in Samalqan Watershed (Iran). *Arabian Journal of Geosciences*, *13*(11). https://doi.org/10.1007/s12517-020-05366-y

Negasa Jaleta, T., Yesuf, M. B., & Hirko, D. B. (2019). Modeling Surface Water Resources for Effective Water Allocation Using Water Evaluation and Planning (WEAP) Model, A Case Study on Finchaa Sub basin, Ethiopia. *Appl. J. Envir. Eng. Sci*, *5*, 402–419.

Negese, A. (2021). Impacts of Land Use and Land Cover Change on Soil Erosion and Hydrological Responses in Ethiopia. *Applied and Environmental Soil Science*, *2021*, 15–17. https://doi.org/10.1155/2021/6669438 Review

Negewo, T. F., & Sarma, A. K. (2021). Estimation of Water Yield under Baseline and Future Climate Change Scenarios in Genale Watershed, Genale Dawa River Basin, Ethiopia, Using SWAT Model. *Journal of Hydrologic Engineering*, *26*(3), 05020051.

Neitsch, S. L., Arnold, J. G., Kiniry, J. R., & Willians, J. R. (2011). *Soil & Water Assessment Tool Theoretical Documentation Version 2009. Texas Water Resources Institute. Texas AgriLife Research and USDA Agricultural Research Service, Temple, Texas, USA*.

Ngongondo, C., Xu, C. Y., Gottschalk, L., & Alemaw, B. (2011). Evaluation of spatial and temporal characteristics of rainfall in Malawi: A case of data scarce region. *Theoretical and Applied Climatology*, *106*(1–2), 79–93. https://doi.org/10.1007/s00704-011-0413-0

Nicholls, E. M., Drewitt, G. B., Fraser, S., & Carey, S. K. (2019). The influence of vegetation cover on evapotranspiration atop waste rock piles , Elk Valley , British Columbia. *Hydrological Processes*, 1–13. https://doi.org/10.1002/hyp.13542

NMA. (2007). *Climate Change National Adaptation Programme of Action (NAPA) of Ethiopia. National Meteorological Agency (NMA), Addis Ababa, Ethiopia.*

NPC. (2016). Federal Democratic Republic of Ethiopia: Growth and Transformation Plan II (GTP II) 2015/16-2019/20), Volume I: Main Text. *World Bank Group*, *I*(GTP II), 236. https://ethiopia.un.org/en/15231-growth-and-transformation-plan-ii

Obeidat, M., Awawdeh, M., & Lababneh, A. (2019). Assessment of land use/land cover change and its environmental impacts using remote sensing and GIS techniques, Yarmouk River Basin, north Jordan. *Arabian Journal of Geosciences*, *12*(22). https://doi.org/10.1007/s12517-019-4905-z

Oliver, J. E. (1980). Monthly precipitation distribution: A comparative index. *Professional Geographer*, *32*(3), 300–309. https://doi.org/10.1111/j.0033-0124.1980.00300.x

Orkodjo, T. P., Kranjac-Berisavijevic, G., & Abagale, F. K. (2022). Impact of climate change on future availability of water for irrigation and hydropower generation in the Omo-Gibe Basin of Ethiopia. *Journal of Hydrology: Regional Studies*, *44*, 101254. https://doi.org/10.1016/j.ejrh.2022.101254

Ougougdal, H. A., Khebiza, M. Y., Messouli, M., & Lachir, A. (2020). Assessment of futurewater demand and supply under IPCC climate change and socio-economic scenarios, using a combination of models in Ourika watershed, High Atlas, Morocco. *Water (Switzerland)*, *12*(6). https://doi.org/10.3390/w12061751

Papa, F., Crétaux, J.-F., Grippa, M., Robert, E., Trigg, M., Tshimanga, R. M., Kitambo, B., Paris, A., Carr, A., Fleischmann, A. S., de Fleury, M., Gbetkom, P. G., Calmettes, B., & Calmant, S. (2023). Water Resources in Africa under Global Change: Monitoring Surface Waters from Space. *Surveys in Geophysics*, *44*(1), 43–93. https://doi.org/10.1007/s10712-022-09700-9

Parkinson, C. L., Vinnikov, K. Y., & Cavalieri, D. J. (2006). Evaluation of the simulation of the annual cycle of Arctic and Antarctic sea ice coverages by 11 major global climate models. *Journal of Geophysical Research: Oceans*, *111*(7). https://doi.org/10.1029/2005JC003408

Pastor, A. V., Ludwig, F., Biemans, H., Hoff, H., & Kabat, P. (2014). Accounting for environmental flow requirements in global water assessments. *Hydrology and Earth System Sciences*, *18*(12), 5041–5059. https://doi.org/10.5194/hess-18-5041-2014

Pechlivanidis, I. G., Jackson, B. M., Mcintyre, N. R., & Wheater, H. S. (2011). Catchment scale

hydrological modelling: A review of model types, calibration approaches and uncertainty analysis methods in the context of recent developments in technology and applications. *Global Nest Journal*, *13*(3), 193–214. https://doi.org/10.30955/gnj.000778

Pedro-Monzonís, M., Solera, A., Ferrer, J., Estrela, T., & Paredes-Arquiola, J. (2015). A review of water scarcity and drought indexes in water resources planning and management. *Journal of Hydrology*, *527*, 482–493. https://doi.org/https://doi.org/10.1016/j.jhydrol.2015.05.003

Pettitt. (1979). A Non-parametric to the Approach Problem. *Applied Statistics*, *28*(2), 126–135. https://doi.org/doi: 10.2307/2346729

Qin, J., Ding, Y. J., Zhao, Q. D., Wang, S. P., & Chang, Y. P. (2020). Assessments on surface water resources and their vulnerability and adaptability in China. *Advances in Climate Change Research*, *11*(4), 381–391. https://doi.org/10.1016/j.accre.2020.11.002

Rathjens, H., Bieger, K., Srinivasan, R., & Arnold, J. G. (2016). *CMhyd User Manual: Documentation for preparing simulated climate change data for hydrologic impact studies*. p.16p. https://swat.tamu.edu/media/115265/bias_cor_man.pdf

Reichle, D. E. (2023). *Chapter 13 - Climate and climate models* (D. E. B. T.-T. G. C. C. and C. C. (Second E. Reichle (Ed.); pp. 389–452). Elsevier. https://doi.org/https://doi.org/10.1016/B978-0-443-18775-9.00010-3

Rheinheimer, D. E. (2011). Modeling Multi-Reservoir Hydropower Systems in the Sierra Nevada with Environmental Requirements and Climate Warming. *University of California, Ph.D. Diss*.

Roba, N. T., Kassa, A. K., Geleta, D. Y., & Harka, A. E. (2021). Streamflow and sediment yield estimation, and area prioritization for better conservation planning in the Dawe River watershed of the Wabi Shebelle River Basin, Ethiopia. *Heliyon*, *7*(12), e08509. https://doi.org/10.1016/j.heliyon.2021.e08509

Samal, D. R., & Gedam, S. (2021). Assessing the impacts of land use and land cover change on water resources in the Upper Bhima river basin, India. *Environmental Challenges*, *5*, 100251. https://doi.org/10.1016/j.envc.2021.100251

Sattari, M.-T., Joudi, A. R., & Kusiak, A. (2017). Assessment of different methods for estimation of missing data in precipitation studies. *Hydrology Research*, *48*(4), 1032–1044. https://doi.org/10.2166/nh.2016.364

Segele, Z. T., & Lamb, P. J. (2005). Characterization and variability of Kiremt rainy season over Ethiopia. *Meteorology and Atmospheric Physics*, *89*((1-4)), 153–180. https://doi.org/10.1007/s00703-005-0127-x

SEI. (2015). *WEAP water evaluation and planning system user guide. Stockholm Environ Institute, Somerville.*

Seleshi, Y., & Zanke, U. (2004). Recent changes in rainfall and rainy days in Ethiopia. *International Journal of Climatology*, *24*(8), 973–983. https://doi.org/10.1002/joc.1052

Sen, P. K. (1968). Estimates of the Regression Coefficient Based on Kendall's Tau. *Journal of the American Statistical Association*, *63*(324), 1379–1389.

https://doi.org/10.1080/01621459.1968.104809

Serdeczny, O., Adams, S., Baarsch, F., Coumou, D., Robinson, A., Hare, W., Schaeffer, M., Perrette, M., & Reinhardt, J. (2017). Climate change impacts in Sub-Saharan Africa : from physical changes to their social repercussions. *Regional Environmental Change*, *17*, 1585–1600. https://doi.org/10.1007/s10113-015-0910-2

Serur, A. B. (2020). Modeling blue and green water resources availability at the basin and sub-basin level under changing climate in the Weyb River basin in Ethiopia. *Scientific African*, *7*, e00299. https://doi.org/10.1016/j.sciaf.2020.e00299

Shaeri Karimi, S., Yasi, M., & Eslamian, S. (2012). Use of hydrological methods for assessment of environmental flow in a river reach. *International Journal of Environmental Science and Technology*, *9*(3), 549–558. https://doi.org/10.1007/s13762-012-0062-6

Shawul, A. A., Alamirew, T., & Dinka, M. O. (2013). Calibration and validation of SWAT model and estimation of water balance components of Shaya mountainous watershed, Southeastern Ethiopia. *Hydrology and Earth System Sciences Discussions*, *10*(11), 13955–13978. https://doi.org/10.5194/hessd-10-13955-2013

Shawul, A. A., Alamirew, T., Melesse, A. M., & Chakma, S. (2016). Climate change impact on the hydrology of Weyb River watershed, Bale mountainous area, Ethiopia. *Landscape Dynamics, Soils and Hydrological Processes in Varied Climates*, 587–613.

Shawul, A., & Chakma, S. (2019). Spatiotemporal detection of land use/land cover change in the large basin using integrated approaches of remote sensing and GIS in the Upper Awash basin, Ethiopia. *Environmental Earth Sciences*, *78*(5), 0. https://doi.org/10.1007/s12665-019-8154-y

Shiferaw, H., Bewket, W., Alamirew, T., Zeleke, G., Teketay, D., Bekele, K., Schaffner, U., & Eckert, S. (2019). Implications of land use/land cover dynamics and Prosopis invasion on ecosystem service values in Afar Region, Ethiopia. *Science of the Total Environment*, *675*, 354–366. https://doi.org/10.1016/j.scitotenv.2019.04.220

Shigute, M., Alamirew, T., Abebe, A., Ndehedehe, C. E., & Kassahun, H. T. (2022). Understanding Hydrological Processes under Land Use Land Cover Change in the Upper Genale River Basin , Ethiopia. *Water*, *14*(23), 3881. https://doi.org/10.3390/w14233881

Shigute, M., Alamirew, T., Abebe, A., Ndehedehe, C. E., & Kassahun, H. T. (2023). Analysis of rainfall and temperature variability for agricultural water management in the upper Genale river basin , Ethiopia. *Scientific African*, *20*, e01635. https://doi.org/10.1016/j.sciaf.2023.e01635

Shiva Shankar, Y., Kumar, A., & Mohan, D. (2021). *Climate Change and Water Resources: Emerging Challenges, Vulnerability and Adaptation in Indian Scenario BT - Climate Change Impacts on Water Resources: Hydraulics, Water Resources and Coastal Engineering* (R. Jha, V. P. Singh, V. Singh, L. B. Roy, & R. Thendiyath (Eds.); pp. 365–376). Springer International Publishing. https://doi.org/10.1007/978-3-030-64202-0_32

Shrestha, M., Acharya, S. C., & Shrestha, P. K. (2017). Bias correction of climate models for hydrological modelling – are simple methods still useful? *Meteorological Applications*,

24(3), 531–539. https://doi.org/10.1002/met.1655

Shrestha, S. (2014). *Climate Change Impacts and Adaptation in Water Resources and Water Use Sectors: Case Studies from Southeast Asia.* Springer International Publishing. https://doi.org/10.1007/978-3-319-09746-6

Shukla, S., & Gedam, S. (2018). Assessing the impacts of urbanization on hydrological processes in a semi-arid river basin of Maharashtra , India. *Modeling Earth Systems and Environment*, *4*(2), 699–728. https://doi.org/10.1007/s40808-018-0446-9

Shumet, A. G., & Mengistu, K. T. (2016). Assessing the Impact of Existing and Future Water Demand on Economic and Environmental Aspects (Case Study from Rift Valley Lake Basin: Meki-Ziway Sub Basin), Ethiopia. *International Journal of Waste Resources*, *6*(2). https://doi.org/10.4172/2252-5211.1000223

Sieber, J., & Purkey, D. (2015). Water evaluation and planning system user guide. *Stockholm Environment Institute, US Center*, *11*.

Sileshi, Z., Tegegne, A., & Tsadik, G. T. (2003). Water resources for livestock in Ethiopia: Implications for research and development. *Integrated Water and Land Management Research and Capacity Building Priorities for Ethiopia*, *66*.

Singh, V. P. (2018). Hydrologic modeling: progress and future directions. *Geoscience Letters*, *5*(1). https://doi.org/10.1186/s40562-018-0113-z

Sisay, G., Gitima, G., Mersha, M., & Alemu, W. G. (2021). Assessment of land use land cover dynamics and its drivers in Bechet Watershed Upper Blue Nile Basin, Ethiopia. *Remote Sensing Applications: Society and Environment*, *24*, 100648. https://doi.org/https://doi.org/10.1016/j.rsase.2021.100648

Sridhar, V., & Nayak, A. (2010). Implications of climate-driven variability and trends for the hydrologic assessment of the Reynolds Creek Experimental Watershed, Idaho. *Journal of Hydrology*, *385*(1–4), 183–202.

Srivastava, A., Kumari, N., & Maza, M. (2020). Hydrological Response to Agricultural Land Use Heterogeneity Using Variable Infiltration Capacity Model. *Water Resources Management*, *34*(12), 3779–3794. https://doi.org/10.1007/s11269-020-02630-4

Stern, R., Rijks, D., Dale, I., & Knock, J. (2006). *Instat Climatic Guide*. Reading, UK: Statistical Services Centre, Reading University.

Stuch, B., Alcamo, J., & Schaldach, R. (2020). Projected climate change impacts on mean and year-to-year variability of yield of key smallholder crops in Sub-Saharan Africa. *Climate and Development*, *13*(3), 1–15. https://doi.org/10.1080/17565529.2020.1760771

Sulamo, M. A., Kassa, A. K., & Roba, N. T. (2021). Evaluation of the impacts of land use / cover changes on water balance of Bilate watershed , Rift valley basin , Ethiopia. *Water Practice and Technology*, *16*(4), 1108–1127. https://doi.org/10.2166/wpt.2021.063

Sun, Y., Zhang, W., Peng, H., Zhou, F., Jiang, A., Chen, X., & Wang, H. (2023). The Impacts of Climate Change on the Hydrological Process and Water Quality in the Three Gorges Reservoir Area, China. *Water (Switzerland)*, *15*(8), 1–20.

https://doi.org/10.3390/w15081542

Sunyer, M. A., Madsen, H., & Ang, P. H. (2012). A comparison of different regional climate models and statistical downscaling methods for extreme rainfall estimation under climate change. *Atmospheric Research*, *103*, 119–128. https://doi.org/https://doi.org/10.1016/j.atmosres.2011.06.011

Suryabhagavan, K. V. (2017). GIS-based climate variability and drought characterization in Ethiopia over three decades. *Weather and Climate Extremes*, *15*, 11–23. https://doi.org/10.1016/j.wace.2016.11.005

Syukuro, M. (2019). Role of greenhouse gas in climate change**. *Tellus A: Dynamic Meteorology and Oceanography*, *71*(1), 1–13. https://doi.org/10.1080/16000870.2019.1620078

Takele, G. S., Gebre, G. S., Gebremariam, A. G., & Engida, A. N. (2022). Hydrological modeling in the Upper Blue Nile basin using soil and water analysis tool (SWAT). *Modeling Earth Systems and Environment*, *8*(1), 277–292. https://doi.org/10.1007/s40808-021-01085-9

Takele, G. S., Gebrie, G. S., Gebremariam, A. G., & Engida, A. N. (2022). Future climate change and impacts on water resources in the Upper Blue Nile basin. *Journal of Water and Climate Change*, *13*(2), 908–925. https://doi.org/10.2166/wcc.2021.235

Tassew, B. G., Belete, M. A., & Miegel, K. (2019). Application of HEC-HMS model for flow simulation in the Lake Tana basin: The case of Gilgel Abay catchment, upper Blue Nile basin, Ethiopia. *Hydrology*, *6*(1), 21. https://doi.org/10.3390/hydrology6010021

Taye, M. T., Dyer, E., Hirpa, F. A., & Charles, K. (2018). Climate change impact on water resources in the Awash basin, Ethiopia. *Water (Switzerland)*, *10*(11), 1–16. https://doi.org/10.3390/w10111560

Taylor, S. D., He, Y., & Hiscock, K. M. (2016). Modelling the impacts of agricultural management practices on river water quality in Eastern England. *Journal of Environmental Mamagement*, *180*, 147–168. https://doi.org/10.1016/j.jenvman.2016.05.002

Teferi, E., Tibebe, D., Bewket, W., Zeleke, G., Alamirew, T., & Centre, L. R. (2020). *Green Water Management for Water and Food Security in the Abbay Basin , Ethiopia : A Review*.

Teklay, A., Dile, Y. T., Asfaw, D. H., & Bayabil, H. K. (2020). Impacts of Climate and Land Use Change on Hydrological Response in Gumara watershed, Ethiopia. *Ecohydrology & Hydrobiology*, *21*(2), 315–322. https://doi.org/10.1016/j.ecohyd.2020.12.001

Temam, D., Uddameri, V., Mohammadi, G., & Hernandez, E. A. (2019). Long-Term Drought Trends in Ethiopia with Implications for Dryland Agriculture. *Water*, *21*, 2571. https://doi.org/10.3390/w11122571

Temesgen, H., Wu, W., Legesse, A., & Yirsaw, E. (2021). Remote Sensing Applications : Society and Environment Modeling and prediction of effects of land use change in an agroforestry dominated southeastern Rift-Valley escarpment of Ethiopia. *Remote Sensing Applications: Society and Environment*, *21*(October 2020), 100469. https://doi.org/10.1016/j.rsase.2021.100469

Tena, T. M., Mwaanga, P., & Nguvulu, A. (2019). Hydrological modelling and water resources assessment of Chongwe River Catchment using WEAP model. *Water (Switzerland)*, *11*(4). https://doi.org/10.3390/w11040839

Tennant, D. L. (1976). Instream Flow Regimens for Fish , Wildlife , Recreation and Related Environmental Resources. *Fisheries*, *1*(4), 6–10. https://doi.org/10.1577/1548-8446(1976)001<0006:IFRFFW>2.0.CO;2

Tesfaw, B. A., Dzwairo, B., & Sahlu, D. (2023). Assessments of the impacts of land use/land cover change on water resources: Tana Sub-Basin, Ethiopia. *Journal of Water and Climate Change*, *14*(2), 421–441. https://doi.org/10.2166/wcc.2023.303

Tesfaye, K., & Walker, S. (2004). Matching of crop and environment for optimal water use : The case of Ethiopia. *Physics and Chemistry of the Earth*, *29*(15–18), 1061–1067. https://doi.org/10.1016/j.pce.2004.09.024

Teshome, A., & Zhang, J. (2019). Increase of Extreme Drought over Ethiopia under Climate Warming. *Advances in Meteorology*, *2019*, 1–18. https://doi.org/10.1155/2019/5235429

Tessema, N., Kebede, A., & Yadeta, D. (2021). Modelling the effects of climate change on streamflow using climate and hydrological models: the case of the Kesem sub-basin of the Awash River basin, Ethiopia. *International Journal of River Basin Management*, *19*(4), 469–480. https://doi.org/10.1080/15715124.2020.1755301

Teutschbein, C., & Seibert, J. (2012). *Bias correction of regional climate model simulations for hydrological climate-change impact studies : Review and evaluation of different methods*. *457*, 12–29. https://doi.org/10.1016/j.jhydrol.2012.05.052

Tewabe, D., & Fentahun, T. (2020). Assessing land use and land cover change detection using remote sensing in the Lake Tana Basin, Northwest Ethiopia. *Cogent Environmental Science*, *6*(1), 1778998.

Theil, H. (1950). *A rank-invariant method of linear and polynomial analysis, part 3.* Nederlandse Akademie van Wettenschappen. Proceedings 53, 1397–1412.

Touch, T., Oeurng, C., Jiang, Y., & Mokhtar, A. (2020). Integrated modeling of water supply and demand under climate change impacts and management options in tributary Basin of Tonle Sap Lake, Cambodia. *Water (Switzerland)*, *12*(9). https://doi.org/10.3390/w12092462

Touseef, M., Chen, L., Masud, T., Khan, A., Yang, K., Shahzad, A., Ijaz, M. W., & Wang, Y. (2020). Assessment of the future climate change projections on Streamflow Hydrology and water availability over upper Xijiang River Basin, China. *Applied Sciences (Switzerland)*, *10*(11). https://doi.org/10.3390/app10113671

Touseef, M., Chen, L., & Yang, W. (2021). Assessment of Surface Water Availability under Climate Change Using Coupled SWAT-WEAP in Hongshui River Basin , China. *International Journal of Geo-Information*, *10*, 298. https://doi.org/10.3390/ijgi10050298

Tripathi, A., & Mishra, A. K. (2016). Knowledge and passive adaptation to climate change: An example from Indian farmers. *Climate Risk Management*, *16*, 195–207. https://doi.org/10.1016/j.crm.2016.11.002

Tripathi, A., Tripathi, D. K., Chauhan, D. K., Kumar, N., & Singh, G. S. (2016). Paradigms of climate change impacts on some major food sources of the world: A review on current knowledge and future prospects. *Agriculture, Ecosystems & Environment*, *216*, 356–373. https://doi.org/https://doi.org/10.1016/j.agee.2015.09.034

Trzaska, S., & Schnarr, E. (2014). A review of downscaling methods for climate change projections. *United States Agency for International Development by Tetra Tech ARD*, *September*, 1–42. https://pdf.usaid.gov/pdf_docs/pa00k67t.pdf

Tufa, F. G., & Sime, C. H. (2020). Stream flow modeling using SWAT model and the model performance evaluation in Toba sub-watershed, Ethiopia. *Modeling Earth Systems and Environment*, *7*(4), 2653-2665. https://doi.org/10.1007/s40808-020-01039-7

UNEP. (2011). *Food Security in the Horn of Africa: The Implications of a Drier, Hotter and More Crowded Future*. https://na.unep.net/geas/getUNEPPageWithArticleIDScript.php?article_id=72.

Urama, K. C., & Ozor, N. (2010). Impacts of climate change on water resources in Africa: the role of adaptation. *African Technology Policy Studies Network*, *29*(1), 1–29.

van Buuren, S., & Groothuis-Oudshoorn, K. (2011). mice: Multivariate imputation by chained equations in R. *Journal of Statistical Software*, *45*(3), 1–67. https://doi.org/10.18637/jss.v045.i03

van Vuuren, D. P., Edmonds, J., Kainuma, M., Riahi, K., Thomson, A., Hibbard, K., Hurtt, G. C., Kram, T., Krey, V., Lamarque, J. F., Masui, T., Meinshausen, M., Nakicenovic, N., Smith, S. J., & Rose, S. K. (2011). The representative concentration pathways: An overview. *Climatic Change*, *109*(1), 5–31. https://doi.org/10.1007/s10584-011-0148-z

Verma, R. K., Murthy, S., Verma, S., & Mishra, S. K. (2017). Design flow duration curves for environmental flows estimation in Damodar River Basin, India. *Applied Water Science*, *7*(3), 1283–1293. https://doi.org/10.1007/s13201-016-0486-0

Viera, A. J., & Garrett, J. M. (2005). Understanding Interobserver Agreement : The Kappa Statistic. *Family Medicine*, *37*(5), 360–363.

Vijayan, D. S., Tadesse, H. T., Yokamo, Y., Divahar, R., Bezabih Bashe, T., & Jebasingh Daniel, J. (2022). A Brief Data on Water Demand Assessment for Sustainable Potable Water Supply in Yergalem Tula Kebele, Ethiopia. *Journal of Environmental and Public Health*, *2022*. https://doi.org/10.1155/2022/1606590

Viste, E., Korecha, D., & Sorteberg, A. (2013). Recent drought and precipitation tendencies in Ethiopia. *Theoretical and Applied Climatology*, *112*(3–4), 535–551. https://doi.org/10.1007/s00704-012-0746-3

von Neumann, J. (1941). Distribution of the ratio of the mean square succesive difference to the variance. *The Annals of Mathematical Statistics*, *12*(4), 367–395. https://doi.org/doi:10.1214/aoms/1177731677

Wagesho, N., Goel, N. K., & Jain, M. K. (2013). Temporal and spatial variability of annual and seasonal rainfall over Ethiopia. *Hydrological Sciences Journal*, *58*(2), 354–373. https://doi.org/10.1080/02626667.2012.754543

Wagesho, N., & Yohannes, E. (2016). Analysis of Rainfall Variability and Farmers ' Perception towards it in Agrarian Community of Southern Ethiopia. *Journal of Environment and Earth Science*, *6*(4).

Wang, L., Fang, L., & Hipel, K. W. (2008). Basin-wide cooperative water resources allocation. *European Journal of Operational Research*, *190*(3), 798–817. https://doi.org/https://doi.org/10.1016/j.ejor.2007.06.045

Wang, R., Kalin, L., Kuang, W., & Tian, H. (2013). Individual and combined effects of land use/cover and climate change on Wolf Bay watershed streamflow in southern Alabama. *Hydrological Processes*, *28*(22), 5530–5546. https://doi.org/10.1002/hyp

Welborn, L. (2018). Africa and climate change Projecting vulnerability and adaptive capacity. *Institute for Security Studies*, *November*, 1–24. https://issafrica.s3.amazonaws.com/site/uploads/ar14.pdf

Weldegerima, T. M., Zeleke, T. T., Birhanu, B. S., Zaitchik, B. F., & Fetene, Z. A. (2018). Analysis of Rainfall Trends and Its Relationship with SST Signals in the Lake Tana Basin, Ethiopia. *Advances in Meteorology*, *2018*. https://doi.org/10.1155/2018/5869010

Weragala, D. K. N. (2010). *Water allocation challenges in rural river basins: A case study from the Walawe River Basin, Sri Lanka*. Utah State University. https://doi.org/https://digitalcommons.usu.edu/etd/589

Wheater, H. S. (2008). Modelling hydrological processes in arid and semi-arid areas: an introduction to the workshop. *Hydrol. Model. Arid. Semi-Arid Areas*, 1–20.

Wijngaard, J. B., Klein Tank, A. M. G., & Können, G. P. (2003). Homogeneity of 20th century European daily temperature and precipitation series. *International Journal of Climatology*, *23*(6), 679–692. https://doi.org/10.1002/joc.906

Williams, J. R. (1990). The erosion-productivity impact calculator (EPIC) model: a case history. *Philosophical Transactions of the Royal Society of London. Series B: Biological Sciences*, *329*(1255), 421–428.

Wodaje, G. G., Asfaw, Z. E., & Denboba, M. A. (2021). Impacts and uncertainties of climate change on stream flow of the Bilate River (Ethiopia), using a CMIP5 general circulation models ensemble. *International Journal of Water Resources and Environmental Engineering*, *13*(1), 64–75. https://doi.org/10.5897/IJWREE2020.0973

Wolde, G. G. (2017). *Local adaptation practice in response to climate change in the Bilate River Basin, Southern Ethiopia[Doctoral thesis, University of South Africa (UNISA)]*. (Issue March). https://1library.net/us/download/888049716837253125

Woldegebriel, T., Garg, V., Gupta, P. K., Srivastav, S. K., & Ranjan, R. (2022). Ethiopia's water resources: an assessment based on geospatial data-driven distributed hydrological modeling approach. *Journal of the Indian Society of Remote Sensing*, *50*(6), 1031–1049.

Woldesenbet, T. A., Elagib, N. A., Ribbe, L., & Heinrich, J. (2018). Catchment response to climate and land use changes in the Upper Blue Nile Sub-basins, Ethiopia. *Science of the Total Environment*, *644*, 193–206. https://doi.org/10.1016/j.scitotenv.2018.06.198

Woldeyohannes, A., Cotter, M., Kelboro, G., & Dessalegn, W. (2018). Land Use and Land Cover Changes and Their Effects on the Landscape of Abaya-Chamo Basin, Southern Ethiopia. *Land*, *7*(2). https://doi.org/10.3390/land7010002

Worku, G., Teferi, E., Bantider, A., & Dile, Y. T. (2020). Statistical bias correction of regional climate model simulations for climate change projection in the Jemma sub-basin, upper Blue Nile Basin of Ethiopia. *Theoretical and Applied Climatology*, *139*(3), 1569–1588. https://doi.org/10.1007/s00704-019-03053-x

Worku, G., Teferi, E., Bantider, A., & Dile, Y. T. (2021). Modelling hydrological processes under climate change scenarios in the Jemma Sub-basin of upper Blue Nile Basin , Ethiopia. *Climate Risk Management*, *31*, 100272. https://doi.org/10.1016/j.crm.2021.100272

Worqlul, A. W., Dile, Y. T., Ayana, E. K., & Jeong, J. (2018). Impact of Climate Change on Streamflow Hydrology in Headwater Catchments of the Upper Blue Nile. *Water*, *10*, 120. https://doi.org/10.3390/w10020120

Xu, C.-Y., & Singh, V. P. (2004). Review on Regional Water Resources Assessment Models under Stationary and Changing Climate. *Water Resources Management*, *18*(6), 591–612. https://doi.org/10.1007/s11269-004-9130-0

Xu, C. (2002). Hydrologic models. *Textbooks of Uppsala University. Department of Earth Sciences Hydrology*.

Xu, M., Li, C., Wang, X., Cai, Y., & Yue, W. (2018). Optimal water utilization and allocation in industrial sectors based on water footprint accounting in Dalian City, China. *Journal of Cleaner Production*, *176*, 1283–1291. https://doi.org/https://doi.org/10.1016/j.jclepro.2017.11.203

Yan, D., Ludwig, F., Huang, H. Q., & Werners, S. E. (2017). Many-objective robust decision making for water allocation under climate change. *Science of The Total Environment*, *607–608*, 294–303. https://doi.org/https://doi.org/10.1016/j.scitotenv.2017.06.265

Yan, Z., Zhou, Z., Sang, X., & Wang, H. (2018). Water replenishment for ecological flow with an improved water resources allocation model. *Science of the Total Environment*, *643*, 1152–1165. https://doi.org/10.1016/j.scitotenv.2018.06.085

Yates, D., Sieber, J., Purkey, D., & Huber-Lee, A. (2005). WEAP21 - A demand-, priority-, and preference-driven water planning model. Part 1: Model characteristics. *Water International*, *30*(4), 487–500. https://doi.org/10.1080/02508060508691893

Yeboah, K. A., Akpoti, K., Kabo-bah, A. T., Ofosu, E. A., Siabi, E. K., Mortey, E. M., & Okyereh, S. A. (2022). Assessing climate change projections in the Volta Basin using the CORDEX-Africa climate simulations and statistical bias-correction. *Environmental Challenges*, *6*, 100439. https://doi.org/10.1016/j.envc.2021.100439

Yesuph, A. Y., & Dagnew, A. B. (2019). Land use/cover spatiotemporal dynamics, driving forces and implications at the Beshillo catchment of the Blue Nile Basin, North Eastern Highlands of Ethiopia. *Environmental Systems Research*, *8*(1). https://doi.org/10.1186/s40068-019-0148-y

Yirga, S. A., Mamo, G., & Mengesha, M. (2017). Rainfall and Temperature Trend Analysis at

Indibir Station, Gurage Zone, Ethiopia. *Journal of Environment and Earth Science*, *7*(9), 1–11.

Zantet oybitet, M., Sambeto Bibi, T., & Abdulkerim Adem, E. (2023). Evaluation of best management practices to reduce sediment yield in the upper Gilo watershed, Baro akobo basin, Ethiopia using SWAT. *Heliyon*, *9*(10), e20326. https://doi.org/https://doi.org/10.1016/j.heliyon.2023.e20326

Zelelew, D. G., & Melesse, A. M. (2018). Applicability of a spatially semi-distributed hydrological model for watershed scale runoff estimation in Northwest Ethiopia. *Water*, *10*(7), 10–12. https://doi.org/10.3390/w10070923

Zewdie, A. (2014). Impacts of Climate Change on Food Security: A Literature Review in Sub Saharan Africa. *Journal of Earth Science & Climatic Change*, *05*(08), 8–11. https://doi.org/10.4172/2157-7617.1000225

Zewdie, W., & Csaplovies, E. (2015). Remote Sensing based multi-temporal land cover classification and change detection in northwestern Ethiopia. *European Journal of Remote Sensing*, *48*(1), 121–139. https://doi.org/10.5721/EuJRS20154808

Zhang, B., Shrestha, N. K., Daggupati, P., Rudra, R., & Shukla, R. (2018). Quantifying the Impacts of Climate Change on Streamflow Dynamics of Two Major Rivers of the Northern Lake Erie Basin in Canada. *Sustainability*, *10*(8), 2897. https://doi.org/10.3390/su10082897

Zhang, X., Srinivasan, R., & Hao, F. (2007). Predicting hydrologic response to climate change in the Luohe River basin using the SWAT model. *American Society of Agriculture and Biological Engineers*, *50*(3), 901–910. https://doi.org/10.13031/2013.23154

APPENDICES

Appendices: Tables

Appendix Table 1. Simulated hydrological variables of the study sub- basin for 1986 LULC

SUB	PRECIPmm	SURQmm	ETmm	WYLDmm	LAT_Qmm
1	879.49	60.63	635.91	198.02	21.68
2	828.44	51.98	598.61	200.91	12.18
3	1307.91	294.52	587.41	689.98	40.27
4	880.22	54.44	730.21	100.60	19.74
5	1598.98	427.51	581.06	985.77	63.31
6	880.22	33.32	699.92	139.65	24.28
7	1338.58	154.05	823.14	452.40	69.47
8	1330.27	110.92	816.38	453.93	64.38
9	1259.26	225.73	617.84	571.57	85.90
10	1338.58	224.34	783.11	489.53	61.06
11	1259.26	250.82	649.52	536.75	51.52
12	1259.26	196.64	625.73	564.01	47.65
13	1338.58	219.52	841.70	430.29	57.02
14	1032.19	189.54	736.17	244.48	44.58
15	1337.81	94.52	968.37	298.23	50.51
16	1032.19	162.41	765.53	221.47	50.62
17	690.91	61.49	614.57	66.80	5.22
18	690.91	35.95	630.46	48.44	12.39
19	690.91	38.56	626.68	52.85	14.19
20	600.35	7.75	586.79	11.35	3.57
21	690.91	42.82	623.36	55.72	12.80
Avg Annual	1060.25	139.88	692.50	324.42	38.68

PRECIPmm, Precipitation in millimeter; ETmm, Evapotranspiration in millimeter; SURQmm, Surface runoff in millimeter; LAT_Qmm, Lateral flow in millimeter; WYLDmm, Total water yield in millimeter.

Appendix Table 2. Simulated hydrological variables of the study sub- basin for 2001 LULC

SUB	PRECIPmm	SURQmm	ETmm	WYLDmm	LAT_Qmm
1	879.49	70.22	617.58	215.15	20.43
2	828.44	70.37	563.61	236.59	11.03
3	1307.91	327.05	588.04	688.51	28.13
4	880.22	77.33	699.38	131.94	21.11
5	1598.98	443.09	579.66	986.89	62.31
6	880.22	45.38	691.81	148.21	21.03
7	1338.58	195.52	800.04	475.48	70.54
8	1330.28	160.43	804.50	465.91	59.30
9	1259.26	258.48	605.59	583.31	88.12
10	1338.58	259.87	744.06	528.26	63.17
11	1259.26	258.90	645.09	540.62	52.15
12	1259.26	208.31	614.16	575.59	48.44
13	1338.58	243.12	816.69	454.97	51.35
14	1032.19	185.86	734.47	245.68	45.46
15	1337.81	159.50	895.00	370.45	51.96
16	1032.19	188.09	739.57	246.39	52.15
17	690.91	61.58	610.59	66.91	5.21
18	690.91	38.00	629.84	50.68	12.59
19	690.91	38.17	625.26	52.22	13.93
20	600.35	7.53	586.71	11.30	3.74
21	690.91	42.82	620.37	57.19	14.25
Avg Annual	1060.25	159.03	676.76	339.63	37.92

PRECIPmm, Precipitation in millimeter; ETmm, Evapotranspiration in millimeter; SURQmm, Surface runoff in millimeter; LAT_Qmm, Lateral flow in millimeter; WYLDmm, Total water yield in millimeter.

Appendix Table 3. Simulated hydrological variables of the study sub- basin for 2016 LULC

SUB	PRECIPmm	SURQmm	ETmm	WYLDmm	LAT_Qmm
1	879.49	63.20	633.93	199.57	15.96
2	828.44	57.10	587.20	212.81	11.06
3	1307.91	327.02	590.36	685.72	31.84
4	880.22	83.57	687.07	142.31	19.07
5	1598.98	476.65	582.21	983.99	55.50
6	880.22	43.96	685.46	155.71	19.50
7	1338.58	209.12	790.78	484.67	69.59
8	1330.28	173.70	787.01	483.34	56.12
9	1259.26	281.48	600.65	588.69	79.07
10	1338.58	291.52	702.71	569.32	61.15
11	1259.26	296.83	636.86	549.33	46.85
12	1259.26	238.94	605.06	584.61	45.36
13	1338.58	274.34	787.32	484.02	51.01
14	1032.19	199.85	730.24	253.51	44.04
15	1337.81	182.64	856.14	409.33	52.95
16	1032.19	197.26	738.98	250.14	48.08
17	690.91	64.65	612.39	70.28	5.55
18	690.91	41.18	628.88	54.89	13.63
19	690.91	40.77	626.34	56.32	15.47
20	600.35	9.72	585.43	13.93	4.19
21	690.91	49.56	622.07	61.23	11.60
Avg Annual	1060.25	171.57	670.34	347.32	36.08

PRECIPmm, Precipitation in millimeter; ETmm, Evapotranspiration in millimeter; SURQmm, Surface runoff in millimeter; LAT_Qmm, Lateral flow in millimeter; WYLDmm, Total water yield in millimeter.

Appendix Table 4. Simulated hydrological variables of the climate model CNRM-CM under RCP4.5

2030s CNRM-CM5-RCP45							2060s CNRM-CM5-RCP45					
YEAR	PRECIP mm	ET mm	SURQ mm	GW_Q mm	LAT_Q mm	WYLD mm	PRECIP mm	ET mm	SURQ mm	GW_Q mm	LAT_Q mm	WYLD mm
2021	1044.19	646.49	139.35	157.40	45.25	350.65	1187.25	706.21	200.97	179.38	46.70	437.74
2022	1284.12	635.21	278.44	260.81	59.80	613.38	1176.73	674.19	149.99	208.76	58.36	429.50
2023	1017.56	651.68	168.23	144.68	36.38	360.30	1289.76	670.97	293.39	324.75	61.96	701.20
2024	1294.74	729.69	167.99	201.44	58.78	441.18	814.42	578.52	81.55	49.25	23.91	158.94
2025	957.87	671.50	92.91	160.46	37.69	303.12	861.30	687.03	97.00	90.53	28.11	222.71
2026	1264.81	695.40	224.82	191.74	54.67	481.01	1045.07	694.94	100.00	142.74	42.34	293.04
2027	850.25	649.49	87.27	114.09	29.36	242.06	873.52	615.99	104.04	71.86	27.07	207.82
2028	1008.44	616.48	131.21	70.21	29.52	234.69	1196.66	758.48	159.87	163.97	48.27	381.74
2029	1105.89	701.54	181.34	219.05	47.77	460.88	1327.91	755.88	252.57	190.15	50.30	505.55
2030	828.14	646.52	80.81	41.36	20.54	147.74	1339.76	737.85	248.12	261.66	57.82	584.35
2031	734.23	646.83	52.79	53.98	20.25	131.02	1201.11	710.19	175.08	132.31	44.46	358.95
2032	1396.92	720.46	250.26	187.21	54.43	499.85	1557.67	739.28	469.30	282.23	63.38	831.65
2033	825.31	663.06	61.04	143.17	34.33	251.38	1174.12	709.50	220.16	154.93	44.83	430.38
2034	1100.46	698.71	141.17	125.43	41.70	316.21	1246.98	694.32	212.60	205.81	54.03	483.83
2035	1532.09	769.88	271.23	312.68	74.01	673.95	828.67	689.13	59.46	120.81	30.57	221.40
2036	794.22	663.16	67.34	72.85	24.27	174.13	1152.68	634.40	237.35	162.48	47.66	458.32
2037	1306.39	789.99	162.67	193.00	48.52	413.60	1317.04	745.19	208.21	219.81	56.53	496.24
2038	1163.04	729.44	161.19	96.36	38.97	303.03	1048.66	686.84	133.25	188.12	44.95	378.95
2039	1524.34	722.43	491.02	269.93	59.09	837.18	770.98	621.39	64.68	68.18	24.12	163.28
2040	915.99	672.10	89.86	94.57	28.82	220.68	1171.30	723.77	148.80	157.62	42.67	355.97
2041	1329.35	729.17	224.70	173.66	51.24	457.45	1380.77	687.88	343.78	242.65	57.15	660.49
2042	813.40	660.27	108.30	90.07	26.03	234.68	1353.24	754.97	220.60	204.55	55.57	492.61
2043	1083.74	669.77	252.47	78.62	28.47	364.19	1318.40	667.63	346.22	227.74	53.38	641.09
2044	755.57	574.18	124.84	82.10	22.67	235.51	708.32	594.66	41.47	58.69	20.55	127.54
2045	1027.32	601.05	201.20	142.84	35.98	387.19	1034.09	715.94	154.45	106.45	34.84	302.82
2046	1219.99	711.86	237.47	134.60	44.35	425.87	1958.05	753.34	459.04	462.12	98.58	1040.87
2047	1565.16	757.37	405.57	216.40	61.31	697.92	1653.73	782.31	377.12	350.86	75.82	826.18
2048	1429.33	769.98	253.50	304.09	65.97	638.60	1036.05	700.58	125.13	164.39	40.88	344.04
2049	641.06	648.73	21.89	15.98	13.69	58.60	874.47	643.27	98.23	95.77	29.77	231.18
2050	908.16	651.39	58.78	73.83	30.86	167.06	1035.68	632.32	156.37	130.27	37.70	330.62
Average	1090.74	683.13	172.99	147.42	40.82	370.77	1164.48	692.23	197.96	180.63	46.74	436.63

PRECIPmm, Precipitation in millimeter; ETmm, Evapotranspiration in millimeter; SURQmm, Surface runoff in millimeter; GW_Qmm, Ground waterflow in millimeter; LAT_Qmm, Lateral flow in millimeter; WYLDmm, Total water yield in millimeter.

Appendix Table 5. Simulated hydrological variables of the climate model CNRM-CM under RCP8.5

2030s CNRM-CM5-RCP85

YEAR	PRECIP mm	ET mm	SURQ mm	GW_Q mm	LAT_Q mm	WYLD mm
2021	1233.20	704.94	203.81	193.58	52.87	461.33
2022	1400.36	718.64	296.72	287.63	63.71	666.07
2023	1336.94	692.64	304.24	234.26	54.99	608.75
2024	1146.40	752.66	131.91	200.72	45.71	392.12
2025	876.19	594.50	111.99	119.32	33.83	273.37
2026	824.43	640.86	56.29	67.27	24.65	153.10
2027	1109.29	679.03	233.76	124.24	35.57	399.71
2028	756.92	627.91	44.45	71.52	21.73	143.85
2029	802.87	617.52	83.77	49.07	23.47	159.76
2030	912.82	697.64	66.63	110.57	29.60	213.47
2031	809.23	626.85	57.22	36.24	20.46	117.65
2032	1518.76	772.51	338.82	296.17	67.39	717.84
2033	1187.34	734.87	135.01	191.91	49.26	387.86
2034	1177.42	717.99	257.87	194.43	44.45	510.18
2035	1119.43	693.63	105.50	120.99	42.76	276.70
2036	928.58	682.31	139.93	135.56	36.69	324.14
2037	837.41	664.56	72.84	22.16	17.40	114.61
2038	1742.48	828.95	459.05	260.36	71.37	803.07
2039	594.51	598.59	11.46	44.12	14.64	79.72
2040	1283.41	751.46	203.76	158.27	46.82	417.13
2041	1709.21	825.14	382.57	306.75	71.99	777.73
2042	998.63	781.94	90.30	156.30	39.33	298.54
2043	1267.09	707.17	179.91	189.53	52.73	431.78
2044	1368.60	691.40	375.31	256.92	57.69	704.03
2045	1087.61	720.73	168.76	131.81	39.54	351.45
2046	1027.76	703.25	126.18	123.80	35.53	294.20
2047	983.58	708.81	140.93	127.98	32.49	309.15
2048	1057.12	730.86	124.91	101.24	33.81	266.43
2049	815.88	690.41	53.77	58.47	21.16	138.95
2050	778.22	595.41	65.62	75.12	23.82	168.44
Average	1089.72	698.44	167.44	148.21	40.18	365.37

2060s CNRM-CM5-RCP85

PRECIP mm	ET mm	SURQ mm	GW_Q mm	LAT_Q mm	WYLD mm
609.92	586.11	28.87	31.52	12.10	76.24
790.08	665.05	25.52	47.45	20.40	97.13
1267.22	732.80	191.92	168.43	50.49	419.46
981.78	764.43	107.25	60.48	25.11	200.49
1118.80	682.92	234.37	158.26	46.42	446.70
1049.58	698.59	158.03	131.41	40.82	339.82
1144.86	784.19	186.65	186.04	43.76	427.21
980.80	699.08	110.60	114.79	33.75	267.02
764.69	691.44	35.76	49.30	21.44	111.30
1220.93	650.53	253.72	198.70	48.64	509.82
729.87	626.29	74.75	68.62	21.52	174.59
1199.84	675.47	305.41	76.68	32.26	418.26
679.98	644.56	37.99	83.07	21.44	150.17
1024.90	648.27	115.52	138.57	37.30	297.66
832.23	689.25	71.36	103.95	26.32	211.58
1686.87	753.17	392.17	311.11	76.54	796.80
1151.86	760.49	198.42	160.94	43.61	415.34
1400.76	765.53	192.72	309.50	68.48	585.40
940.60	732.68	95.04	125.53	31.53	264.04
706.07	587.94	41.66	64.07	20.36	130.71
1053.53	726.35	103.17	129.33	35.84	275.40
1192.18	775.39	172.94	196.14	48.03	428.69
1207.68	757.65	238.24	134.55	39.14	420.95
1099.95	720.15	175.32	136.87	39.91	361.26
1396.91	772.46	356.06	217.21	54.29	641.12
731.00	686.19	37.53	29.15	15.49	88.15
1342.28	762.43	294.41	174.08	50.34	527.72
975.89	681.75	121.66	126.54	35.43	291.76
1046.49	702.28	187.80	114.18	34.55	345.79
1160.82	785.07	149.17	163.24	43.09	363.78
1049.61	706.95	156.47	133.66	37.28	336.15

Appendix Table 6. Simulated hydrological variables of the climate model EC-EARTH under RCP4.5

2030s EC-EARTH-RCP45

YEAR	PRECIP mm	ET mm	SURQ mm	GW_Q mm	LAT_Q mm	WYLD mm
2021	1014.95	676.05	152.93	97.43	28.53	285.22
2022	1156.14	703.42	298.07	148.20	36.03	490.01
2023	935.96	682.24	126.52	115.96	29.79	278.28
2024	989.68	710.84	110.38	101.29	29.98	246.95
2025	879.12	700.46	103.04	108.31	27.88	245.07
2026	1085.95	679.57	158.38	145.33	37.24	347.97
2027	1079.33	743.00	168.60	114.52	30.18	319.85
2028	1012.64	699.77	137.92	138.10	33.89	317.20
2029	809.86	678.14	87.77	81.40	24.61	198.35
2030	1519.68	727.85	359.32	209.00	55.36	632.55
2031	1046.33	702.13	198.11	149.79	35.30	392.24
2032	1193.33	760.10	214.55	154.87	40.00	417.50
2033	744.58	665.35	65.22	78.25	18.97	168.03
2034	1191.23	712.31	212.91	162.51	45.01	427.18
2035	1064.28	715.67	159.07	132.86	34.92	334.54
2036	876.50	702.76	106.41	101.00	26.57	240.10
2037	806.27	656.77	81.60	58.08	20.28	163.71
2038	881.87	671.52	91.82	104.03	29.15	229.52
2039	1048.33	690.15	148.68	104.33	31.86	290.54
2040	960.51	717.52	128.31	74.35	21.63	228.90
2041	1187.13	721.32	233.04	175.16	44.46	460.58
2042	795.81	660.76	71.09	70.04	20.61	166.61
2043	937.25	708.81	113.06	90.60	26.71	234.92
2044	748.21	637.44	61.18	84.83	23.02	173.76
2045	924.18	657.07	85.08	76.59	25.29	190.85
2046	1195.13	743.68	208.30	164.38	43.71	423.79
2047	1182.68	730.50	204.21	171.32	42.95	427.42
2048	1012.09	713.92	158.22	98.56	27.17	290.60
2049	879.94	709.30	89.67	112.22	28.98	236.64
2050	883.21	663.18	80.72	85.29	26.75	197.43
Average	1001.41	698.05	147.14	116.95	31.56	301.88

2060s EC-EARTH-RCP45

PRECIP mm	ET mm	SURQ mm	GW_Q mm	LAT_Q mm	WYLD mm
1148.33	733.81	226.13	141.53	38.63	412.99
916.04	678.36	104.32	101.80	27.27	239.47
935.64	701.62	118.89	115.97	32.01	272.61
1179.41	729.62	173.63	159.02	43.11	383.78
1036.80	703.12	143.40	123.86	34.63	308.65
1035.63	722.31	158.57	120.44	31.66	317.26
948.77	722.37	115.53	93.37	26.90	241.02
908.53	693.54	101.68	116.75	28.96	253.02
1233.20	721.88	244.79	149.15	39.34	441.50
945.81	713.42	140.08	95.43	25.94	266.96
1053.71	706.70	183.77	118.05	32.29	339.51
1013.20	700.51	140.31	123.75	32.08	302.58
858.08	692.86	85.83	68.09	22.09	180.59
717.94	618.18	60.04	76.54	21.22	161.66
750.49	633.62	56.95	61.08	19.69	141.10
1037.70	697.38	140.46	77.65	28.65	250.78
1167.95	738.69	206.10	152.96	39.77	405.86
748.20	664.88	61.54	71.71	19.77	157.97
995.26	687.72	137.31	129.70	32.49	305.82
1153.56	749.31	208.13	122.15	35.03	371.62
930.27	710.02	132.10	96.29	27.52	261.24
1002.58	699.51	157.69	82.94	24.85	270.47
996.31	718.78	117.36	103.80	29.93	255.78
899.20	670.30	133.56	79.14	23.44	240.72
908.95	691.84	109.74	88.56	25.13	228.06
1040.56	700.56	153.12	116.61	32.03	307.26
1243.57	747.05	240.84	157.57	41.63	448.18
1057.40	704.07	183.67	145.47	35.67	373.15
862.45	675.34	94.99	81.07	23.03	203.86
922.21	690.35	149.03	66.16	20.15	238.99
988.26	700.59	142.65	107.89	29.83	286.08

Appendix Table 7. Simulated hydrological variables of the climate model EC-EARTH under RCP8.5

2030s EC-EARTH-RCP85

YEAR	PRECIP mm	ET mm	SURQ mm	GW_Q mm	LAT_Q mm	WYLD mm
2021	1042.78	698.08	158.21	170.81	38.21	376.10
2022	1086.61	733.52	166.98	135.69	33.36	343.32
2023	1135.23	712.23	218.01	189.65	42.25	459.99
2024	934.79	682.49	141.98	112.26	28.26	289.93
2025	982.59	693.71	156.36	93.21	28.42	283.16
2026	942.56	717.26	171.07	98.19	27.81	303.34
2027	1076.28	723.31	155.76	100.22	32.00	293.95
2028	886.41	696.06	90.02	106.66	28.89	232.19
2029	1016.01	712.06	162.50	110.45	31.31	310.65
2030	917.29	680.30	125.63	66.05	21.75	218.71
2031	1116.53	745.86	209.04	134.74	37.27	387.83
2032	911.39	726.29	89.63	75.74	24.75	195.65
2033	922.88	695.17	130.03	107.61	28.74	272.56
2034	1163.15	692.91	199.89	171.43	46.25	426.54
2035	1036.05	725.55	179.18	125.49	32.93	345.75
2036	838.79	659.92	79.01	90.34	25.89	201.91
2037	732.75	632.35	58.99	65.75	20.51	149.33
2038	1093.39	720.63	157.87	113.12	32.10	309.57
2039	981.02	709.78	134.10	111.14	31.99	283.09
2040	1134.09	735.36	175.77	128.25	36.07	348.13
2041	1418.43	785.25	343.99	223.09	53.00	632.06
2042	876.82	675.16	102.31	108.42	28.59	247.48
2043	976.59	707.44	127.92	104.82	29.62	268.87
2044	991.42	730.62	172.63	110.02	30.14	319.15
2045	893.24	691.55	91.84	75.78	24.95	197.85
2046	801.87	677.01	64.60	75.42	23.43	167.83
2047	879.25	664.53	79.27	96.75	27.87	209.27
2048	1023.19	687.76	146.33	153.09	37.38	344.97
2049	792.28	643.61	79.46	46.25	18.55	148.97
2050	1136.01	729.92	222.10	101.49	32.20	361.17
Average	991.32	702.86	146.35	113.40	31.15	297.64

2060s EC-EARTH-RCP85

PRECIP mm	ET mm	SURQ mm	GW_Q mm	LAT_Q mm	WYLD mm
919.78	700.89	112.59	137.66	32.21	289.33
836.49	652.57	78.34	89.00	22.88	195.78
874.77	691.02	90.23	82.49	22.45	199.83
952.55	669.84	88.41	101.35	28.73	223.13
979.31	707.44	131.13	162.81	34.11	336.26
804.49	669.76	65.04	71.92	20.20	162.02
917.41	691.10	86.22	88.12	24.91	203.49
1128.45	722.95	175.91	162.16	39.01	385.71
1272.80	744.25	262.28	191.80	45.07	510.05
1004.32	710.09	161.84	127.70	31.48	330.01
974.92	695.62	132.73	100.64	29.17	268.14
1006.50	709.51	134.83	111.91	31.36	284.72
1010.46	749.26	132.80	107.20	28.95	275.61
1020.77	720.70	119.73	111.69	30.83	269.01
1170.11	749.61	202.18	133.55	36.09	379.17
1648.92	818.61	458.54	286.17	60.73	820.76
914.63	685.36	135.26	107.78	27.23	278.51
814.58	679.21	82.37	81.72	22.27	192.11
701.99	629.87	51.52	41.13	16.58	112.22
1185.14	725.72	164.58	115.87	37.41	323.12
1124.76	757.21	211.92	170.35	37.50	429.27
908.69	689.03	108.08	83.33	23.90	221.92
847.16	665.93	87.62	71.87	24.30	188.15
1361.12	772.66	286.54	187.34	48.40	531.66
1023.43	702.52	154.98	143.24	35.39	342.42
1029.35	717.48	147.57	154.25	36.60	347.34
1125.02	703.15	181.17	151.13	40.09	381.13
997.15	716.78	137.57	113.40	30.66	289.77
958.28	681.16	144.74	98.82	28.45	278.14
1074.77	729.52	177.18	128.19	32.83	345.89
1019.60	708.63	150.13	123.82	31.99	313.156

Appendix Table 8. Simulated hydrological variables of the climate model MIRCOS under RCP4.5

2030s MIRCOS-RCP45

YEAR	PRECIP mm	ET mm	SURQ mm	GW_Q mm	LAT_Q mm	WYLD mm
2021	1077.82	763.34	149.22	143.80	35.57	337.58
2022	888.74	653.15	108.08	130.75	30.47	277.75
2023	810.39	662.40	58.52	107.18	25.08	197.58
2024	885.16	677.03	101.34	90.83	26.77	225.23
2025	885.44	658.72	129.14	77.85	25.55	237.60
2026	869.11	734.40	98.39	60.37	23.15	186.28
2027	960.29	731.48	135.74	81.72	28.58	251.44
2028	906.47	657.86	177.98	83.65	24.77	290.75
2029	889.37	670.71	102.30	107.78	28.25	245.35
2030	817.22	649.00	63.31	115.41	27.31	213.04
2031	763.52	639.71	56.80	66.26	21.90	150.30
2032	757.47	670.05	75.90	48.58	19.45	147.32
2033	764.53	678.45	48.21	48.70	20.19	119.97
2034	920.66	661.21	110.32	110.24	28.88	255.92
2035	989.44	705.58	151.17	115.66	30.48	304.05
2036	849.13	680.91	98.75	85.18	24.12	214.63
2037	951.09	746.90	112.73	70.87	26.53	215.09
2038	1056.37	755.76	169.58	91.88	31.55	299.67
2039	916.94	701.12	131.87	90.23	25.74	253.77
2040	851.69	652.69	103.93	97.07	26.30	233.48
2041	897.47	710.48	97.23	85.77	25.82	214.82
2042	759.52	695.03	55.73	31.24	18.24	108.55
2043	1052.48	699.25	167.63	101.84	31.55	306.73
2044	952.14	754.22	108.94	136.77	31.34	285.46
2045	868.14	675.94	83.48	107.30	27.17	224.56
2046	773.65	654.61	75.92	63.78	22.03	166.38
2047	981.97	696.04	138.03	103.29	30.40	278.67
2048	1191.91	763.14	252.09	111.59	34.11	405.10
2049	1149.79	735.55	212.80	182.10	39.54	445.10
2050	1026.09	720.98	199.72	112.83	29.67	349.80
Average	915.47	695.19	119.16	95.35	27.35	248.07

2060s MIRCOS-RCP45

PRECIP mm	ET mm	SURQ mm	GW_Q mm	LAT_Q mm	WYLD mm
1006.83	723.81	157.11	111.08	31.55	307.77
1108.66	750.63	225.73	137.09	33.72	404.86
749.61	690.73	54.28	37.55	19.28	115.72
915.65	767.97	103.53	73.30	24.34	205.66
792.03	691.38	84.95	50.62	20.54	159.59
970.32	724.18	158.96	90.78	27.90	282.45
712.46	670.57	47.76	52.35	19.36	124.02
861.18	696.18	85.10	93.19	26.44	209.57
1199.00	760.51	251.86	90.60	32.60	381.90
970.79	747.18	127.29	144.91	33.84	314.72
934.46	727.81	112.86	116.48	29.29	266.37
892.68	694.80	116.94	112.46	27.70	263.70
1050.52	711.88	158.03	112.48	30.35	307.98
871.32	723.77	116.44	112.82	29.61	265.93
855.57	718.83	86.74	49.67	21.36	162.25
1156.10	757.27	210.83	160.70	38.84	419.23
1053.13	737.45	160.89	155.25	35.35	361.01
995.16	721.15	139.35	132.20	32.53	313.88
623.78	634.67	40.98	26.17	14.64	84.84
610.60	606.66	36.32	9.70	12.31	59.59
1227.37	785.50	222.44	141.59	38.24	409.55
721.51	688.59	55.75	57.60	19.67	138.22
763.57	679.82	54.14	57.36	20.52	136.41
1132.32	707.86	205.44	162.19	37.23	413.28
1037.15	766.43	148.74	147.43	34.06	340.38
860.41	679.36	132.84	81.46	24.15	243.88
825.16	703.39	63.87	45.31	20.13	132.94
1149.83	755.98	224.98	106.63	34.21	373.55
786.41	729.28	98.72	33.93	18.53	154.89
882.49	750.14	93.97	80.53	26.73	205.64
923.87	716.79	125.89	92.78	27.17	251.99

Appendix Table 9. Simulated hydrological variables of the climate model MIRCOS under RCP8.5

2030s MIRCOS-RCP85

YEAR	PRECIP mm	ET mm	SURQ mm	GW_Q mm	LAT_Q mm	WYLD mm
2021	949.23	660.60	136.67	123.24	28.53	296.92
2022	848.60	689.15	83.29	97.10	25.92	213.39
2023	986.95	711.48	148.75	86.38	26.26	267.18
2024	988.70	752.04	151.35	113.17	29.78	299.97
2025	974.05	726.14	130.05	128.37	30.84	297.28
2026	681.84	622.77	31.76	67.57	18.60	123.40
2027	1065.49	711.82	183.54	119.06	31.65	340.16
2028	1180.40	783.41	221.17	115.57	32.94	377.12
2029	1039.40	755.47	134.29	139.45	33.53	316.35
2030	918.62	722.35	92.94	118.64	27.88	247.77
2031	810.04	644.98	68.89	113.99	27.06	217.23
2032	920.43	662.26	110.05	141.46	30.89	290.84
2033	780.99	659.47	69.61	55.28	20.22	149.80
2034	878.17	719.52	95.95	83.78	24.08	208.92
2035	644.84	595.79	47.32	40.45	15.31	105.74
2036	780.32	602.74	71.68	66.97	22.37	165.29
2037	1151.58	742.45	194.89	167.63	38.08	410.17
2038	1089.03	765.83	157.48	104.98	29.44	300.00
2039	1054.79	772.09	128.75	179.75	38.66	356.94
2040	805.55	672.58	69.23	87.51	23.10	186.99
2041	930.63	685.44	103.07	113.74	29.78	253.97
2042	852.58	656.87	118.62	61.92	21.48	207.04
2043	1217.00	767.98	199.58	191.52	43.42	444.41
2044	891.45	751.61	79.50	80.73	22.94	190.81
2045	756.04	684.45	45.10	64.84	20.03	134.09
2046	1158.77	742.81	266.00	108.22	31.87	411.99
2047	796.39	696.23	68.88	46.41	18.76	138.88
2048	1183.49	745.93	245.96	125.23	34.95	412.23
2049	1172.00	776.00	205.53	184.09	40.81	441.92
2050	898.36	725.74	87.02	88.55	24.87	208.04
Average	946.86	706.87	124.90	107.19	28.14	267.16

2060s MIRCOS-RCP85

PRECIP mm	ET mm	SURQ mm	GW_Q mm	LAT_Q mm	WYLD mm
804.47	697.32	63.37	102.46	24.95	196.50
791.42	715.25	95.42	57.33	20.52	177.03
870.02	757.99	80.97	76.03	24.43	185.17
654.55	638.50	44.72	38.97	17.98	104.62
868.73	691.17	85.28	81.56	27.44	199.30
979.44	761.47	158.76	47.47	24.11	234.29
647.86	683.29	52.13	32.66	16.71	104.54
800.56	709.10	83.03	46.36	22.58	154.68
1197.82	787.24	273.87	82.96	33.16	395.41
940.00	779.05	118.59	105.88	28.69	260.36
1079.71	727.78	146.54	161.56	38.26	355.73
875.32	741.50	107.12	127.04	30.27	273.67
821.89	704.43	85.27	67.71	22.30	180.07
689.67	654.23	46.23	40.15	18.45	108.27
967.33	747.52	129.86	79.64	29.10	243.27
1038.47	780.96	146.05	84.19	29.82	266.12
881.73	759.28	106.67	82.40	26.97	221.90
621.18	658.21	33.07	32.71	15.78	84.59
838.47	688.88	68.67	104.29	27.68	206.55
766.68	624.62	106.42	22.70	17.09	149.02
1030.14	783.09	208.68	78.30	31.99	323.94
917.30	765.51	113.02	86.47	27.03	233.20
975.58	748.60	156.62	92.16	29.08	283.13
958.53	774.37	102.45	123.10	31.59	265.23
858.14	726.93	110.47	81.48	26.52	224.38
884.54	717.93	114.46	64.92	25.92	209.64
1199.35	789.68	239.74	159.92	41.67	450.57
875.33	702.57	120.66	90.67	28.05	245.90
1038.80	742.97	157.37	169.08	37.03	373.02
901.09	732.45	94.89	98.40	28.40	229.80
892.47	726.40	115.01	83.95	26.79	231.33

Appendix Table 10. Simulated hydrological variables of the climate model MPI-ESM-LR- under RCP4.5

2030s MPI-ESM-LR-RCP45

YEAR	PRECIP mm	ET mm	SURQ mm	GW_Q mm	LAT_Q mm	WYLD mm
2021	1250.12	705.73	289.01	118.86	39.65	453.04
2022	1620.65	761.83	296.25	476.61	75.01	872.46
2023	699.79	672.89	36.53	41.94	18.04	106.48
2024	957.41	727.73	103.99	82.32	26.54	218.52
2025	1672.62	796.14	368.46	299.34	65.79	746.49
2026	904.51	698.15	117.88	182.62	32.87	348.84
2027	947.26	691.12	72.45	104.20	30.72	214.89
2028	551.50	541.25	46.04	22.47	13.25	84.46
2029	1325.89	784.20	249.16	186.07	47.94	492.98
2030	528.17	559.44	13.75	11.76	9.74	38.37
2031	1540.62	732.16	338.45	209.36	57.64	615.59
2032	887.18	646.98	90.54	41.56	27.32	166.51
2033	976.45	706.89	180.13	174.24	34.41	400.51
2034	1058.23	772.51	118.31	117.73	33.21	274.99
2035	894.61	719.42	78.80	69.63	25.55	179.69
2036	1051.39	711.00	122.56	51.54	29.19	206.82
2037	1639.19	779.16	456.80	391.87	73.20	945.54
2038	754.65	661.14	63.17	44.15	18.36	130.60
2039	548.46	545.26	19.07	14.38	12.26	47.93
2040	783.69	689.18	35.43	10.39	15.31	61.95
2041	1014.47	633.82	171.68	82.05	32.18	289.92
2042	1347.46	789.86	221.92	218.40	48.46	501.08
2043	921.87	725.22	139.29	81.15	28.65	258.30
2044	1261.10	796.53	194.07	116.80	38.67	356.98
2045	697.39	700.42	48.60	77.08	18.81	151.00
2046	907.86	704.51	51.11	85.78	27.52	169.85
2047	1492.79	775.13	351.67	231.36	52.90	650.72
2048	877.13	691.29	122.37	89.27	28.28	247.25
2049	1143.00	778.99	129.65	82.03	33.93	249.79
2050	530.38	602.88	21.49	29.01	12.90	68.15
Average	1026.19	703.36	151.62	124.80	33.61	318.32

2060s MPI-ESM-LR-RCP45

PRECIP mm	ET mm	SURQ mm	GW_Q mm	LAT_Q mm	WYLD mm
766.76	657.78	35.22	19.26	20.34	76.31
1083.55	759.11	168.54	119.30	37.91	332.66
1176.26	861.14	213.50	126.57	35.00	385.07
757.87	679.78	87.18	29.80	21.32	142.11
909.28	755.06	70.23	54.71	27.18	155.51
839.41	766.68	88.24	125.94	27.94	249.53
558.59	567.56	42.26	41.80	14.10	102.64
919.38	680.27	138.78	46.49	27.24	215.71
918.12	731.01	116.00	94.21	29.71	244.48
768.32	737.93	60.48	69.93	19.66	156.77
1053.70	874.05	74.97	86.12	29.87	195.57
1355.26	650.32	408.53	117.05	45.59	576.74
994.45	816.45	97.40	166.88	35.87	314.32
606.11	706.13	19.52	29.39	12.80	66.45
455.76	567.96	4.00	3.36	7.94	15.96
1166.95	762.71	180.88	91.62	37.64	315.02
812.35	711.76	137.88	100.77	26.64	273.37
848.88	714.07	53.47	19.17	22.32	97.50
1008.16	798.38	96.25	69.54	30.44	199.97
556.29	653.35	42.69	61.03	17.29	127.35
1006.99	740.44	157.10	90.20	29.23	280.21
611.26	653.27	11.03	34.91	15.16	66.15
658.72	678.42	14.25	16.75	14.97	47.53
863.29	630.32	106.50	75.77	29.74	218.88
1394.97	752.19	315.79	170.67	49.75	544.27
698.23	724.98	63.37	118.83	23.77	216.46
527.86	608.36	13.04	9.09	9.38	33.69
923.46	756.61	61.38	65.56	26.53	156.73
1371.76	852.82	213.68	168.54	49.41	439.90
839.32	677.12	82.08	78.10	30.78	198.85
881.71	717.53	105.81	76.71	26.85	214.86

Appendix Table 11. Simulated hydrological variables of the climate model MPI-ESM-LR- under RCP8.5

2030s MPI-ESM-LR-RCP85

YEAR	PRECIP mm	ET mm	SURQ mm	GW_Q mm	LAT_Q mm	WYLD mm
2021	957.01	710.83	85.00	64.50	30.44	192.92
2022	979.09	859.04	77.79	95.59	24.85	216.88
2023	706.22	741.27	27.35	40.35	14.35	94.35
2024	1051.61	781.20	107.32	89.36	30.70	243.89
2025	858.99	736.83	47.07	39.33	21.21	116.68
2026	772.72	719.45	52.17	25.20	12.72	97.77
2027	755.32	687.23	61.40	60.11	24.41	154.54
2028	593.82	650.00	18.15	21.31	9.39	57.76
2029	684.18	635.57	35.16	12.97	12.35	67.79
2030	952.73	772.98	86.66	89.46	27.90	218.80
2031	621.24	625.73	27.29	20.10	11.67	67.79
2032	1378.33	799.33	259.08	175.74	44.35	533.58
2033	802.68	705.54	32.38	8.08	16.80	62.03
2034	1841.09	937.95	445.25	373.46	67.66	922.04
2035	576.43	698.77	2.39	11.45	7.40	33.52
2036	864.86	710.89	56.69	80.27	23.44	172.14
2037	846.96	703.51	81.77	39.84	18.84	152.48
2038	789.91	701.11	60.02	73.71	21.13	165.70
2039	1268.92	806.12	197.60	139.29	38.97	411.50
2040	1140.17	873.65	190.49	93.96	27.78	331.63
2041	427.44	561.78	0.68	0.52	3.99	9.25
2042	927.09	577.82	122.51	17.86	26.45	171.03
2043	1852.84	841.67	564.35	289.68	65.19	962.34
2044	889.54	847.01	60.74	109.99	21.42	217.16
2045	542.95	607.29	33.24	25.54	9.90	78.75
2046	495.65	538.80	8.50	1.53	6.47	20.17
2047	1008.25	783.00	46.30	64.75	26.71	146.44
2048	754.33	733.32	58.85	49.98	17.89	140.75
2049	299.35	382.13	0.73	0.05	3.03	5.83
2050	670.82	578.92	49.08	3.11	14.38	68.51
Average	877.02	710.29	96.53	70.57	22.73	204.47

2060s MPI-ESM-LR-RCP85

PRECIP mm	ET mm	SURQ mm	GW_Q mm	LAT_Q mm	WYLD mm
527.08	605.07	8.44	7.10	10.38	28.62
1138.57	718.23	246.31	77.89	34.80	407.05
1135.96	824.82	163.90	74.05	33.28	292.52
965.68	836.41	75.77	75.68	25.76	188.56
1505.97	895.52	265.34	275.67	57.23	632.38
1040.96	762.20	192.69	144.51	32.22	387.07
725.07	733.30	69.61	44.52	18.42	142.82
1161.79	786.08	177.08	76.65	32.82	299.11
1057.22	797.76	204.60	147.24	32.17	409.86
898.36	727.27	78.97	72.55	25.33	183.05
653.08	713.18	17.53	30.37	14.91	73.44
1217.98	765.36	182.43	101.57	34.83	332.19
648.28	644.30	56.59	45.17	19.80	130.66
1242.90	852.34	194.99	164.11	40.26	418.47
1027.78	825.69	144.36	125.71	31.26	325.57
926.98	788.81	64.59	100.58	25.94	203.79
771.17	706.48	60.74	52.51	19.51	141.64
520.14	507.41	57.73	8.26	11.55	79.26
1436.79	772.27	323.42	223.62	56.04	623.65
568.48	595.60	44.04	69.52	16.60	143.06
671.73	615.46	34.53	48.10	18.42	108.93
1170.83	706.06	144.45	116.27	43.04	312.72
1266.79	875.73	179.86	232.62	48.85	485.87
646.40	730.36	42.38	52.81	17.61	125.94
704.72	701.94	39.19	19.05	17.68	83.97
662.15	570.75	45.83	19.30	20.62	85.55
1640.77	719.21	412.58	287.36	66.99	790.69
1084.86	861.66	116.20	171.37	36.44	357.12
984.13	669.74	145.49	211.67	43.67	415.24
692.75	639.57	72.72	48.86	15.47	148.33
956.51	731.62	128.75	104.16	30.06	278.57

Appendix Table 12. Population number (portion of zone found in study area) and their respective daily water consumption

Zones	Parts of Zone Population	Daily demand &CIWD (lit/day)	Daily total(lit/day) consumption	Daily total (m3/day) consumption	Daily Population and CIWD)(lit/day)
WEST Arsi	440086	25+10%	12102365	12102.365	27.5
Sidama	1353400	25+10%	37218500	37218.5	27.5
Guji	369206	25+10%	10153165	10153.165	27.5
Bale	84514	25+10%	2324135	2324.135	27.5
Total	2247206	25+10%	61798165	61798.165	

*CIWD is Commercial and Institutional Water Demand

Appendix Table 13. Small towns population number and their respective daily water consumption

Woreda	Towns	Population	Daily Domestic and CIWD (Lit/day)	Daily total consumption (lit/day)	Daily total consumption (m3/day)
Arbegona	Yaya	17061	44	750684	750.684
Bensa	Daye	29318	44	1289992	1289.992
Bursa	Bursa	5832	44	256608	256.608
Bona Zuria	Bona	15266	44	671704	671.704
Aroresa	Mejo	7563	44	332772	332.772
Chere	Chere	5977	44	262988	262.988
Kokosa	Kokosa	6310	44	277640	277.64
Nensebo	Werka	11885	44	522940	522.94
Bore	Bore	17142	44	754248	754.248
Bore	Yirba Muda	2947	44	129668	129.668
Hula	Hageselam	16234	44	714296	714.296
Meda Welabu	Bidre	5855	44	257620	257.62
Total		141390	44	6221160	6221.16

Appendix Table 14. Livestock Population and their respective daily water consumption in the study area

Livestock	Population	Dail demand (lit/day)	Daily total(lit/day) consumption	Daily total (m3/day) consumption
Cattel	1648964	50	82448200	82448.2
Sheep	1404874	10	14048740	14048.74
Goats	168494	10	1684940	1684.94
Horse	108726	45	4892670	4892.67
Donkey	60128	45	2705760	2705.76
Mule	110447	45	4970115	4970.115
Camel	333005	43	14319215	14319.215
Poultry	594150	0.4	237660	237.66
Total	4428788	248.4	125307300	125307.3

Appendix Table 15. Existing small-scale irrigation in the study area

Project Name	UTM 37N		Area (ha)
	Longitude E	Latitude N	
Ababa	489763	673787	32.22
BadessaAdibar	493027	665765	34.12
BoltuGirisa	488337	689490	70.6
Kame	462886	707475	4.95
Genale oda Kalacha	497696	678143	60
Harawa Hebo	524633	723648	50
Dodie	488703	674129	32.3
Hila	490683	677129	40.6
Galana	470877	723406	52
Galalicha	468939	711679	50
Rewo	474707	719665	60
Racha	493572	691336	60
Girja	491442	691470	22
Malawe	470662	733281	97
Morodo	457808	726235	100
Gase	444749	719984	18
Wirma	446449	718822	25
Namieha	470262	712261	138
Asaro	485237	729081	42
Bebeko	466169	740394	25
Tulicha	474721	734637	10
Total			1023.79

Appendix Table 16. Potential Future Irrigation Location and their respective Area

Project Name	UTM 37N		Area (ha)
	Longitude E	Latitude N	
Korke	547913	680450	210
Bedessa	516836	700392	275
Genale	562747	630073	5000
Iya	540558	694539	3700
Chembe	489488	674075	4300
Berecha	495543	668732	5000
Raro kobo	478362	673403	5200
Michicha	496742	679325	7000
Dereha	525889	722628	70
Fechea	545442	733818	90
Chabi	525920	721184	110
Youko	541154	675962	165
Bunaka	507943	725052	65
Gabata	470249	731596	48
Wonjala	459667	724262	60
Erерte	465504	722623	65
Konkana	479802	719429	60
Bisanguddu	505111	702642	65
Gambeltu	489345	697812	75
Malgaancho	459234	720773	55
Namicha	463274	710967	100
Shadada	461237	727336	61
Total			31774

Source: (MoWE, 2007f).

Appendices: Figures

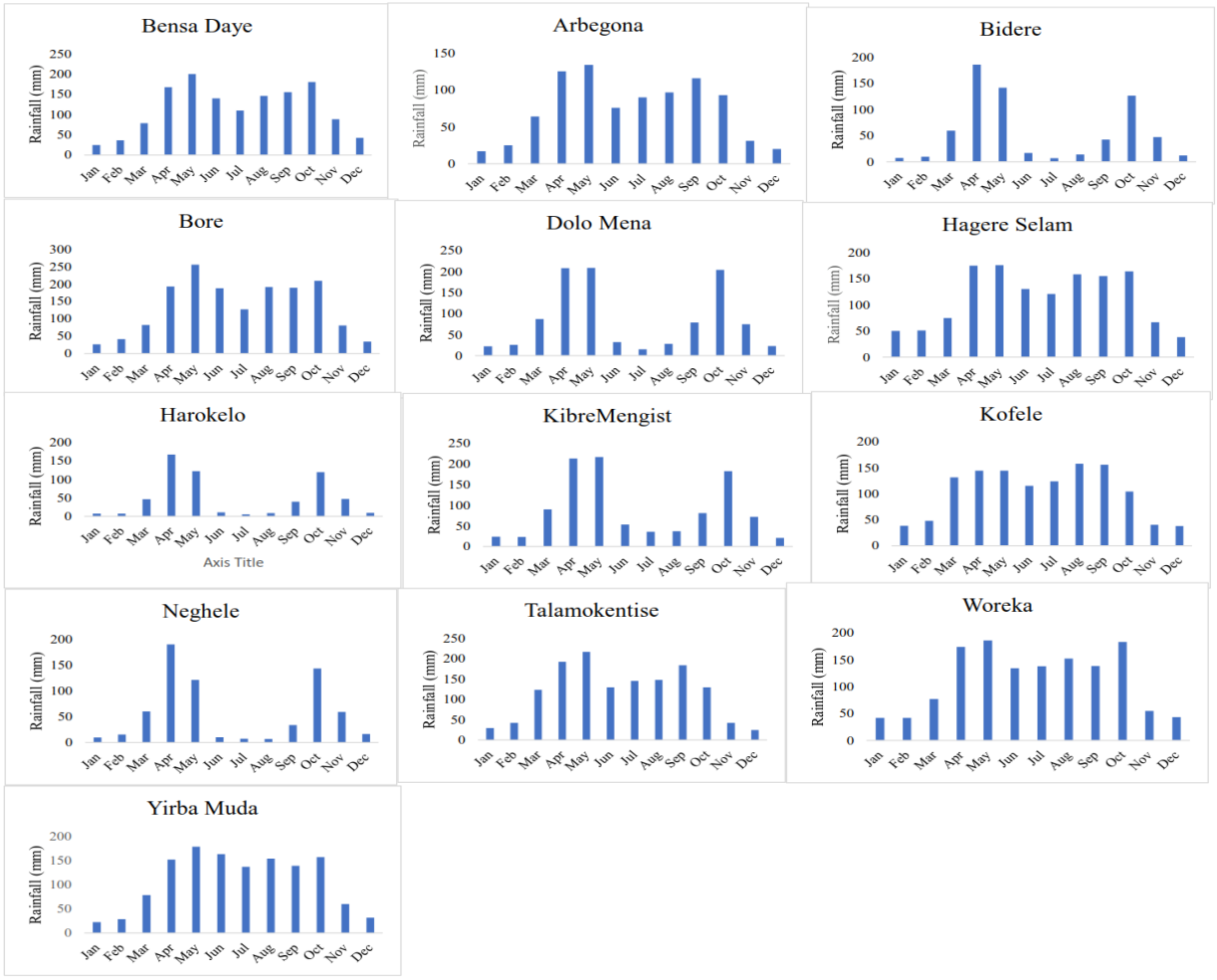

Appendix Figure 1. Monthly average rainfall distribution for each station

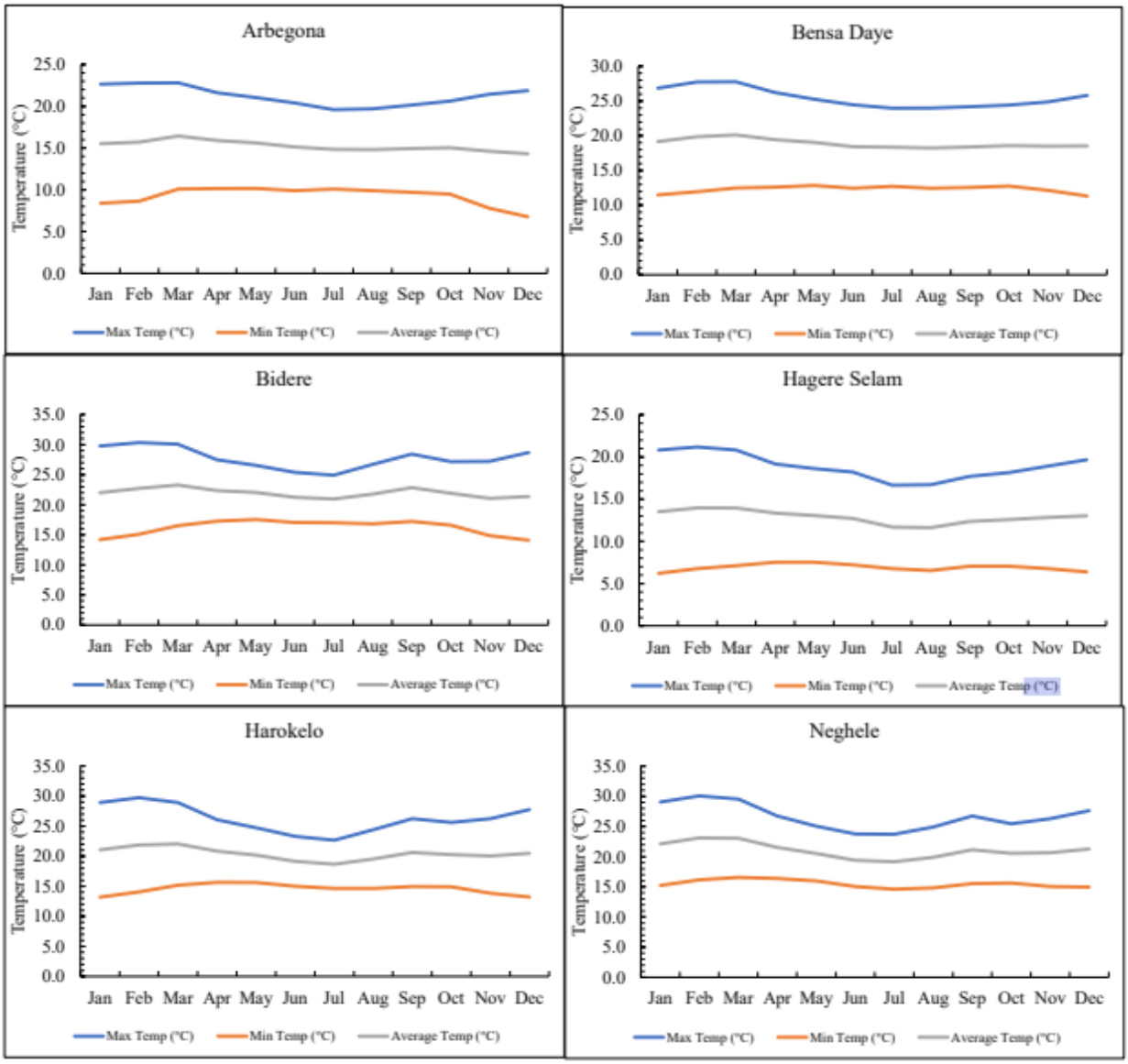

Appendix Figure 2. Monthly average maximum and minimum temperature distribution for selected station

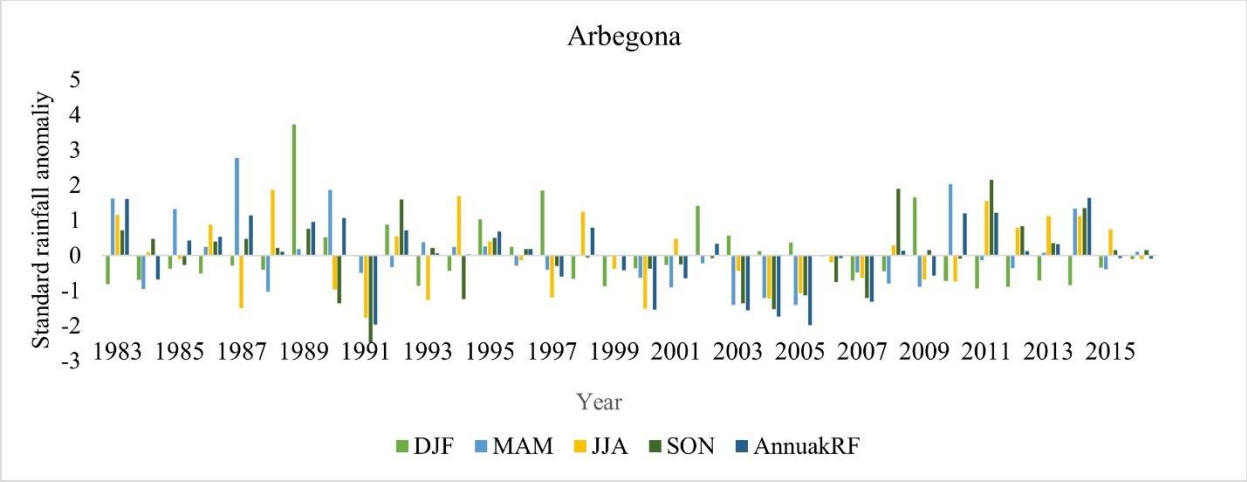
Arbegona
Standard rainfall anomaliy
5
4
3
2
1
0
-1
-2
-3
1983 1985 1987 1989 1991 1993 1995 1997 1999 2001 2003 2005 2007 2009 2011 2013 2015
Year
DJF MAM JJA SON AnnuakRF

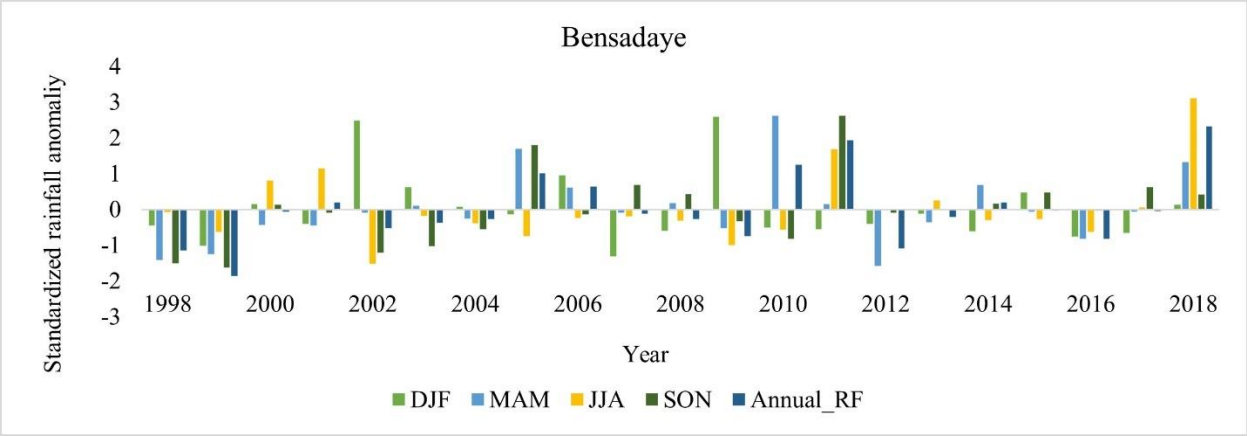
Bensadaye
Standardized rainfall anomaliy
4
3
2
1
0
-1
-2
-3
1998 2000 2002 2004 2006 2008 2010 2012 2014 2016 2018
Year
DJF MAM JJA SON Annual_RF

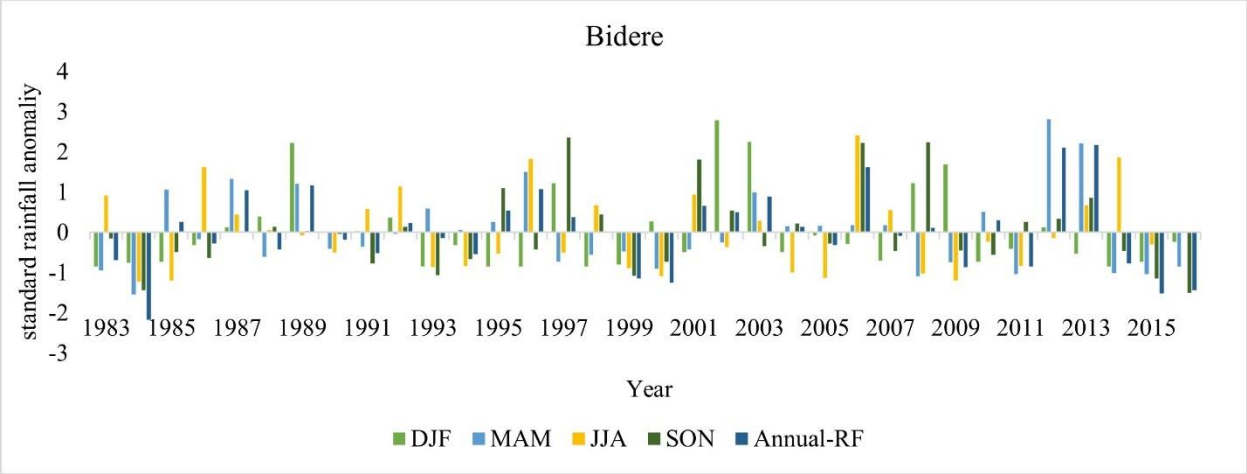
Bidere
standard rainfall anomaliy
4
3
2
1
0
-1
-2
-3
1983 1985 1987 1989 1991 1993 1995 1997 1999 2001 2003 2005 2007 2009 2011 2013 2015
Year
DJF MAM JJA SON Annual-RF

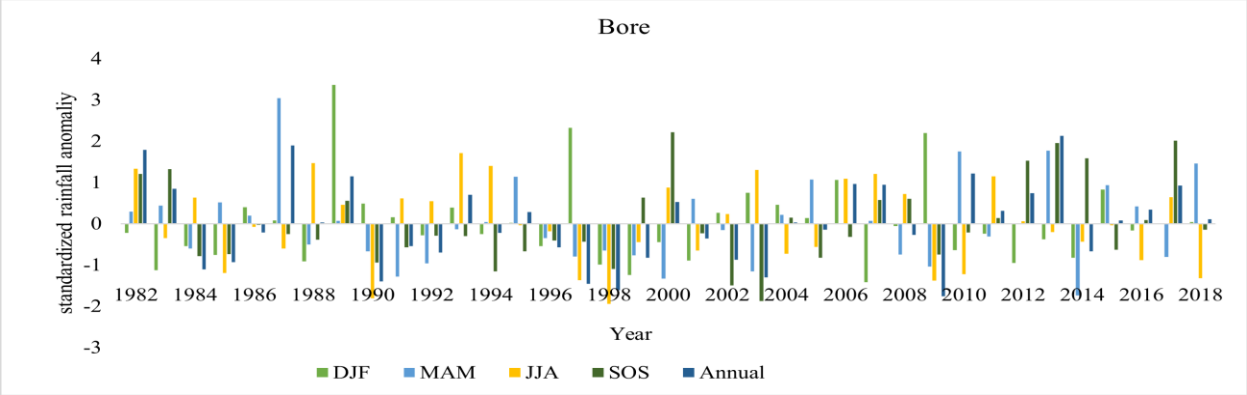
Bore
standardized rainfall anomaliy
4
3
2
1
0
-1
-2
-3
1982 1984 1986 1988 1990 1992 1994 1996 1998 2000 2002 2004 2006 2008 2010 2012 2014 2016 2018
Year
DJF MAM JJA SOS Annual

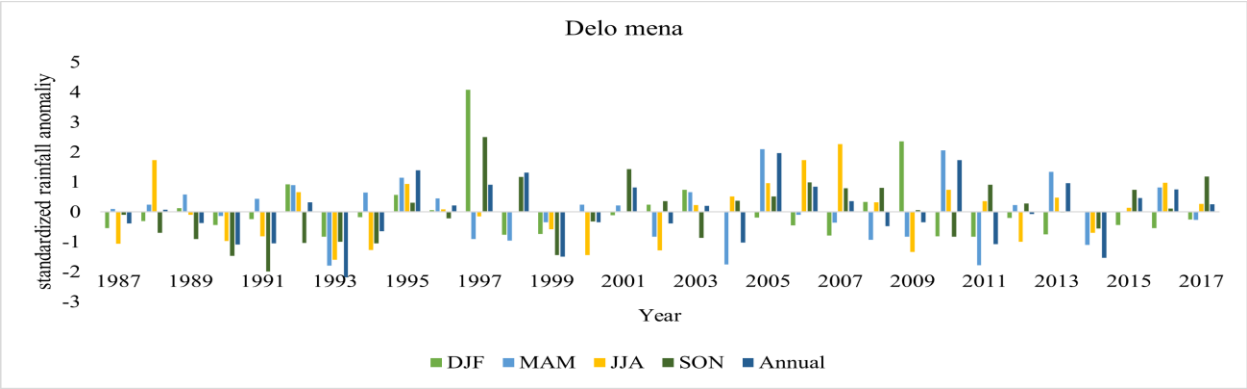
Delo mena
standardized rainfall anomaliy
5
4
3
2
1
0
-1
-2
-3
1987 1989 1991 1993 1995 1997 1999 2001 2003 2005 2007 2009 2011 2013 2015 2017
Year
DJF MAM JJA SON Annual

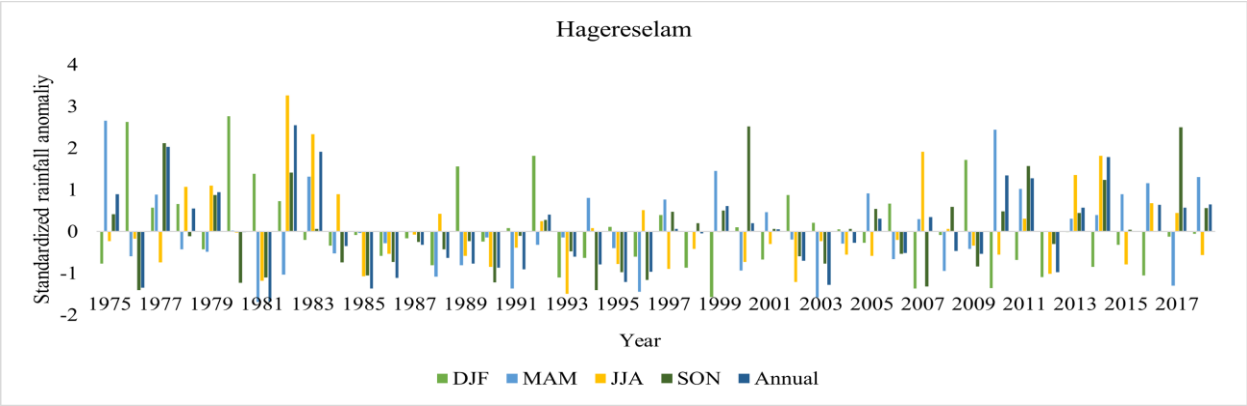
Hagereselam
Standardized rainfall anomaliy
4
3
2
1
0
-1
-2
1975 1977 1979 1981 1983 1985 1987 1989 1991 1993 1995 1997 1999 2001 2003 2005 2007 2009 2011 2013 2015 2017
Year
DJF MAM JJA SON Annual

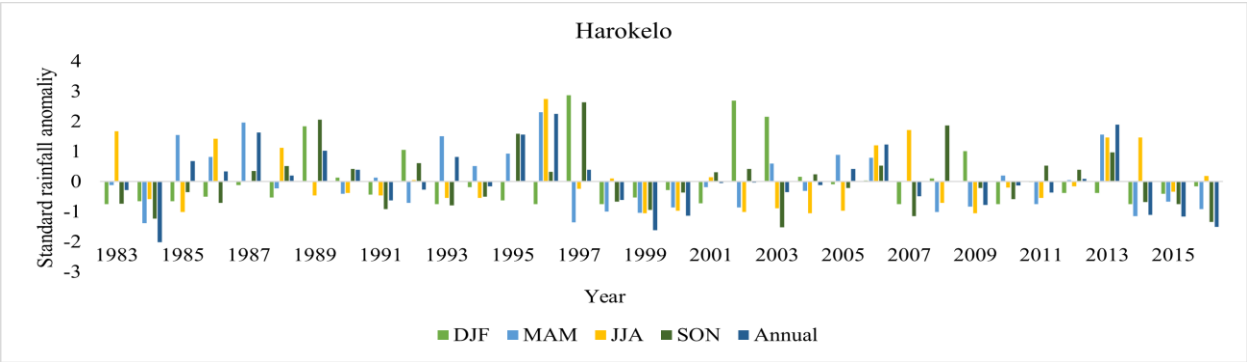
Harokelo
Standard rainfall anomaliy
4
3
2
1
0
-1
-2
-3
1983 1985 1987 1989 1991 1993 1995 1997 1999 2001 2003 2005 2007 2009 2011 2013 2015
Year
DJF MAM JJA SON Annual

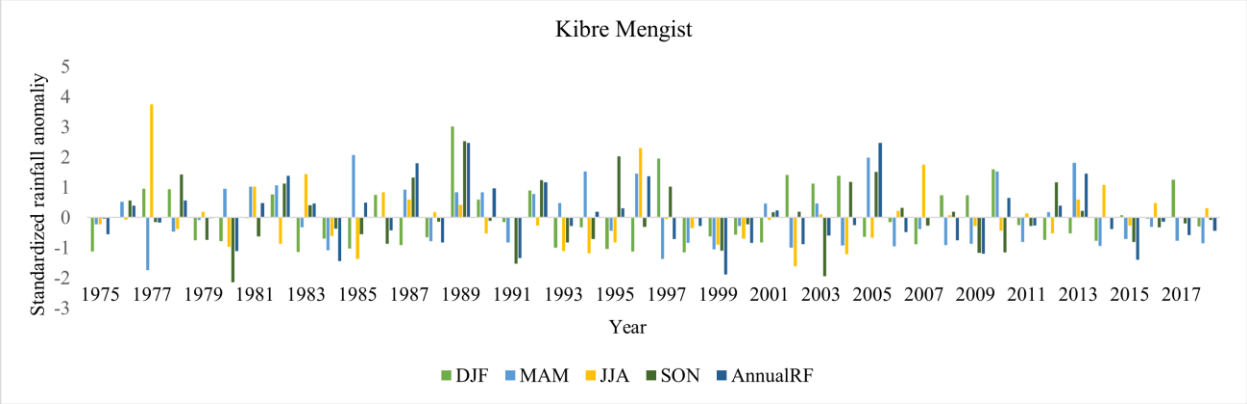
Kibre Mengist
Standardized rainfall anomaliy
5
4
3
2
1
0
-1
-2
-3
1975 1977 1979 1981 1983 1985 1987 1989 1991 1993 1995 1997 1999 2001 2003 2005 2007 2009 2011 2013 2015 2017
Year
DJF MAM JJA SON AnnualRF

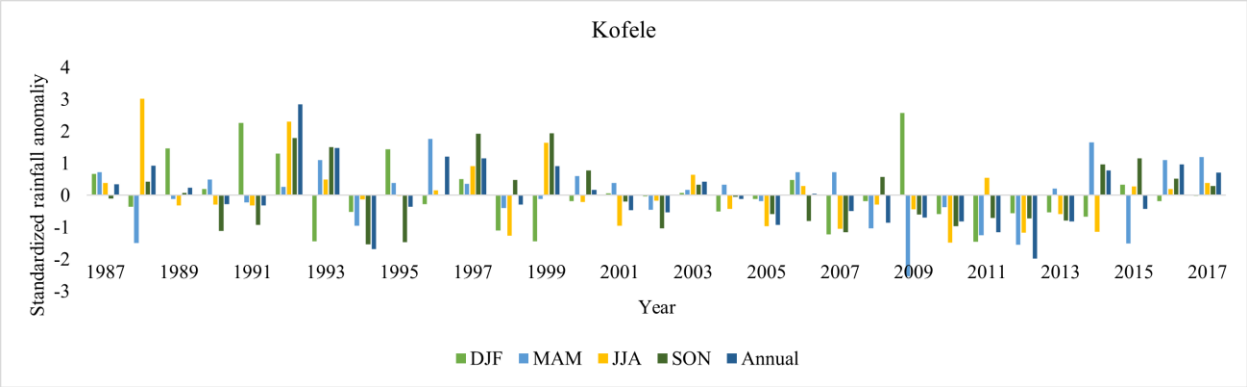
Kofele
Standardized rainfall anomaliy
4
3
2
1
0
-1
-2
-3
1987 1989 1991 1993 1995 1997 1999 2001 2003 2005 2007 2009 2011 2013 2015 2017
Year
DJF MAM JJA SON Annual

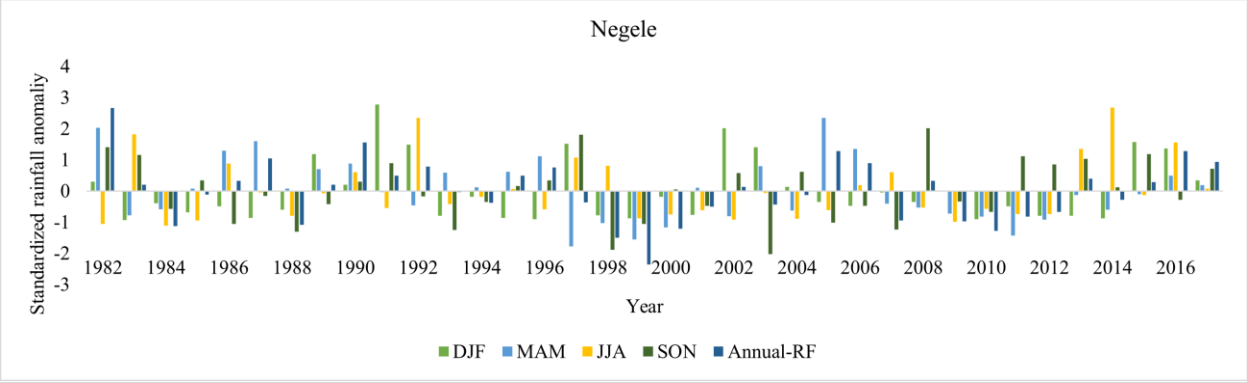
Negele
Standardized rainfall anomaliy
4
3
2
1
0
-1
-2
-3
1982 1984 1986 1988 1990 1992 1994 1996 1998 2000 2002 2004 2006 2008 2010 2012 2014 2016
Year
DJF MAM JJA SON Annual-RF

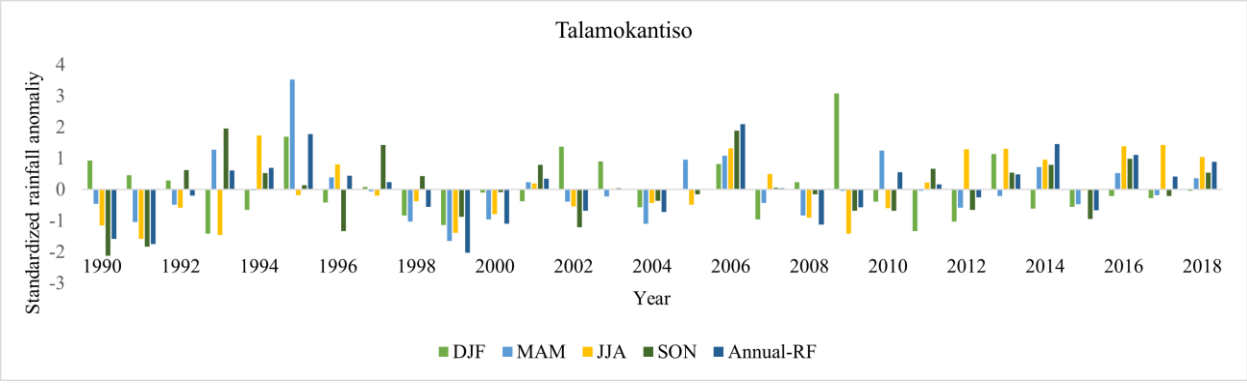
Talamokantiso
Standardized rainfall anomaliy
4
3
2
1
0
-1
-2
-3
1990 1992 1994 1996 1998 2000 2002 2004 2006 2008 2010 2012 2014 2016 2018
Year
DJF MAM JJA SON Annual-RF

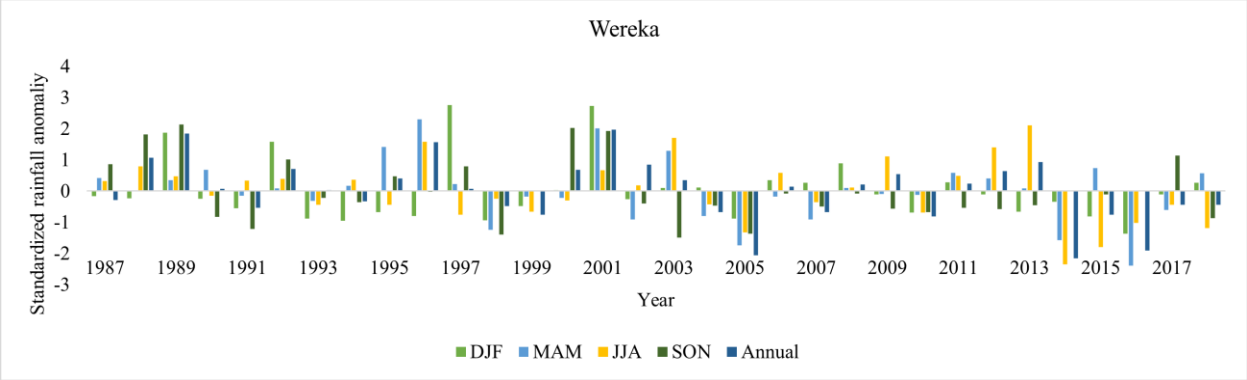

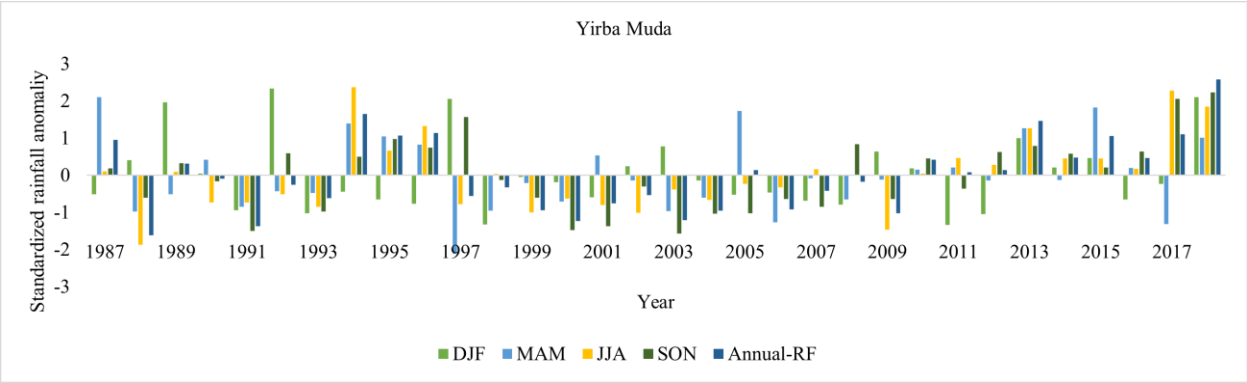

Appendix Figure 3. Annual and seasonal standardized rainfall anomaly for each station

Crop Water Requirements

ETo station: HAGERE-SELAM
Rain station: HAGERE-SELAM
Crop: MAIZE (Grain)
Planting date: 20/03

Month	Decade	Stage	Kc	ETc	ETc	Eff rain	Irr. Req.
			coeff	mm/day	mm/dec	mm/dec	mm/dec
Mar	3	Init	0.30	1.13	12.5	18.8	0.0
Apr	1	Deve	0.31	1.14	11.4	32.1	0.0
Apr	2	Deve	0.49	1.76	17.6	42.2	0.0
Apr	3	Deve	0.73	2.60	26.0	41.1	0.0
May	1	Deve	0.98	3.40	34.0	39.9	0.0
May	2	Mid	1.16	3.93	39.3	40.6	0.0
May	3	Mid	1.17	3.85	42.3	36.0	6.3
Jun	1	Mid	1.17	3.74	37.4	29.9	7.5
Jun	2	Mid	1.17	3.63	36.3	25.4	10.9
Jun	3	Late	1.07	3.20	32.0	25.0	7.0
Jul	1	Late	0.80	2.29	22.9	23.8	0.0
Jul	2	Late	0.53	1.45	14.5	22.4	0.0
Jul	3	Late	0.36	1.02	2.0	4.8	2.0
					329.3	**383.0**	**34.8**

Crop Water Requirements

ETo station: Dello Mena | Crop: SORGHUM (Grain)

Rain station: Dello Mena | Planting date: 05/04

Month	Decade	Stage	Kc	ETc	ETc	Eff rain	Irr. Req.
			coeff	mm/day	mm/dec	mm/dec	mm/dec
Apr	1	Init	0.30	1.26	7.6	24.6	0.0
Apr	2	Init	0.30	1.20	12.0	52.7	0.0
Apr	3	Deve	0.33	1.30	13.0	50.9	0.0
May	1	Deve	0.49	1.84	18.4	51.8	0.0
May	2	Deve	0.65	2.39	23.9	53.6	0.0
May	3	Deve	0.82	2.96	32.6	36.6	0.0
Jun	1	Mid	0.95	3.35	33.5	8.0	25.5
Jun	2	Mid	0.95	3.31	33.1	0.0	33.1
Jun	3	Mid	0.95	3.14	31.4	0.0	31.3
Jul	1	Late	0.91	2.77	27.7	0.1	27.6
Jul	2	Late	0.76	2.16	21.6	0.0	21.6
Jul	3	Late	0.61	1.81	19.9	0.1	19.8
Aug	1	Late	0.51	1.61	3.2	0.2	3.2
					277.8	**278.7**	**162.1**

Crop Water Requirements

ETo station: ADOLA-(KIBREMENGIS | Crop: MAIZE (Grain)

Rain station: | Planting date: 20/03

Month	Decade	Stage	Kc	ETc	ETc	Eff rain	Irr. Req.
			coeff	mm/day	mm/dec	mm/dec	mm/dec
Mar	2	Init	0.30	1.36	1.4	1.3	1.4
Mar	3	Init	0.30	1.31	14.4	24.3	0.0
Apr	1	Deve	0.31	1.29	12.9	39.6	0.0
Apr	2	Deve	0.48	1.94	19.4	51.8	0.0
Apr	3	Deve	0.73	2.85	28.5	49.8	0.0
May	1	Deve	0.97	3.72	37.2	50.1	0.0
May	2	Mid	1.14	4.29	42.9	51.6	0.0
May	3	Mid	1.15	4.19	46.1	36.2	10.0
Jun	1	Mid	1.15	4.07	40.7	14.4	26.3
Jun	2	Mid	1.15	3.95	39.5	0.0	39.5
Jun	3	Late	1.06	3.49	34.9	1.2	33.7
Jul	1	Late	0.79	2.52	25.2	4.2	21.1
Jul	2	Late	0.52	1.61	16.1	3.7	12.4
Jul	3	Late	0.36	1.16	2.3	0.7	2.3
					361.6	**328.8**	**146.6**

Appendix Figure 4. CROPWAT 8.0 output for selected stations

Appendices: Published Articles

Scientific African 20 (2023) e01635

Contents lists available at ScienceDirect

Scientific African

journal homepage: www.elsevier.com/locate/sciaf

Analysis of rainfall and temperature variability for agricultural water management in the upper Genale river basin, Ethiopia

Mehari Shigute[a,b], Tena Alamirew[a,c], Adane Abebe[d], Christopher E. Ndehedehe[e,f,*], Habtamu Tilahun Kassahun[e]

[a] Ethiopian Institute of Water Resources (EIWR), Addis Ababa University, Addis Ababa, P. O. Box 150461, Ethiopia
[b] Natural Resource Management, Dilla University, Dilla, P. O. Box 419, Ethiopia
[c] Water and Land Resource Center (WLRC), Addis Ababa University, Addis Ababa, P. O. Box 3880, Ethiopia
[d] Arba Minch Water Technology Institute, Arba Minch University, Arba Minch, P. O. Box 21, Ethiopia
[e] Australian Rivers Institute, Griffith University, Nathan, QLD 4111, Australia
[f] Griffith School of Environment & Science, Griffith University, Nathan, QLD 4111, Australia

ARTICLE INFO

Article history:
Received 17 May 2022
Revised 17 November 2022
Accepted 7 March 2023

Editor: DR B Gyampoh

Keywords:
Upper Genale river basin
Rainfall and temperature trend
Rainfall variability
Mann-Kendall trend test

ABSTRACT

A better understanding of climate-induced changes and support for adaptation strategies requires knowledged of the spatiotemporal dynamics of climatic variables. This study aims to assess long-term changes in annual and seasonal rainfall and temperature for agricultural water management in the upper Genale river basin, Ethiopia. To achieve this objective, long-term climate data from 13 stations between 1975 and 2018, as well as maximum and minimum temperatures for six stations were collected from the Ethiopian National Meteorological Service Agency (NMA). The characteristics of rainfall (onset, cessation, length of growing season, and crop water requirement) were assessed using the Coefficient of Variation (CV), Standard Rainfall Anomaly (SRA), and Precipitation Concentration Index (PCI). Additionally, the Mann–Kendall test and Sen's slope estimator were used to assess the trend and magnitude of changes in rainfall and temperature. The annual, winter, spring, summer and autumn CVs were 20%, 89%, 30%, 45%, and 32%, respectively. The standardized anomalies of annual and seasonal rainfall for the climate stations indicated that the basin had a drier season than a wet season. The mean length of the growing season in Belg and Kiremt ranged from 43 to 79 days and 38 to 170 days, respectively. On an annual, summer, and autumn season basis, most rainfall stations showed a non-significant trend. In contrast, in the spring season, rainfall showed a decreasing but statistically insignificant trend in all stations except Bensadaye, Bore, Telamokentise, and Yirba Muda stations. According to the analysis of the crop water requirements in the studied basin, supplemental irrigation is essential to reducing yield reduction and crop failure during spring and autumn. In these seasons, maize and sorghum varieties required supplementary irrigation up to 202 mm and 252 mm, respectively. Annual and seasonal maximum and minimum temperatures showed an increasing trend at all the stations except Hagre Selam station. Generally, there was a spatially and temporally variable trend in rainfall while the temperature trend was increasing irrespective of the temporal and spatial factors. Thus, this study

* Corresponding author at: Australian Rivers Institute and School of Environment & Science, Griffith University, Nathan, QLD 4111, Australia.
E-mail address: c.ndehedehe@griffith.edu.au (C.E. Ndehedehe).

Appendix: Published Article 1. Analysis of rainfall and temperature variability for agricultural water management in the upper Genale river basin , Ethiopia. Scientific African, 20, e01635 (2023). https://doi.org/10.1016/j.sciaf.2023.e01635

water

MDPI

Article

Understanding Hydrological Processes under Land Use Land Cover Change in the Upper Genale River Basin, Ethiopia

Mehari Shigute [1,2,*], Tena Alamirew [1,3], Adane Abebe [4], Christopher E. Ndehedehe [5,6] and Habtamu Tilahun Kassahun [5]

[1] Ethiopian Institute of Water Resources (EIWR), Addis Ababa University, Addis Ababa P.O. Box 150461, Ethiopia
[2] Natural Resource Management, Dilla University, Dilla P.O. Box 419, Ethiopia
[3] Water and Land Resource Center (WLRC), Addis Ababa University, Addis Ababa P.O. Box 3880, Ethiopia
[4] Arba Minch Water Technology Institute, Arba Minch University, Arba Minch P.O. Box 21, Ethiopia
[5] Australian Rivers Institute, Griffith University, Nathan, QLD 4111, Australia
[6] Griffith School of Environment & Science, Griffith University, Nathan, QLD 4111, Australia
* Correspondence: meharishigute@gmail.com

Abstract: The expansion of cultivated land in place of natural vegetation has a substantial influence on hydrologic characteristics of a watershed. However, due to basin characteristics and the nature and intensity of landscape modification, the response varies across basins. This study aims to evaluate the performance of a soil and water assessment tool (SWAT) model and its applicability in assessing the effects of land use land cover (LULC) changes on the hydrological processes of the upper Genale River basin. The results of satellite change detection over the past 30 years (between 1986 and 2016) revealed that the landscape of the basin has changed considerably. They showed that settlement, cultivated, and bare land areas had increased from 0.16% to 0.28%, 24.4% to 47.1%, and 0.16% to 0.62%, respectively. On the contrary, land cover units such as forest, shrubland, and grassland reduced from 29.6% to 13.5%, 23.9% to 19.5%, and 21.8% to 18.9%, respectively. Based on monthly measured flow data, the model was calibrated and validated in SWAT-CUP using the sequential uncertainty fitting (SUFI-2) algorithm. The result showed that the model performed well with coefficient of determination (R^2) $\geq$ 0.74, Nash–Sutcliffe efficiency (NSE) $\geq$ 0.72, and percent bias (PBIAS) between −5% and 5% for the calibration and validation periods. The hydrological responses of LULC change for the 1986, 2001, and 2016 models showed that the average annual runoff increased by 13.7% and 7.9% and groundwater flow decreased by 2.85% and 2.1% between 1986 and 2001 and 2001 and 2016, respectively. Similarly, the total water yields increased from 324.42 mm to 339.63 mm and from 339.63 mm to 347.32 mm between 1986 and 2001 and 2001 and 2016, respectively. The change in hydrological processes, mainly the rise in runoff and total water yield as well as the reduction in lateral and groundwater flow in the watershed, resulted from LULC changes. This change has broader implications for the planning and management of the land use and water resource development.

Keywords: upper Genale River basin; SWAT model; LULC change

Citation: Shigute, M.; Alamirew, T.; Abebe, A.; Ndehedehe, C.E.; Kassahun, H.T. Understanding Hydrological Processes under Land Use Land Cover Change in the Upper Genale River Basin, Ethiopia. *Water* **2022**, *14*, 3881. https://doi.org/10.3390/w14233881

Academic Editor: František Petrovič

Received: 28 October 2022
Accepted: 25 November 2022
Published: 28 November 2022

Publisher's Note: MDPI stays neutral with regard to jurisdictional claims in published maps and institutional affiliations.

1. Introduction

Land use and land cover (LULC) changes are dynamic and uninterrupted processes that are often influenced by both anthropogenic and natural factors [1,2]. Human activities have been identified as the primary drivers of LULC changes [3,4]. Although humans have been altering land for thousands of years to obtain livelihoods and other necessities, the amount, rate, and severity of LULC modification are significantly larger now than they were previously [5]. Population growth, societal development, overgrazing, the inappropriate utilization of forest resources, and agricultural land expansion have all contributed to a substantial rise in the rate of LULC changes [6–9]. These human actions

Appendix: Published Article 2. Understanding Hydrological Processes under Land Use Land Cover Change in the Upper Genale River Basin, Ethiopia. Water, 14(23), 3881 (2022). https://doi.org/10.3390/w14233881

Environmental Earth Sciences (2024) 83:297
https://doi.org/10.1007/s12665-024-11586-2

ORIGINAL ARTICLE

Assessing the impacts of climate change on hydrological processes in the upper Genale River basin, Ethiopia

Mehari Shigute[1,2] · Tena Alamirew[1,3] · Adane Abebe[4] · Christopher E. Ndehedehe[5,6] · Habtamu Tilahun Kassahun[5]

Received: 3 October 2023 / Accepted: 5 April 2024

Abstract

The aim of this research is to assess the impact of future climate change on hydrological parameters (e.g., precipitation and temperature) in Ethiopia's upper Genale River basin. Future climate scenarios for the 2021–2050 and 2051–2080 periods were developed from four different GCM–RCM combinations of CORDEX-Africa projections using the Representative Concentration Pathways (RCP 4.5 and RCP 8.5). These climate models were bias corrected and used as input to the Soil and Water Assessment Tool (SWAT) model. During the 2030s (2021–2050) and 2060s (2051–2080), under the two RCPs, the projected precipitation in the annual and seasonal periods tends to decrease while temperatures increase. The simulated result revealed a significant change in hydrological components (e.g., During the 2060s), under the RCP4.5 scenario, CNRM-CM5 climate model runoff, ground water flow, and total water yield increased by 24.47%, 27.98%, and 28.56%, respectively. On the contrary, during the 2060s under the MIROC5 climate model, runoff, ground water flow, and total water yield reduced by 20.84%, 34.34%, and 25.8%, respectively. The annual hydrological components of the study area under MPI-ESM-LR, EC-EARTH, and MIROC5 showed a decrease in total water yield, surface runoff, ground waterflow, and lateral flow. However, due to a rise in temperature, evapotranspiration showed an increase up to 8.1% under all climate models (MPI-ESM-LR, EC-EARTH, CNRM-CM5, and MIROC5). The reduction in rainfall, which coincides with rising temperatures, is expected to reduce annual water yield, surface runoff, ground waterflow, and lateral flow by up to 39.8%, 39.3%, 50%, and 40.1%, respectively, across MPI-ESM-LR, EC-EARTH, and MIROC5 scenarios for the entire study basin in future projections. Our study helps to give a better insight into understanding climate change in watershed and can benefit the planning of water resources by strengthening adaptation strategies against the impacts of future climate change.

Keywords Upper Genale River basin · Climate change · Regional climate models · Hydrological processes · SWAT model

Introduction

Emissions of greenhouse gases (GHGs) into the atmosphere have increased since the pre-industrial era, primarily due to the expansion of intensive agriculture, industrialization, the utilization of fossil fuels, and urbanization (Hussain et al. 2018; IPCC 2014; Shrestha 2014). Changes in GHG concentrations in the atmosphere primarily tend to raise the temperature (Syukuro 2019). The change in climate has caused the mean temperature to rise across the globe. Since the 1900s, it has risen by about 0.8 °C, and by the end of the twenty-first century, it is expected to rise by 1.4–2.0 °C (IPCC 2013). A warmer climate accelerates and changes the hydrological cycle, causing long-term changes in evapotranspiration, rainfall, and runoff volume and timing, and resulting in negative impacts on natural water resources in a

✉ Mehari Shigute
meharishigute@gmail.com

[1] Ethiopian Institute of Water Resources (EIWR), Addis Ababa University, P. O. Box 150461, Addis Ababa, Ethiopia

[2] Natural Resource Management, Dilla University, P. O. Box 419, Dilla, Ethiopia

[3] Water and Land Resource Center (WLRC), Addis Ababa University, P. O. Box 3880, Addis Ababa, Ethiopia

[4] Arba Minch Water Technology Institute, Arba Minch University, P. O. Box 21, Arba Minch, Ethiopia

[5] Australian Rivers Institute, Griffith University, Nathan, QLD 4111, Australia

[6] Griffith School of Environment and Science, Griffith University, Nathan, QLD 4111, Australia

Published online: 04 May 2024

Appendix: Published Article 3. Assessing the Impacts of Climate Change on Hydrological Processes in the Upper Genale River Basin, Ethiopia. *Environ Earth Sci* **83**, 297 (2024). https://doi.org/10.1007/s12665-024-11586-2